

TNO report

TNO 2012 R10670

4D Basin modelling of the Broad Fourteens Basin and offshore West Netherlands Basin; Erosion and heat flow reconstruction and its influence on temperature, maturity and hydrocarbon generation

Princetonlaan 6
3584 CB Utrecht
P.O. Box 80015
3508 TA Utrecht
The Netherlands

www.tno.nl

T +31 88 866 42 56
F +31 88 866 44 75
infodesk@tno.nl

Date	25 September 2012
Author(s)	R. Abdul Fattah J.M. Verweij N. Witmans J.T.Veen
Copy no	
No. of copies	
Number of pages	168 (incl. appendices)
Number of appendices	7
Sponsor	
Project name	4D Geomodellen
Project number	056.01549

All rights reserved.

No part of this publication may be reproduced and/or published by print, photoprint, microfilm or any other means without the previous written consent of TNO.

In case this report was drafted on instructions, the rights and obligations of contracting parties are subject to either the General Terms and Conditions for commissions to TNO, or the relevant agreement concluded between the contracting parties. Submitting the report for inspection to parties who have a direct interest is permitted.

© 2012 TNO

draft

Summary

3D basin modelling is used to analyze the basin evolution and the maturity and hydrocarbon generation history of the source rock units in the NCP-2F area in the Dutch offshore. Additional focus was on quantitative analysis of two main processes: erosion and basal heat flow history. The latest results of the mapping project of the Dutch offshore. are used in the modelling.

The study area covers the Broad Fourteens Basin, the offshore part of the West Netherlands Basin as well as the Zandvoort Ridge and the surrounding platforms. The input model consists of 24 layers including a basement. New thickness and erosion maps of the Carboniferous formations are included in the model. Six formations have been defined in the model as source rock. In addition to the oil-prone Namurian Unit, three Westphalian age gas-prone source rocks are defined in the Carboniferous (Baarlo, Ruurlo and Maurits). Two Jurassic formations are introduced as oil-prone source rocks; the Aalborg and the Posidonia formations.

Four erosional phases are included in the initial model; the Saalian (Late Carboniferous-Early Permian), the Late Kimmerian (Late Jurassic), the Subhercynian-Laramide inversion (Late Cretaceous) and the Pyrenean (Late Eocene). Special attention is paid to improve the erosion model and to determine the amount of erosion for the different layers. An iterative approach is used where calculated maturity, based on initial erosion thicknesses, are calibrated to measured well data (temperature and vitrinite reflectance).

The erosion scenario that provided the best fit with measured maturity and temperature data and which was consistent with new stratigraphic concepts and data was selected for maturity simulation. A new erosion scenario is proposed and a number of refined erosion thickness maps have been generated.

This erosion scenario suggests that during the Saalian event, the Hunze sub group, the Maurits formation and parts of the Ruurlo formation were eroded in the study area. The Kimmerian erosion is divided into two phases; the Mid-Late Kimmerian I and the Late Kimmerian II. In the Mid-Late Kimmerian I, parts of the Jurassic Altena Group was eroded. During the Late Kimmerian II, the Late Jurassic Schieland Group was eroded in almost the whole area. In the central part of the area, the Schieland was preserved together with the underlying Altena formations. During the Subhercynian inversion, Cretaceous formations were eroded as well as the remaining patches of Jurassic Schieland and Altena groups in the central part of the study area. The Late Cretaceous inversion in the central part of the Broad Fourteens Basin went deep and reached the Upper Triassic formations. Therefore, Jurassic formations were eroded in two phases; the Later Kimmerian and the Subhercynian-Laramide phases.

A detailed study was carried out to model the basal heat flow in the area. The heat flow was modelled in six wells covering different structures in the study area. The interpolated heat flow maps were then calibrated with measured temperatures and vitrinite reflectance in a number of wells over the whole area. The new generated heat flow maps are then used for maturity analyses.

New surface-water interface temperatures and paleo water depth data, based on recent geo-biological studies, have been used for the upper boundary condition and the tectonic reconstruction.

draft

The calibrated heat flow maps and the new erosion scenario and maps are used to model the maturity and hydrocarbon generation history of the source rocks in the area. The models are calibrated to field data including temperature and vitrinite reflectance measurements.

The simulation shows that the burial history has an important role in temperature and maturity evolution of the area. The model indicates that the Namurian source rock is overmature at present-day. Hydrocarbon generation started in the Permian and increased during the Jurassic rifting phases to reach the present-day status in the Late Cretaceous. Most of its convertible organic matter was consumed during the Permian through gas generation.

In some places, the remaining organic matter in the Namurian was transformed to hydrocarbons during the Mesozoic. This might have contributed to later gas accumulations in the area.

Most of the hydrocarbon generation from the Westphalian formations took place in the Jurassic and Cretaceous in the whole area. Maturity of these formations started in the Early Jurassic and experienced a jump in Late Cretaceous. The model indicates that the Baarlo Formation is predominantly overmature at present-day. The Ruurlo and the Maurits formations are overmature in the basins and appear to be in the gas generating window at the platforms. The gas generating Westphalian formations are still capable of hydrocarbon generation as the modelled transformation ratio shows.

Jurassic source rocks (Aalburg and Altena formations) generally appear to be in the oil window at present-day. Some small patches in the basins are in the gas generating window and some have already overmature. The maturity started in the Late Jurassic and increased during the Cretaceous to reach a peak at the Late Cretaceous. The maturity has slightly increased during the Tertiary, especially to the south (the West Netherlands Basin).

The maturity and the timing of hydrocarbon generation can be related to the major tectonic events and the associated structures to understand the distribution of the accumulations. Most of the charging could have taken place prior to the inversion event. But later generation, during the Tertiary, might have contributed to charging the traps.

Contents

1	Introduction	6
1.1	Mapping of the deep subsurface of the Netherlands offshore (NCP-2 project).....	6
1.2	Definition of mapping areas in the Netherlands offshore.....	7
1.3	Detailed mapping of the NCP-2F area	7
1.4	Geological setting.....	8
1.5	Petroleum systems.....	9
2	Basin modelling: Workflow, input data and boundary conditions.....	12
2.1	Assumptions and conditions underlying the basin modelling approach.....	12
2.2	Basin modelling workflow	12
2.3	Database.....	13
2.4	Input: Geological model (thickness maps).....	13
2.5	Input: Properties.....	21
2.6	Input: Boundary conditions	24
2.7	Input: Sequence of events (initial scenario).....	25
2.8	Input: Erosion maps (initial scenario)	26
2.9	Basin modelling: Default set-ups, calibration wells	35
2.10	Basal Heat Flow modelling: Input parameters and modelling results	36
3	Modelling results: evaluation of different erosion scenarios.....	42
3.1	Scenario I : Initial model	42
3.2	Scenario II: Reduced original thickness of the Chalk.....	48
3.3	Scenario III: Subhercynian erosion of Jurassic formations.....	51
3.4	Scenario IV: Subhercynian erosion of Jurassic formations: modified erosion thicknesses	57
3.5	Scenario V: Kimmerian and Subhercynian erosion of Jurassic formations	62
3.6	Scenario VI: Late Kimmerian (I and II) erosion of Jurassic formations (New deposition ages).....	65
4	Burial history and history of maturity and hydrocarbon generation	76
4.1	Burial history	76
4.2	Maturity and hydrocarbon generation history.....	82
5	Discussion.....	92
5.1	Temperature, burial history and maturity.....	92
5.2	Heat flow calibration	93
5.3	Source rock maturity.....	94
5.4	Migration and trapping.....	95
6	Conclusions.....	98
7	References.....	103
8	Annex.....	107
8.1	Annex I : Input thickness maps	108
8.2	Annex II: Basin modelling parameters, default relations	111
8.3	Annex III: List of calibration wells	114
8.4	Annex IV: 1D Heat flow modelling parameters	117
8.5	Example of basal heat-flow modelling : Well P06-1 (Broad Fourteens Basin)	121

8.6	Annex V: 3D Heat flow calibration.....	136
8.7	Annex VI: Calibration of well data	150
8.8	Annex VII: Erosion maps (Maturity scenario).....	159
9	Signature	168

1 Introduction

There is a rapidly growing demand for improved understanding of the Dutch subsurface for finding and producing more conventional and unconventional oil and gas and because of the need for alternative energy supplies. We use basin modelling to integrate the wealth of new data and information that is increasingly available on the Dutch subsurface (sections 1.1 -1.3) for evaluating the interdependencies of the different processes that affect rocks and fluids during geological history. Special attention is paid to processes and conditions affecting hydrocarbon potential. In addition we develop different approaches to improve the basin modelling results. Here we pay special attention to two such approaches. The first one involves probabilistic tectonic heat flow modelling to calculate the basal heat flow history and construct paleo and present-day heat flow maps (the most important thermal boundary condition for basin modelling). The second approach is the reconstruction of erosion history that directly influences burial history modelling.

This report shows results of the tectonic heat flow modelling and erosion reconstruction and its application in 3D basin modelling of the burial history and the history of temperature, source rock maturity and timing of hydrocarbon generation in the study area from 320 Ma to present-day.

1.1 Mapping of the deep subsurface of the Netherlands offshore (NCP-2 project)

The detailed mapping of seven offshore areas on the Netherlands Continental Shelf was initiated in late 2005 and was finalised in 2011. It builds on and goes one step beyond the previous regional mapping of the Netherlands onshore and offshore. In 2004 the publication of the Geological Atlas of the Subsurface of the Netherlands – onshore rounded off the onshore regional mapping project and a ‘quick and dirty’ offshore mapping (NCP-1 project) was completed in 2006 (viz. on the <http://www.nlog.nl>; Duin et al. 2006).

The main aim of the detailed mapping of seven sub-areas is to present a more comprehensive model of the subsurface to future and current operators in the oil industry and to governmental and non-governmental organisations for, amongst other things, the spatial planning of the Dutch subsurface. The deliverables include:

- 3D geological framework (depth and thickness grids)
- Rock and fluid parameters (petrophysical parameters, P, T, Vr) 3D burial histories
- Petroleum system analysis

All deliverables, such as maps, grids and graphs, can be downloaded from <http://www.nlog.nl> site. When applicable, regular updates will be made available on the site. The outcome of this study, including final report, will also be made available on the site.

1.2 Definition of mapping areas in the Netherlands offshore

Based on consultation with the exploration departments of the oil companies operating in the Netherlands it was decided to divide the offshore area into seven sub-areas (Figure 1). These areas represent more or less structural entities at the Late Jurassic to Early Cretaceous times (Figure 2). One of these sub-areas is the 2F area. Area 2F is predominantly occupied by the Broad Fourteen Basin and the offshore part of the West Netherlands Basin. It also includes the offshore part of the Zandvoort Ridge, parts of the Noord-Holland Platform, parts of the Central Offshore Platform and the Cleaver Bank High as well as parts of the Winterton Platform. The area covers the K, L, P, Q quadrants.

1.3 Detailed mapping of the NCP-2F area

The detailed mapping was focussed on the assessment of the present-day stratigraphic and structural framework of the sedimentary fill of the area as well as on the properties of rocks and fluids it contains, such as reservoir porosities, pressures, salinities, source rock maturity, characteristics of oil and gas.

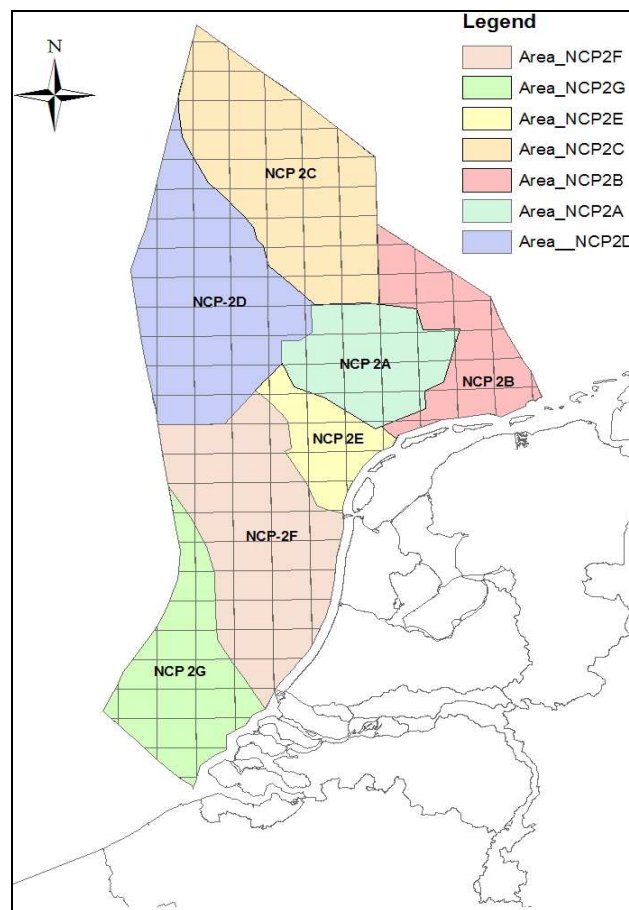


Figure 1: Mapping areas of the NCP-2 project for mapping the deep subsurface of the Dutch offshore area.

1.4 Geological setting

The NCP-2F area is composed of basins, highs and platforms (Figure 2).

Most of the area is occupied by the Broad Fourteens Basin and the offshore part of the West Netherlands Basin. The geological setting of these basins has been studied and described in detail by various authors (Van Wijhe, 1987; Huyghe and Mugnier, 1994, 1995; Hooper et al., 1995; Nalpas et al., 1995; Brun and Nalpas, 1996; De Jager et al., 1996; Van Balen et al., 2000; De Jager, 2003; De Lugt et al., 2003; Verweij, 2003). The Broad Fourteens Basin was formed during the Mesozoic and was subject of major inversion movements during the Late Cretaceous and to less extent during the Early Tertiary. Its southwestern boundary is formed by major graben faults, whereas its northeastern boundary is formed by a gradual transition to adjacent platform areas. The northern area of the basin is affected by salt tectonics and movements, whereas the southern parts of the basin are less affected by salt movements (Nalpas et al., 1995; Brun and Nalpas, 1996;) (Figure 3).

The present-day structure and sedimentary record of the BFB reflect a complex history of extension and inversion. Active extension stress regimes dominated from Triassic to Early Cretaceous. Compressional stress regimes dominated the basin from the Late Cretaceous onward. Pre- and early rift phases resulted in thick sedimentary sequences that includes the Upper Rotliegend, Zechstein, and Germanic Triassic Groups. During the main syn-rift phase, the Altena Group and Schieland Group were developed in the deepest axial parts of the basin followed by a post-rift thermal subsidence phase where Rijnland and Chalk Groups were deposited. This was interrupted by Late Cretaceous inversion of the BFB. The inversion of the basin resulted in deep erosion of the uplifted sedimentary deposits. At the same time, syn-inversion deposition of chalk continued in the adjacent areas (Verweij et al., 2003). The Cainozoic post-inversion development of the basin was dominated by subsidence interrupted by phases of compression and erosions like the Eocene-Oligocene which led to the erosion of the Lower North Sea Group sediments. For more details on the geological settings and development of the BFB the reader is referred to Verweij (2003), and references therein.

The West Netherlands Basin has a similar tectonic history as the Broad Fourteens Basin. It is part of the Late Jurassic/Early Cretaceous transtensional basins that include, in addition to the WNB and the BFB, the Roer Valley Graben. The Late Permian-Middle Jurassic regional thermal subsidence resulted in the deposition of Rotliegend sandstones, claystones and carbonates of the Zechstein Group, and the shales and sandstones of the Germanic Triassic Groups. During the Late Jurassic to Early Cretaceous rifting the Altena and the Schieland Groups were deposited. Late Jurassic-Early Cretaceous rifting was accompanied by igneous activities, especially in the south-eastern part of the basin (van Balen et al. 2000). During the Cretaceous, thermal subsidence led to the deposition of the Rijnland and the Chalk Groups. During the Late-Cretaceous compressive forces dominated and caused uplift of the basin fill and erosion. The compressional stress that caused the inversion is mainly related to the onset of convergence of Africa with Eurasian plate (the Alpine collision). Major fault zones developed and were re-activated. At the end of the Early Palaeocene and during the Eocene-Oligocene, renewed uplift occurred and almost all Palaeogene sediments were removed.

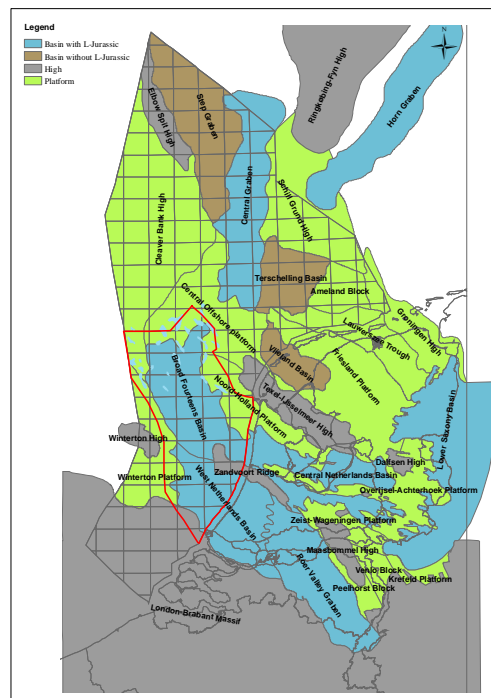


Figure 2: The structural settings in the region in the Late Jurassic-Early Cretaceous, with the location of the NCP_2F area.

1.5 Petroleum systems

Many oil and gas fields have been discovered in the area. Most of the discoveries are located along the margins of the major tectonic elements (Figure 3). In the BFB, major gas accumulations are present in the Slochteren Formation (Upper Rotliegend Group), Main Buntsandstein Subgroup (Lower Germanic Trias Group) and Zechstein Carbonate Member. The main top seal for the Slochteren reservoir in the Broad Fourteens Basin consists of Zechstein evaporites. The major source rocks for gas in BFB are gas-prone Westphalian coal measures of the Limburg Group. The kerogen is of type III and the TOC content of the coals is at least 70 % (Verweij et al., 2003). The Namurian shales might also have contributed as a source rock to the gas accumulations in the area. The Namurian shale is of kerogen type II which is an oil-prone type. However, under deep burial conditions it would generate gas. Commercial oil accumulations are found in the Vlieland Sandstone Formation (Rijnland Group) and the Delfland Subgroup (Schieland Group). The Vlieland Claystone is forming the top seal for the oil accumulations; the traps are mainly faulted anticlines that formed during the Late Cretaceous inversion. The source rock of the oil accumulations is the Posidonia Shale Formation (Altena Group). The Aalburg Formation (Altena Group) is also considered as a source rock for the oil accumulations. Both source rocks are of kerogen type II.

In the West Netherlands Basin, hydrocarbon systems are comparable to those in the Broad Fourteens Basin. The Main Buntsandstein Subgroup and the Röt Fringe Sandstone Member (Upper Germanic Trias Group) contain mainly gas and minor quantities of oil (van Balen et al., 2000). Other reservoir horizons include: Zechstein Sandstone, the Middle Werkendam Member and Brabant Formation (Middle Jurassic), sand intervals in the lower Cretaceous Rijnland Group and Lower Tertiary Dongen Sand Member. As in the BFB, the major source rocks in the WNB are the thick successions of the Westphalian sediments, and the Posidonia and

Aalburg Formations. Westphalian source rocks consist of gas prone coal measures of kerogen type III. Jurassic source rocks are oil prone shales of kerogen type II. Similar to the BFB, in the WNB the Namurian shales are also considered to be a source rock of kerogen type II (Van Balen et al., 2000; Van Bergen, 1998).

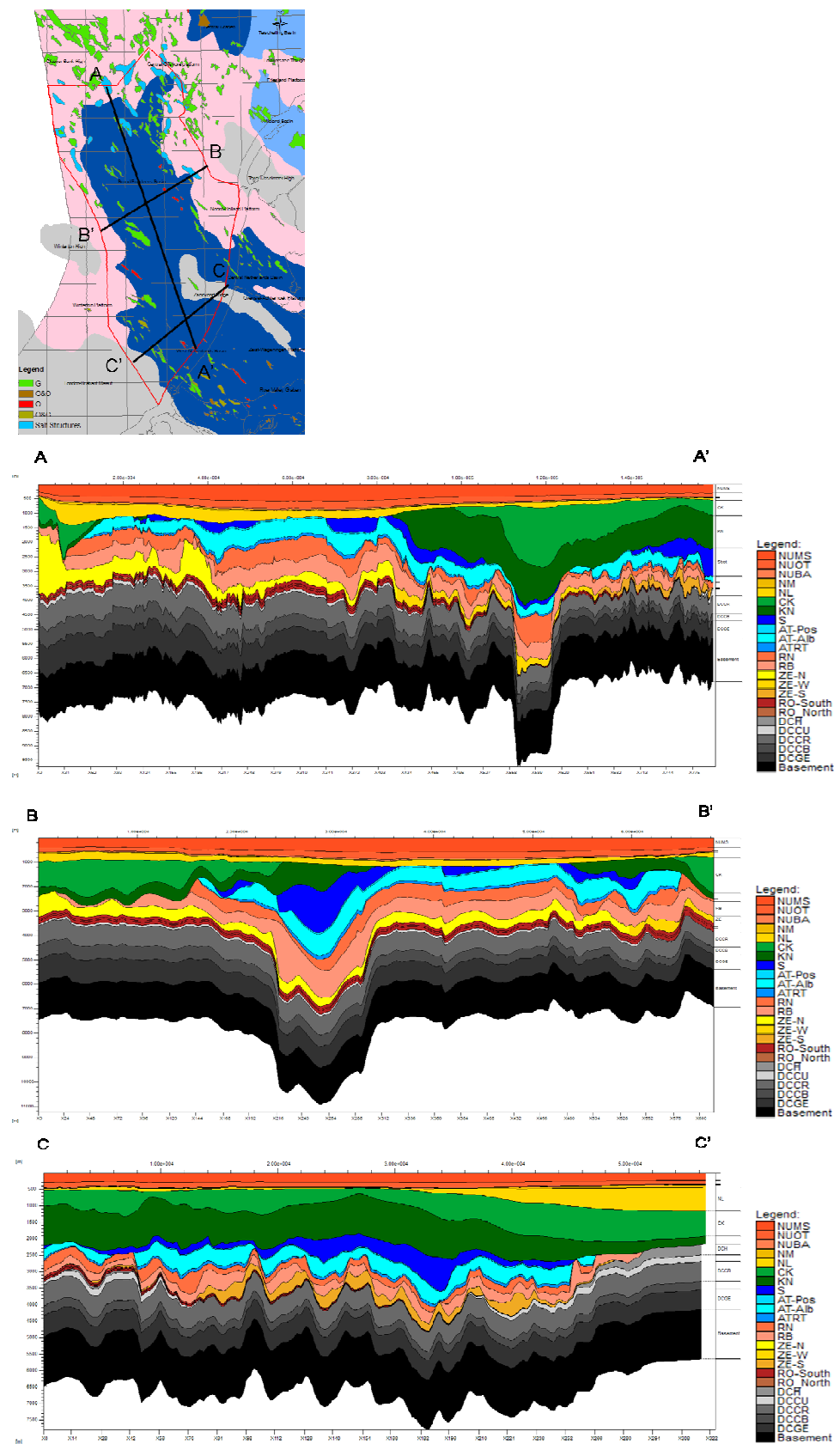


Figure 3: Three profiles through the study area. The map of the study area shows the distribution of gas fields in the NCP-2F area.

2 Basin modelling: Workflow, input data and boundary conditions

2.1 Assumptions and conditions underlying the basin modelling approach

The 1D-3D basin modelling was performed with the basin modelling programme PetroMod version 11 of Schlumberger.

General assumptions and conditions inherent in basin modelling:

- Geological history:
 - the model is laterally constrained, no horizontal compression or extension of the basin fill is taken into account.
 - vertical movement only (no lateral deformation of the sediments in the model, except for salt movement)
 - salt movement has no direct relation to changes in stress
 - compaction of the basin fill is vertical
 - compaction is mechanical according to vertical effective stress-based rock property model
- History pore water fluids
 - density of pore water is constant
- Thermal history
 - conductive heat flow

The basin modelling scenarios presented here are based on a geological model without faults and assumed open fluid flow boundaries. In addition to these general limiting assumptions and conditions, default set-ups of the modelling package influence simulation results. Such default set-ups include default relations between standard lithologies and properties through compaction approaches, porosity-permeability relations, thermal models, kinetic models; mixing rules lithology. The selection of the proper set-up is an important part of the basin modelling workflow.

2.2 Basin modelling workflow

Initially 1D simulations for individual well locations were carried out to verify the conceptual models of subsidence and erosion history.

The general workflow with respect to the full 3D basin modelling of the NCP-2F area included the following steps:

- 1- Building 3D geological model. This includes reviewing and editing the input depth maps for the different formations as well as establishing initial scenarios for the erosion phases;
- 2- Selection proper PetroMod default porosity-depth and porosity-permeability relations;
- 3- Running 3D model for reconstructing burial history;
- 4- Selection proper thermal conductivity model (using measured temperature data and published information on thermal conductivities); the default Sekiguchi model of PetroMod was selected;
- 5- Generating Surface Water Interface Temperatures (SWIT) and Paleo Water Depths boundary conditions. The SWIT are corrected for paleo water depths. Generating basal heat flow boundary conditions based on the 1D modelling of

tectonic evolution of the area and using the in-house probabilistic modelling tool PetroProb;

- 6- Running 3D model for reconstructing history of temperature and source rock maturity (using the Pepper and Corvi (1989)_Type III-IV F kinetic model and tectonic heat flow boundary condition);
- 7- Running 3D heat flow model for calibrating and refining the basal heat flow boundary condition input maps;
- 8- Running 3D model for reconstructing the history of hydrocarbon generation, using the Pepper and Corvi (1989)_Type III-IV F kinetic model introducing the salt movement tool where incorporated. The new newly calibrated and refined heat flow maps are used;
- 9- Running multiple simulations dealing with various erosion scenarios;
- 10- Discussing the best scenario for hydrocarbon generation and source rock maturity.

2.3 Database

The basic data requirements for the 3D modelling involve: present-day geometry (stratigraphy; property/facies boundaries within stratigraphic units, fault geometries, water depth); lithological properties (lithological composition of each stratigraphic unit and eroded (part of) unit and of each facies); quantified uninterrupted time-sequence of events during geological history (3D history of sedimentation, uplift and erosion; estimated thickness of erosion; 3D history of water depth, basal heat flow, surface temperature; timing of salt movement); calibration data (such as present-day temperatures, porosities, permeabilities, pressures, vitrinite reflectance measurements).

The results of the detailed mapping of the NCP_2F area provided the basic conceptual model of the geological evolution required for the numerical modelling.

2.4 Input: Geological model (thickness maps)

The present-day 3D litho-stratigraphic model was the basic input for the 3D modelling. Depth and thickness maps of 13 stratigraphic units were loaded from Petrel into PetroMod and horizons were adjusted. Twelve new maps were created and included in the model to achieve a more comprehensive and realistic model.

The model input maps obtained from the Petrel model included:

- Sediment Surface (Sea Water Depth)
- Upper North Sea Group
- Lower North Sea Group
- Chalk Group
- Rijnland Group
- Schieland Group
- Altena Group
 - Upper Altena
 - Posidona Formation
 - Lower Altena
- Upper Germanic Trias Group
- Lower Germanic Trias Group
- Zechstein Group

The input maps of these groups are shown in Annex I. This basic 3D lithostratigraphic model of the area was extended to greater depths with Upper Rotliegend, Carboniferous and Namurian and basement. The final geological input model consists of 24 layers, including the basement. The twelve additional maps were created by splitting of a basic input map or by interpolation from well data, as follows:

- Upper North Sea formations

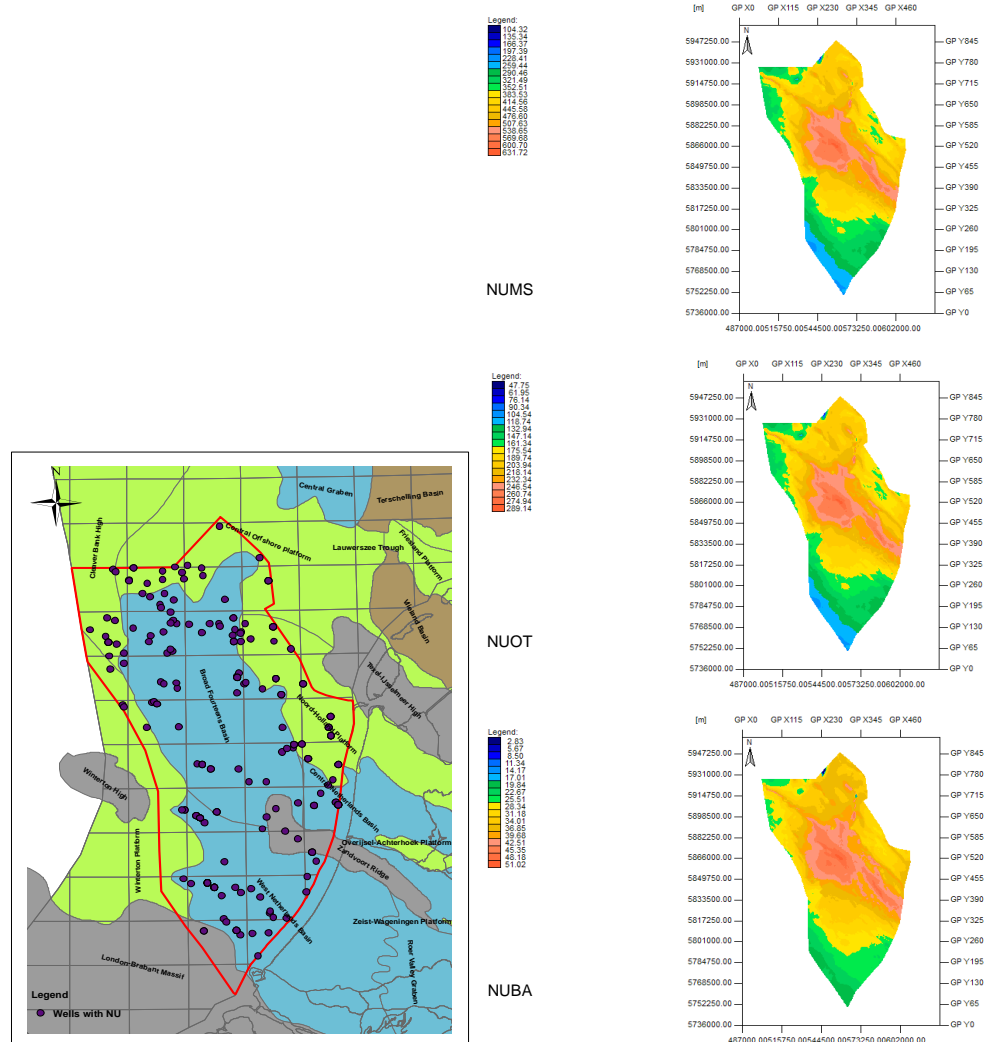
The Upper North Sea Group was subdivided into three formations; the Maassluis Formation (NUMS), the Oosterhout Formation (NUOT) and the Breda Formation (NUBA). The main purpose of the subdivision is to be able to include the effect of the paleo water depth (PWD) for these periods, especially since detailed PWD curves were available for the study (see below). The subdivision and splitting of the map between the three formations was based on well analyses in the area. The splitting ratio according to the well analysis is: 60 % for the Maassluis Formation (NUMS), 35 % for the Oosterhout Formation (NUOT) and 5% for the Breda Formation (NUBA). The generated new maps are shown in Figure 4. All other properties, such as lithology and facies, were kept the same as used for the original input map of the North Sea Group.

- Middle and Lower North Sea groups

The map of the lower North sea group was split into two maps, the Middle North Sea Group and the Lower North Sea Group. Based on well data, the split ratio was set to 90 % for the Lower North Sea Group and 10 % for the Middle North Sea Group (Figure 5).

- The Aalburg and Sleen Altena formations

Three main thickness maps were provided for the Altena Group. A map representing the Posidonia Shale Formation (the main Jurassic source rock). A map representing the upper part of Altena (above Posidonia Formation), as well as a map of the Altena Group below the Posidonia. Since the Aalburg Formation was also considered as a source rock in our model, the lower part of the Altena was subdivided into two sub-layers representing the Aalburg Formation (ATAL) and Sleen Formation (ATRT). Based on well analysis, the splitting ratio was set to 85 % for the Aalburg Formation and 15% for the Sleen Formation (Figure 6). This way the Altena Group was introduced into the model as four layers, Upper Altena, Posidonia, Aalburg and Sleen formations.



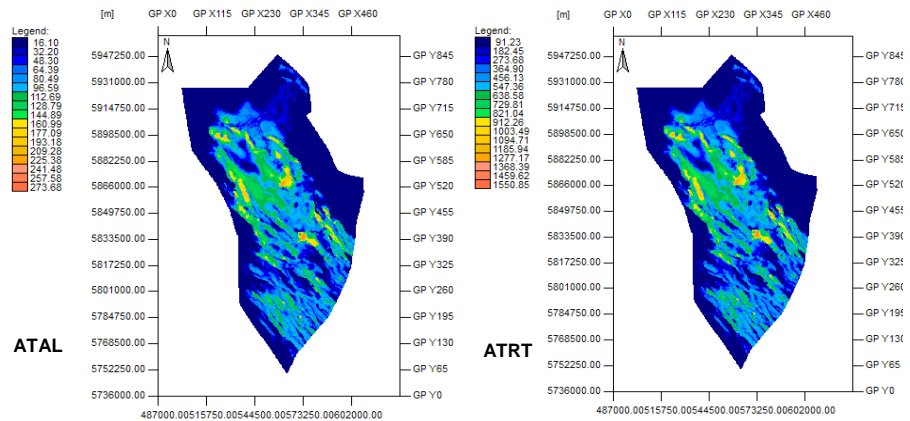


Figure 6: Thickness maps of the Aalborg and Sleen Formations.

- The Rotliegend Group

The Rotliegend thickness map was created by interpolation of the observed thicknesses in wells in the study area. (Figure 7).

The map was generated based on the interpreted upper horizon of the Rotliegend from the seismic tied to well top marks in the wells. The base of the Rotliegend was constructed from wells that reached the top of the Limburg Group (Figure 7) (Stegers and Mijnlief, 2009).

This thickness map of the Rotliegend was subdivided into three sub-layers to take facies distributions into account: Upper Rotliegend (40 %), Middle Rotliegend (20 %) and Lower Rotliegend (40 %). The splitting was based on well data and followed the facies distribution (see below for more details).

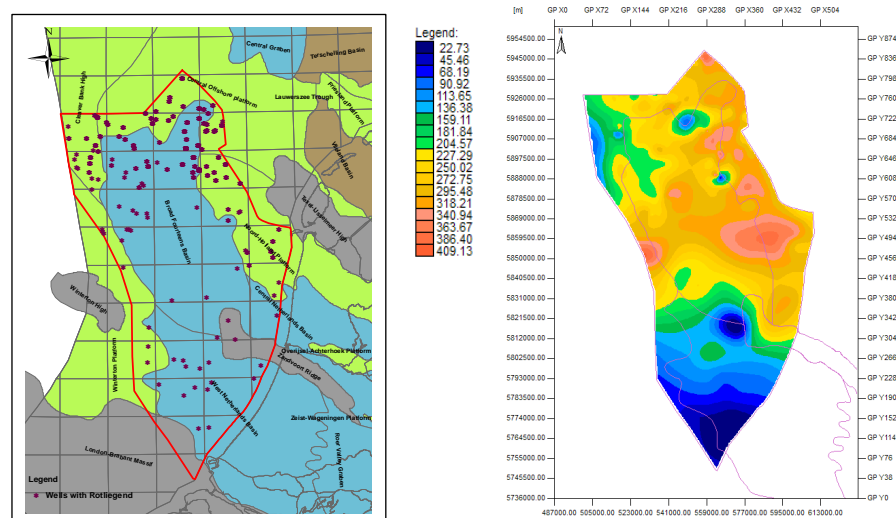


Figure 7: Wells used for generating the Rotliegend thickness map.

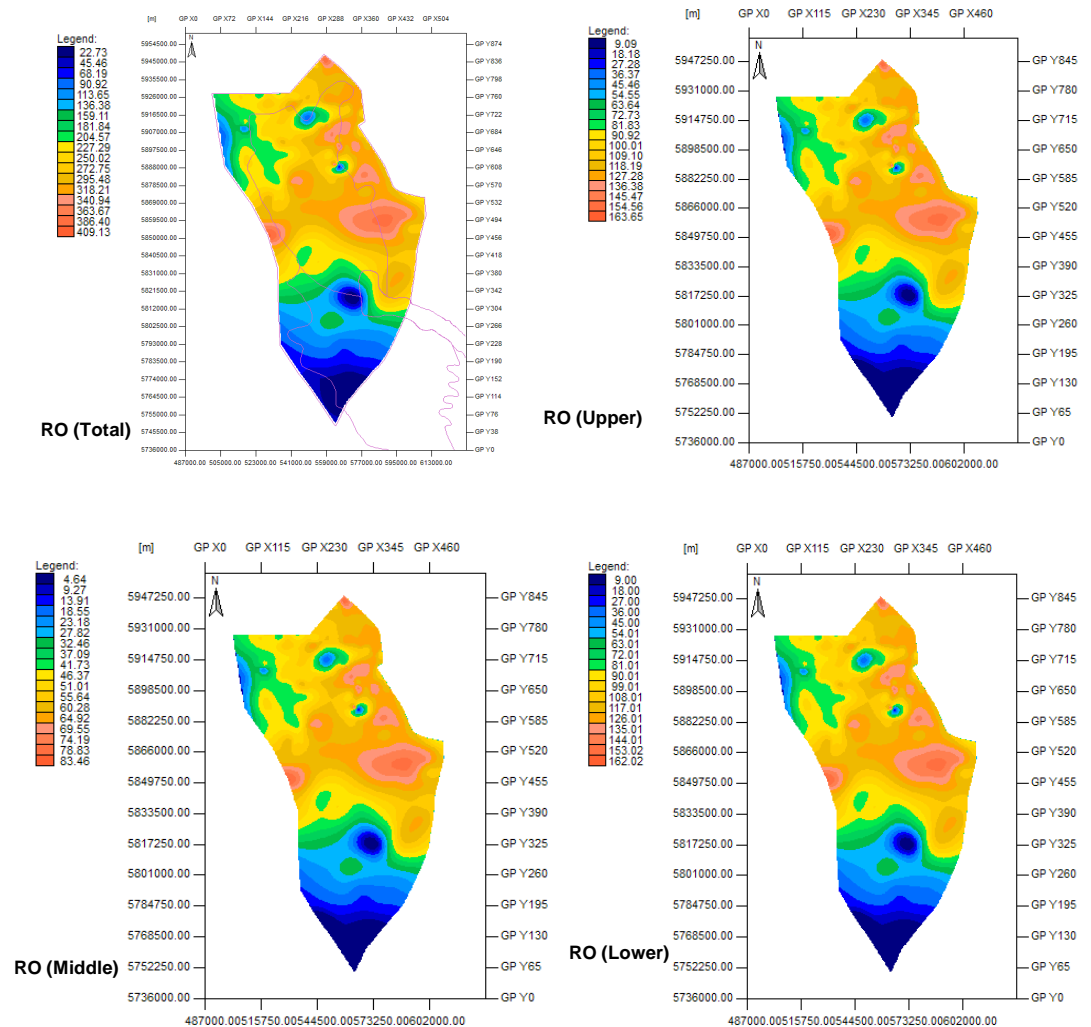


Figure 8: Generated thickness maps of sub-layers of the Rotliegend Group.

- The Carboniferous layers:

The stratigraphic model was extended to greater depths by adding extra Carboniferous layers including; the Hunze Subgroup, Maurits, Ruurlo and Baarlo and the Namurian formations of the Limburg Group. The thickness maps of these layers were based on the subcrop map of the area which was derived from well analysis as well as initial thickness values for the layers that were based on regional paleo-geographic and stratigraphic models (Kombrink et al., 2010). Figure 9 shows the subcrop map of the Carboniferous formations and the wells that penetrate the formations in the area. This map was refined based on the re-interpretation of some wells. The present-day thickness maps of the Carboniferous layers were derived from the refined version of the subcrop maps. The original deposition thicknesses as well as the present-day thickness maps of the Carboniferous formations are shown in Figure 10.

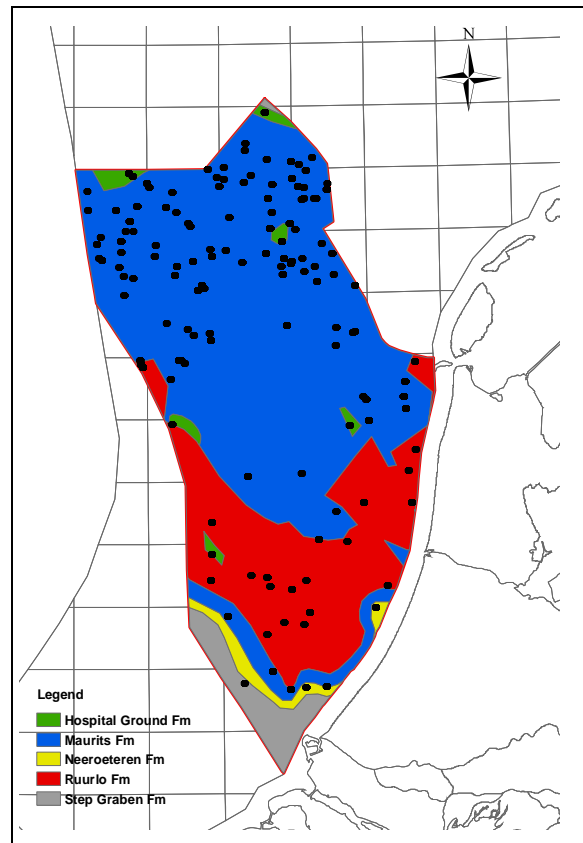
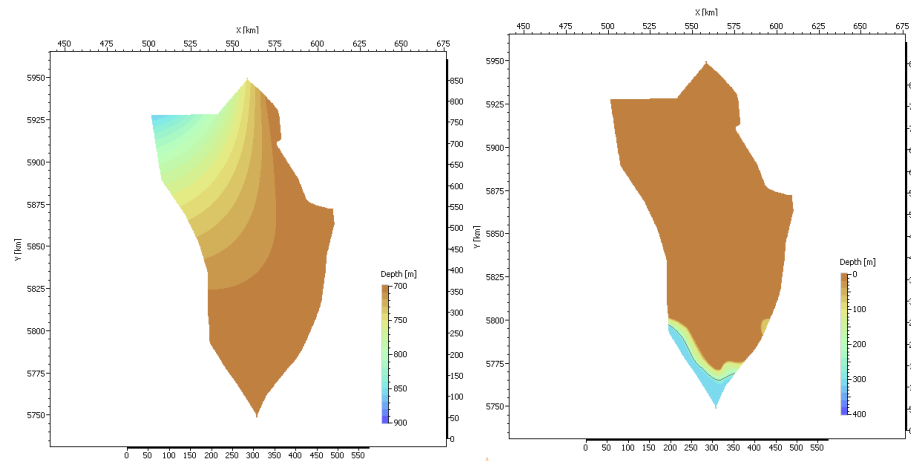
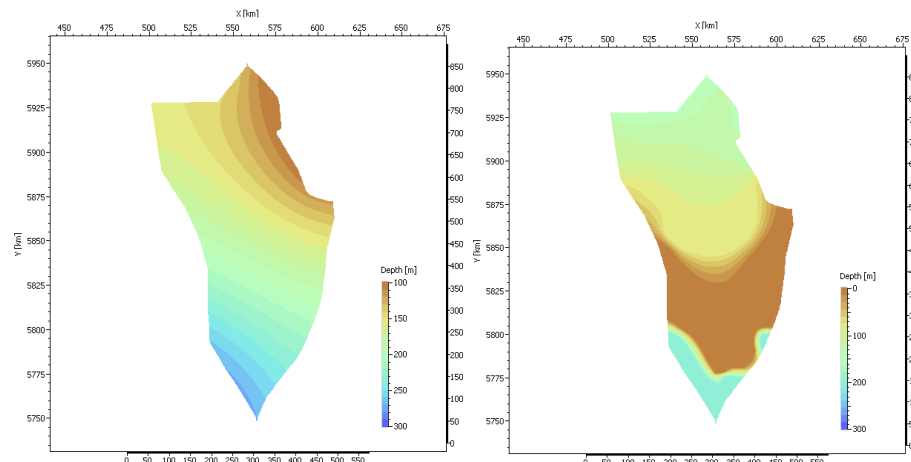
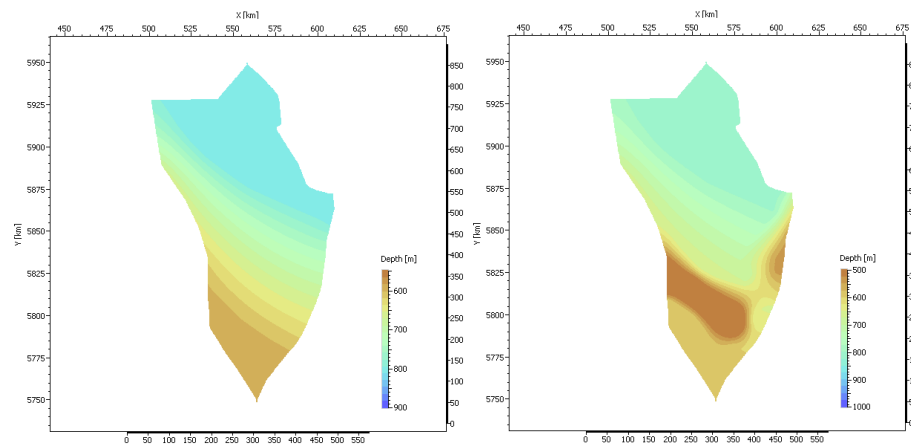
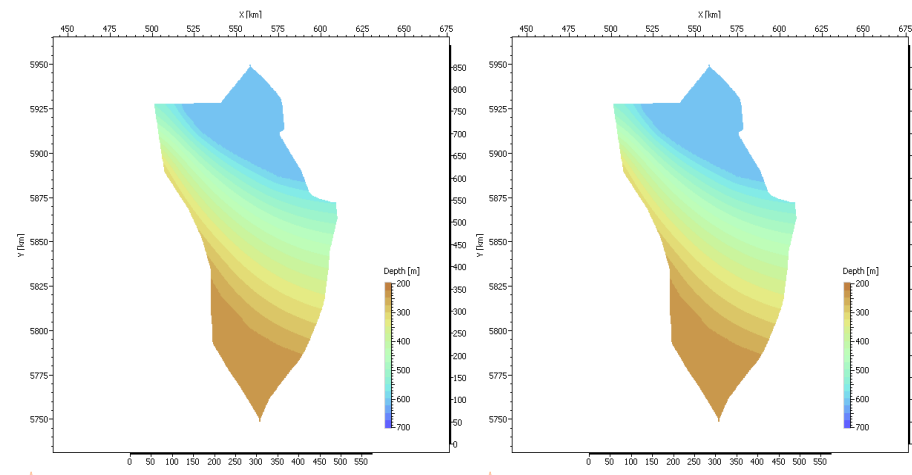


Figure 9: Initial subcrop map of the Carboniferous formations in the NCP-2F area. Wells that penetrate the Carboniferous formations are shown as black dots. This map was slightly modified for the purpose of this study. The Step Graben and Hospital Ground formations are grouped together in the Hunze Subgroup.

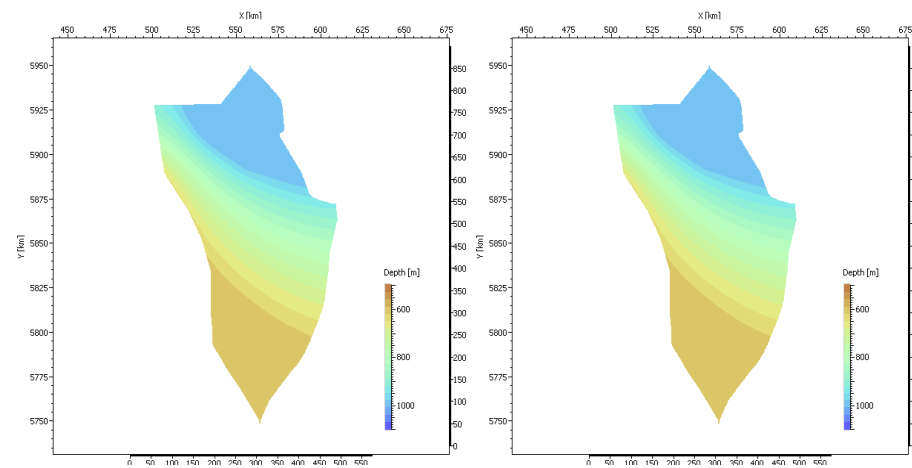
A basement with a uniform thickness of about 1500 m was added to the bottom of the model.

The final 3D input model used for the simulation included 23 layers plus the basement and a Sea Water layer (Figure 11, Table 1). The input model consisted of 575 * 900 gridpoints with a distance of 250 m between gridpoints. The model does not include faults.

**The Hunze Sub-Group (DCH)****The Maurits Formation (DCCU)****The Ruurlo Formation (DCCR)**



The Baarlo Formation (DCCB)



The Epen Formation (DCGE) (Namurian)

Figure 10: Original thicknesses (left) and present-day thicknesses (right) of the Carboniferous formations in the NCP-2F area.

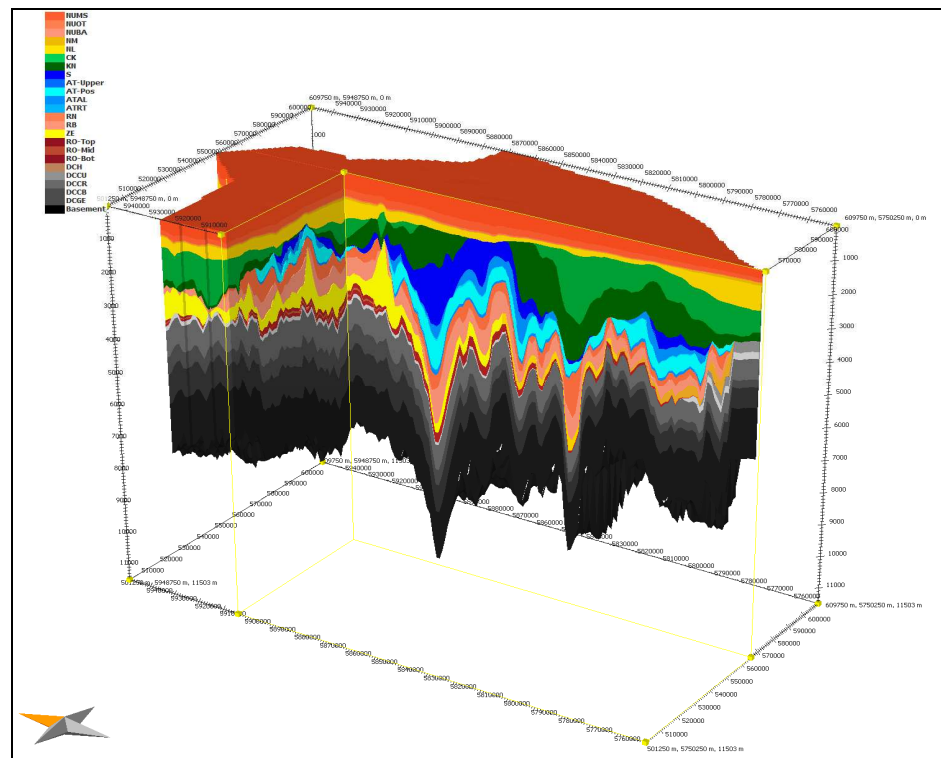


Figure 11: The present-day 3D geometrical model of the NCP-2F area used as input for the basin modelling .

2.5 Input: Properties

Lithology: Lithological compositions were assigned to each layer. The lithology for each of the layers is based on the generalized description of its lithology rather than an exact description based on information from individual wells. Facies changes were taken into account for the Rotliegend and Zechstein groups. The facies distributions were mainly based on well observations (Table 1) (Figures 11, 12).

Table 1. Model stratigraphy: 24 layers and assigned lithological composition in NCP-2F area. Note the facies assigned to the Rotliegend Group and the Zechstein Group.

Layer		Layer	Lithology
			Facies
1	NUMS	Upper North Sea _ Maassluis Formation	Sand/Shale_75
2	NUOT	Upper North Sea _ Oosterhout Formation	Sand/Shale_75
3	NUBA	Upper North Sea _ Breda Formation	Sand/Shale_75
4	NM	Middle North Sea Group	Sand/Shale_50
5	NL	Lower North Sea Group	Sand/Shale_50
6	CK	Chalk	Chalk (typical)
7	KN	Rijnland Group	Shale/Sand/Marl_50/25/25
8	S	Schieland Group	Sand/Shale_50
9	AT-Upper	Altena Group Upper	Shale/Silt_75
10	AT-Pos	Altena Posidonia Formation	Shale (typical)_100
11	ATAL	Altena Aalborg Formation	Shale/Silt_75
12	ATRT	Altena Sleen Formation	Shale (typical)_100
13	RN	Upper Germanic Trias Group	Shale/Sand/Marl_50/25/25
14	RB	Lower Germanic Trais Group	Sand/Shale_70

15	ZE	Zechstein Group	
		<i>Zechstein (North)</i>	Salt/Lime_85/15
		<i>Zechstein (West)</i>	Shale/Lime-70/30
		<i>Zechstein (South)</i>	Sand/Lime/Shale_40/30/30_1
16	RO-Top	Rotliegend Group-Top	Sandstone_100
17	RO-Mid	Rotliegend Group-Middle	
		<i>Rotliegend Middle (North)</i>	Shale/Silt_50
		<i>Rotliegend Middle (South)</i>	Sandstone_100
18	RO-Bot	Rotliegend Group-Bottom	Sandstone_100
19	DCH	Hunze Sub-Group	Shale/Sand_75
20	DCCU	Maurits Formation	Shale/Sand/Coal_80/15/5
21	DCCR	Ruurlo Formation	Shale/Silt/Sand/Coal_48/25/25/02
22	DCCB	Baarlo Formation	Shale/Silt/Sand/Coal_48/25/25/02
23	DCGE	Namurian Unit	Shale/Sand_60/40
24	Basement	Basement	BASEMENT

Two facies were assigned to the middle layer of the Rotliegend layer. The northern part of the middle layer of the Rotliegend were considered a bit more shaly and silty, while the southern part was kept sandy. The upper and lower parts of the Rotliegend were kept homogenous and sandy. The Zechstein layer was given three facies, the northern part contained more salt. While the middle part of the layer was assigned a more shale and lime lithology, the southern part was considered a mixture of shale, sand and lime (Table 1).

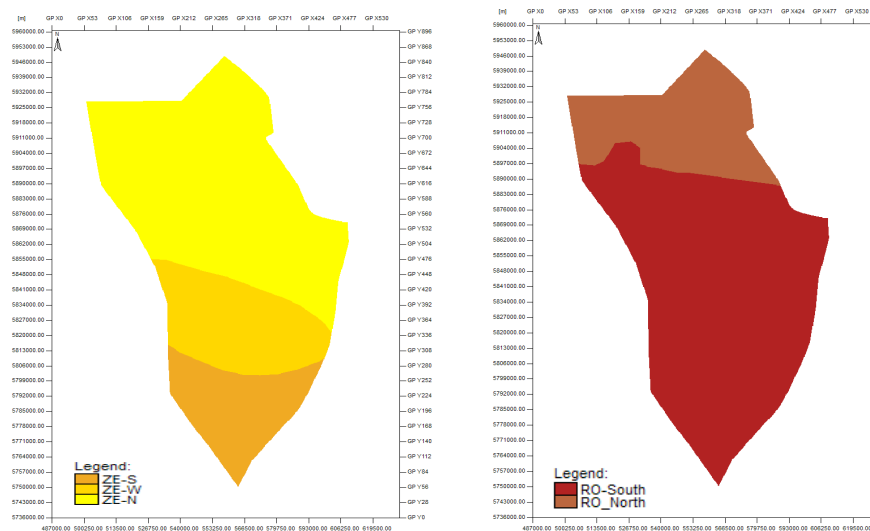


Figure 12: Facies distribution for the Rotliegend Group-Middle (right) and the Zechstein Group (left).

Thermal properties: The thermal conductivity values for the lithologies were defined based on a default thermal conductivity model (the Sekiguchi Model available in PetroMod 11). The radiogenic heat production was calculated for each of the lithologies. The calculation of the radiogenic heat is based on assumed default concentrations of certain minerals (Uranium, Thorium and Potassium) in the major lithological units. The Rybach equation was used to derive the heat production from the concentrations of the minerals. For mixed lithologies, the heat production for various lithological components was arithmetically averaged.

Mechanical Compaction: For all major lithologies, a default compaction model was applied. The model is based on the Hydrostatic Athy's law Model where the porosity versus depth curve is theoretical curve that assumes a hydrostatic pressure and a uniform lithological column. The solid rock is incompressible. Salt is impermeable ($k = 10^{-16}$ mD).

Source rock properties: The model includes 6 source rocks. The major source rock intervals in the model are the Baarlo, Ruurlo and Maurits coal bearing formations of the Limburg Group (gas-prone source rocks of kerogen type III) and the organic rich shales of the Aalburg and Posidonia Shale formations of the Altena Group (oil-prone source rocks of kerogen type II). In addition, the Namurian shale was included as oil-prone source rocks of type II kerogen. Table 2 shows the characteristics of the source rocks that were used as input for the initial simulations of the timing of hydrocarbon generation. The TOC and HI contents of the source rocks were chosen based on Verweij et al. (2003), Verweij (2003), van Balen et al. (2000). The hydrocarbon generation potential kinetics for the source rock formations was based on Pepper & Corvi (1995) with variations based on the simulation scenario chosen for each run (See below)

Table 2. Average source rock parameters used for simulating timing of hydrocarbon generation.

Source rock	TOC Input PM (wt%)	HI input PM (mgHC/gTOC)	Kinetics
Namurian	2.0	200	Pepper&Corvi(1995)_TII(B)
Maurits	4.0	200	Pepper&Corvi(1995)_TIII-IV(F)
Ruurlo	3.0	100	Pepper&Corvi(1995)_TIII-IV(F)
Baarlo	3.0	100	Pepper&Corvi(1995)_TIII-IV(F)
Aalburg	3.00	400	Pepper&Corvi(1995)_TII(B)
Posidonia	6.00	400	Pepper&Corvi(1995)_TII(B)

Pore water/formation water properties: In the model the pore water is of constant density that is the density of the water is independent of changes in temperature and salinity. The water is incompressible.

Salt deformation: Salt deformation can be incorporated in the 3D simulations (i.e. not in the 1D simulation at well locations). When implemented, the 'Salt movement' tool of PetroMod was used to simulate the movement of Zechstein salt, taking the calculated original thickness of the Zechstein Group as original depositional thickness. This original constant thickness of the Zechstein Group over the whole area was derived from the present-day volume of the Zechstein Group. In this study, salt movement was implemented without any detailed salt deformation scheme. A uniform thickness was giving to the salt layer at deposition time. The program then interpolates the thickness variations between deposition thickness and present-day thickness over the geological history.

2.6 Input: Boundary conditions

Paleo water depths: Detailed paleo water depth (PWD) values were used in the modelling. The PWD curve was constructed from TNO in-house database which is largely based on the geobiology studies. The paleo water depths were allowed to vary in time but were kept constant over the entire area at a certain time (Figure 13).

Paleo surface temperature: The paleo surface temperature at the sediment water interface was calculated with an integrated PetroMod tool that takes into account the paleo water depth and the evolution of ocean surface temperatures through time depending on paleo latitude of the area (Wygrala, 1989). For the Tertiary and Quaternary history of SWIT's more detailed temperature boundary conditions were reconstructed. The temperatures at a certain time are kept constant over the entire area (Figure 14) (Verweij et al., 2009).

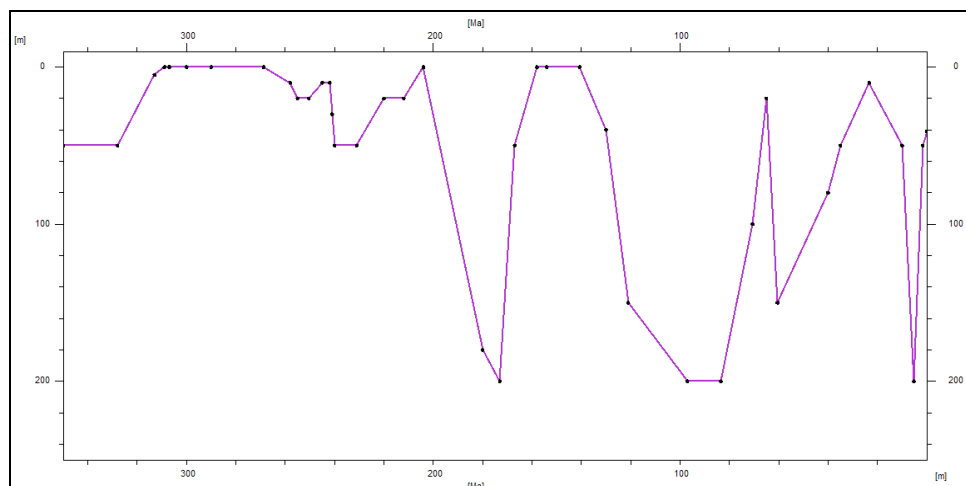


Figure 13: Detailed Paleo Water Depth curve used for the modelling. The curve is based on the TNO in-house database.

Basal heat flow: Basal heat flow was modelled in the area using the 1D tectonic heat flow modelling tool PetroProb (Van Wees et al., 2009). The tool uses the sedimentation, uplift and erosion history for single wells to predict the evolution of the basal heat flow in that well. PetroProb takes into account the tectonic evolution of the basin and requires a user-defined model of the lithosphere. Uncertainties in the input parameters are taken into account during the calculations and as a result the modelled heat flows are expressed in a probabilistic way. The models are calibrated to measured temperatures and vitrinite reflectance data from the well and the heat flow model that gives the best fit is selected (Van Wees et al., 2009). The tool provides 1D basal heat flow models from individual wells. Since the NCP-2F area comprises several tectonic elements (with different tectonic structures and development), several wells (covering the different structures) were used for heat flow modelling. The resulted heat flow models were then interpolated to generate heat flow maps that cover the whole area. Six heat flow models (modelled in six wells) were used for creating heat flow maps (Figure 15). The created heat flow maps were later calibrated over the whole model area using the 3D Heat Flow Calibration tool provided by PetroMod. The calibration tool resulted in refining the initial heat flow maps which were used for maturity modelling. More details about the modelling the basal heat flow and the applied parameters are presented below.

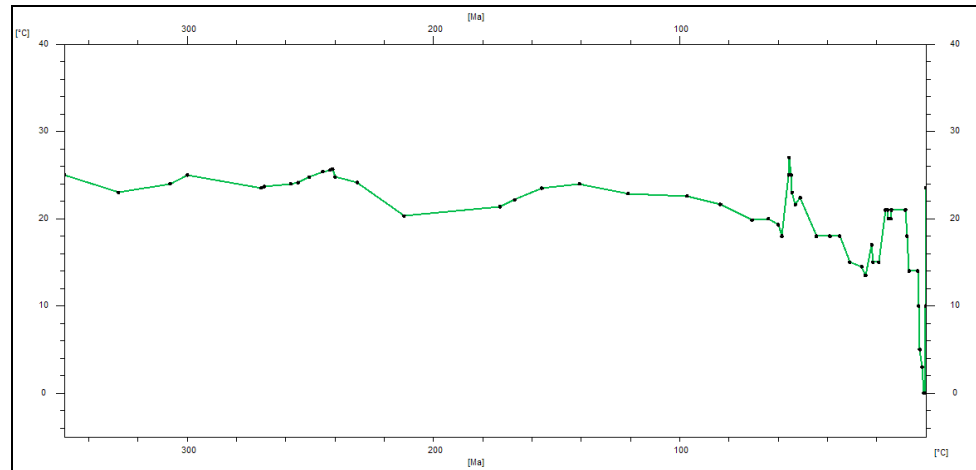


Figure 14: Detailed Paleo Surface Water Interface Temperature curve (Verweij et al.2009).

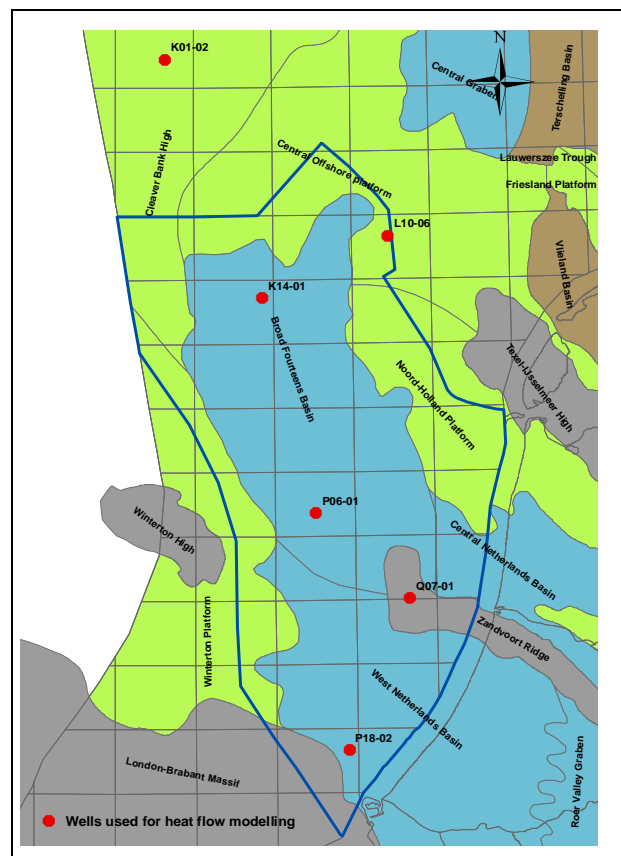


Figure 15: Wells used for basement heat flow modelling. The calculated models were interpolated between the location of the wells to produce 18 paleo heat flow maps. The maps were later calibrated to temperature and maturity data from the whole area in a full 3D calibration process (see below).

2.7 Input: Sequence of events (initial scenario)

Table 3 shows the timing and duration of periods of sedimentation, erosion and non-deposition from Late Carboniferous to present-day. These values are used for the geological model for the initial scenario. Updated ages, and even sequences

are modified during this study to account for different scenarios (see below). Ages of the event and layers are based on the Stratigraphic nomenclature of the Netherlands where the ages are following the Geological Time Scale as published by Gradstein et. al. (2004). The geological evolution includes four phases of erosion, the Saalian, Mid-Kimmerian to Late-Kimmerian, Subhercynian-Laramide inversion and the Pyrenean phase. In addition, periods of non-deposition are included, for example in the Tertiary.

Table 3. Timing and duration of periods of sedimentation, erosion and non-deposition as used for the initial scenario. Modified ages and events are introduced for other scenarios.

Layer	Layer	Deposition Age from [Ma]	Deposition Age to [Ma]	Erosion Age from [Ma]	Erosion Age to [Ma]
NUMS	Upper North Sea Maassluis Formation	3.1	0	0	0
NUOT	Upper North Sea Oosterhout Formation	5.8	3.1	0	0
NUBA	Upper North Sea Breda Formation	20.1	9.6	0	0
NM	Middle North Sea Group	35.4	20.4	0	0
NL	Lower North Sea Group	61.7	40	40	35
CK	Chalk	99.1	85	85	70
KN	Rijnland Group	138.7	99.1	70	61.7
SL	Schieland Group	154.7	149	149	147.5
AT-Upper	Altena Group Upper	177.6	170.1	147.5	145
AT-Pos	Altena_Posidonia Formation	183	177.6	145	144
ATAL	Altena_Aalburg Formation	199.6	183	144	142
ATRT	Altena_Sleen Formation	203.6	200.51	142	140.5
RN	Upper Germanic Trias Group	243	203.6	140.5	138.7
RB	Lower Germanic Trais Group	251	246.2	0	0
ZE	Zechstein Group	258	251	0	0
RO-Top	Rotliegend Group-Top	261.8	258	0	0
RO-Mid	Rotliegend Group-Middle	263.74	261.8	0	0
RO-Bot	Rotliegend Group-Bottom	267.46	263.74	0	0
DCH	Hunze Sub-Group	311	299	290	280
DCCU	Maurits Formation	312.3	311	280	275
DCCR	Ruurlo Formation	313.1	312.3	275	268
DCCB	Baarlo Formation	313.6	313.1	0	0
DCGE	Namurian Formation	326.27	313.6	0	0
Basement	Basement	340	326.27	0	0

2.8 Input: Erosion maps (initial scenario)

The initial 3D geometry of the eroded sediments was estimated based on available stratigraphic correlation. The assumed original thicknesses were used to create

original thickness maps that were later used together with present-day thicknesses of the layers to generate erosion maps.

The assumed erosion thicknesses were calibrated to maturity data in order to restrict and refine the erosion thickness of the layers. This is done in several erosion scenarios until satisfactory results are achieved.

For the four erosion episodes that were introduced to the initial model, 12 erosion maps were prepared.

Table 4 gives an overview of the main erosion phases and the erosion layers that were assigned to each phase. This description was used for the initial model and the base scenario. These values and the sequence of events were modified later in the study.

Table 4: Main erosion phases and the related erosion maps as used for the input of the initial scenarios.

Erosion phase	Related Erosion maps	Erosion Age from [Ma]	Erosion Age to [Ma]
Pyrenean	Lower North Sea Group	40	35
Subhercynian -Laramide	Chalk	85	61.7
	Rijnland Group		
Late Kimmerian	Schieland Group	149	138.7
	Altena Group Upper		
	Altena_Posidonia Formation		
	Altena_Aalburg Formation		
	Altena_Sleen Formation		
	Upper Germanic Trias Group		
Saalian	Hunze Sub-Group	290	268
	Maurits Formation		
	Ruurlo Formation		

A general description of the main erosion phases are presented here:

1. Saalian erosion phase (290 Ma – 268 Ma): The Carboniferous deposits underwent strong uplift and subsequent erosion as result of a regional thermal doming during Early to Middle Permian. In our model we assume (based on the subcrop map (Figure 9)) that the Saalian event affected the Hunze Sub-group, Maurits Formation and the Ruurlo Formation. Deeper layers were not affected by the erosion. Figure 16 presents the original thickness maps of these layers and the erosion maps that were calculated by subtracting the present-day thickness maps from the original thickness maps.(Figure 10).
2. Mid –Late Kimmerian erosion phase (149 Ma – 138.7 Ma): In Early and Mid Jurassic a thermal dome developed in the central part of the North Sea. The development of this transient mantel plume head was related to the extensional stresses that dominated in the region that started in Early Jurassic. The domal uplift during Mid- and Late Kimmerian resulted in regional-scale erosion. The whole NCP-2F area was deeply eroded. The intensity and depth of the erosion varied in the area depending on the tectonic element (basin, high or platform). Nevertheless, the Late Jurassic – Early Cretaceous uplift caused deep erosion and partial removal of the

Lower to Middle Jurassic and sometimes the Upper Triassic sediments. This was particularly the case at the highs and the platforms in the area (such as the North Holland Platform, the Central Offshore platform and the Cleaver Bank High). In our model, the layers that were affected by this erosion phase included; Schieland Group, Altena Group and the Upper Germanic Trias Group. Similar to the Carboniferous erosion maps, the erosion maps of the Kimmerian phase were calculated based on maps of the original thicknesses of the layers. Table 5 shows that original thickness values for each of the layers and in each tectonic element in the area as used in the initial scenario. The values were provided by the mapping department at TNO (N. Witmans, Pers. Comm, 01-2011). The original deposition thickness maps were generated through interpolation between the values (shown in the Table 5) over the whole NCP-2F area. The difference between these maps and the present-day thickness maps were used as the erosion maps (Figure 17). The generated erosion maps were adjusted to the model details. For example, the Altena original thickness maps were subdivided into four sub-layers so that erosion maps can be made for the sub-layers that were used in the model. In addition, the erosion maps were adjusted so that all the layers were eroded in one phase (Mid-Late Kimmerian). The original thickness of the Altena Group in the West Netherlands Basin was given 1300 m. The thickness of the Altena Group in the Broad Fourteen Basin was 900 m. These values were changed and modified according to the different scenarios in the study. This will be discussed later in the report.

3. The Late Cretaceous witnessed a major inversion event. The sedimentary fill of the basin was uplifted and deeply eroded in different pulses. The Subhercynian phase started already in pre-Campanian and peaked in Campanian times and was followed by the Paleocene Laramide inversion phases (De Jager, 2007)., It is suggested that the uplift and erosion were diachronous: the central parts of the basins were affected first and later spread to the margins (Hooper et al., 1995; Verweij, 2003). During uplift and erosion in the central parts of the basins, deposition continued outside the inverted basins (Huyghe and Mugnier, 1994; Nalpas et al., 1995, 1996 Verweij, 2003). Due to the complexity and interference of the different erosion episodes in the upper part of the Cretaceous section it is difficult to distinguish the different erosion phases in the Cretaceous sequence. For this reason, in our model we consider a single phase (Subhercynian-Laramide) of erosion of the upper Cretaceous section. This erosion phase is assigned the age of the Subhercynian -Laramide event (Table 4). Since it is not possible to include a depositional phase simultaneous with erosion phase in PetroMod version 11, we neglect any syn-erosion deposition. In the initial model (scenario) we assumed that the Subhercynian-Laramide erosion phase only affected the Chalk and Rijnland Groups, and not the underlying Jurassic layers (which were assumed to be eroded during the previous Kimmerian event only). This assumption was later modified. The erosion maps of the Rijnland and Chalk groups were based on maps of the original thicknesses of the groups that were constructed in-house (Witmans, Per. Comm, 01-2011) (Table 5). Different erosion scenarios were proposed for the Chalk Group. In the first scenario the Chalk Group is

given an original thickness of 1300 (m), and in the second scenario the Chalk was given 600 (m).

4. Initially different depositional thickness maps of Jurassic layers were constructed depending on their location on the different structural elements in the area. Subsequently these original thickness maps were interpolated. Erosion maps were calculated based on these thickness maps of the Jurassic layers (Figure 18). The post-inversion development of the area in the Cainozoic was generally characterized by regional subsidence, especially in the BFB and the WNB. The subsidence was however interrupted by inversion pulses. A major compressive phase took place during the Eocene-Oligocene Pyrenean phase (40-35 Ma. This caused uplift and erosion of the Lower North Sea Group. Another erosion phase (Savian phase) took place in early Eocene that affected the Middle North Sea Group). This phase is neglected in our model, because the removed thicknesses from the Middle North Sea Group remains limited (~ 100 m) which has a negligible effect on the maturity calculations. The Pyrenean phase, on the other hand, is included in the model and an erosion map of the Lower North Sea Group is generated. The map is also based on original thickness values for each of the structural elements in the study area (Table 5) (Figure 19).

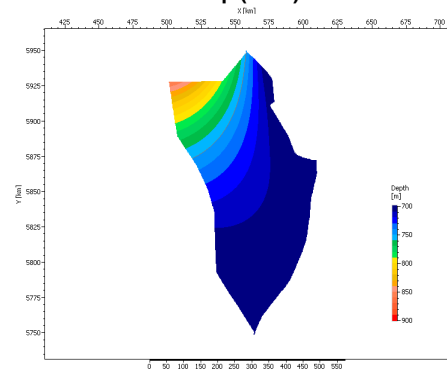
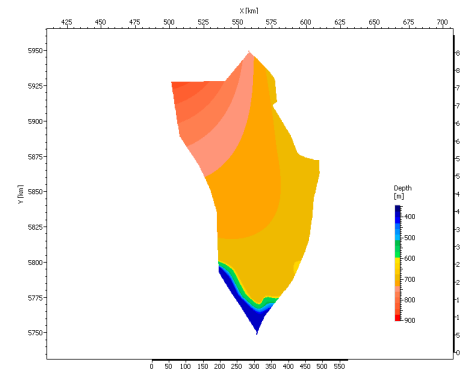
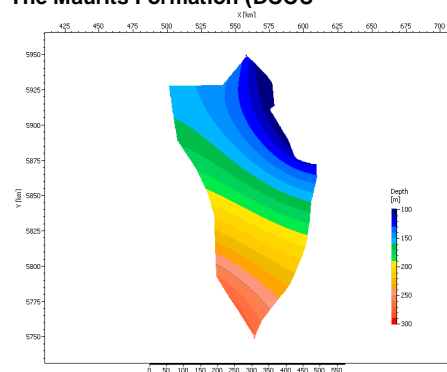
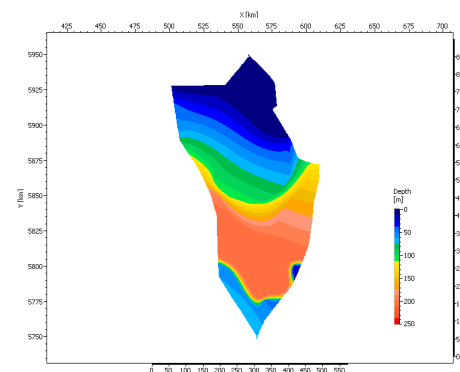
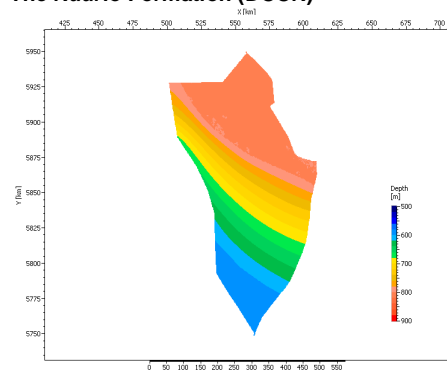
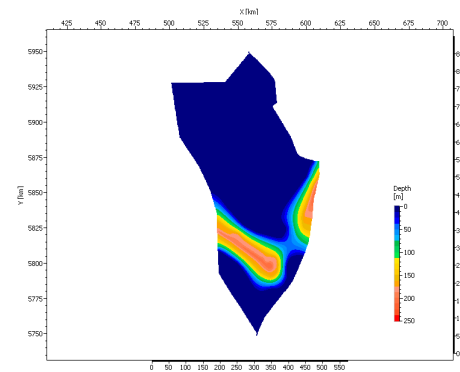
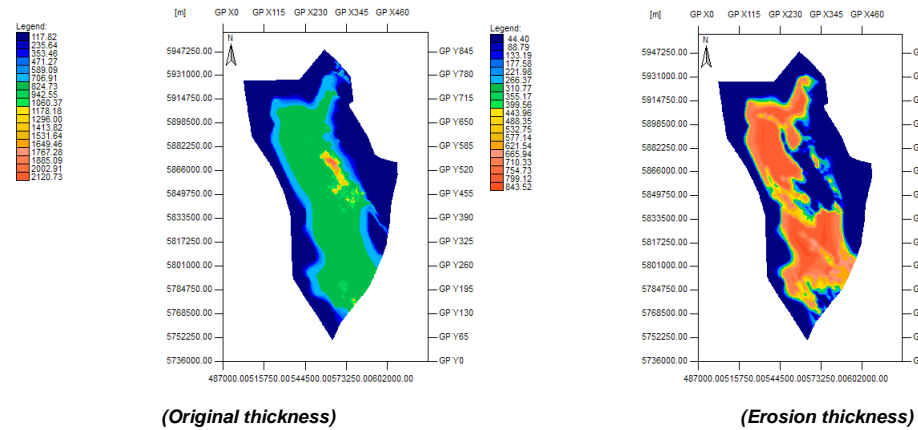
The Hunze Sub-Group (DCH)**(Original thickness)****(Erosion thickness)****The Maurits Formation (DCCU)****(Original thickness)****(Erosion thickness)****The Ruurlo Formation (DCCR)****(Original thickness)****(Erosion thickness)**

Figure 16: Original thicknesses (left) and erosion thickness maps(right) of the eroded Carboniferous formations during the Saalian event in the NCP-2F area.

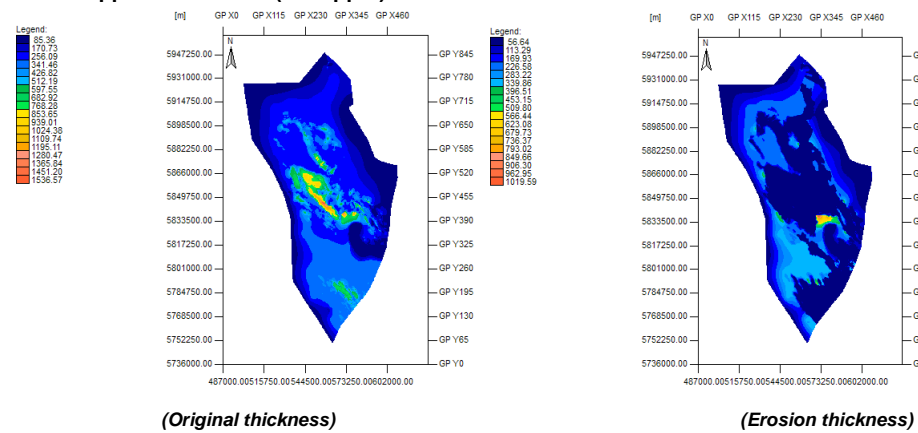
Table 5: Estimated original deposition thicknesses and erosion of various tectonic elements in the NCP-2F area. These values represent the initial scenario and were modified for various scenarios.

	Estimated original thicknesses (m)				Estimated erosion (m)			
	COP/WH	B14	WNB	NHP	COP/WH	B14	WNB	NHP
NU	600	900	500	600	0	0	0	0
NL+NM	400	500	500	700	50-200	55-400	200-500	50-300
CK	1100	600 -1300	600 -1300	1600	100	>600	0-900	100
KN	650	1000	1000	650	100	600-1000	0-50	100
SL	0	800	800	0	0	0-650	0-650	0
AT	200	900-1300	1300	200	200	0-900	0-900	200
RN	400	500	700	400	0-400	0-300	0-200	400
RB	500	700	500	500	0-100	0-50	0-50	0

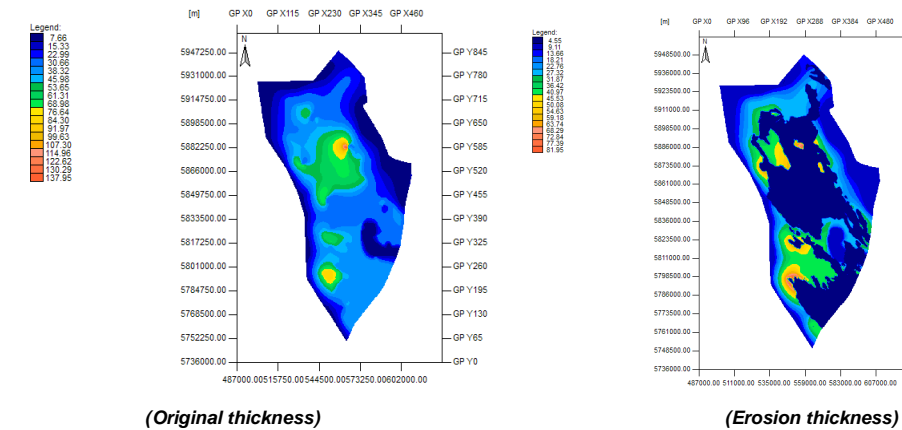
The Schieland Group (SL)



Altena Upper subdivision (AT-Upper)



Altena Posidonia Formation (ATPO)



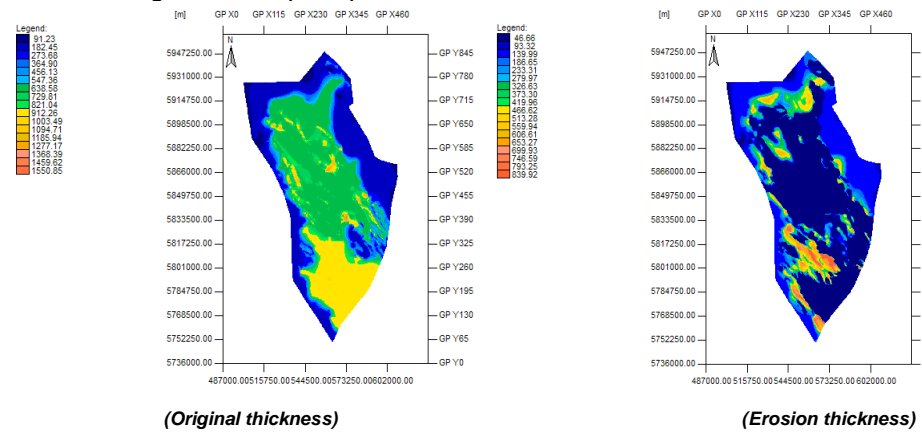
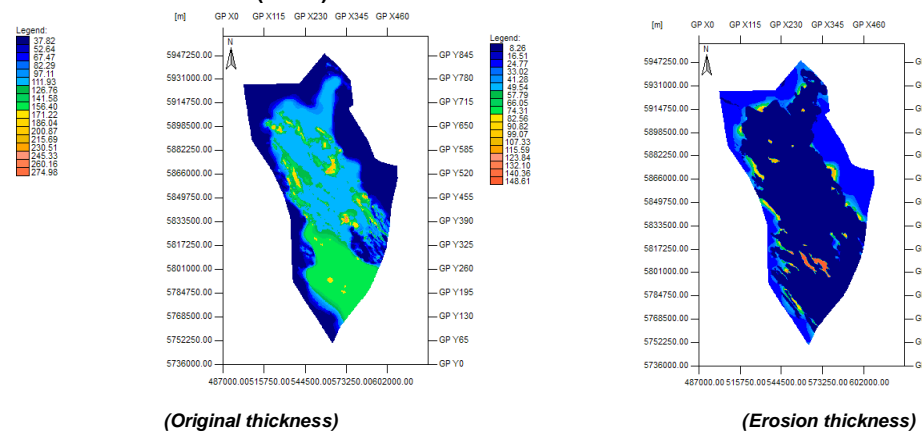
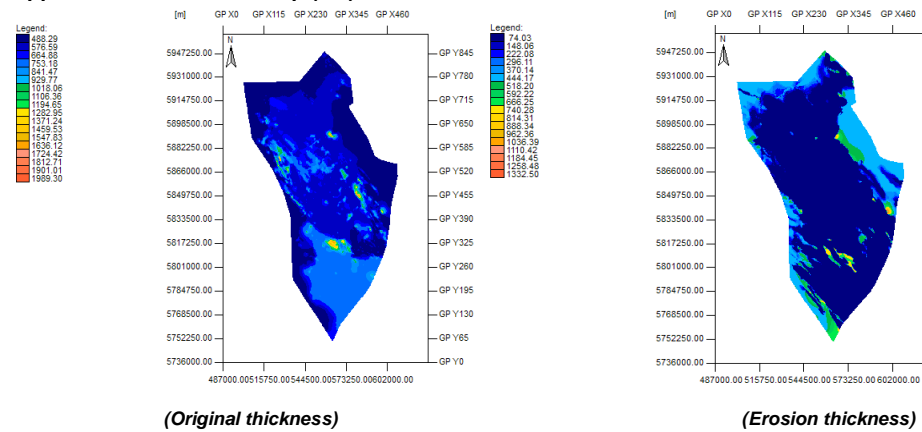
Altena Aalborg Formation (ATAL)**Altena Sleen Formation (ATRT)****Upper Germanic Trias Group (RN)**

Figure 17: Original thicknesses (left) and erosion thickness maps (right) of the eroded layers during the Kimmerian erosion event (initial scenario).

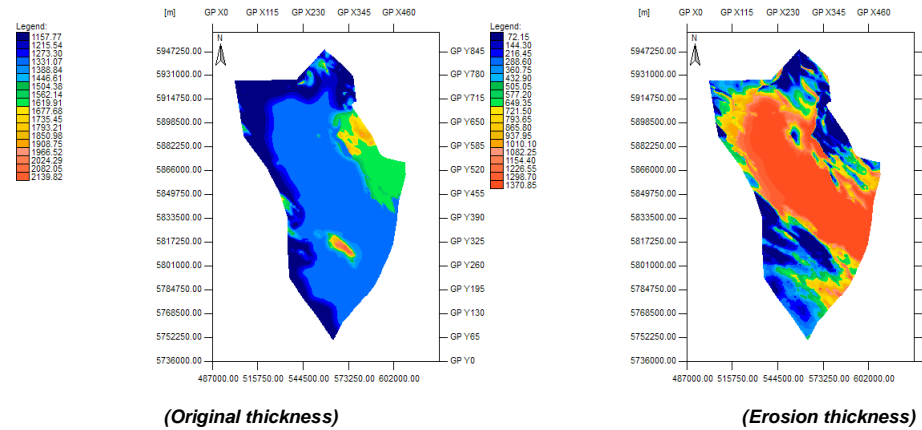
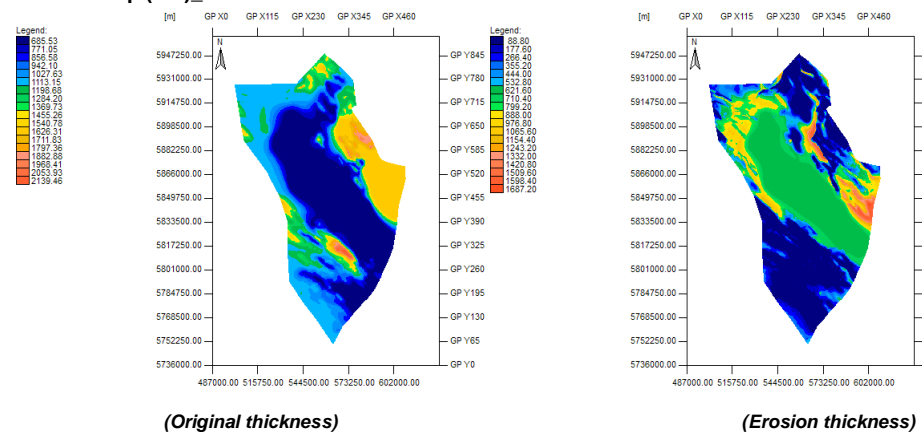
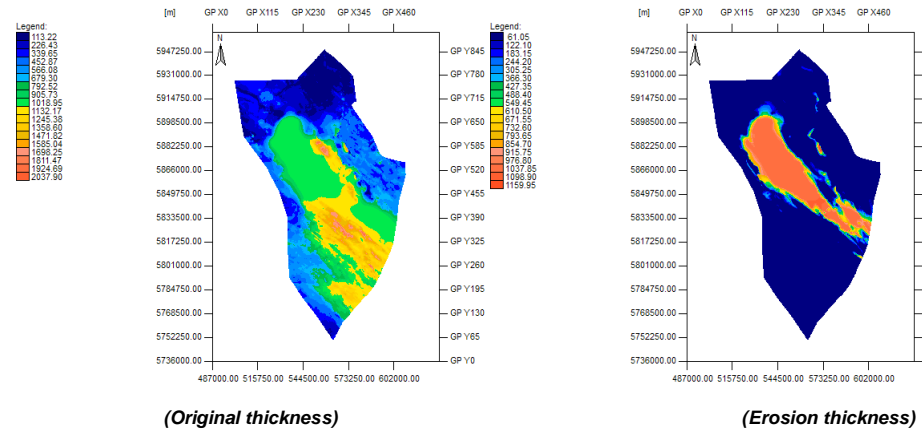
Chalk Group (CK) Scenario I**Chalk Group (CK) Scenario II****Rijnland Group (KN)**

Figure 18: Original thicknesses (left) and erosion thickness maps (right) of the eroded layers during the Subhercynian-Laramide erosion event (initial scenario).

Rijnland Group (KN)

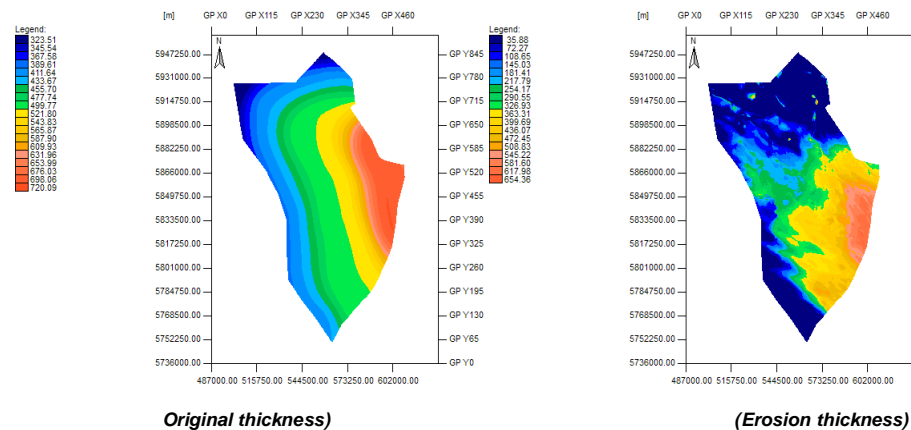


Figure 19: Original thicknesses (left) and erosion thickness (right) maps of the eroded Lower North Sea Group during the Pyrenean erosion event (initial scenario).

2.9 Basin modelling: Default set-ups, calibration wells

PetroMod provides an extensive suit of default set-ups. Default set-ups that were used in the simulations concern the lithology and mixed lithology and their associated default properties (thermal conductivity, radiogenic heat production, heat capacity), default mechanical compaction equations and default porosity-permeability relations (Annex II provides more detailed information). Measured porosities and permeability provided the basis for selecting the proper compaction and porosity-permeability relations.

Measured present-day temperature and vitrinite reflectance data from 93 wells were used to calibrate the 1D and later the 3D input model, including the heat flow models (Annex III). The calibration was conducted first to calibrate the 1D heat flow models. More wells and data were later used to calibrate the heat flow maps in the 3D model as well as the maturity modes. The data were also used to restrain the erosion thicknesses that were assumed for the model. The list of wells and the availability of calibration data are presented in (Annex III). The quality of the measured data (temperature and vitrinite reflectance) is an important source of uncertainty in the model results. The quality of the different data is taken into account in the calibration process.

2.10 Basal Heat Flow modelling: Input parameters and modelling results

Basal heat flow is an essential boundary condition for temperature, maturity and hydrocarbon generation modelling. Often a constant heat flow is used as an input where a single value is assumed for the whole basin and during the development history of the basin. TNO, however, uses a modelling tool (PetroProb) to calculate the basal heat flow based on the tectonic evolution of the basin. The modelling result is a heat flow model that varies over time expressed in a probabilistic way that takes the uncertainties in the inputs into account (Van Wees et al., 2009). For the NCP-2F area, we used six wells to model the heat flow in the area (Figure 15). The heat flow models were then interpolated over the whole area to produce heat flow maps to be used in the simulation.

2.10.1 Selection of wells

The NCP-2F area comprises different tectonic elements. The area has also a relatively complex tectonic history which is reflected in the stratigraphy and the burial history of area. Therefore, a varying heat flow pattern was expected over the area which can not be represented by a single heat flow model that is based on a single well. Five wells were chosen for heat flow modelling. The wells were selected so that the tectonic elements in the area were represented by at least one well (Figure 15). In addition to the location, the selection of the wells was based on the several criteria. The selection criteria included: the depth of the well, absence of faults, proximity to salt domes and the availability and the quality of calibration data such as measured temperature and vitrinite reflectance. The basal heat flow in well K01-02, which is located in Cleaver Bank High in the area NCP-2D area, was used to generating heat flow maps in the NCP-2F area. The well was used as there was no wells with suitable data in the Cleaver Bank High within the NCP-2F area. Figure 20 shows the stratigraphic column for each of the wells used for heat flow modelling. The indicated stratigraphy is based on the 3D model that is used for the 3D temperature and maturity modelling. This stratigraphy was not used for heat flow modelling. A more detailed stratigraphy was used for each of the wells for tectonic heat flow modelling. The lithologies were based on the lithostratigraphic description available for each well for TNO well database. Modelling parameters are presented in Annex IV.

Table 6. List of wells used for 1D heat flow modelling and the available calibration data.

Well	Number of Temperature data points	Number of Vitrinite Reflectance data points
L10-06	3	6
K01-02	23	18
K14-01	20	32
P06-01	6	62
Q07-01	11	3
P18-02	15	4

The modelled tectonic heat flow for each of the wells we calibrated to measured temperatures and vitrinite reflectance.

For more details about the modelling procedures, the input parameters and the calibration process the reader is referred to (Abdul Fattah et al., 2008; Van Wees et al., 2009).

Figure 21 presents the modelled heat flows and the tectonic subsidence model for each of the modelled wells. The heat flow models in all the modelled wells indicate two major heat flow peaks that are related to major tectonic events. The first heat flow peak is modelled in the Permian (~ 300 Ma) which is related to the Saalian uplift and erosion phase (Figure 21). The second heat flow peak is observed in the Late Jurassic-Early Cretaceous (~ 150 Ma). This phase is related to the Mid-Late-Kimmerian domal uplift and erosion. Both events are reflected in the tectonic model that is based on the stratigraphy of the well as well as the tectonic evolution as it is described in the model.

The calculated heat flow models were interpolated over the whole NCP-2F area and the created maps were used as input heat flow maps for maturity modelling.

The interpolated maps show that there are variations in basal heat flow in the NCP-2F area between the different tectonic elements (Figure 22). The variations are not only observed between the basin and the highs and platforms, but also between the basins themselves within the area. The Zandvoort Ridge seem to have high heat flow value not only at present-day but also during various time intervals.

Although the six 1D models were originally calibrated to temperature and vitrinite data, heat flow values in the rest of the area result from interpolation between the six models and are not directly calibrated to measured data in these wells. For this reason, we run the 3D heat flow calibration tool (PetroMod v. 11) in order to fine-tune the interpolated heat flow maps to the measured data at all wells. The new (calibrated) heat flow maps are re-used in modelling the area again. In other words, the refined heat flow maps were reused as input for maturity simulation (see below) (See Annex V). Examples of the new heat flow maps are shown in figure 22.

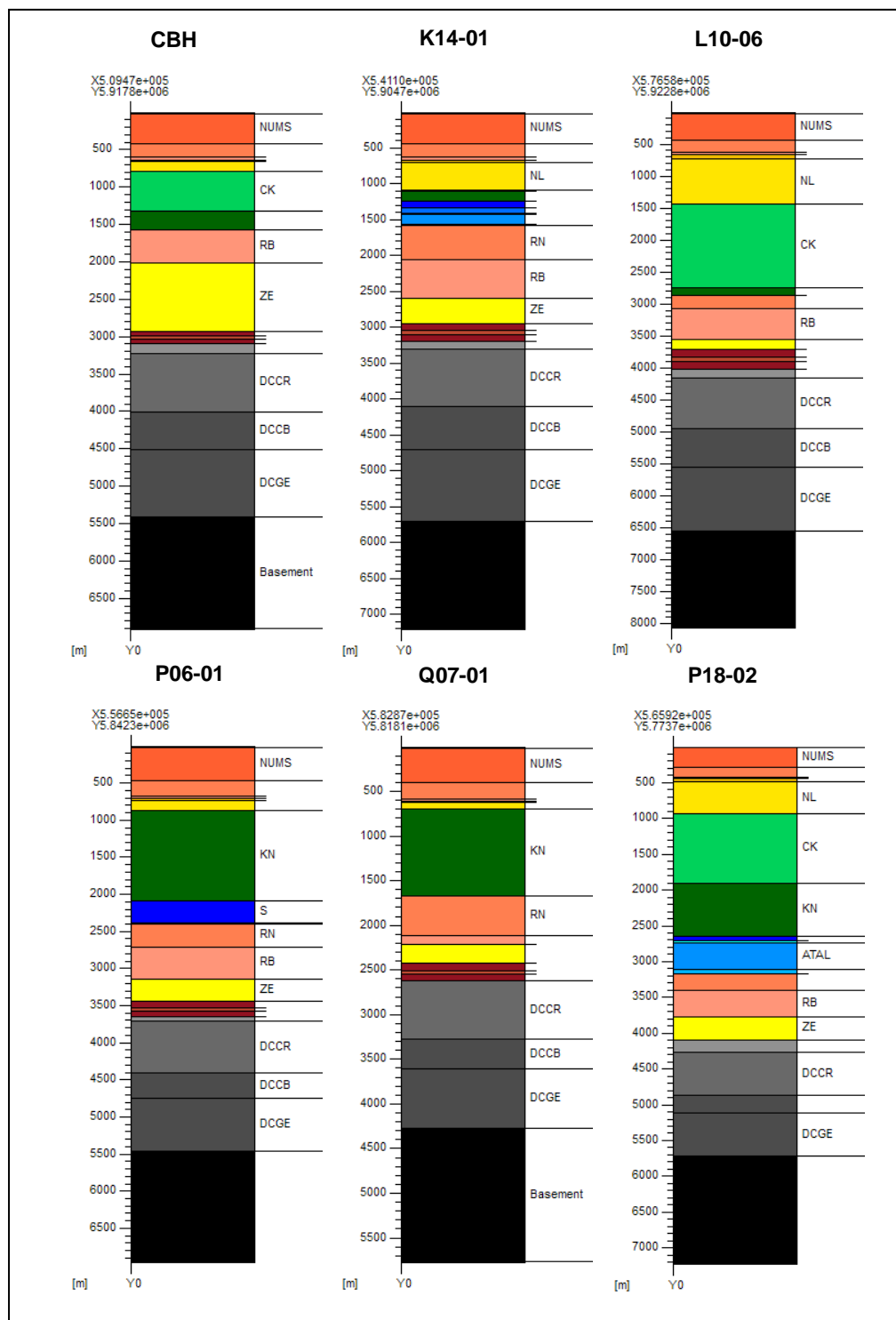


Figure 20: The stratigraphic column for each of the wells used for heat flow modelling. Location of the wells are indicated in Figure 21.

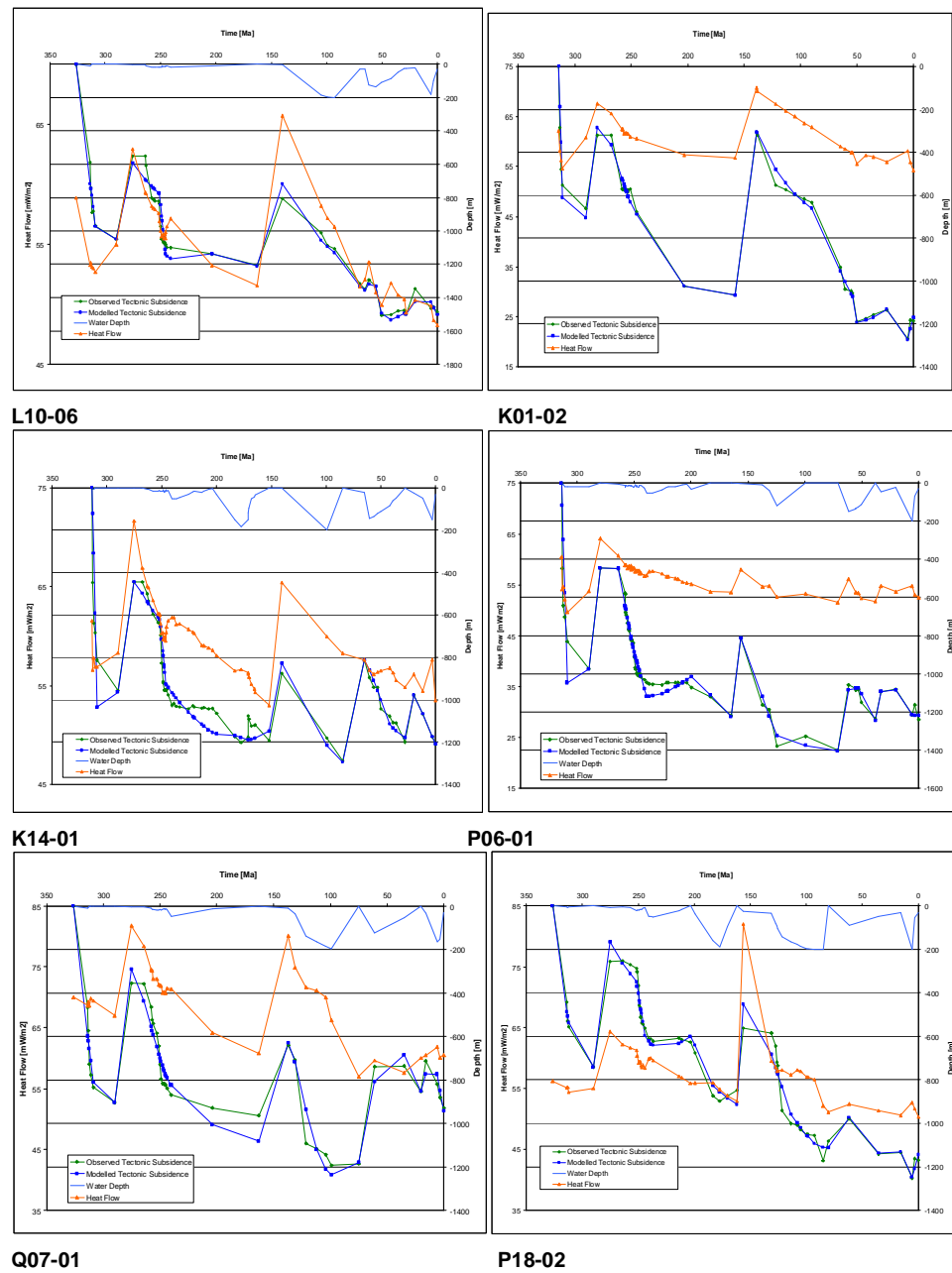
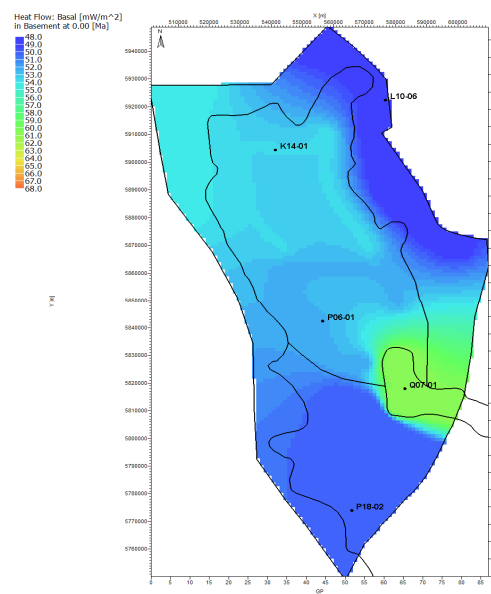
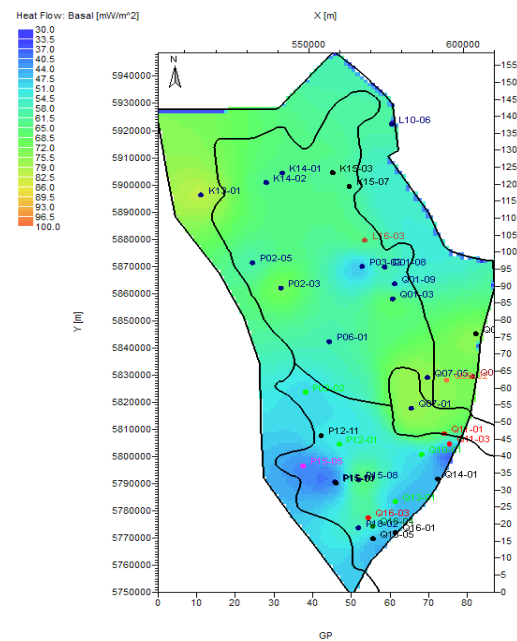


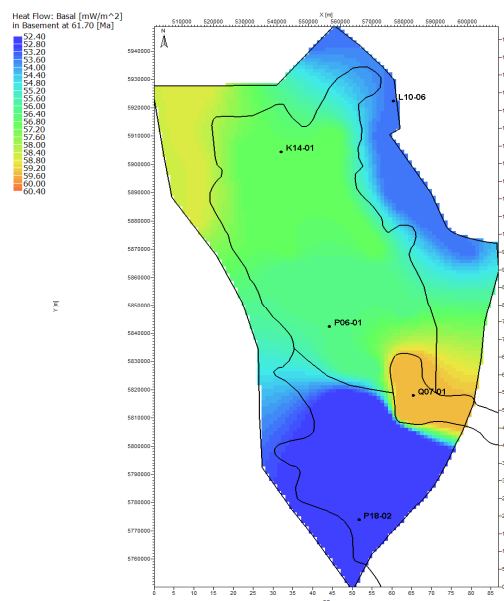
Figure 21: Modelled tectonic heat flow and tectonic subsidence of the selected wells.



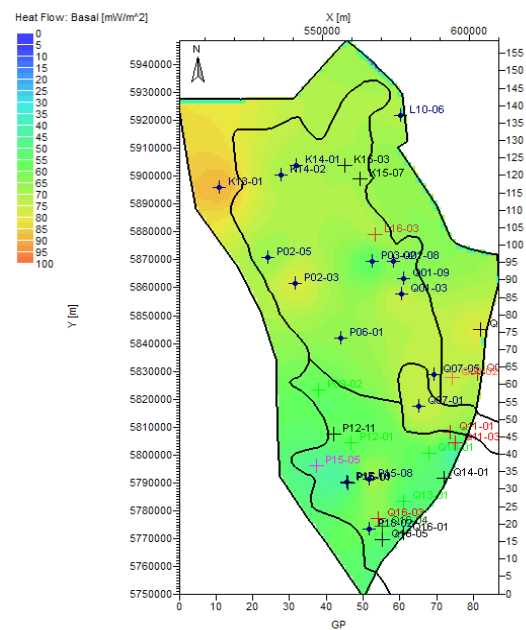
0 Ma. (Present day) Heat flow before calibration



Heat flow after calibration



61 Ma. Heat flow before calibration



Heat flow after calibration

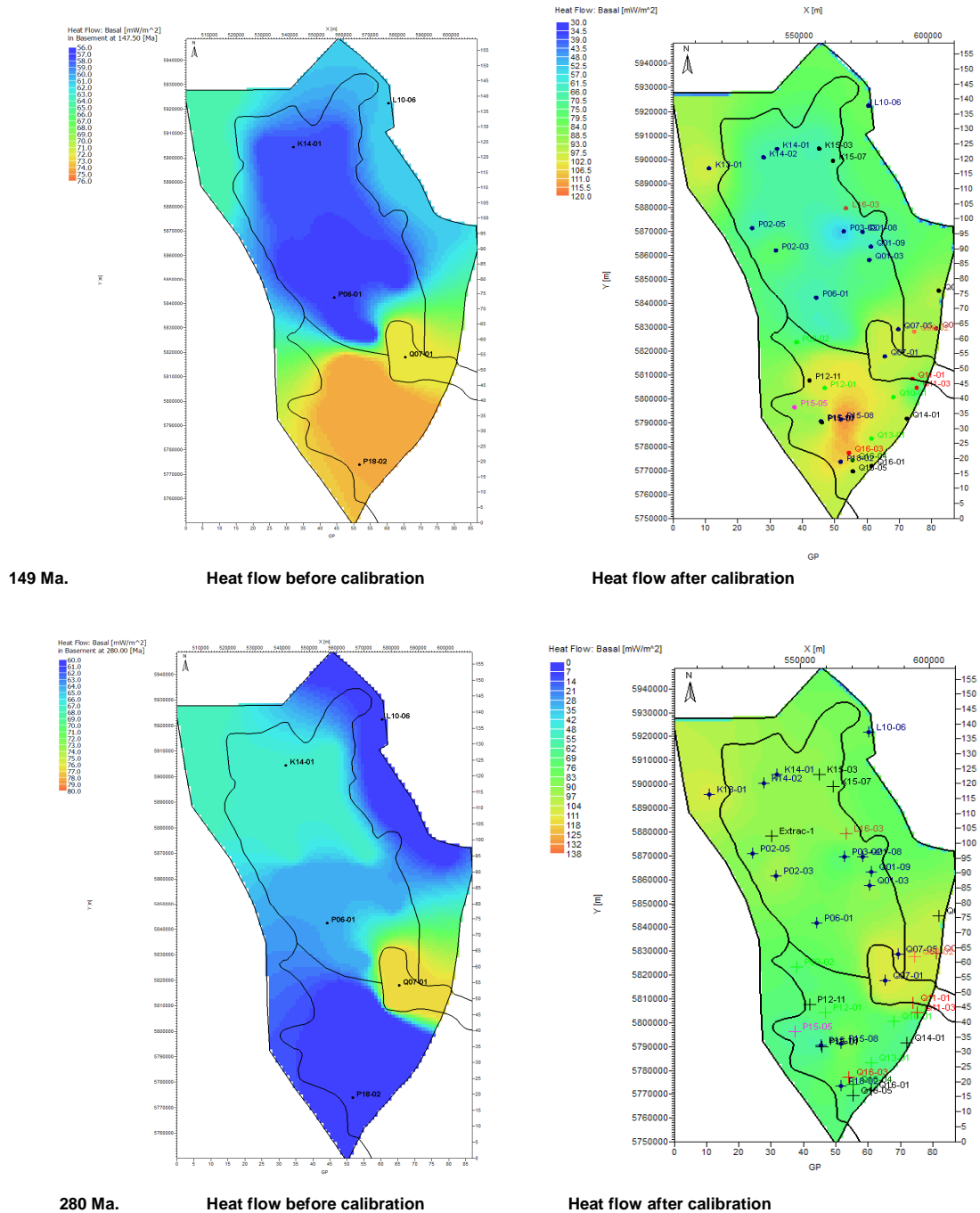


Figure 22: Comparison between initial basal heat flow maps (left) and calibrated (right) basal heat flow maps for selected four time intervals. The initial maps are interpolated between six heat flow models calculated in six wells (five wells are shown on the map, the sixth well is well K01-02 located in NCP-2D area). The maps are calibrated to measured data (temperature and vitrinite reflectance) in the wells that are shown on the maps (right).

3 Modelling results: evaluation of different erosion scenarios

In the NCP-2F area, erosion models and thicknesses are essential unknowns and significant sources of uncertainty. Through applying different erosion scenarios and thicknesses and comparing the modelled maturity with measured data, the best erosion scenario is chosen. In this study we evaluated:

- The effect of using different erosion thicknesses (especially during the Mid-Late Kimmerian phase) on maturity history.
- The effect of using different timings of erosion on maturity history.

The input geological model, input parameters and boundary conditions were kept constant (as described in chapter 2) for all scenarios, and any changes relating to the timing and magnitude of erosion are clearly indicated in the text below.

Measured data (temperature and/or vitrinite reflectance) were compared to the modelled results at well locations in the 3D model. A list of wells with calibration data is presented in Annex III.

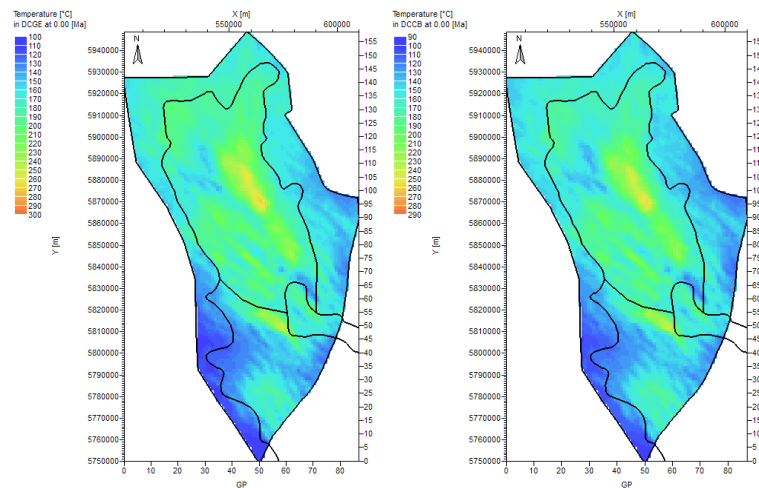
3.1 Scenario I : Initial model

In the first scenario the initial geological model was run using the basic input parameters and conditions (as described in Chapter 2):

- The erosion thicknesses of the layers were based on the initial original thicknesses as shown in figures 16, 17, 18 and 19;
 - The description and ages of the major erosion phases as presented in Table 4;
- The erosion map of the Chalk Group based on a minimum original thickness of Chalk of 1300 m. The basal heat flow maps constructed by interpolation between six 1D heat flow models (Figure 15, 21 and 22). These maps were later modified through calibration with well data from the region (see Annex V). The modified maps are used as basal heat flow boundary condition.
- The erosion scenarios in this chapter are evaluated by comparing results of calculated present-day temperatures and maturities with measured data. Below we first present a short introduction on factors of influence on temperature and maturity history.

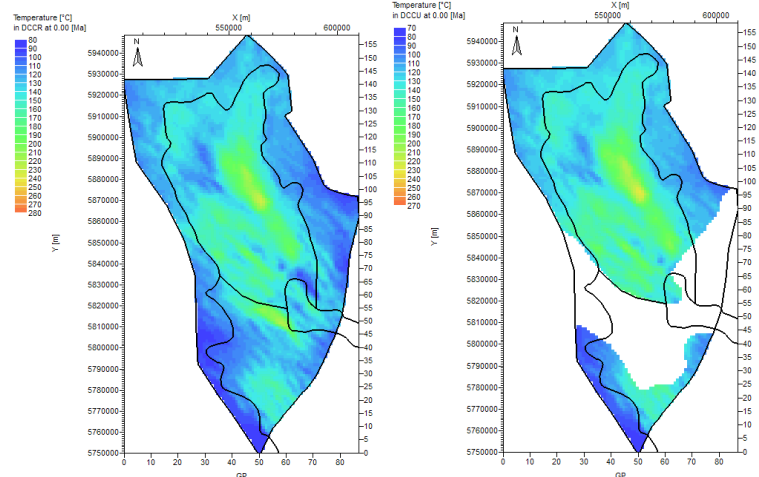
3.1.1 Temperature history

The 3D temperature history was reconstructed using the calibrated tectonic heat flow boundary condition (Figure 22). The paleo water depth (PWD) and sediment water interface temperatures (SWIT) are very important factors in determining the temperature history (Figure 14). Compaction parameters as well as thermal conductivity parameters have a significant effect on the thermal evolution of the basin. Standard compaction and thermal conductivity models were used for this scenario (Annex I). The temperature distribution in a sedimentary basin at a certain time during history, principally depends on the spatial variation in basal heat flow input, the distribution of bulk thermal conductivities of the subsurface and the sediment water interface temperatures.



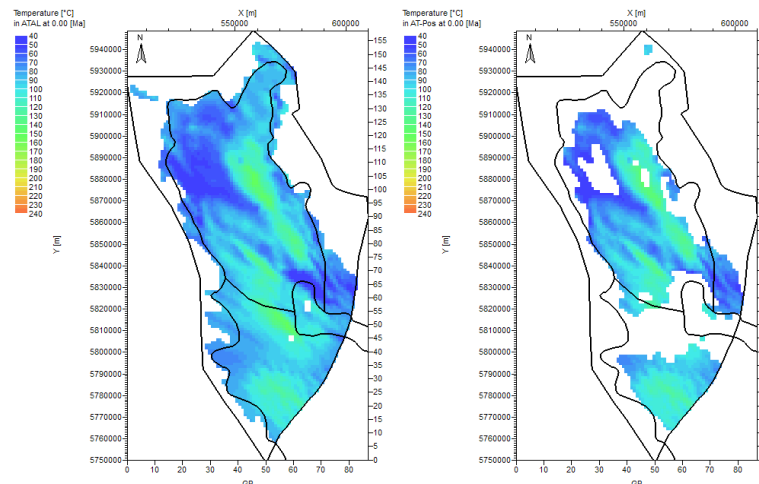
The Namurian (Depth: 2.8-9.0 Km)

The Baarlo Formation (Depth: 2.4-8.5 Km)



The Ruurlo Formation (Depth: 1.8-7.4 Km)

The Maurits Formation (Depth: 3.8-7.7 Km)



The Aalburg Formation (Depth: 0.3-4.5 Km)

The Posidonia Formation (Depth: 0.3-4.5 Km)

Figure 23: Modelled temperatures of the top of the major source rocks in the area (Carboniferous and Upper Jurassic formations) at present-day (scenario I). The Hunze Sub-Group is not shown because of its limited distribution in the area.

The modelled temperature at present-day for the major Carboniferous source rock units in the model are shown in Figure 23. The temperature values include the transient effect of variable factors, such as paleo boundary conditions (e.g. paleo surface temperatures) and effects of rapid sedimentation or uplift on the temperature distribution at a certain time.

The figure shows that higher temperatures are modelled within the basins and in areas with deepest burial. This is demonstrated by a cross section through area where the temperatures are overlaid on the layers (Figure 24). Basal heat flow at present-day seems to have less determining role than the burial depth.

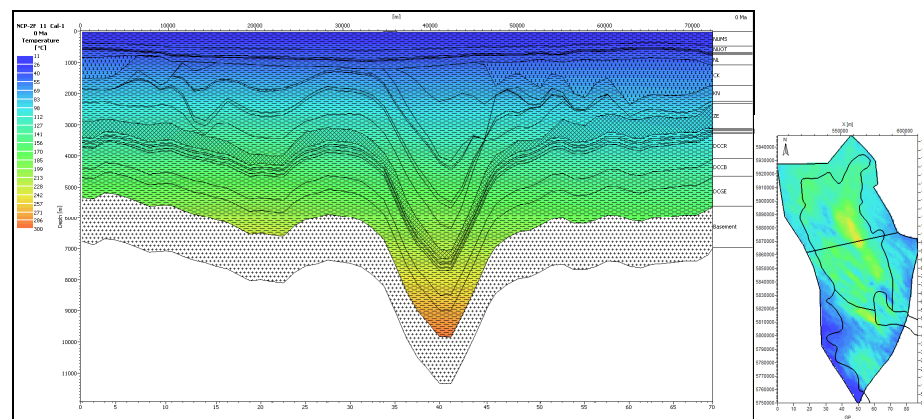


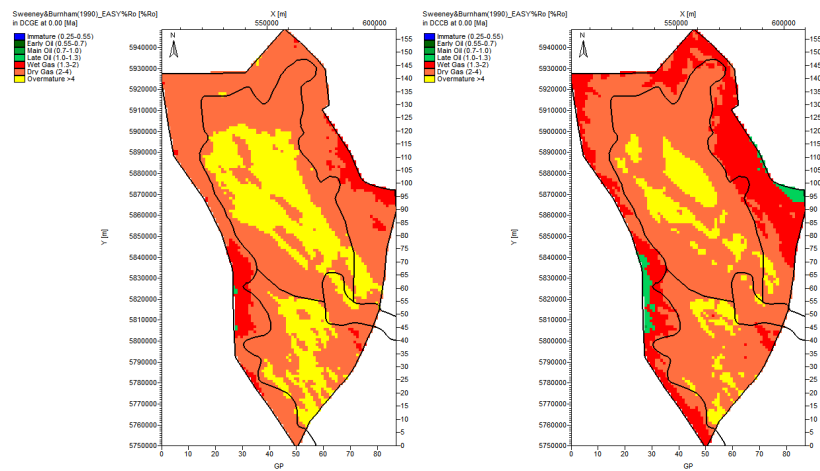
Figure 24: Cross-section through the study area showing that highest temperatures are located in areas with deepest burial.

3.1.2 History of maturity and hydrocarbon generation

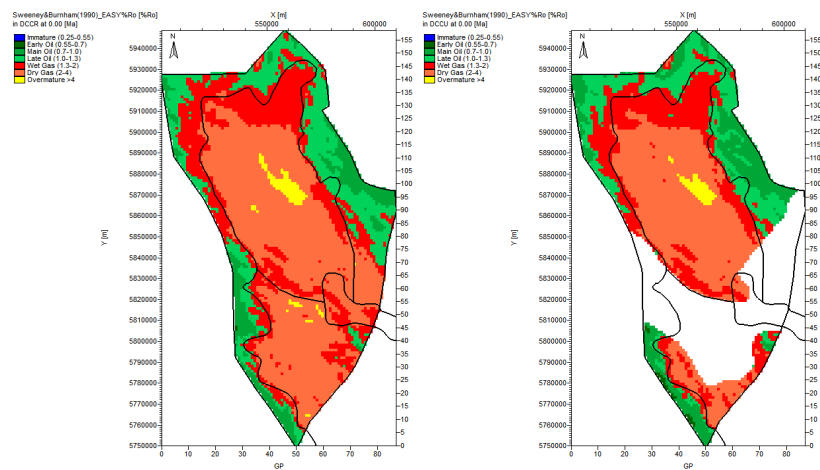
Maturity indicators such as vitrinite reflectance values (according to Sweeney and Burnham 1990) and transformation ratios are calculated in PetroMod. Vitrinite reflectance values are calculated for all stratigraphic units. The calculated maturity of the main Carboniferous formations (Maurits, Ruurlo and Baarlo and Namurian) and the Upper Jurassic formations (Aalburg and Posidonia) at present-day is shown in figure 25.

Present-day maturity maps show that the central parts of the basin generally have higher maturity than the edges and the platforms. Similar to the temperature, maturity is strongly related to burial depth as deeper parts show higher maturity. According to this scenario, the majority of the Namurian and the Baarlo Formation appears to be ranging between gas generating to overmature ($R_o\%$: 1.3-> 4). The Ruurlo and the Maurits formations, on the other hand, are still in the oil window especially at the highs and platforms. The Jurassic source rocks however, fall predominantly within the oil window ($R_o\%$: 0.55-1.3) (Figure 25).

Before discussing the thermal and maturity evolution of the area, it is important to evaluate the model and its assumptions. This can be done through comparing the modelled maturity and temperature with measured data in the wells. A map of the area indicating the location of wells used in the calibration and the comparison is shown in figure 25. Annex III provides a list of the wells and the data available from the wells for the calibration.

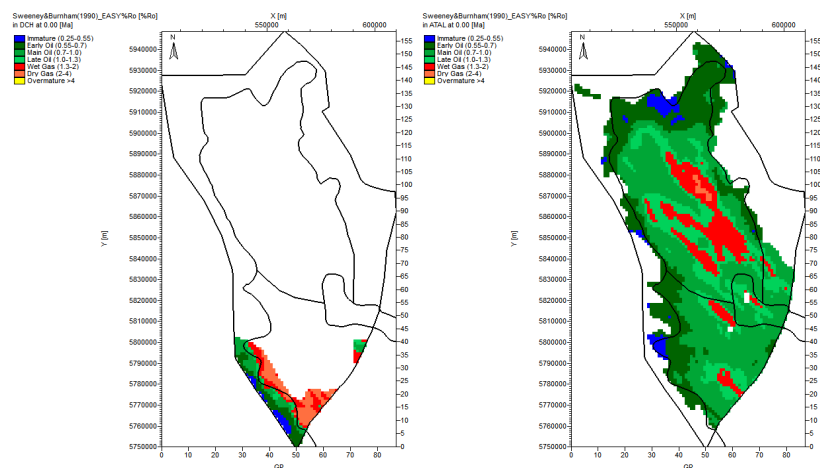


The Namurian Unit



The Baarlo Formation

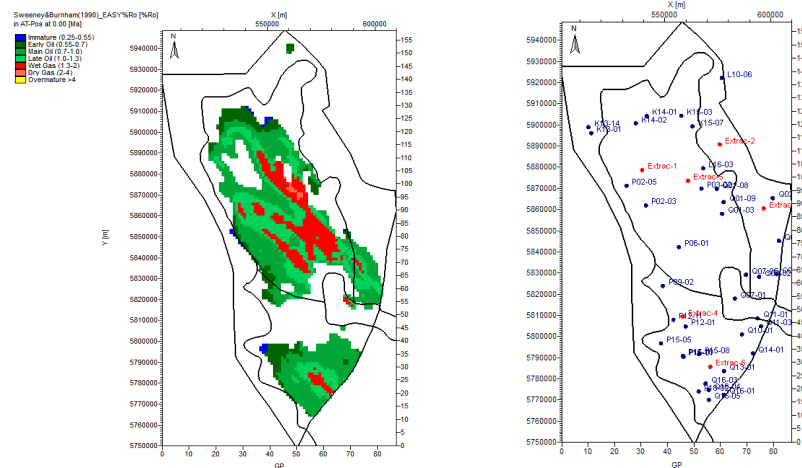
The Ruurlo Formation



The Maurits Formation

The Hunze Sub-group Formation

The Aalburg Formation

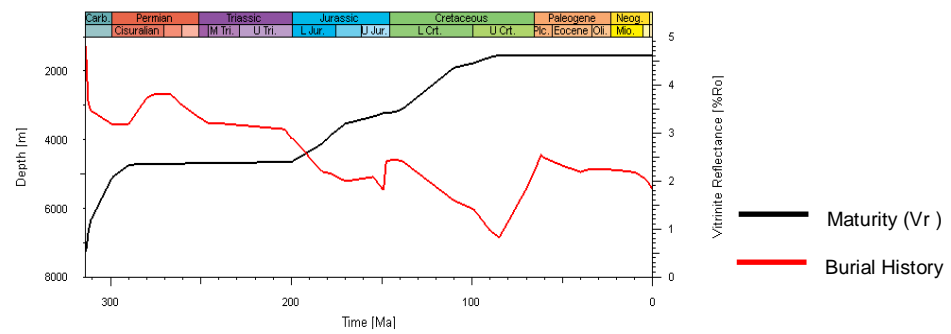
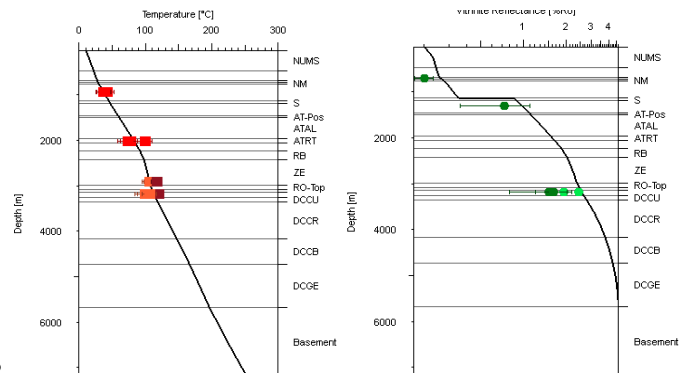
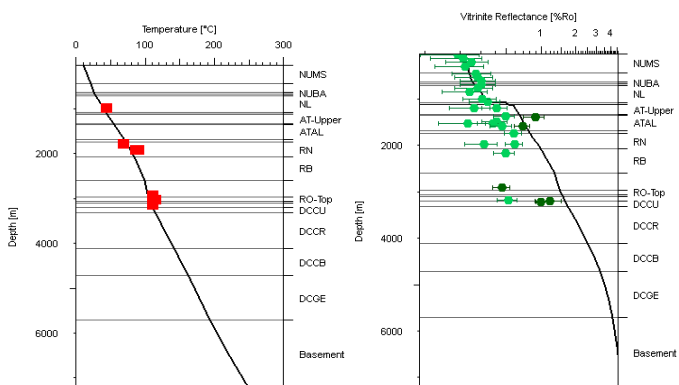
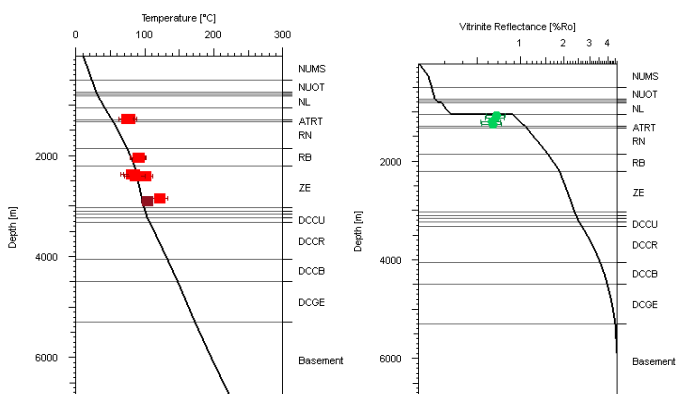


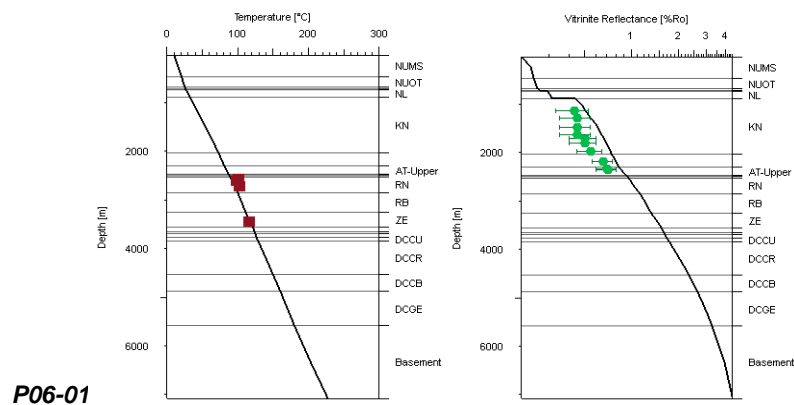
The Posidonia Formation

Figure 25: Modelled maturity of the top of the major source rocks in the area (Carboniferous and Upper Jurassic formations) at present-day (scenario I). Wells used for calibrating the models are indicated in the figure above.

A total of 93 wells were used to compare the measured data (temperature, vitrinite reflectance) with our model. Some examples of the comparison are shown in figure 26.

The selected wells indicate that a good fit is achieved between the measured and the modelled temperature. This mainly indicates an appropriate heat flow at present-day as obtained from our calibration process. Maturity data however show that the modelled values are slightly overestimated in comparison to the measured data. The deepest burial at the selected wells occur during the Cretaceous and before the Subhercynian-Laramide inversion. As a result, the maximum maturity is achieved in the Cretaceous (Figure 26). This implies that the overestimated maturity in this scenario can be reduced if less erosion is assigned to this erosion phase. In this initial scenario (scenario I) an initial original thickness of 1300 m was assigned to the Chalk formation in the BFB and WNB (see above). In an alternative scenario, less original thickness can be assigned to the Chalk formation which will result in less erosion during this phase and thus lower maturity values.

**K14-02****K14-01****K17-02**



P06-01

Figure 26: Modelled vitrinite reflectance (maturity) and temperature in a selection of wells from the area. Whereas good fit is achieved for the temperature, the maturity is overestimated. The burial and maturity history of one of the wells is indicated in the top.

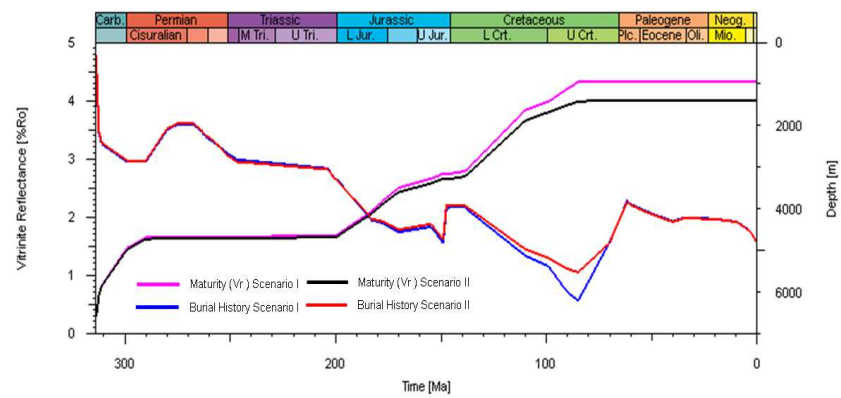
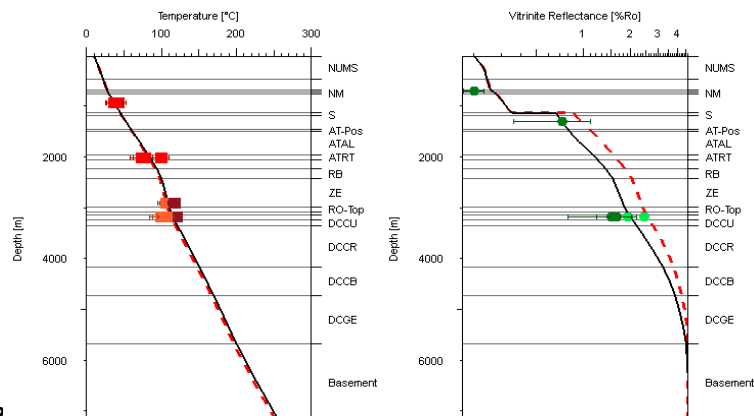
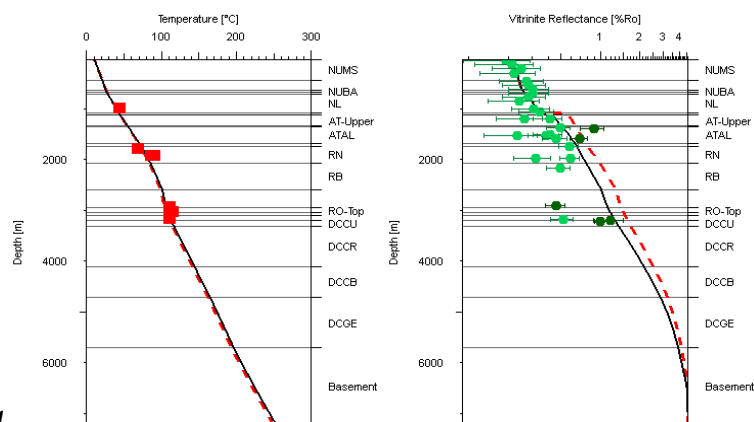
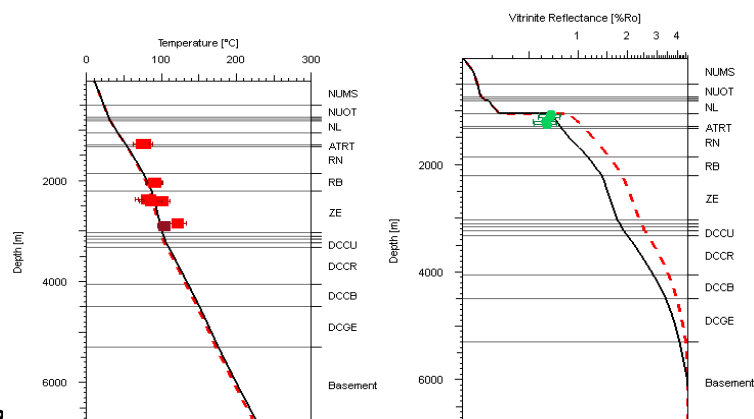
3.2 Scenario II: Reduced original thickness of the Chalk

In Scenario I, the Chalk Group has an original thickness of 1300 m. (Figure 18). This original thickness resulted in an overestimation of the calculated maturity and a misfit with the measured data in several wells. Scenario II assumes an original thickness of 600 m for the Chalk Group. A reduced thickness of the Chalk in the basins is consistent with regional stratigraphic correlations and concepts for the Chalk in the Upper Cretaceous (N. Witmans, Pers. Comm, 01-2011). The thickness of 600 m is assumed to be a minimum original thickness for the Chalk Group in the area.

The reduced original thickness will reduce the erosion during the Subhercynian event (Figure 6).

Simulation parameters were kept similar to those used in scenario I. The simulation results of this scenario compared to the previous scenario are shown in figure 27.

The figure indicates that modelled maturity at present-day in the selected wells are reduced compared to scenario I and fit the observed vitrinite reflectance data. Modelled present-day temperatures, on the other hand, have not changed by reducing the original thickness and erosional thickness of the Chalk Group. The burial history of well K14-02 shows that the deepest burial was reached during the Late Cretaceous. As a consequence the reduction of the original (and erosional) thickness of the Chalk reduced its maximum burial and its maximum maturity and therefore its present-day maturity (Figure 27).

**K14-02****K14-01****K17-02**

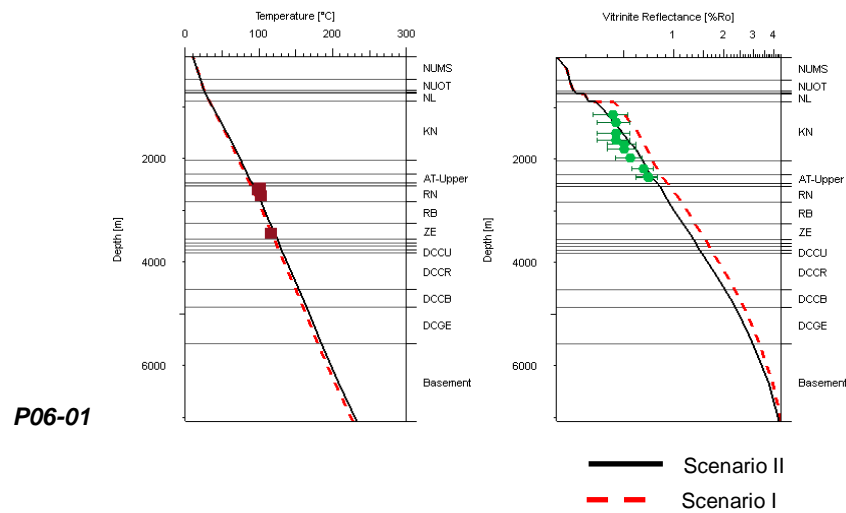


Figure 27: Modelled temperature and maturity in scenario II where less erosion is assumed for the Chalk Group (600 m Chalk is assumed as depositional thickness in the basins). Modelling results of Scenario I, where 1300 m Chalk is assumed as depositional thickness in the basins are also indicated.

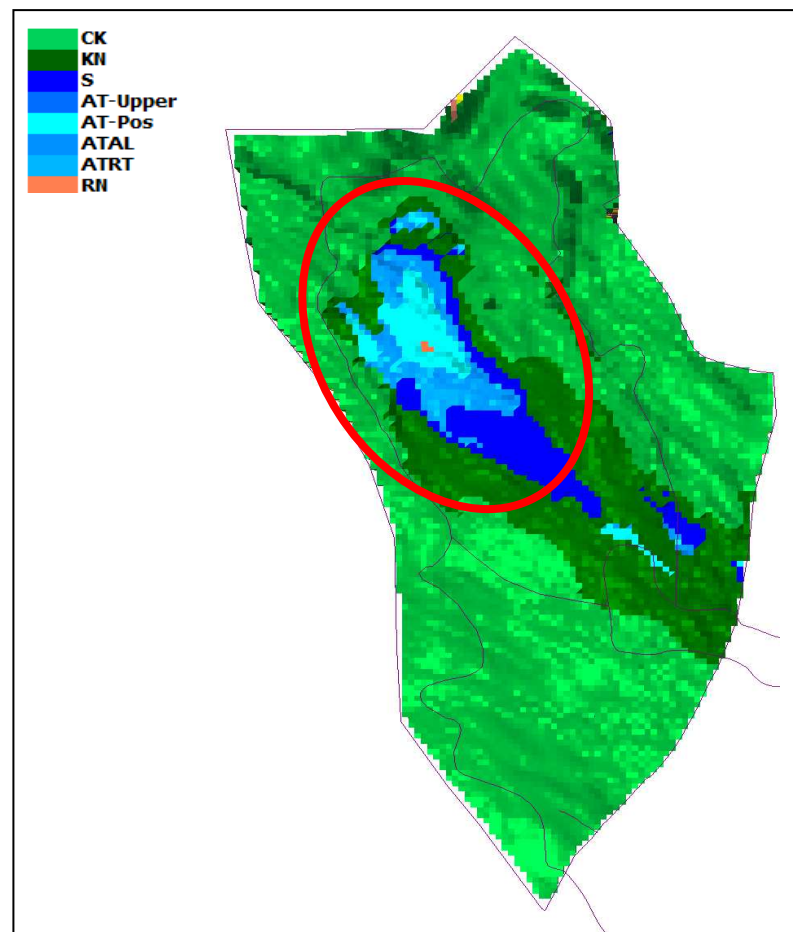


Figure 28: A subcrop map of the Cretaceous and Jurassic formations below the Tertiary deposits. The circle shows the area where the Subhercynian inversion and erosion is expected to have eroded the Jurassic layers.

3.3 Scenario III: Subhercynian erosion of Jurassic formations

In previous scenarios, the Jurassic formations were assumed to be eroded to their present-day thicknesses during the Late Kimmerian erosion phase (Table 4); erosion during the Subhercynian and Laramide inversion phase stopped at the Late Jurassic unconformity.

The subcrop pattern of the Cretaceous and Jurassic formations below the Tertiary in the central part of the BFB indicates a co-centred erosion pattern similar to erosion pattern in anticlinal structures (Figure 28). It is likely that inversion was stronger in the central part of the BFB which led to more erosion than on the flanks of the basin. As a result Jurassic formations were also partly eroded in the central parts of BFB during the late Cretaceous.

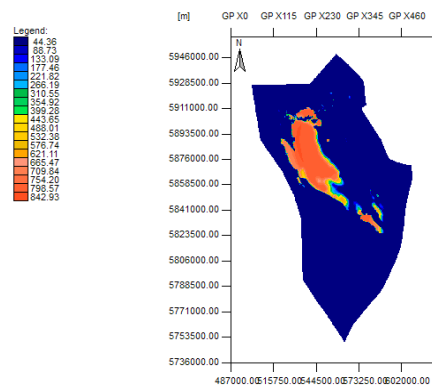
Therefore a new scenario is proposed where the Altena and Schieland groups, in the central part of the BFB, are eroded during the Subhercynian-Laramide inversion.

Basic assumptions underlying the constructing of new erosion maps for scenario III include:

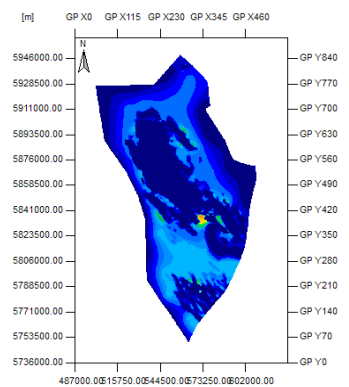
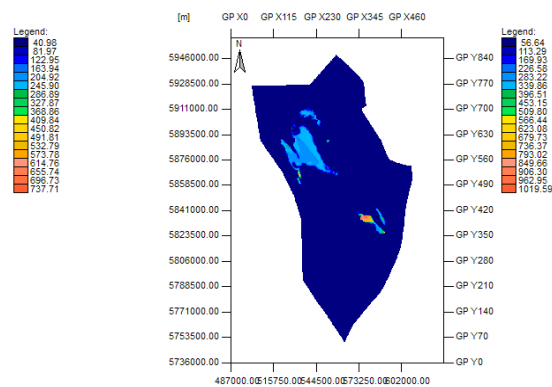
- Schieland Group is entirely eroded during the Subhercynian phase in the Late Cretaceous (68.00 to 66.00 Ma). This means that the erosion and depositional thickness map of the Schieland Group has to be modified (Figure 29).
- The Altena Group and its subdivisions are modified in such a way that the layers are divided in two phases. While this is not possible in the present version of PetroMod, some modifications to the input table had to be done so that a single layer can be eroded in two phases (see below).
- The Altena Group is first eroded in Late Kimmerian phase on the highs, the platform and part of the basins. In the Subhercynian inversion phase, part of the Altena, located in the central part of the BFB, is eroded (Figure 29).

The erosion ages of the Altena Groups are modified so that they are partly eroded in the Late Jurassic (170.1 to 154.7 Ma), and partly in Late Cretaceous (66.00 to 61.7 Ma) (the central part of the Broad Fourteens Basin). Following the new depositional ages, the Late Jurassic erosion is now defined as the Late Kimmerian I. This is because, according to this scenario, the Schieland Group is deposited after the Late Kimmerian erosion and the erosion of Schieland is taking place during the Subhercynian (Table 7).

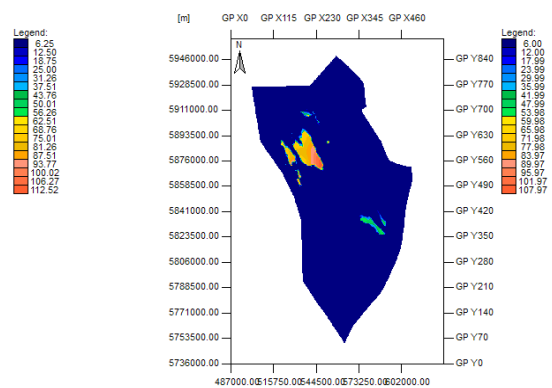
The erosion thicknesses of the layers are kept the same as in the previous scenarios. The changes in this scenario are limited to the ages of erosion and the distribution of the erosional thicknesses of each of the layers (Altena and Schieland).



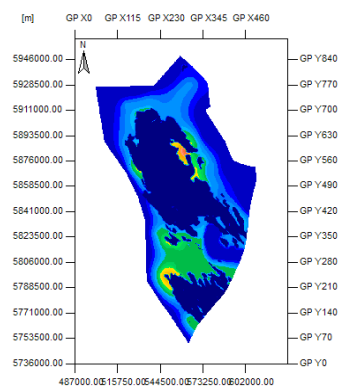
SL: erosion thickness (SubHer-LRM)



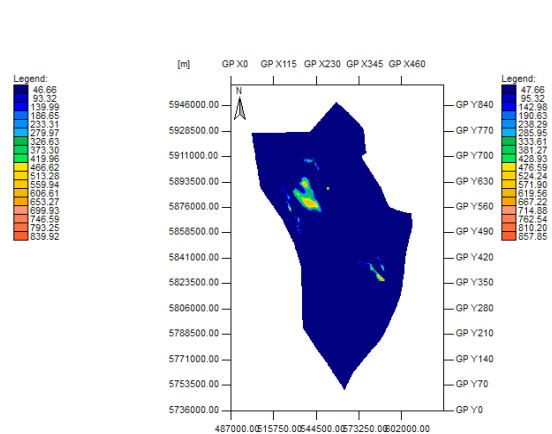
AT-Upper: erosion thickness (SubHer-LRM)



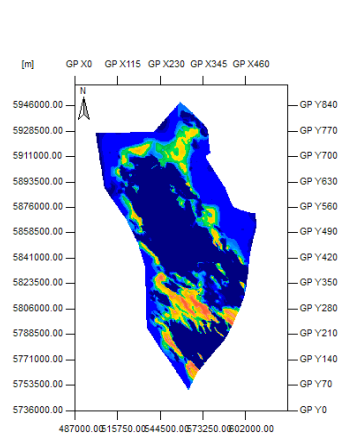
AT-Upper: erosion thickness (KIMM)



AT-Pos: erosion thickness (SubHer-LRM)



AT-Pos: erosion thickness (KIMM)



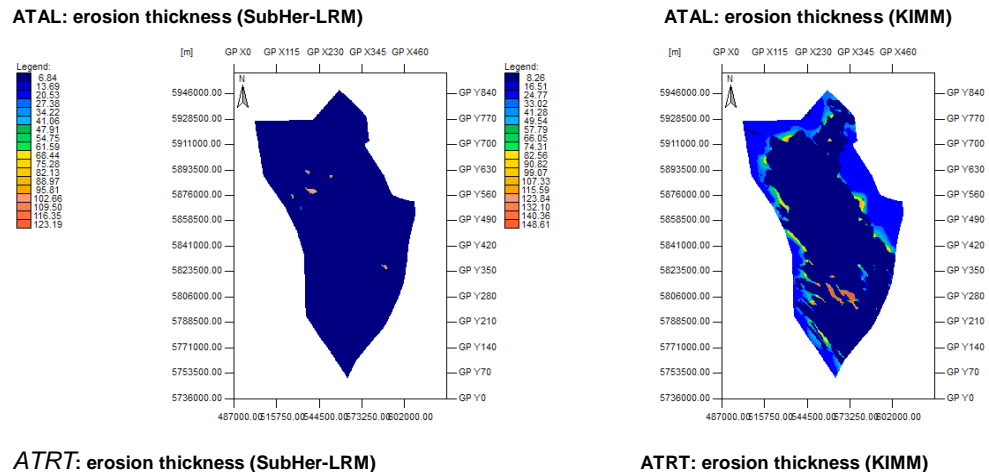


Figure 29: Erosion maps of the Schieland and Altena Groups as used in scenario III. Left; erosion maps of formation eroded in the Subhercynian and Laramide inversion. Right; erosion maps of formations eroded in the Kimmerian uplift phase. No change in the thicknesses is implemented.

The simulation of this erosion scenario III is run for the same boundary conditions, using the same simulation and gridding parameters as in the previous runs. A good optimization quality is achieved (~ 0.1 %).

To evaluate the effect of this scenario on the maturity and thermal evolution of the basin, we studied 1D extractions for the maturity and temperature at the location of the wells in the central part of the Broad Fourteens Basin, where the new erosion scenario is implemented. The simulation results for scenario III are compared with those of the previous scenarios. (Figure 31).

Figure 31 shows that while a good fit is still obtained between modelled temperatures and measured ones, the modelled maturities for scenario III are higher than measured data. Comparison with maturity calculations using the previous scenario (where Schieland and the whole Altena Group are eroded in the Late Kimmerian (II)), shows a higher maturity for scenario (III) (Figure 31).

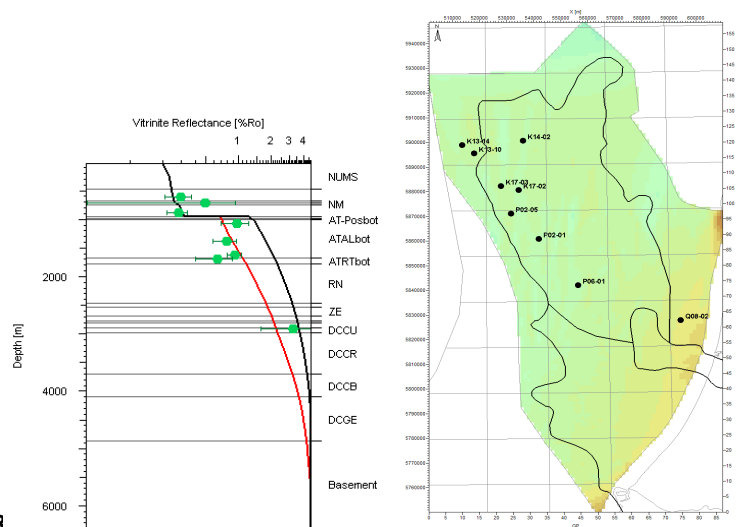
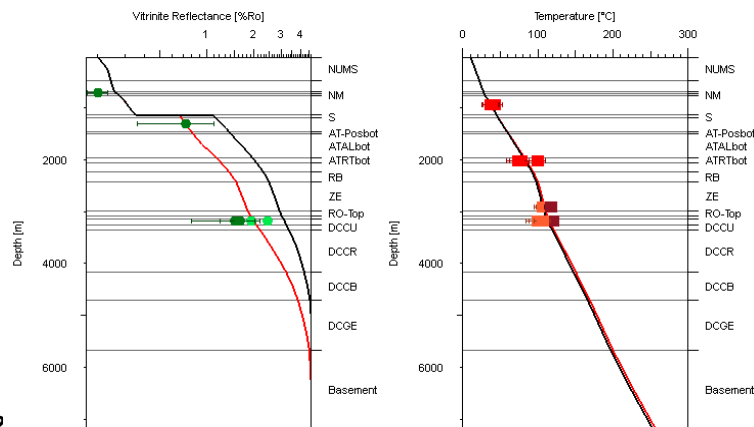
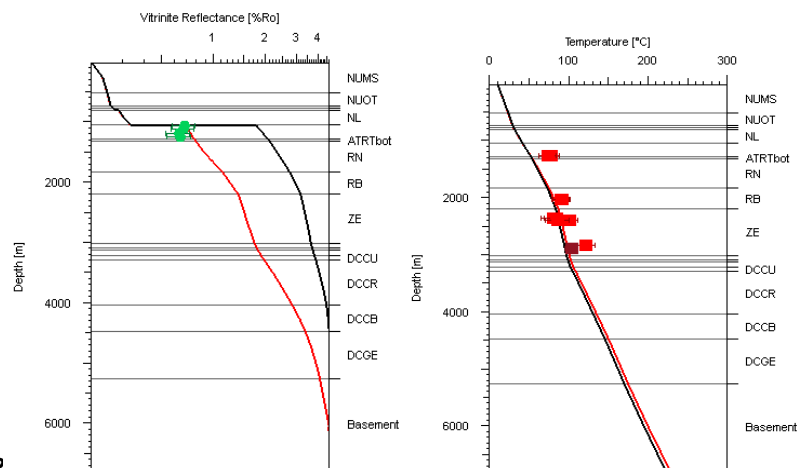
Table 7: Adjusted deposition and erosion ages following this scenario (Scen III). Green coloured ages represent Cretaceous events. Blue coloured ages represent Jurassic events.

Layer	Layer Erosion phase	Deposition Age from [Ma]	Deposition Age to [Ma]	Erosion Age from [Ma]	Erosion Age to [Ma]
CK	Chalk				
	<i>Er. Subhercynian</i>	99.1	85	85	72
KN	Rijnland Group				
	<i>Er. Subhercynian</i>	138.7	99.1	72	68
S	Schieland Group				
	<i>Er. Subhercynian</i>	154.7	149	68	66
AT-Upper (SubHer)	Altena Group Upper				
	<i>Er. Subhercynian</i>	170.18	170.1	66	64
AT-Upper (L.Kim_I)	Altena Group Upper				
	<i>Er. Late Kimmerian I</i>	177.6	170.18	170.1	165.5
AT-Pos (SubHer)	Altena_Posidonia				
	<i>Er. Subhercynian</i>	177.65	177.6	64	63
AT-Pos (L.Kim_I)	Altena_Posidonia				
	<i>Er. Late Kimmerian I</i>	183	177.6	165	162
ATAL (SubHer)	Altena_Aalburg				
	<i>Er. Subhercynian</i>	183.17	183	63	62
ATAL (L.Kim_I)	Altena_Aalburg				
	<i>Er. Late Kimmerian I</i>	199.6	183.17	162	160.2
ATRT (SubHer)	Altena_Sleen				
	<i>Er. Subhercynian</i>	200.54	200.51	62	61.7
ATRT (L.Kim_I)	Altena_Sleen Er. Late				
	<i>Kimmerian I</i>	203.6	200.54	160	157.3
RN	Upper Germanic Er.				
	<i>Late Kimmerian I</i>	243	203.6	157.3	154.7

The burial history of well K14-02 shows that when the Schieland and parts of the Altena Group are eroded in the Subhercynian (scenario III), deeper burial and more subsidence is reached in the area. This results in a higher modelled maturity (Figure 32). Reducing the amount of erosion during the Subhercynian inversion event will lower the maturity during the Cretaceous (section 3.4).

The calculated maturities in some wells from the highs and platforms indicate that modification of the initial amount of erosion might result in a better fit (Figure 33). The modelled maturity in wells K13-14 and K13-10, located on the Cleaver Bank High, is lower than measured values. The modelled maturity in well Q08-02, located in the Central Netherlands Basin, is lower than observed vitrinite reflectance in the well. This is also the case for both scenarios (II and III). Increasing the erosion thicknesses during the Cretaceous might result in a better fit with measured data. This will be discussed in the following scenario.

Well P06-02 is presented here as an example of a good fit obtained between measured and modelled maturity in the Central part of the study area (Figure 33). In the WNB the new scenario is not reflected in the maturity data. Therefore no modification in the erosion amounts is implemented.

K17-03**K14-02****K17-02**

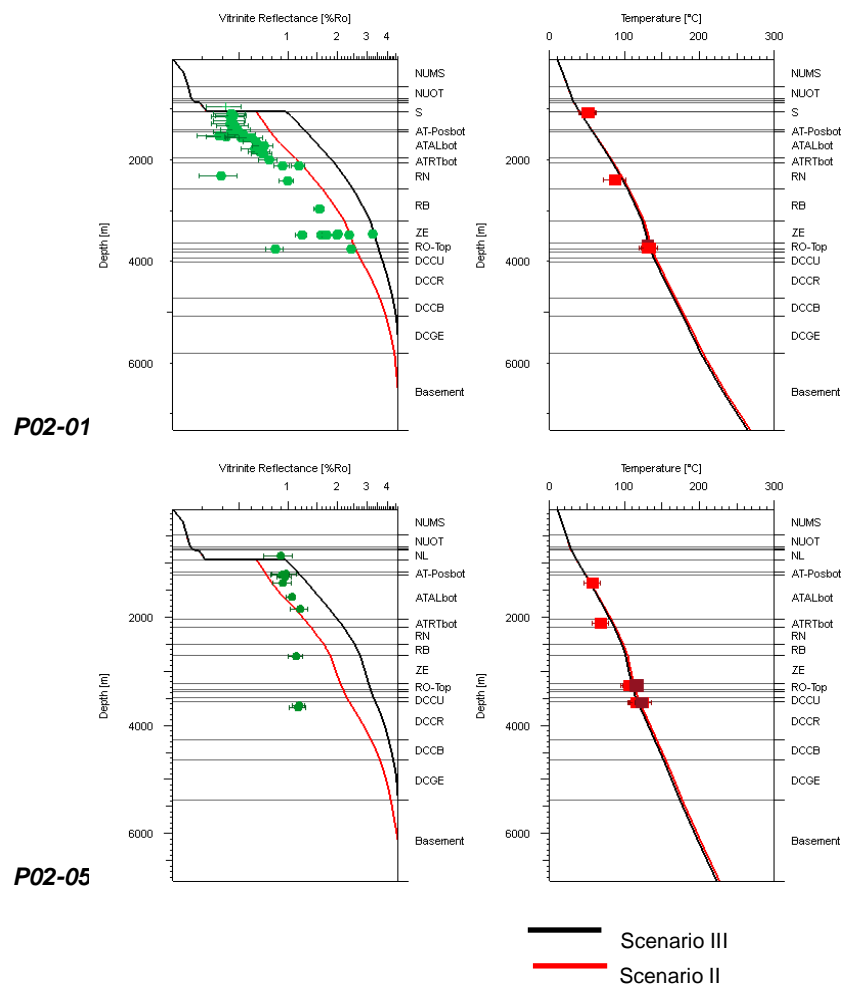


Figure 31: Modelled maturity and temperature at a selection of wells in scenario III (Schieland and parts of the Alena Group are eroded in the Subhercynian). Modelling results of Scenario II are also indicated. Wells are located in the central part of the Brouard Fourteen Basin.

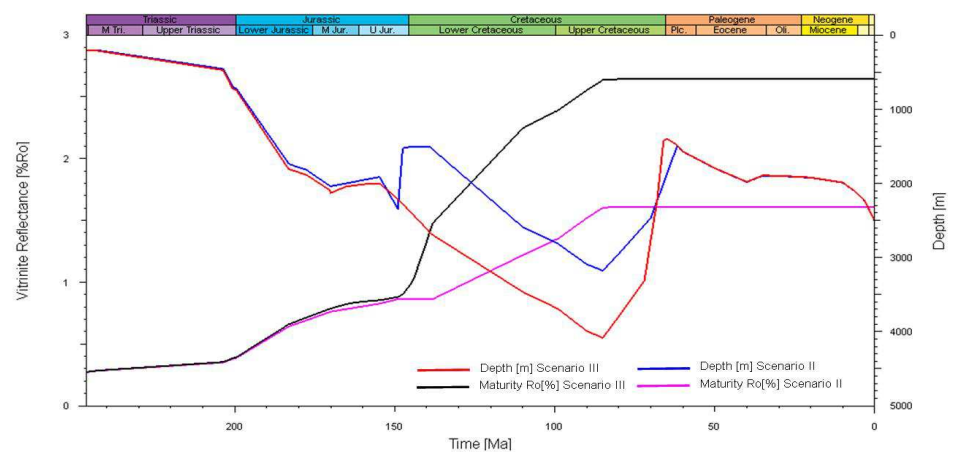


Figure 32: The burial history and maturity model of well K14-02 as modelled in scenario III and II. In scenario III deeper burial is achieved during the Cretaceous which caused higher maturity. (The Lower Triassic formation is shown here).

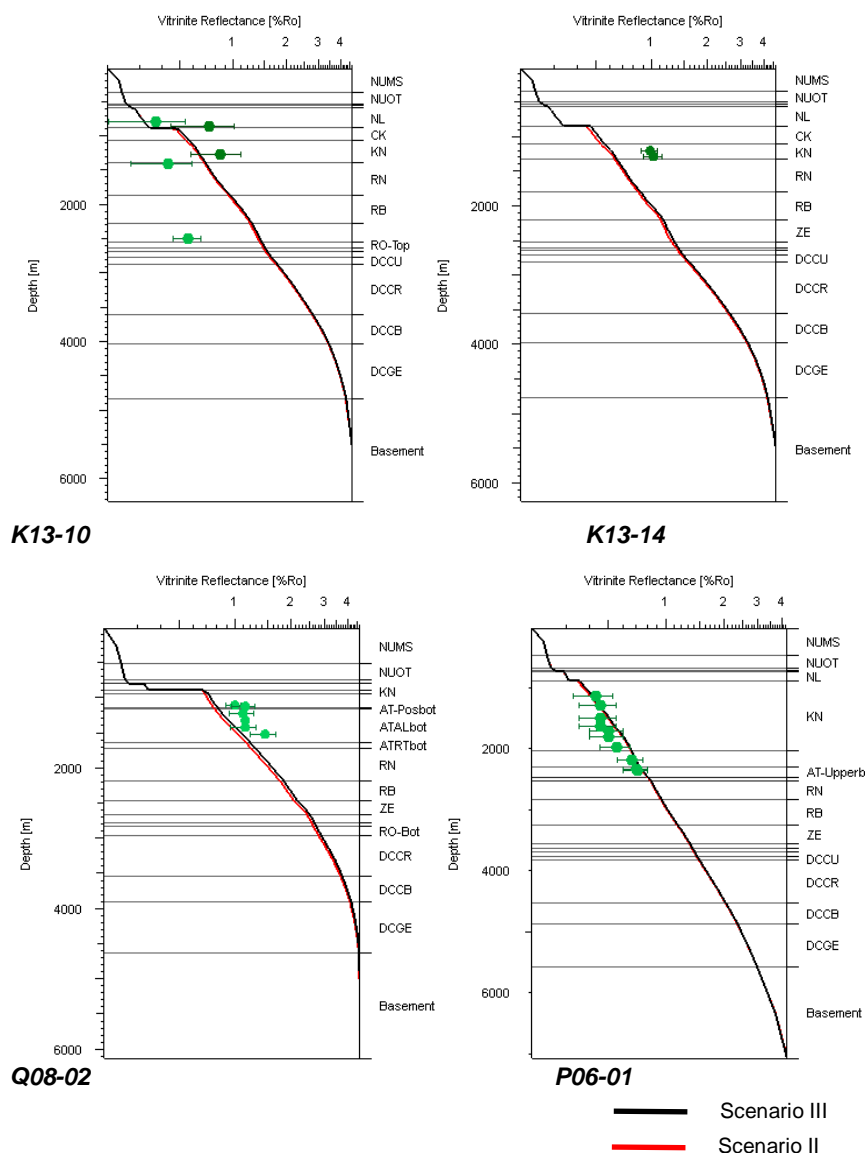


Figure 33: Modelled maturity in a selection of wells in scenario III and II. Well K13-10, K13-14 are located on the Cleaver Bank High. Well Q08-02 on the Noord Holland Platform. Well P06-01 in the Broad Fourteen Basin.. For the location of the wells, please see figure 31.

3.4 Scenario IV: Subhercynian erosion of Jurassic formations: modified erosion thicknesses

The previous scenario showed that the erosion assumptions have to be modified in the platforms as well so that a better fit can be obtained. In scenario IV we propose new erosion thicknesses for the layers but we keep the same erosion scenario as in III. The modified erosion thicknesses are shown in table 8 and figure 34.

The erosion amount of Chalk was increased by 300 m in some limited parts of the Cleaver Bank High adjacent to the BFB. The Chalk thickness is also increased by 200 m in the area of the Central Netherlands Basin (Figure 34). In the Cleaver Bank High, only the erosion thickness of the Chalk Group can be modified since the Rijnland Group is not eroded. The thickness of the eroded Rijnland Group is reduced by 400 m in the northern part of the BFB. Erosion of Schieland is decreased by 300 m. Erosion of the Altena Group is reduced with 150 m.

In scenario IV (and scenario III) the Schieland Group can only be deposited and eroded in a limited part of the BFB and WNB. It is safe to assume that the Schieland Group was not deposited in areas where the Schieland is absent under present-day Cretaceous deposits. This assumption is valid the Schieland Group was eroded in the Cretaceous, which is the case in this scenario,

Table 8: Modified erosion thicknesses in Scenario IV. Compare to Table 5.

	Modified and initial erosion (m)			
	COP/WH	B14	WNB	CNB
CK	+ 300	Not modified	Not modified	+ 200
KN	Not modified	- 400	Not modified	Not modified
SL	Not modified	- 300	- 300	Not modified
AT				
AT-UP	Not modified	- 50	- 50	Not modified
AT-Po	Not modified	- 20	- 20	Not modified
AT-AL	Not modified	- 80	- 80	Not modified
AT-RT	Not modified	Not modified	Not modified	Not modified
RN	Not modified	Not modified	Not modified	Not modified

The modelled maturity is compared to measured values in a set of wells. The results are shown in figure 35. The figure shows that a better fit is achieved in some of the wells, such as well K14-02, K17-03 and P02-05. Other wells (K17-02, P02-01) show a lower maturity but it remains high for the measured values (Figure 35). The burial history of well K14-02 shows the effect of using less erosion on the maturity (Figure 36). It is clear from the figure that the maximum maturity of the displayed formation is reached during the Cretaceous just prior to the uplift phase. Wells located outside the basins, where the thicknesses are also modified, show small change in the modelled maturity. In the Cleaver Bank High (well K13-14 and K13-10), increasing the erosion thickness of the Chalk Group with 300 m didn't result in a higher maturity. The same is observed in the Central Netherlands Basin (well Q08-02) (Figure 37). Our analysis showed that in order to get higher maturity and therefore a better fit in both locations, high erosion thicknesses have to be assumed. This would require an increase in the erosion thickness of around 800 m, which doesn't agree with stratigraphic settings of the area (N.Witmans, Pers.Comm, 01-2011). Increasing the heat flow will result in higher maturity in the wells. However, since there are no temperature data available for the wells, it is difficult to judge any heat flow modification.

Although reducing the thicknesses in the basins has resulted in lower maturity and thus a relatively better fit, the comparison clearly shows that more reduction of erosion thicknesses is required in the basins. This is not possible when the stratigraphy and the paleo-geographic settings of the region are considered. Further reduction of erosion (and thus the depositional thickness) of the Chalk and Rijnland in the northern part of the BFB is not likely. This is because the area was in the depositional centre of the basin during the Cretaceous. On the contrary, it is more likely that the depositional thicknesses were maximum in this part of the basin. In addition to that, it is not possible to reduce the erosion thickness of the Schieland Group as this will result in a depositional thickness that is lower than the minimum stratigraphic thickness of Schieland Group.

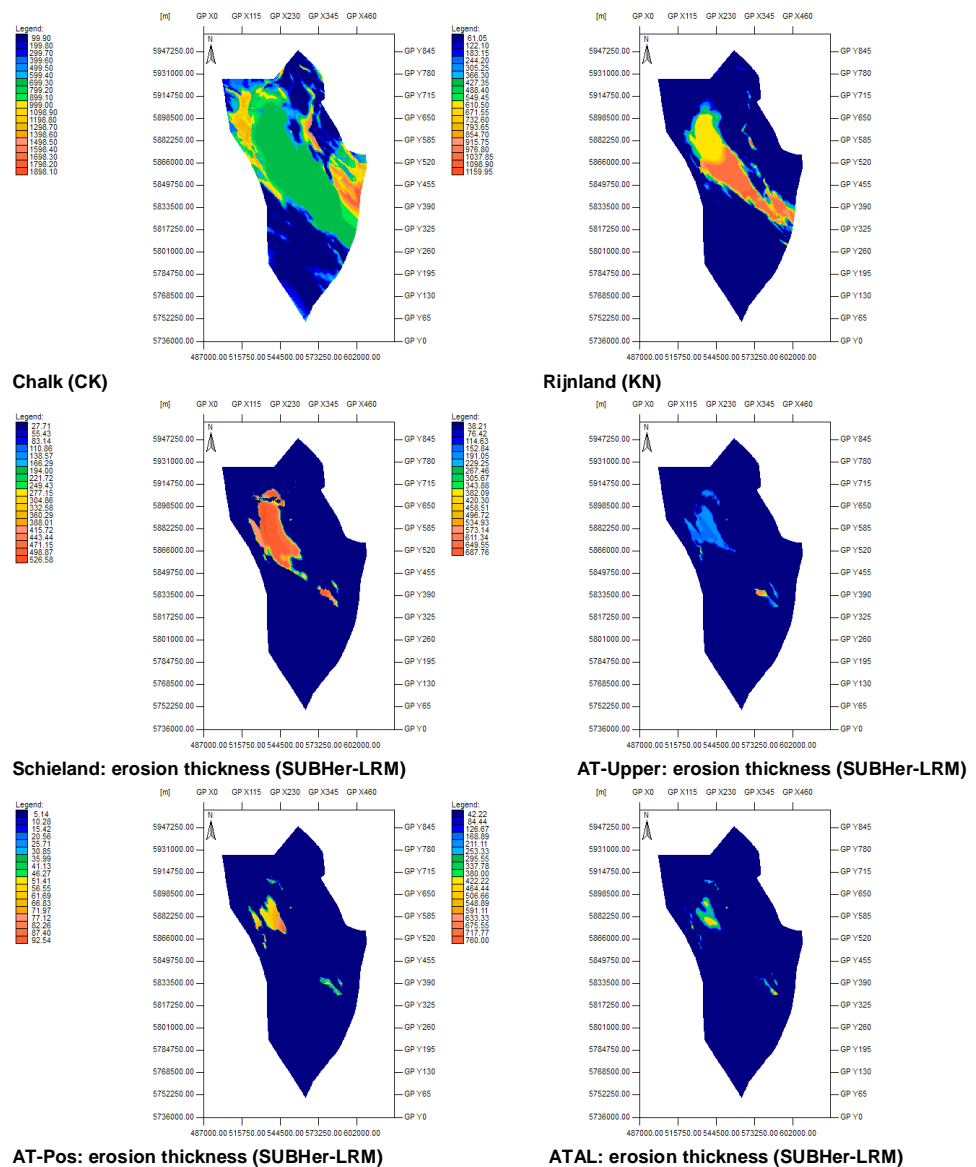


Figure 34: Modified erosion maps as used in scenario IV. Only the erosion maps of the Alena Group that are eroded during the Subhercynian and Laramide phases are modified.

An alternative scenario can be suggested in order to lower the erosion thicknesses during the Cretaceous and thereby reducing the burial depth during the Cretaceous. In the new scenario less burial will be reached without reducing the erosion thicknesses .

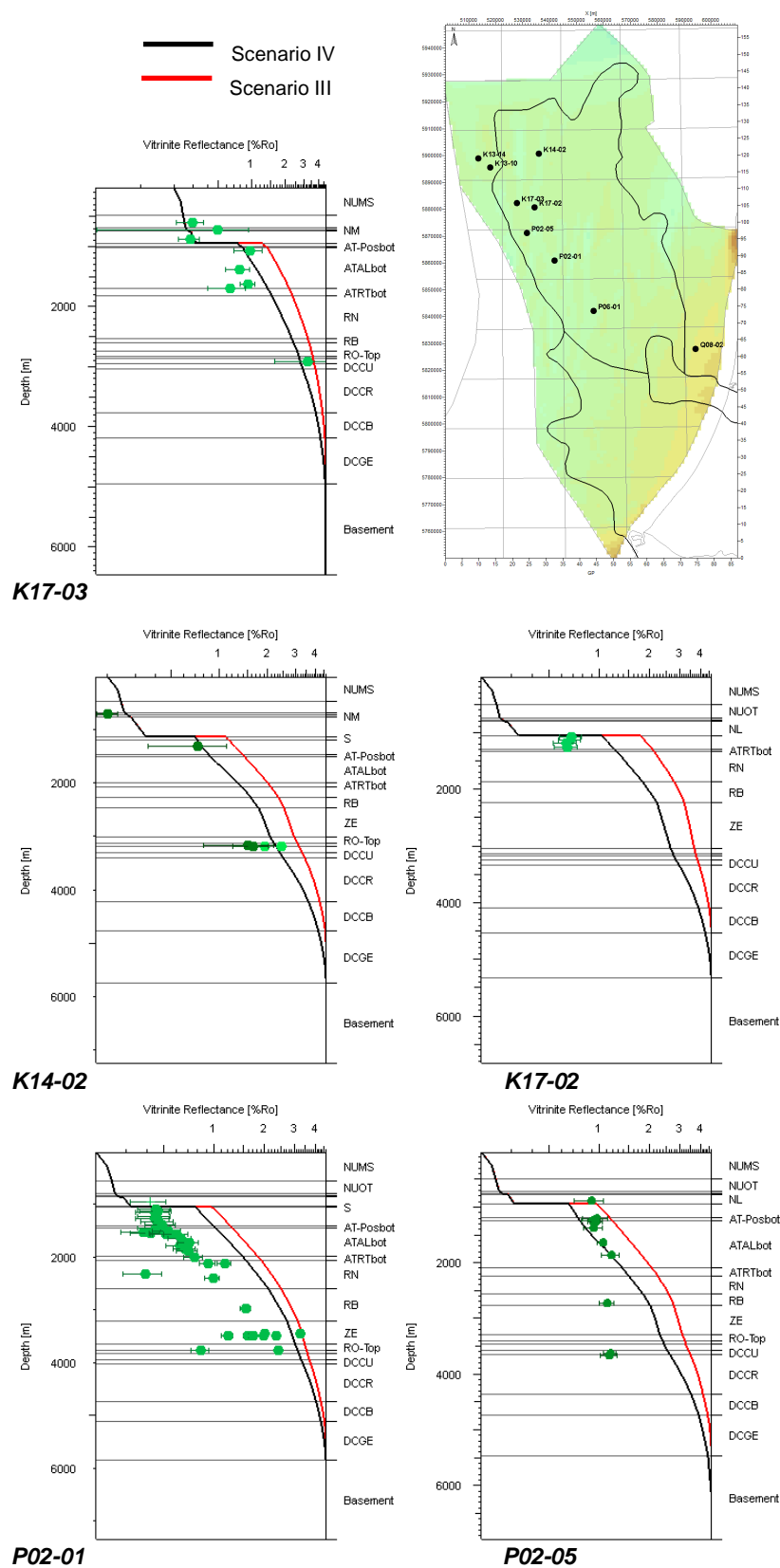


Figure 35: Modelled maturity and temperature at a selection of wells in the basins in scenario IV. Modelling results of Scenario III are also indicated.

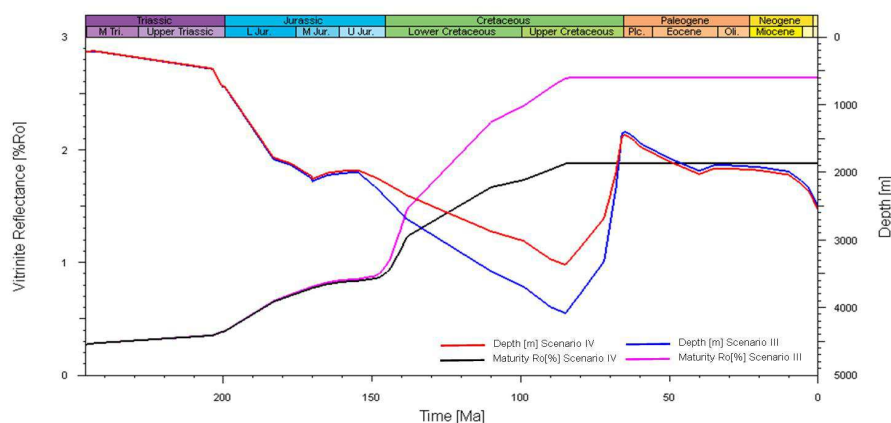
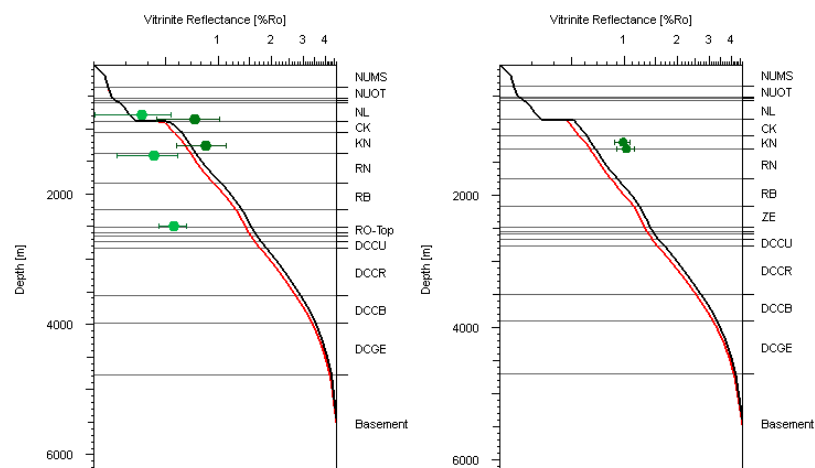
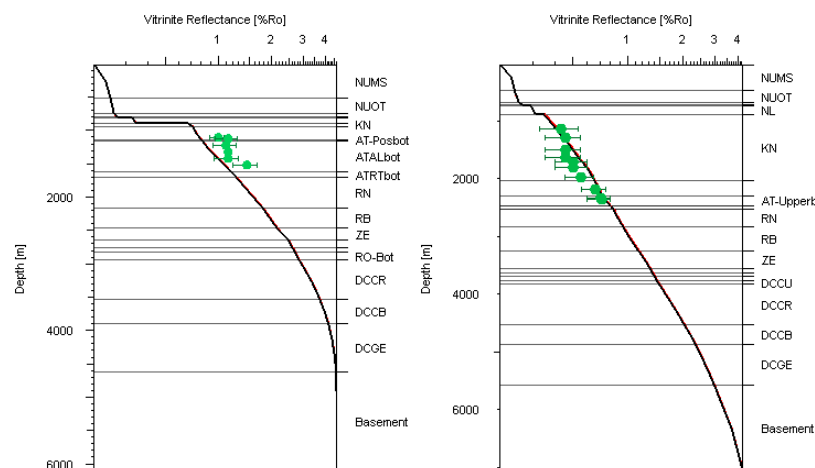


Figure 36: The burial history and maturity model of well K14-02 as modelled in scenario IV and III. The new erosion thicknesses resulted in shallower burial and thus less maturity. (The lower Triassic formation is shown here).



K13-10

K13-14



Q08-02

P06-01

Figure 37: Modelled maturity in a selection of wells in scenario IV and III. The applied modifications of erosion did not cause a better fit.

3.5 Scenario V: Kimmerian and Subhercynian erosion of Jurassic formations

In this scenario the Schieland Group is divided into two phases (sub layers). The upper part of the group is eroded during the Late Kimmerian phase together with most of the Altena Group. The bottom part of the Schieland is eroded in the Subhercynian-Laramide event together with parts of the Altena Group. Applying this geological model, we can assume that most of the Schieland Group is eroded during the Late Jurassic and only small part at the bottom of the group is preserved to be later eroded during the Late Cretaceous inversion. By doing so, it is possible to reduce the burial depth of the formations during the Cretaceous and therefore lower the maturity which is reached its maximum in the Cretaceous. This scenario also allows us to recover the initial erosion thickness of the Rijnland Group as it is possible now to compensate this thickness with erosion from the Schieland Group. Moreover, it is now possible to introduce initial deposition of the Schieland group in the rest of the study area (similar to scenario II and I). This part of the Schieland Group will be eroded during the Kimmerian phase.

In scenario V the Kimmerian erosion starts after the Schieland Group is deposited and therefore it is defined as the Late Kimmerian II erosion phase (Table 9).

Table 9: Adjusted deposition and erosion ages following this scenario (Scen V). Green coloured ages represent Cretaceous events. Blue coloured ages represent Jurassic events.

Layer	Layer Erosion phase	Deposition Age from [Ma]	Deposition Age to [Ma]	Erosion Age from [Ma]	Erosion Age to [Ma]
CK	Chalk <i>Er. Subhercynian</i>	99.1	85	85	72
KN	Rijnland Group <i>Er. Subhercynian</i>	138.7	99.1	72	68
S (SubHer)	Schieland Group <i>Er. Late Kimmerian II</i>	168	165	165	161
S (L.Kim.II)	Schieland Group <i>Er. Subhercynian</i>	170.1	168	68	66
AT-Upper (SubHer)	Altena Group Upper <i>Er. Subhercynian</i>	170.18	170.1	66	64
AT-Upper (L.Kim.II)	Altena Group Upper <i>Er. Late Kimmerian II</i>	177.6	170.18	161	158
AT-Pos (SubHer)	Altena_Posidonia <i>Er. Subhercynian</i>	177.65	177.6	64	63
AT-Pos (L.Kim.II)	Altena_Posidonia <i>Er. Late Kimmerian II</i>	183	177.65	158	152
ATAL (SubHer)	Altena_Aalborg <i>Er. Subhercynian</i>	183.17	183	63	62
ATAL (L.Kim.II)	Altena_Aalborg <i>Er. Late Kimmerian II</i>	199.6	183.17	152	149
ATRT (SubHer)	Altena_Sleen <i>Er. Subhercynian</i>	200.54	200.51	62	61.7
ATRT (L.Kim.II)	Altena_Sleen <i>Er. Late Kimmerian II</i>	203.6	200.54	149	145
RN	Upper Germanic <i>Er. Late Kimmerian II</i>	243	203.6	145	138.7

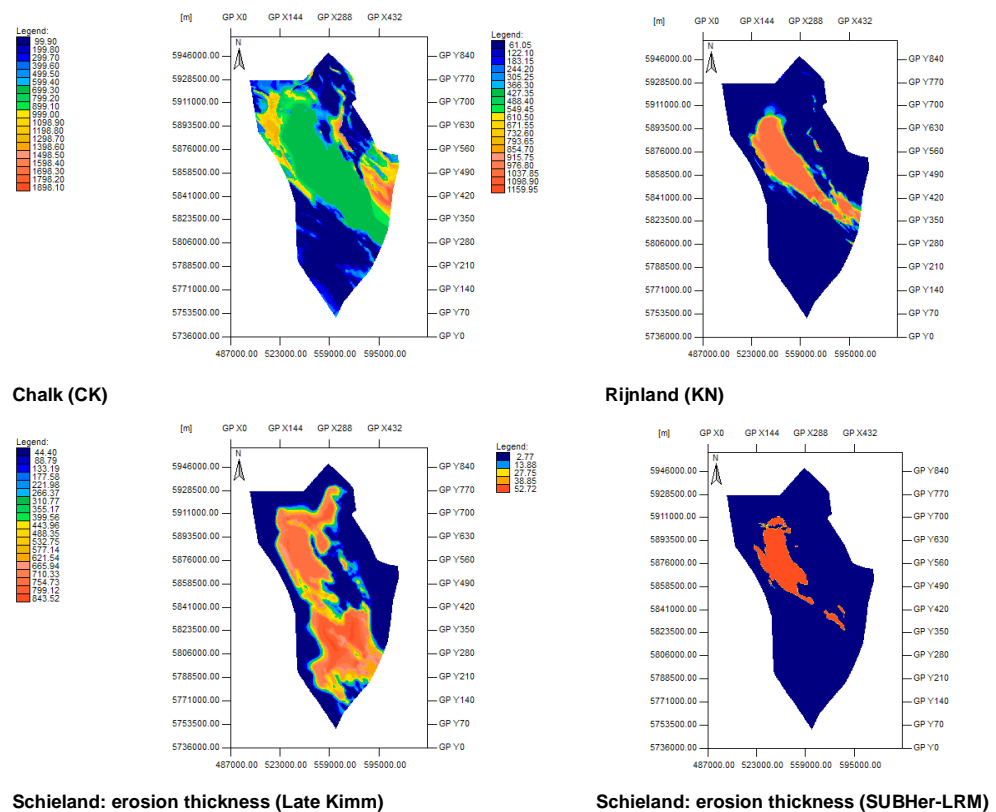


Figure 38: Modified erosion maps as used in scenario V. Only modified erosion maps of the Chalk, Rijnland and the Schieland Groups are shown here. Alena erosion maps are similar to scenario III.

The erosion thicknesses of the Rijnland and Alena groups are recovered and set equal to those in scenario II. Modifications of the Chalk Group are kept as in scenario IV. The Schieland Group is divided into two sub-layers; upper Schieland, with a varying thickness and eroded during the Late Kimmerian, and lower Schieland, which is given a fixed thickness and eroded during the Subhercynian. Modified erosion maps according to this scenario are shown in figure 38. Other simulation parameters and boundary conditions are kept similar to the previous scenarios. The results of the simulation of this scenario are presented in figure 39.

Maturity models for a selection of wells in this scenario show no significant improvement in the calibration and fit quality. Besides, no clear trend of maturity can be observed in the scenario. In some wells the modifications resulted in elevated maturity (as in well K17-03 and K17-02), while in others lower maturity is modelled (well K14-02, P02-01) (Figure 39).

The burial and maturity history of two wells show that the new erosion thicknesses and scenario is clearly reflected in the maturity evolution the wells (Figure 40). While recovering the original thickness of Rijnland has resulted in deeper burial during the Cretaceous, eroding the Schieland in the Upper Jurassic caused less burial and therefore less maturity. Depending on the thicknesses of the layers at the location of the wells or the extraction, the burial history and the maturity at that location is varying.

Although this scenario has not resulted in a better fit, it allows us to restore erosional thicknesses of some formations with minimum effect on the maturity.

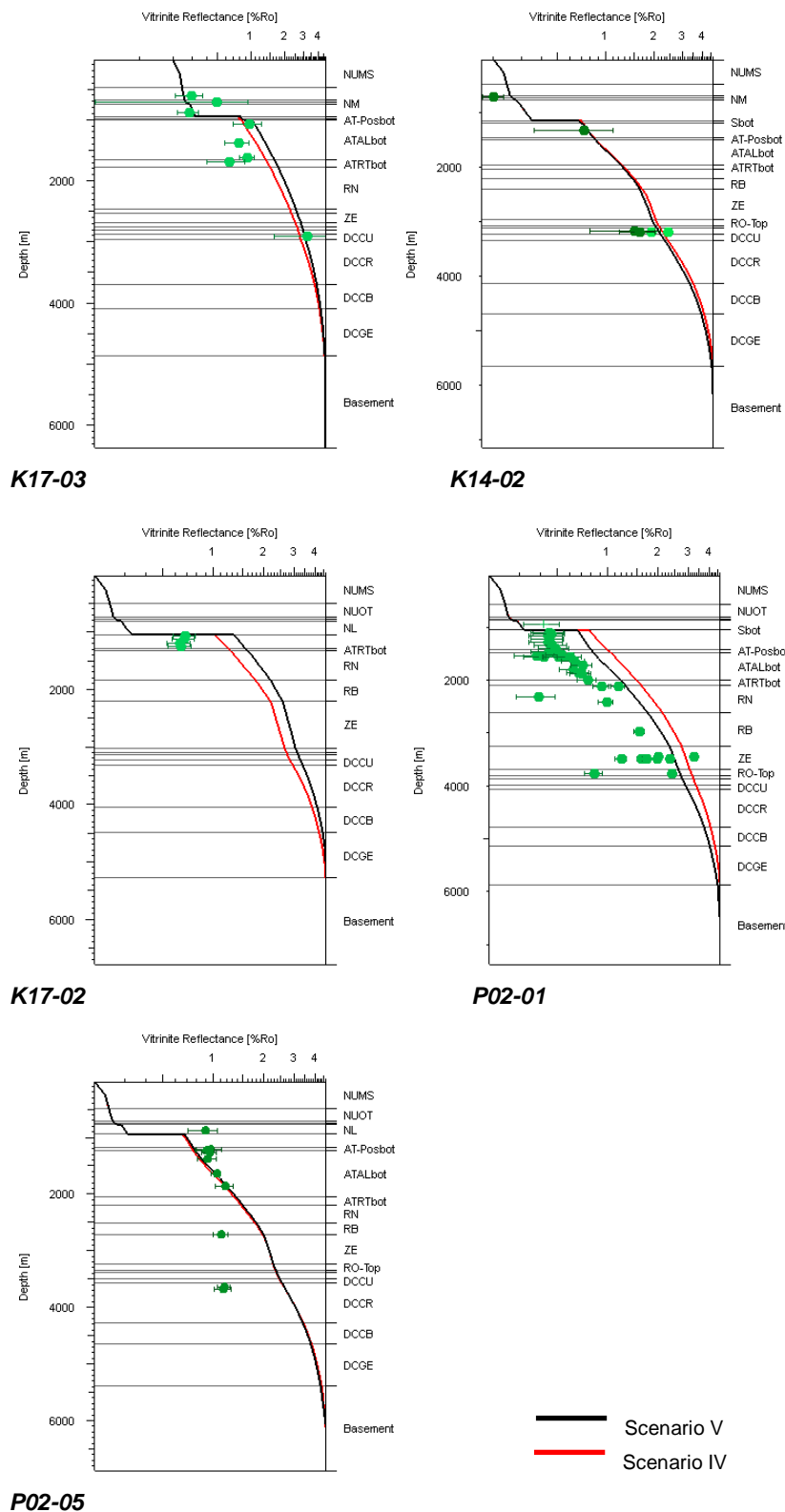


Figure 39: Modelled maturity and temperature at a selection of wells in the basins in scenario V.

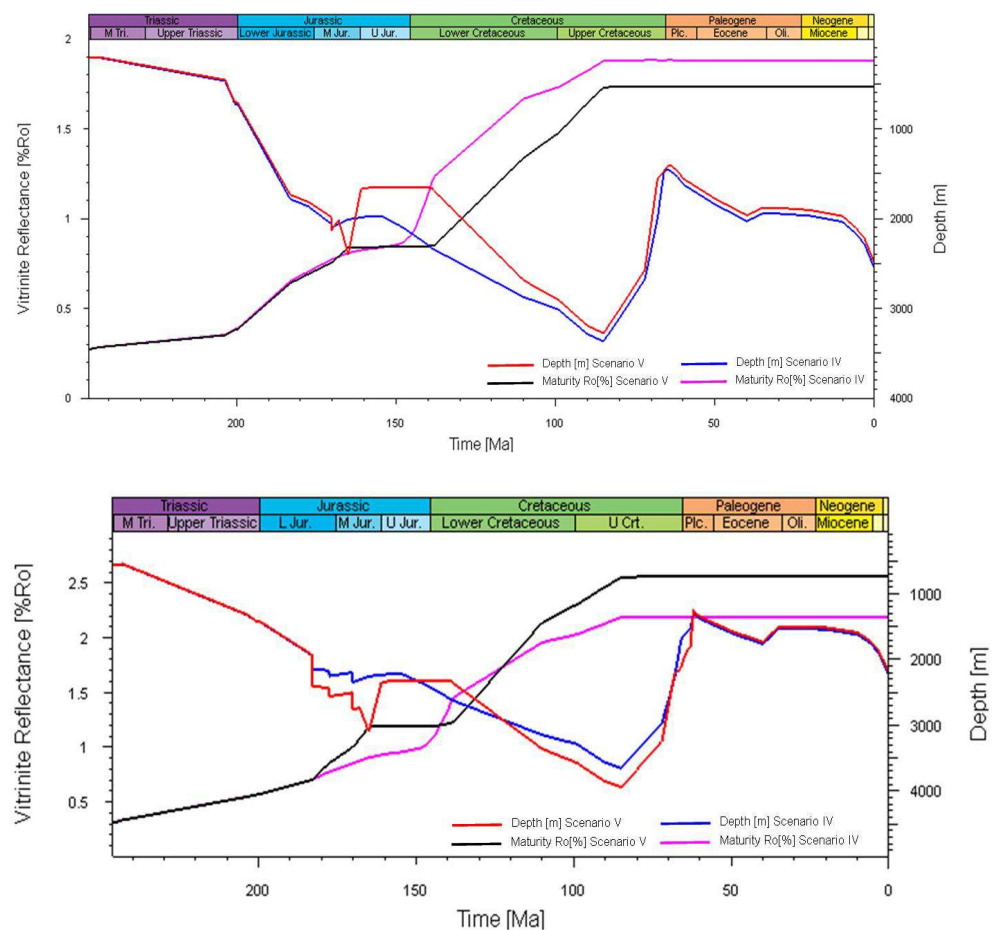


Figure 40: The burial history and maturity model of well K14-02(top) and well K17-02(bottom) as modelled in scenario V and IV. New erosion thicknesses resulted in varying burial and maturity patterns. The figure shows the modelling results for the Lower Germanic Trias Group.

3.6 Scenario VI: Late Kimmerian (I and II) erosion of Jurassic formations (New deposition ages)

In previous scenarios, the erosion of Jurassic sediments (Altena and/or Schieland groups) took place in the Late Kimmerian. This means that erosion took place after the deposition of the Schieland Group.

A new erosion scenario is proposed here based on new stratigraphic data and ages provided by the mapping department of TNO.

The new deposition ages are slightly different from the ones used in previous scenarios (Table 3). The new timescale and ages are mostly following Gradstein et al (2004) (Table 10). The Triassic ages are according to Kozur & Bachmann (2008) and the Upper Jurassic ages are according to Munsterman & Verreussel (in prep). The Quaternary ages follow the International Commission on Stratigraphy (2009) and the Western European nomenclature is used for the Carboniferous series and stages.

New tectono-stratigraphic charts prepared by Witmans (Pers. Comm. 2011) for the NCP-2F area provided new insights to create erosion scenario VI (Figure 41).

Table 10. Timing and duration of periods of sedimentation, erosion and non-deposition.

Layer	Layer	Deposition Age from [Ma]	Deposition Age to [Ma]
NUMS	<i>Upper North Sea Maassluis Formation</i>	2.6	0
NUOT	<i>Upper North Sea Oosterhout Formation</i>	4.5	2.6
NUBA	<i>Upper North Sea Breda Formation</i>	20	10
NM	<i>Middle North Sea Group</i>	34	29
NL	<i>Lower North Sea Group</i>	61	37
CK	<i>Chalk</i>	100	85
KN	<i>Rijnland Group</i>	140	100
S	<i>Schieland Group</i>	155	140
AT-Upper	<i>Altena Group Upper</i>	179	167
AT-Pos	<i>Altena Posidonia Formation</i>	183	179
ATAL	<i>Altena Aalburg Formation</i>	200	183
ATRT	<i>Altena Sleen Formation</i>	206	200
RN	<i>Upper Germanic Trias Group</i>	247	206
RB	<i>Lower Germanic Trias Group</i>	252	247
ZE	<i>Zechstein Group</i>	263	252
RO-Top	<i>Rotliegend Group-Top</i>	264	263
RO-Mid	<i>Rotliegend Group-Middle</i>	265	264
RO-Bot	<i>Rotliegend Group-Bottom</i>	267	265
DCH	<i>Hunze Sub-Group</i>	308	299
DCCU	<i>Maurits Formation</i>	310	308
DCCR	<i>Ruurlo Formation</i>	312	310
DCCB	<i>Baarlo Formation</i>	313.5	312
DCGE	<i>Namurian Formation</i>	326	313.5
Basement	<i>Basement</i>	340	326

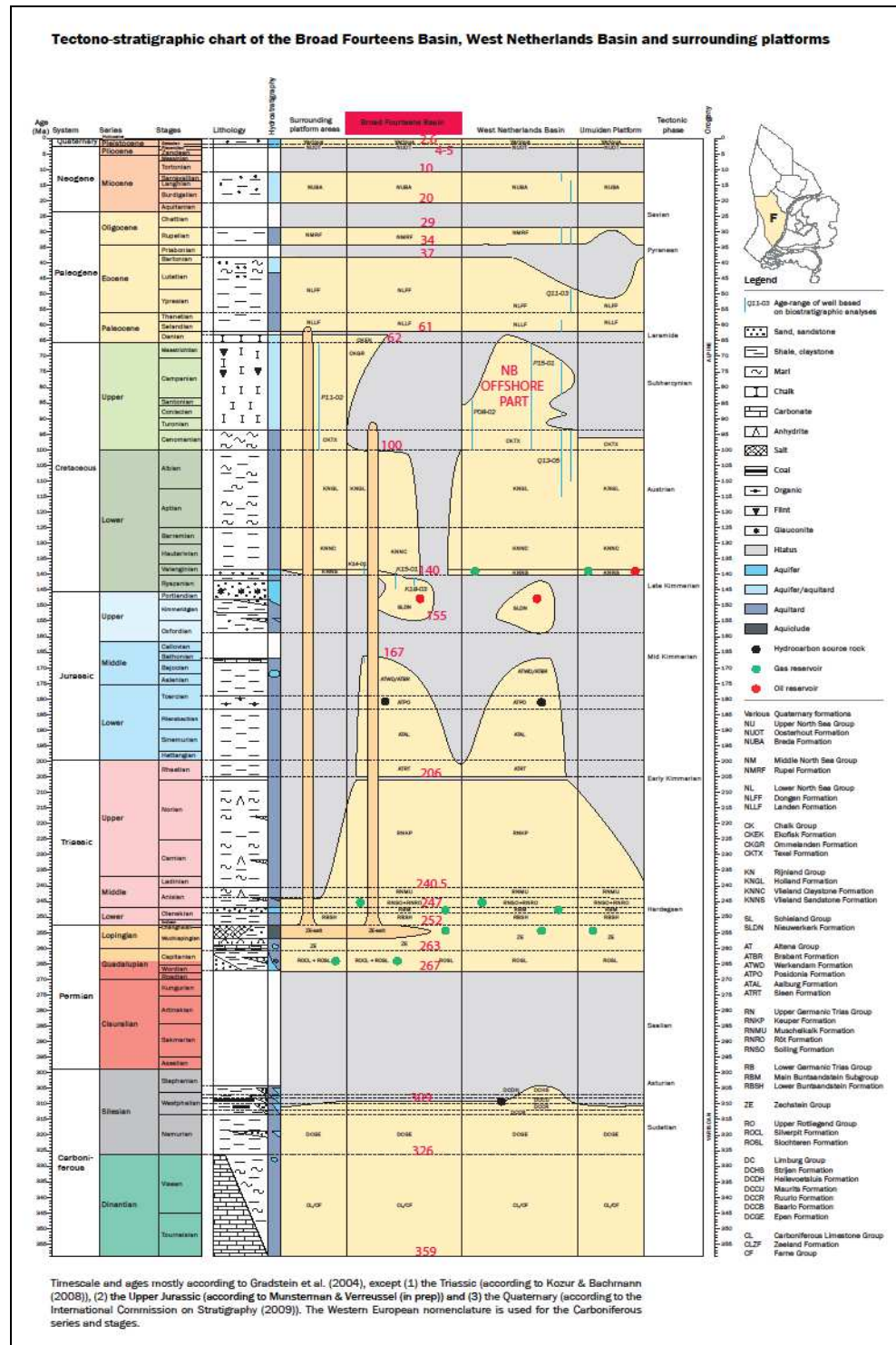


Figure 41: Updated tectono-stratigraphic chart of the NCP-2F area. Erosion scenario VI is based on this chart.

The new erosion scenario is schematically demonstrated in figure 42. Three erosion phases are defined. The first phase is the Late Kimmerian I phase where most of the Altena Group is eroded (167 Ma–155 Ma). A small patch of the Altena is left uneroded in the northern part of the BFB. The second phase is the Late Kimmerian (II) (146 Ma – 140 Ma) phase where most of the Schieland Group is eroded except for a small patch in the northern part of the BFB. It is also possible that this phase in

some places eroded parts of the Altena Group and even Upper Triassic (Figure 42). This is however not included in the model for the sake of simplicity and as it is difficult to prove this from the stratigraphic record. The third erosion phase in this scenario is the Subhercynian-Laramide erosion phase (85 Ma – 61 Ma) where the Chalk and the Rijnland Groups are partly eroded. The remaining parts of the Schieland and the Altena Groups in the inverted centre parts of the BFB is also eroded during this phase (Figure 42).

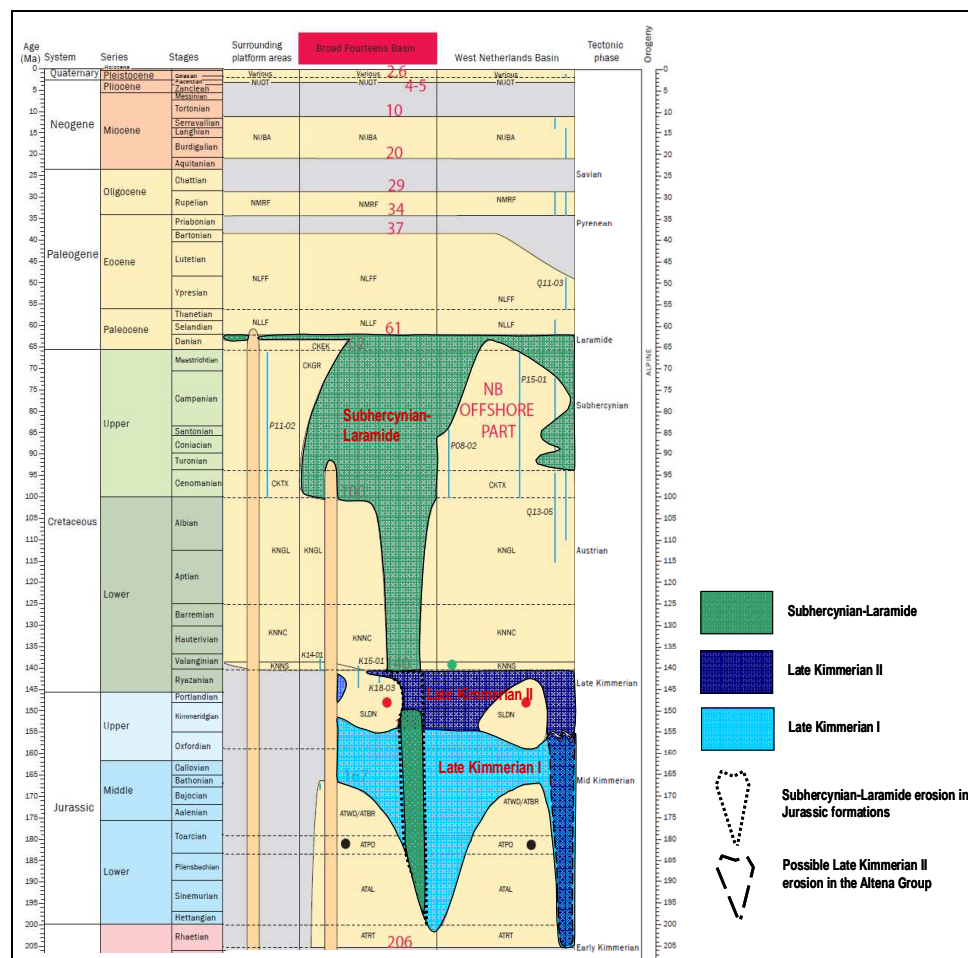


Figure 42: Schematic overview showing the main erosion phases as used in the model of scenario VI overprinted on the updated tectono-stratigraphic chart of the NCP-2F area.

Erosion thicknesses for all eroded layers are kept similar to those used in scenario (V). Simulation parameters are also set identical to those used in previous scenarios.

The simulation results of this scenario are presented in the form of present-day temperature and vitrinite reflectance for a selection of wells (Figure 43). The presented wells are grouped into three sets, wells within the BFB, wells within the WNB and wells from the remaining surrounding area (highs and platforms). The modelled vitrinite reflectance of the wells are presented in figures 44, 45 and 46. The figures show that generally a good fit with the measurements is achieved. However, the modelled maturity appears to be overestimated in some wells, especially in the basins (for example well K15-01, P02-01, P12-01, Q10-01; Figure 44, 45). As in the previous scenarios, the quality of the measured vitrinite

reflectance data is an important source of uncertainty. A significant portion of the measured data is considered less reliable as the lab measurements are conducted by external parties and no information is available on the number of measurements and the standard deviation. The most reliable data (presented in the figures below in dark green colour), which are measured at TNO laboratory, do provide a good fit with the model.

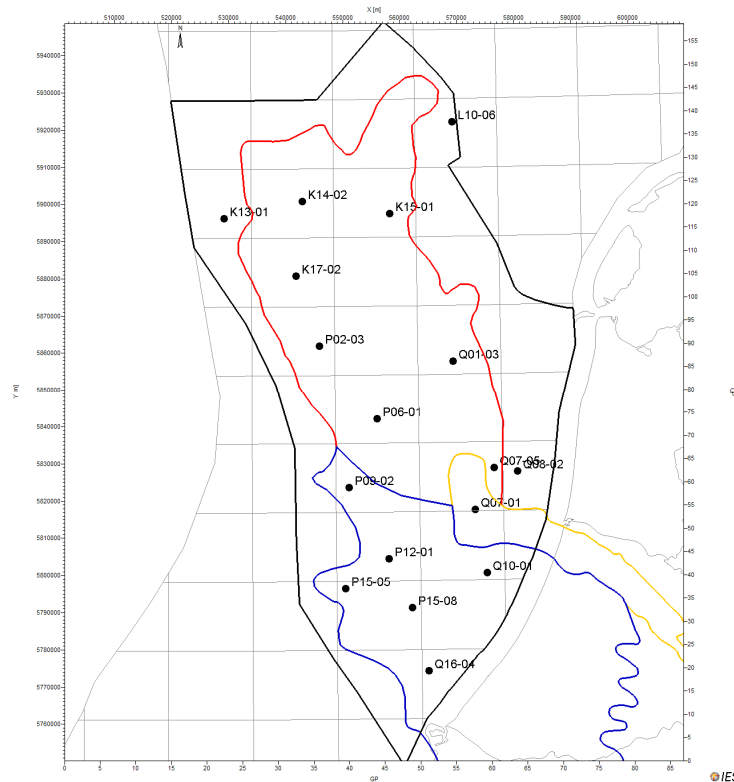


Figure 43: Location of the wells used for model calibration with measured data.

The modelled vitrinite reflectance in wells in the third group (outside the two basins area) is shown in figure 46. The modelled maturity is generally comparable to the measurements in the wells. The measurements have a degree of uncertainty that makes the calibration of the model difficult (for example well Q07-01; Figure 46).

In addition to the quality of the measurements, there remain some questions and uncertainties involved with the model assumptions and boundary conditions. For example, the model does not include the effects magmatic activities which have been recorded in the area (Van Bergen & Sissingh, 2007). Magmatism can result in anomalously high temperatures and maturity in the nearby sediments. In addition to that, faults can form paths for circulating fluids which might change the thermal regime in the surrounding sediments. Since these factors are not taken into account in the model, this might explain the mismatch between the model the measurements. Nonetheless, in the majority of the wells and over the whole study area, a good fit is achieved between the modelled maturity and the measurements. The figures show that introducing this erosion scenario (scenario VI) did not result in a significant change in the maturity. The burial history and the modelled maturity history in two wells and for both scenarios are shown in figure 47. Although the new scenario (new erosion model and ages) has resulted in a different burial history, the maturity is not affected significantly.

Modelled temperatures show a good fit with the measured temperatures in the wells (Figure 48). This indicates that the applied basal heat flow model, in combination with other lithological properties, are acceptable.

A more elaborated and perhaps realistic geological scenario that describes deposition and erosion in the area is not included due to the limitations imposed by the software package. It is not possible in the current version of PetroMod to include a phase of simultaneous erosion and deposition for a given layer. This is, however, a likely scenario for two major formations in our model. The Chalk Group for example is likely to be deposited on the platforms at the same time that it was being eroded in the basin during the Subhercynian inversion phase. Since combining both events in one single phase in the model is not possible, they can only be introduced as two separate events. This can have important effect on modelled maturity as it will influence the timing and the amount of burial of the layers below the Chalk Group.

A similar case is also expected during Jurassic tectonic events. The Schieland Formation was deposited in the centre of the basin during the Late Kimmerian while the Altena Group was being eroded on the surrounding rising platforms. The erosion material might have provided the deposition material for the centre of the basin. Again, such a scenario cannot be included in the model due to software limitations. This can have significant impact on maturity models.

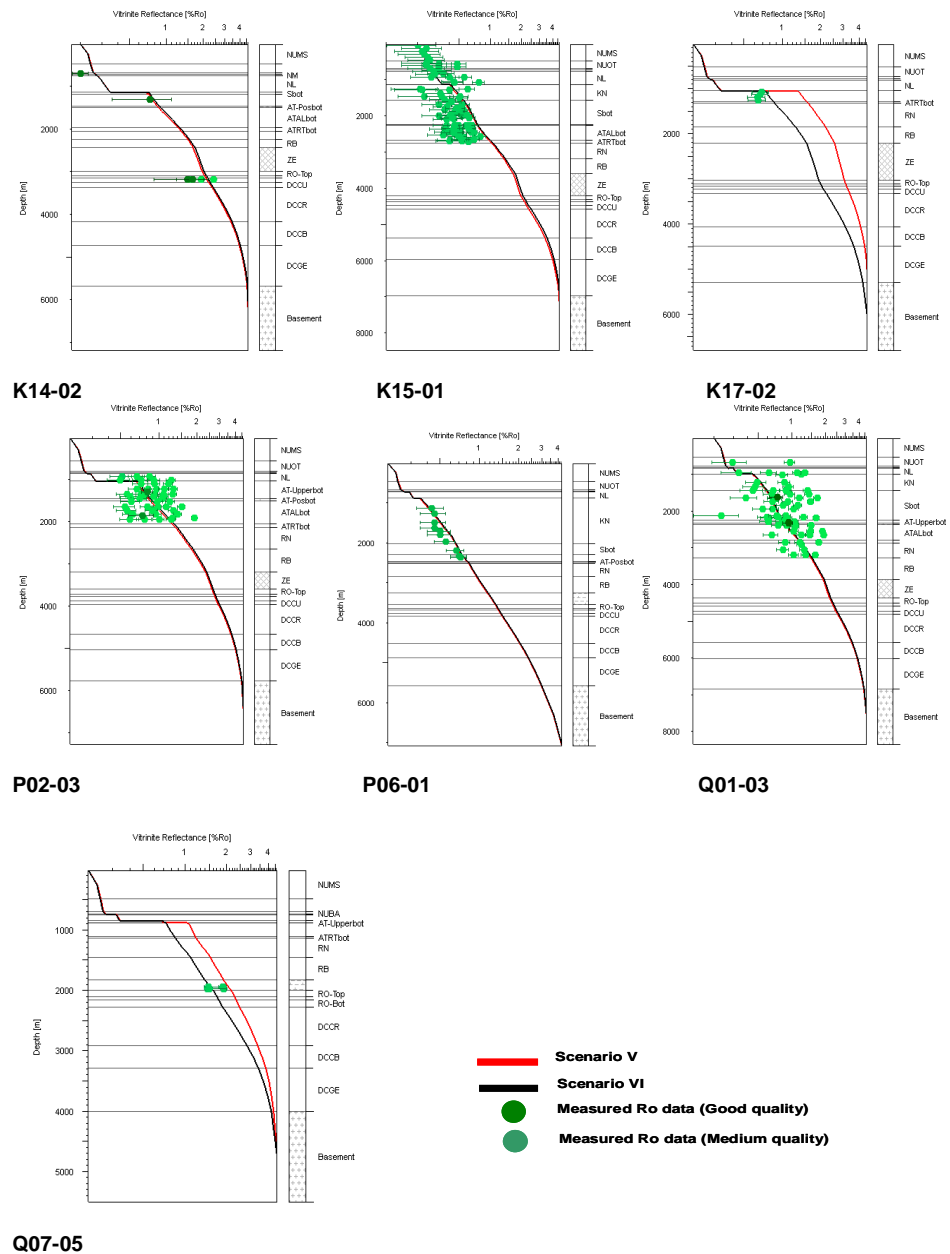


Figure 44: Comparison between modelled maturity (Ro %) and measured values in a selection of wells in the Broad Fourteen Basin. Generally, good fit is obtained with data with good quality.

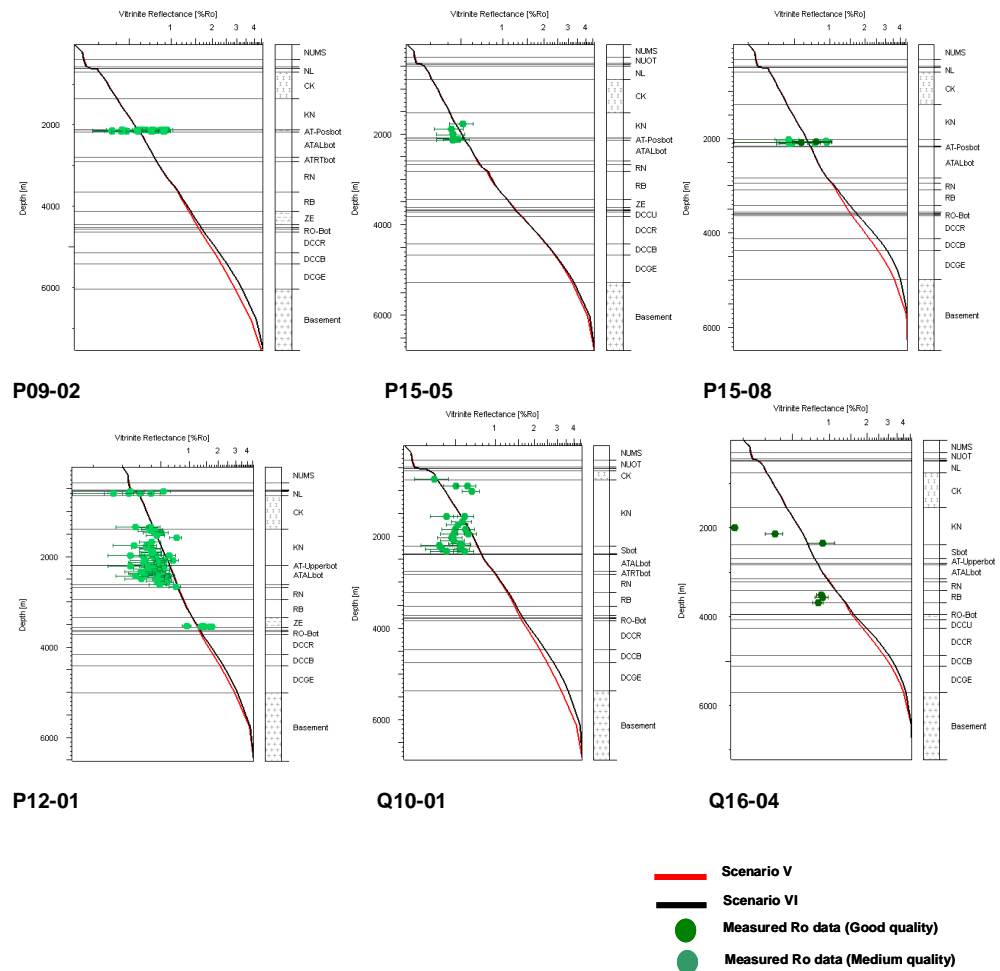


Figure 45: Comparison between modelled maturity (Ro %) and measured values in a selection of wells in the West Netherlands Basin.

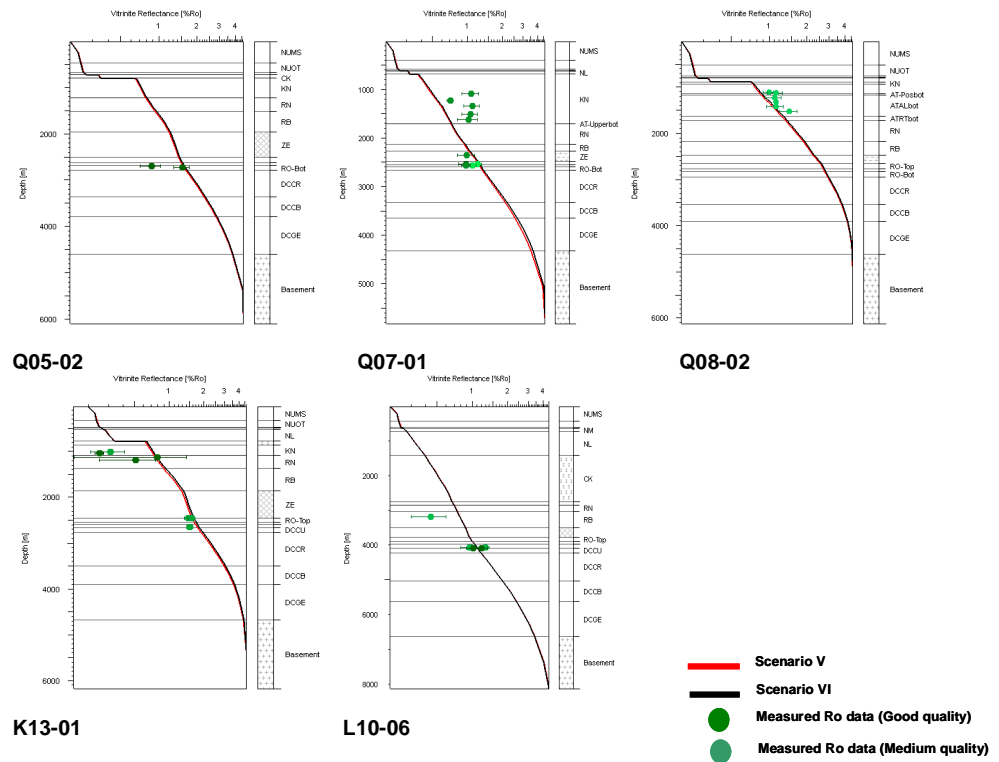


Figure 46: Comparison between modelled and measured maturity (Ro %) in a selection of wells in the NCP-2F area outside the Broad Fourteen Basin and West Netherlands Basin.

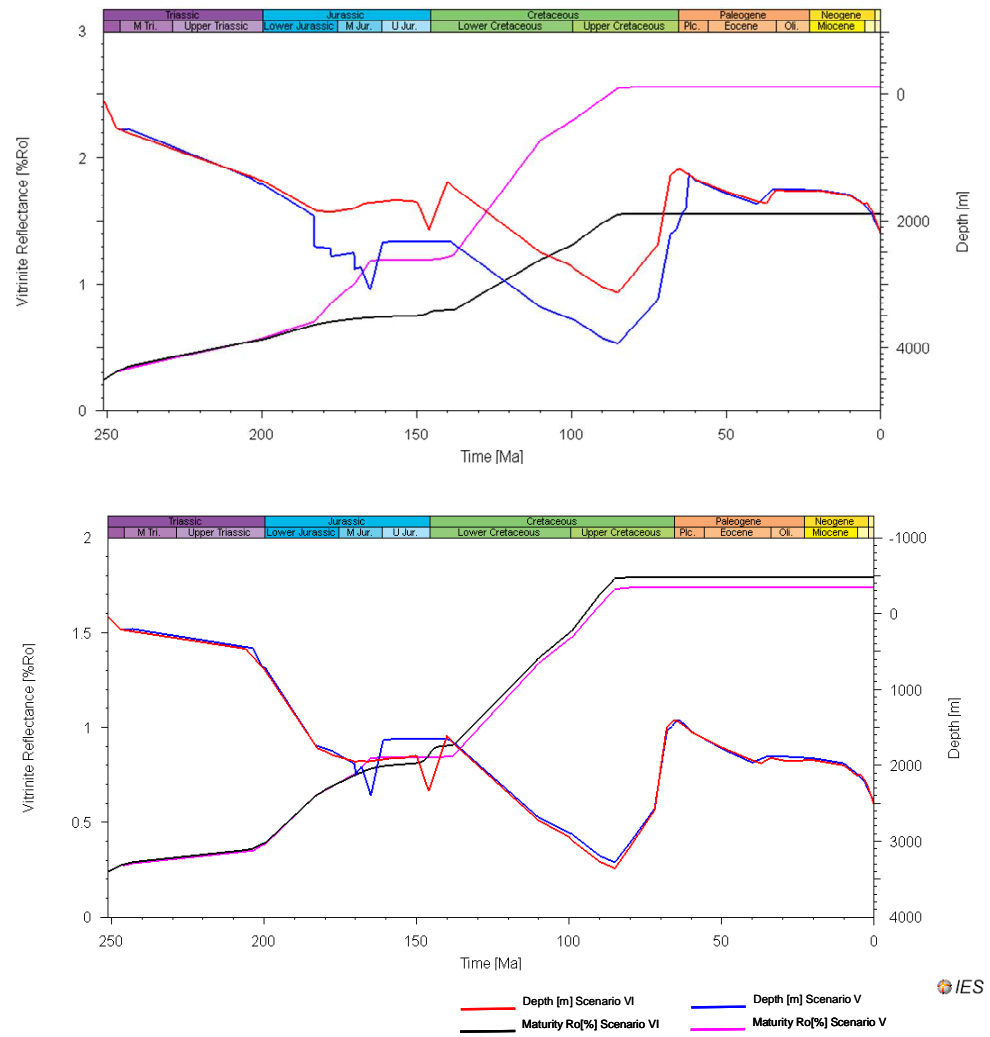


Figure 47: The burial history and maturity model of well K17-02 (top) and well K14-02 (bottom) as modelled in scenario VI and V. The Lower Germanic Trias Group is shown here. Notice how the new erosion scenario has affected the burial history, and thus the maturity, during the Jurassic in well K17-02.

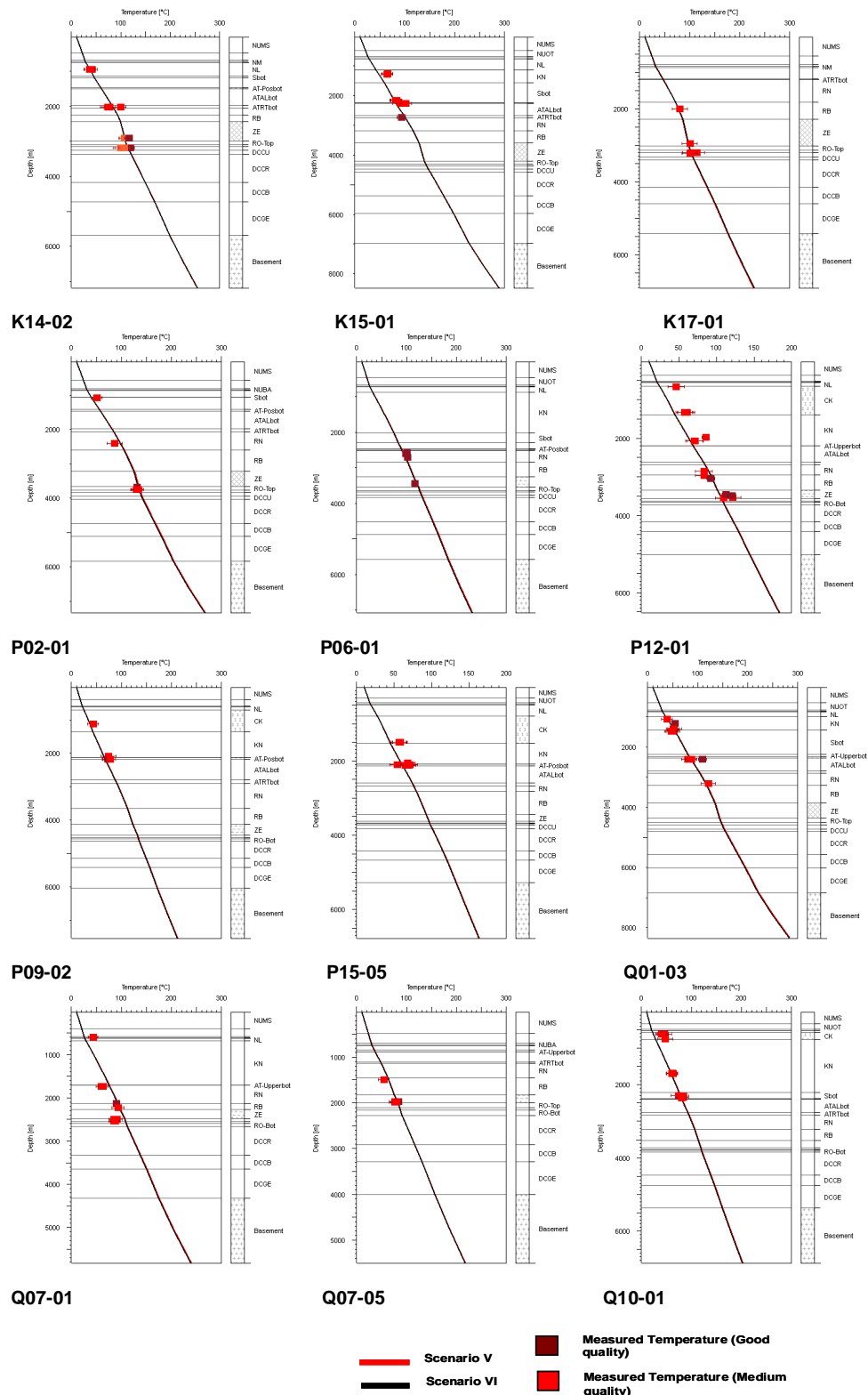


Figure 48: Modelled present-day temperatures in a selection of wells compared to measured values in the wells.

4 Burial history and history of maturity and hydrocarbon generation

In the previous chapter we discussed various scenarios that can be applied to modelling the NCP-2F area. The scenarios were focused on the erosion, in terms of thicknesses and sequence. As a result of the comparisons between the scenarios, a final model was chosen to simulate the burial and maturity history in the area. Based on the results of the evaluation of the different scenarios, we have concluded that scenario (VI) is the most reliable one. It is most consistent with the general geological settings and stratigraphic concepts in the area. The comparison between the calculated vitrinite reflectance and temperature and measured values in several wells shows a good fit. Therefore we adopt the modelling parameters from the scenario for further analysis. This includes the erosion scenario but also model parameters and properties, regarding the heat flow, the amounts of erosion, the lithology and the thermal parameters of the strata in the model.

4.1 Burial history

The burial history of a number of representative 1D extractions in each of the structures in the area are presented below. The locations of the 1D extractions are shown in Figure 49.

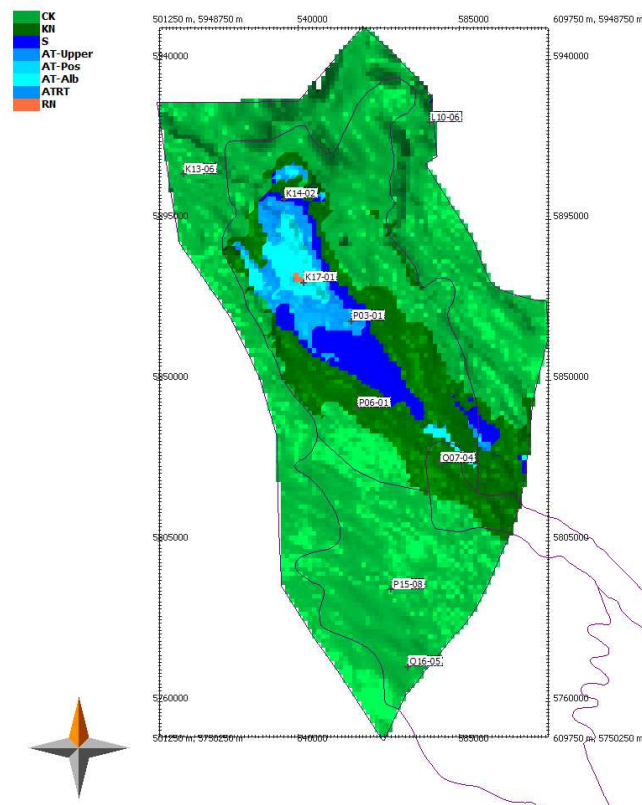


Figure 49: Map of the study area showing the location of the 1D extractions used for burial history analysis.

4.1.1 *The Broad Fourteens Basin*

The burial histories of four wells in the Broad Fourteens Basin are shown in Figure 50. Well K17-01 is located in the central part of the basin where the Subhercynian-Laramide inversion and erosion has reached almost the Upper Triassic. The Late-Kimmerian II erosion continued until the Early Cretaceous and removed the whole Upper Jurassic Schieland Group. The Subhercynian-Laramide erosion has removed the whole Cretaceous and almost all of the remaining Altona. In this well, the Late Kimmerian I phase does not seem to have affected the Jurassic formations on a large scale. The burial history of well P03-01 is similar to the burial history of well K17-01. However, the Subhercynian-Laramide erosion stopped at the Upper Altona and did not cut deeper.

At the location of well K14-02, the Late Kimmerian II removed only the upper part of the Schieland. The Subhercynian-Laramide phase removed the entire Cretaceous and a limited part of the Schieland which is still present in the well. The Late Kimmerian I erosion does not seem to have affected the Jurassic at this location. The burial history of well P06-01 in the southern part of the BFB, shows that Late Kimmerian I phase eroded parts of the Lower Jurassic formations (Figure 50). The Late Kimmerian II resulted in the erosion of the Schieland Group. During the Subhercynian-Laramide, the Chalk was eroded as well as the upper part of the Rijnland Group.

The Late Eocene Pyrenean uplift, which resulted in the erosion of parts of the Lower North Sea Group, can be seen in the burial history of all the wells.

The Saalian event, where parts of Carboniferous formations have been eroded, is seen in all burial histories.

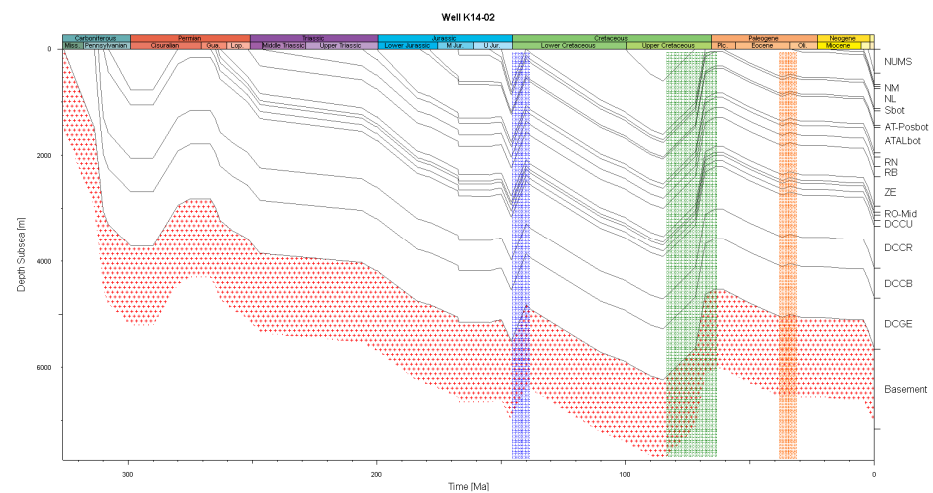
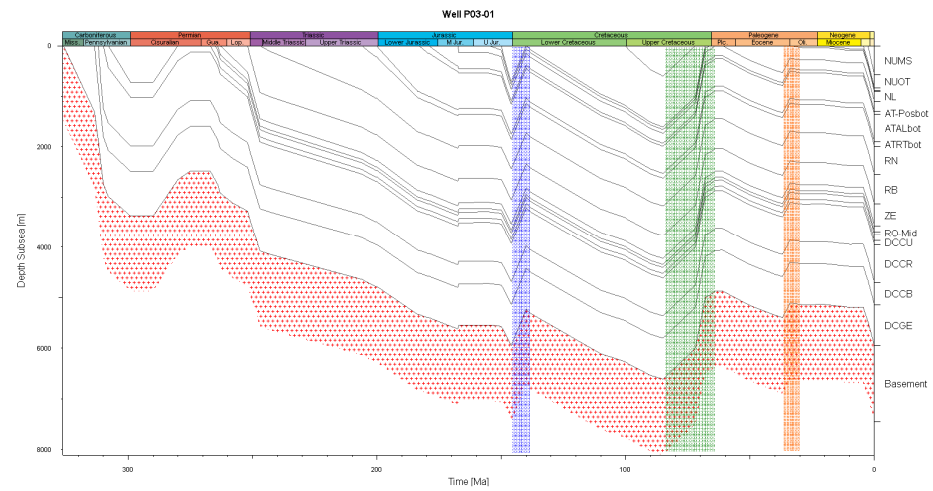
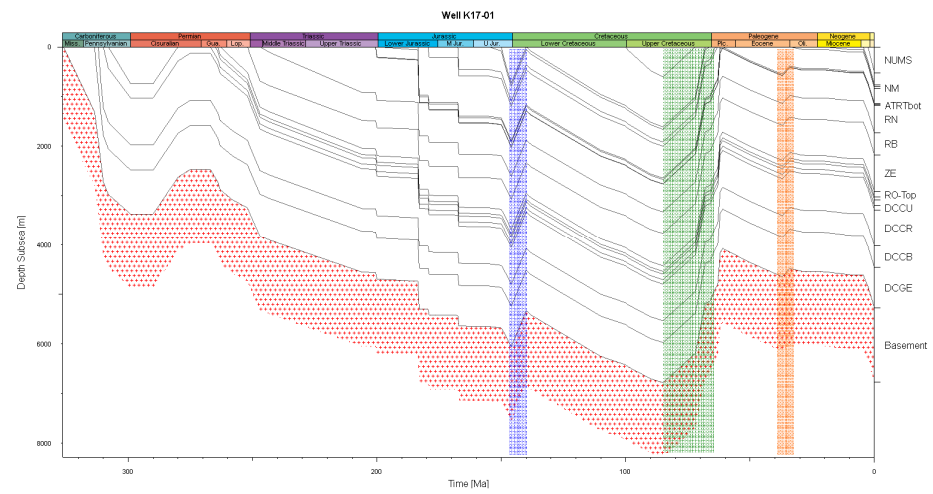
The burial history shows that the deepest burial of the formations was reached during the upper Cretaceous and prior to the inversion.

4.1.2 *The West Netherlands Basin*

The burial histories of two selected wells from the West Netherlands Basin (offshore) indicate that the Subhercynian-Laramide erosion did not affect the basin on a large scale (Figure 51). Neither the Cretaceous Rijnland nor the Chalk seem to have been eroded on a large scale. The Late Kimmerian II eroded parts of the Upper Jurassic where most of the Schieland is absent. Less erosion took place during this phase in the southern parts of the basin (well Q16-05).

The Permian Saalian erosion can be seen in the burial histories as well. The intensity of the uplift and erosion seems however less to the south of the basin (well Q16-05) than to the north (well P15-08).

Some erosion of the Lower North Sea Group has taken place during the Pyrenean uplift. The amount of uplift, however, is higher in wells located to the north (well P15-08). The deepest burial in both wells seem to be at present day.



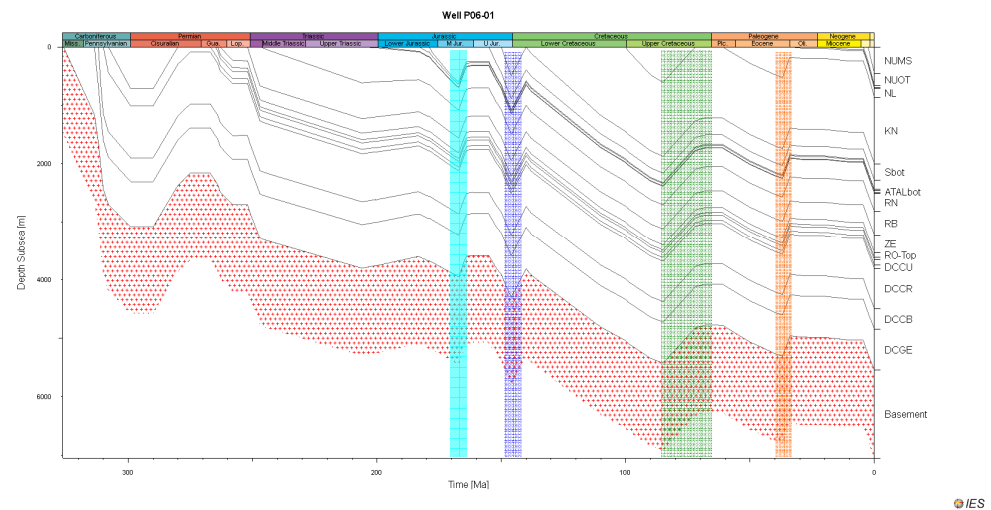


Figure 50: The burial history of a number of wells from the Broad Fourteens Basin. The main erosion phases are indicated with the highlighted bars. See figure 49 for the location of the wells.

4.1.3 Zandvoort Ridge

The burial history in the Zandvoort Ridge (well Q07-04) indicates that, in addition to the Saalian uplift phase, the other four uplift phases have strongly affected the structure (Figure 52). The Late Kimmerian I removed parts of the Lower and Mid Jurassic sediments. The ridge was uplifted again during the Late Kimmerian II phase and the entire Schieland was removed from the section. The Subhercynian-Laramide erosion events affected Cretaceous sediments and removed the whole Chalk and part of the Rijnland Group. After the deposition of the Lower North Sea Group in the Palaeogene, the Pyrenean uplift began and resulted in the removal of parts of the Lower North Sea.

The deepest burial in the Zandvoort Ridge was reached during the Cretaceous prior to Subhercynian-Laramide uplift. A comparable burial was reached afterward during the Late Eocene and at present day.

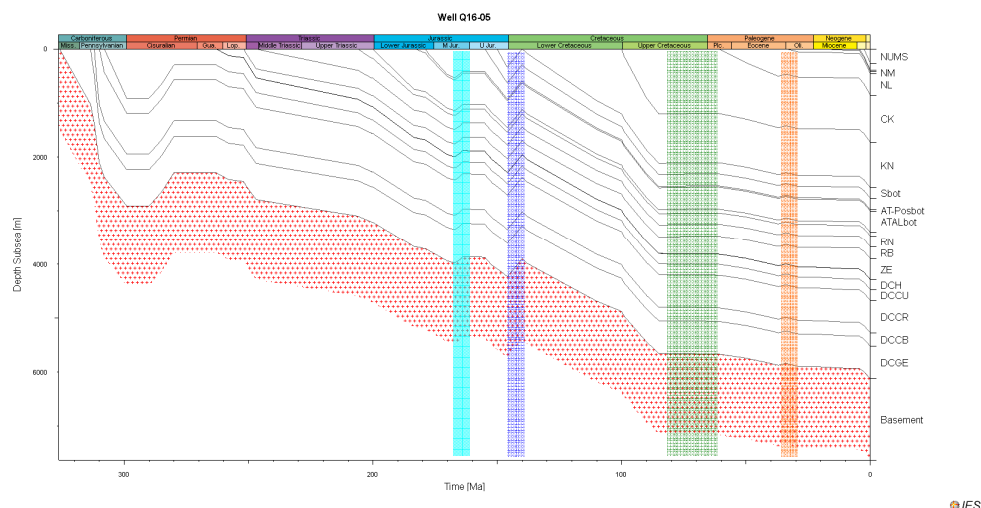
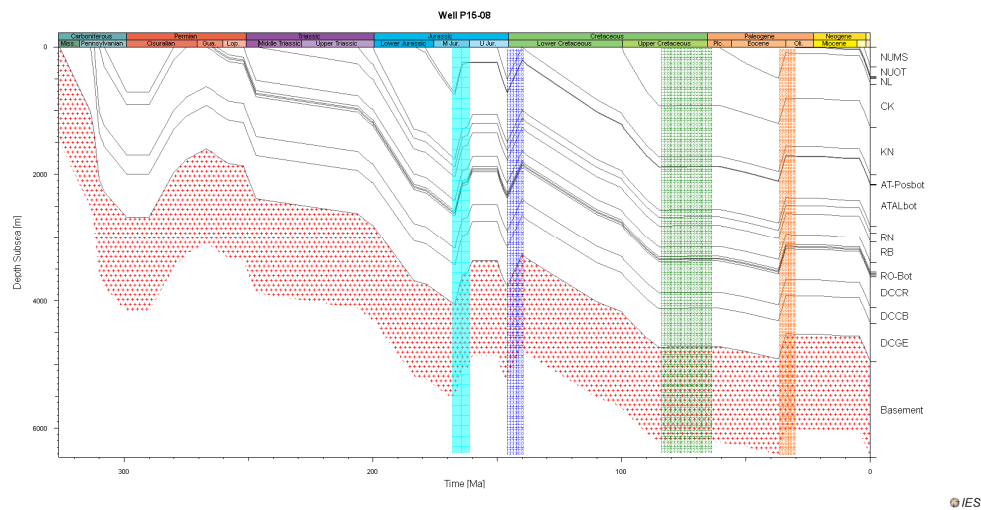


Figure 51: The burial history of two wells from the West Netherlands Basin. The main erosion phases are indicated with the highlighted bars. See figure 49 for the location of the wells.

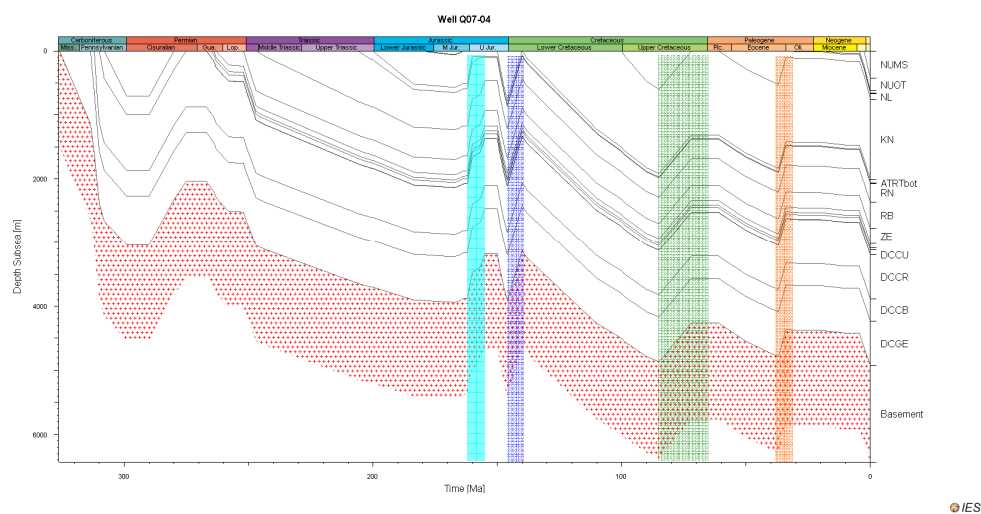


Figure 52: The burial history of well Q07-04 located in the Zandvoort Ridge.

4.1.4 Surrounding Platforms

Two wells are selected to present the burial history in the platform areas surrounding the basins. These include: well K13-06 located to the west of the BFB, and well L10-06 located to the east of the BFB in the Noord Holland Platform (Figure 49: 53).

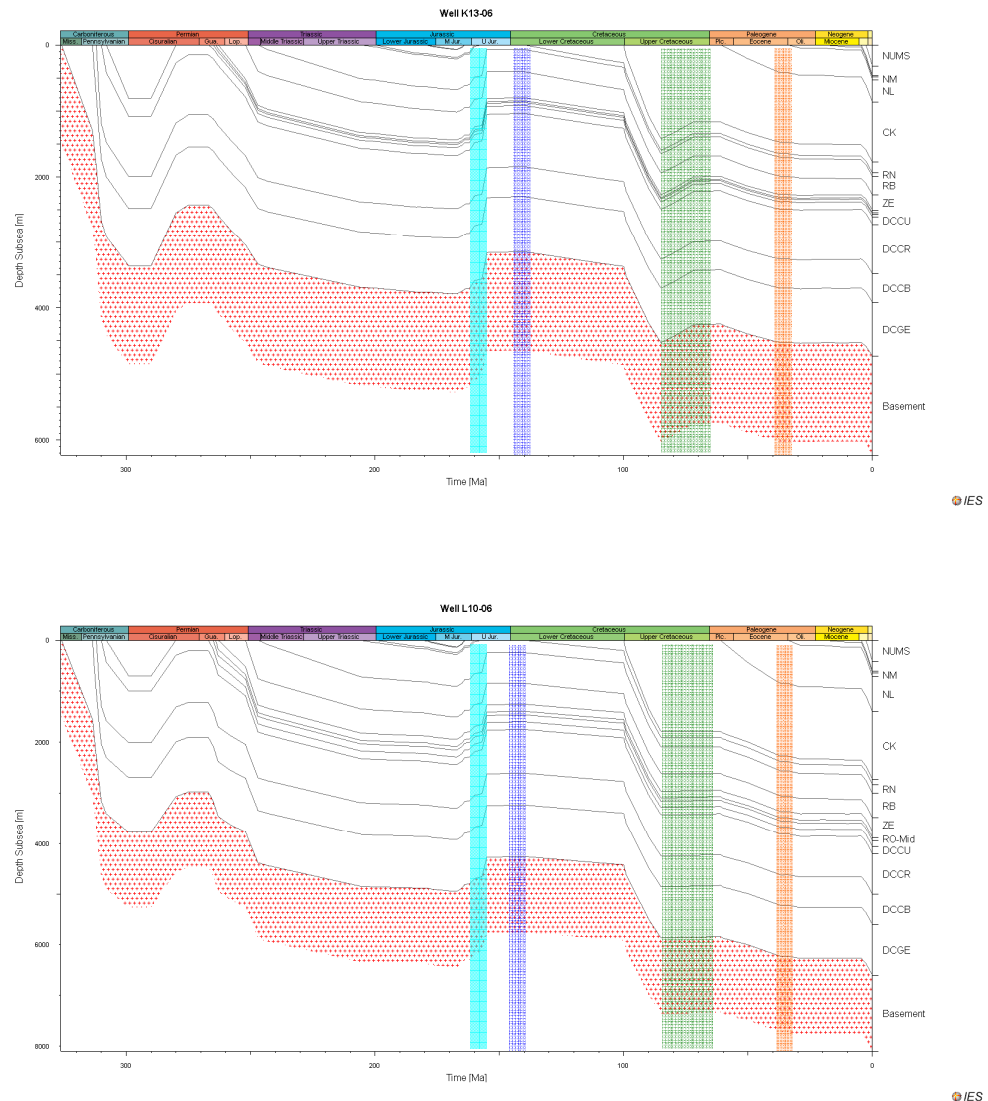


Figure 53: The burial history of well K13-06 and well L10-06 located in the platforms.

Both burial histories show that only the Late Kimmerian I phase affected the platforms in the area. This event resulted in the erosion of the entire Lower and Mid Jurassic from the platforms. No Upper Jurassic sediments (of the Schieland Group) were deposited in the platforms on a large scale. The Late Kimmerian II phase therefore is not reflected in the burial history. Relatively thick sections of the Rijnland are deposited on the platforms. However, high thicknesses of the Chalk Group are observed in the burial histories.

The Chalk Group was partly eroded during the Subhercynian-Laramide erosion event. The amount of eroded Chalk in the platforms is less than that eroded in the basins and the platforms preserve a thick Chalk section at present-day (Figure 53).

The burial histories also indicate that the Pyrenean uplift did not have a significant impact on the platforms. Not much sediments seem to have been removed by erosion from the Palaeogene sections during the Pyrenean event.

The Saalian event seems to have affected the platforms as it was the case in the other parts of the study area.

The deepest burial of the sediments seem to be reached at present-day in the platform areas.

4.2 Maturity and hydrocarbon generation history

The present-day maturity of each of the main source rock units are presented and discussed below. The maturity and temperature evolution of each of the source rocks is discussed in 1D extractions at the location of different wells from the area. The transformation ratios of the main source rock units are also discussed below. The transformation ratio is the ratio of generated petroleum to potential petroleum in a source rock. The transformation ratio provides information on the timing of hydrocarbon generation and level of maturity and organic matter consumption within the source rock units. The calculation of the transformation ratio is based on the Pepper and Corvi (1995)_TII and TIII kinetic model for the Carboniferous and Jurassic source rocks.

The Namurian Unit

The present-day maturity of the Namurian is shown in Figure 54. The figure shows high maturity of the Namurian over the area (V_r 2-4 %Ro). The maturity increases in the central part of the BFB ($V_r > 4$ %Ro). The distribution of the maturity in the Namurian does not seem to be related to specific structural units. Within the same structural unit there appears to be variations in maturity. Modelled hydrocarbon zones, using the Pepper & Corvi (1995) TII kinetics, of the Namurian indicate that the Namurian is overmature at present day (Figure 54).

The history of maturity and transformation ratio of the organic material in the Namurian in a selection of 1D extractions (6 extractions) are presented in Figure 55. The extractions location is selected to represent the major tectonic elements as well as areas with different maturity level. The figure shows that the majority of the area has reached its present-day status in the Upper Cretaceous. This is not the case in the western part of the WNB (well P12-01), which reached the highest maturity in the Lower Cretaceous (Figure 55). The figure also shows that the area entered the gas window (> 1.3 %Ro) already in late Permian. As explained before, the major maturity events are related to the deepest burial before major erosion events. The transformation ratio in the well extractions indicates that, starting from the Upper Cretaceous, all the organic matter has been transformed to hydrocarbons. In most of the extractions (except for well P12-01), almost 85 % of the organic material was transformed into hydrocarbons already in the Permian. The transformation witnessed another small peak in the Jurassic. The Namurian is therefore in the whole area in an overmature state and no hydrocarbons are currently generated in this source rock (Figure 54).

The Baarlo Formation

The present-day maturity of the Baarlo shows high maturity in most of the area (V_r 2-4 %Ro) (Figure 56). Higher values of vitrinite reflectance are observed in the central part of the BFB. The surrounding platforms show relatively lower maturity (V_r 1.3-2 %Ro). The Baarlo formation is overmature in most of the study area

(Figure 56). Only in some locations on the margins of the study area, the Baarlo is still in the gas window. The hydrocarbon generation zones are modelled using the Pepper & Corvi (1995) TIII kinetics.

The 1D extractions at the location of the 6 wells shows that the formation reached its present-day maturity status in the Upper Cretaceous (Figure 57). As in the Namurian, the first maturity peak was in the Lower Permian and the second significant maturity phase started in the Lower Jurassic just to reach the peak in the Upper Cretaceous. The transformation ratio of the well extractions also reflects the maturity history of the formation (Figure 57). It shows that in some places, the maturity and the transformation of the organic matter is still going on. In the central part of the BFB and the western platform area (well K13-14), all the organic matter has been consumed and thus the Baarlo is overmature.

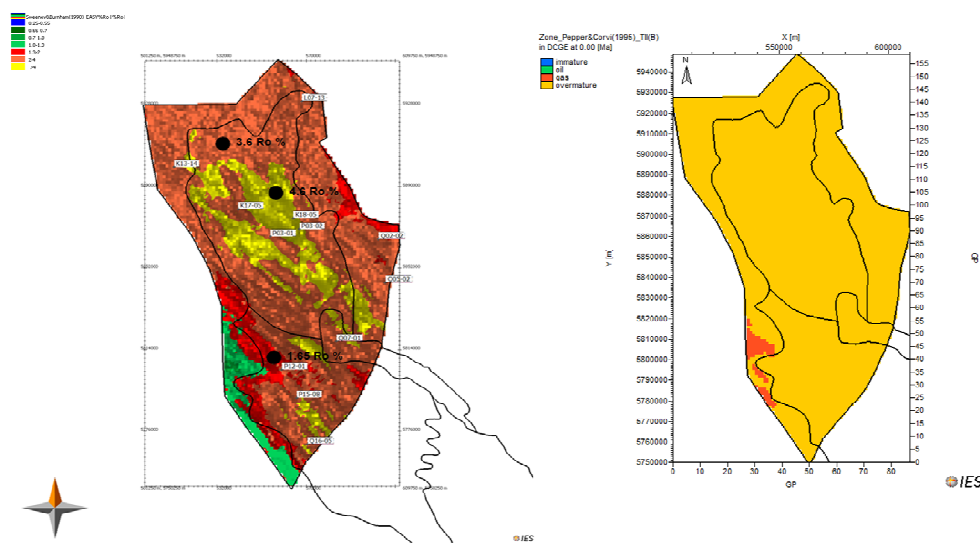


Figure 54: Left: Present-day maturity of the Namurian Unit in the study area. The Locations of the well extractions are also indicated on the map. Right: Hydrocarbon generation zones of the Namurian.

The Ruurlo Formation

The modelled present-day maturity of the Ruurlo formation shows lower values than Baarlo and the Namurian unit. Higher maturity values (Vr 2-4 %Ro) are modelled in most of the basin areas (BFB and WNB) (Figure 58). Modelled maturity in the surrounding platforms are considerably lower (Vr 0.5-1.3 % Ro). The model show that Ruurlo formation is overmature in the basins area (BFB, WNB) (Figure 58). Parts the West Netherlands Basin are still in the gas window. Areas surrounding the basins are in the gas window (Figure 58). The hydrocarbon generation zones for the Ruurlo formation are modelled using the Pepper & Corvi (1995) TIII kinetics. Maturity history at the location of the 6 well extractions show similar maturity pattern as in the Baarlo Formation. Maturity started in the Lower Permian and increased during the Permian and Triassic (Figure 59). The second maturity pulse is modelled in the Lower Jurassic just to reach the present-day maturity in the Upper Cretaceous. History of transformation ratio in the well extractions show that, except for well K18-05 in the central part of the BFB, the area is still capable of hydrocarbon generation. This is because the model indicates that not all of the convertible organic material in the source rock has been consumed during previous maturity events. Transformation of the transformable organic matter went parallel

with the maturity evolution of the Ruurlo. Most of the transformation of the organic matter took place during the Jurassic and the Cretaceous.

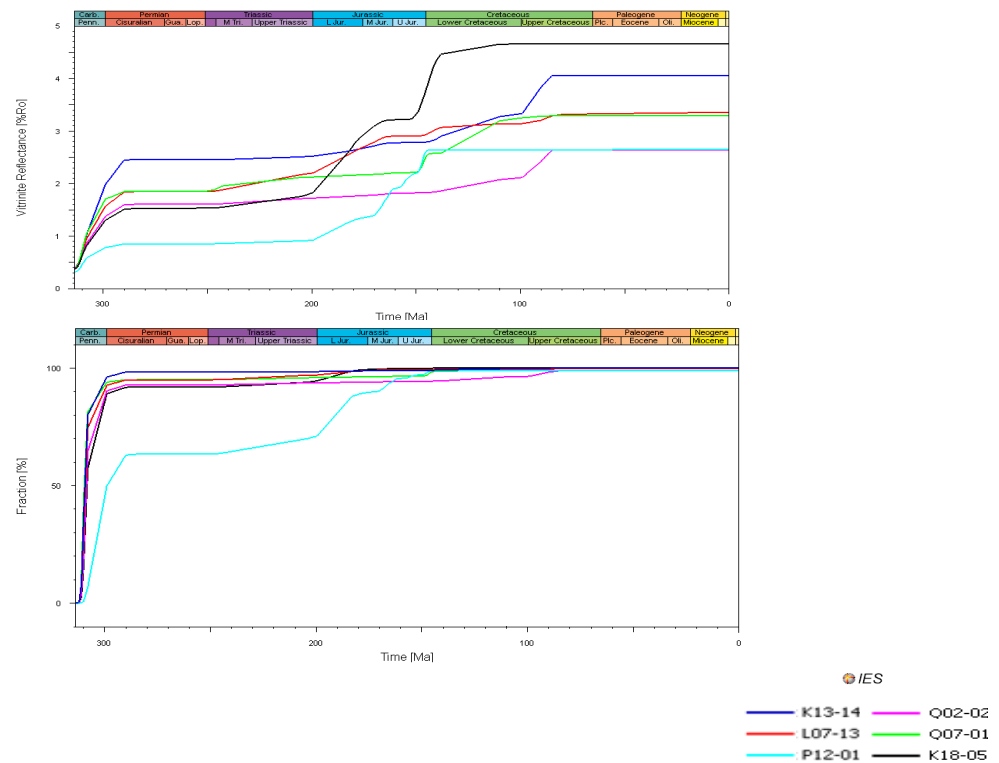


Figure 55: History of maturity (top) and transformation ratio (bottom) of the Namurian in 6 well extractions. Location of the well extractions are shown in Figure 54.

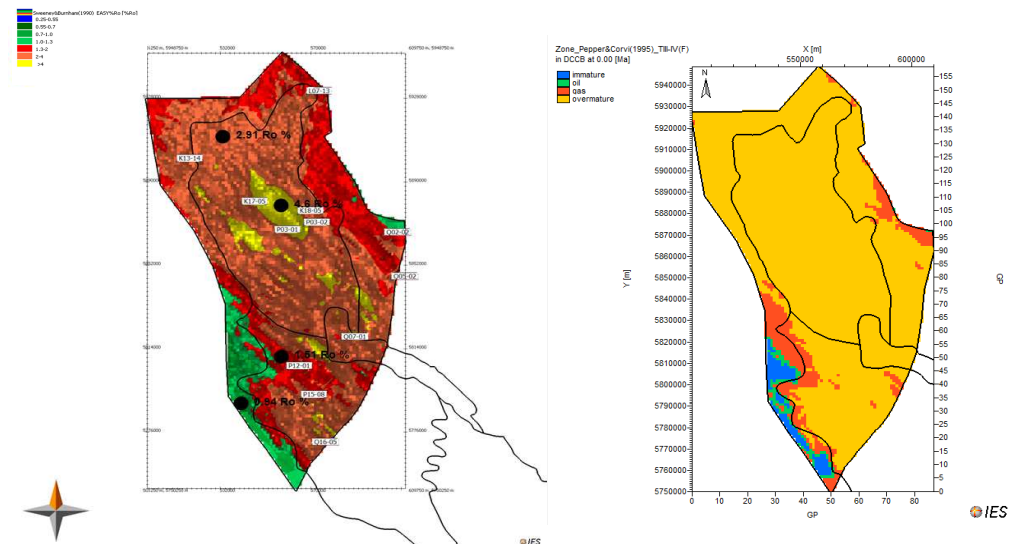


Figure 56: Left: Present-day maturity of Baarlo in the study area. The Locations of the well extractions are also indicated on the map. Right: hydrocarbon generation zones of the Baarlo formation.

The Maurits Formation

The modelled present-day maturity in the remaining parts of the Maurits Formation shows some similarity with the Ruurlo Formation (Figure 60). Higher maturity is modelled in the BFB (Vr 2 – 4 % Ro). The platform areas show lower maturity at present-day. The model show that Maurits is overmature at present-day in the Broad Fourteens Basin and it is gas generating from the surrounding areas (Figure 60).

The maturity and transformation ratio history of 5 well extractions, show large similarities with the maturity history in the Ruurlo Formation (Figure 61). In most of the wells, the present-day maturity was reached in the Upper Cretaceous. In the well extraction from the WNB (Q16-05) however, the present-day maturity was reached in the Upper Jurassic.

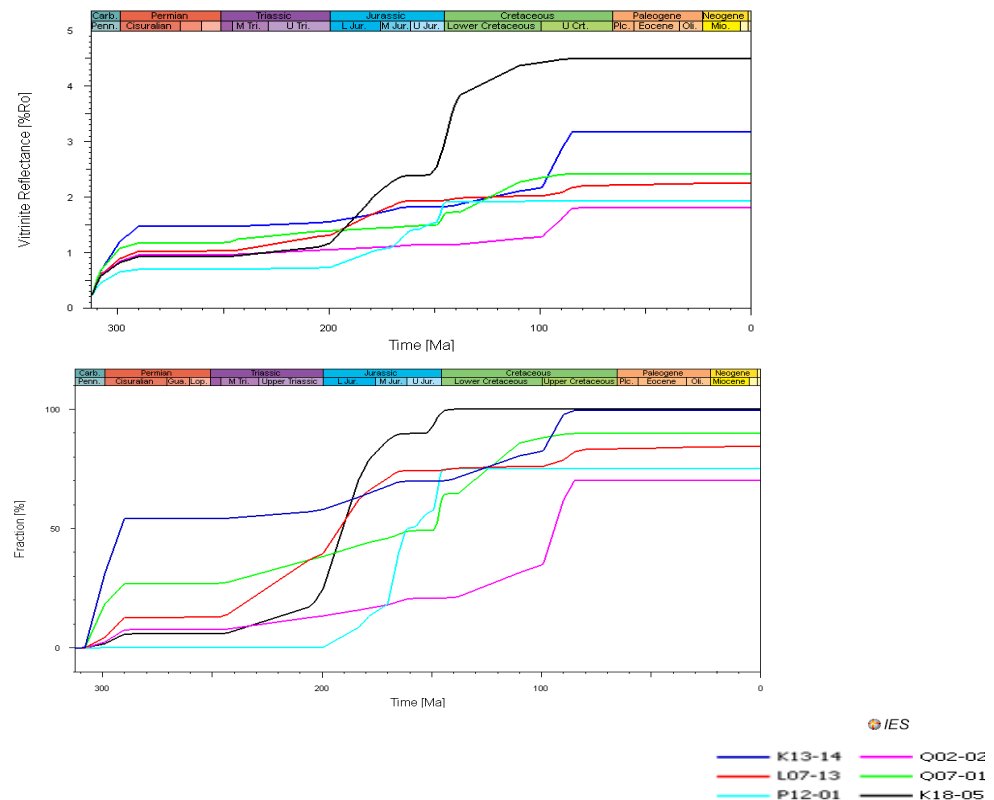


Figure 57: History of maturity (top) and transformation ratio (bottom) of the Baarlo Formation in 6 well extractions. Location of the well extractions are shown in Figure 51-1

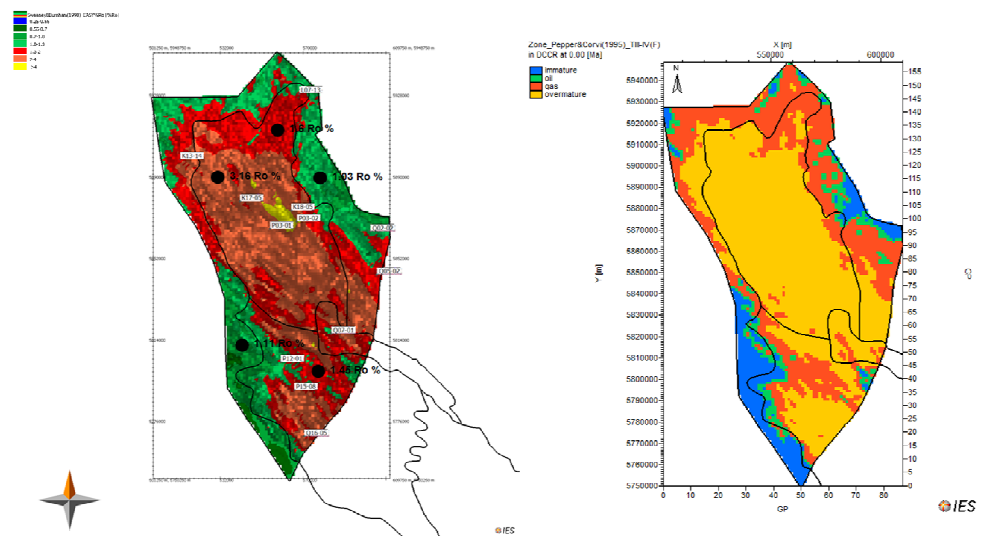


Figure 58: Left: present-day maturity map of the Ruurlo Formation in the study area. The locations of the well extractions are also indicated on the map. Right: hydrocarbon generation zones of the Ruurlo formation.

The Aalborg Formation

The Jurassic Aalborg Formation is found at present-day in the basin area, particularly the BFB and WNB. The modelled present-day maturity ranges in most of the formation between V_r 0.55 and 1.3 %Ro (Figure 62). Modelled hydrocarbon zones, using the Pepper & Corvi (1995) TII kinetics, shows some variations. While most of the formations appears to be in the oil window, it has reached the gas and the overmature phases in the central parts of the Broad Fourteens Basin (Figure 62).

The history of source rock maturity at the location of 6 well extractions show that maturity started in different places at different ages. In some parts of the BFB, maturity started already during the Middle Jurassic (well K17-05). Lower Cretaceous witnesses an increase in maturity especially in the BFB. In that area, the formation reached its present-day maturity (in the oil window) in the Upper Cretaceous (Figure 62). Similar to the Carboniferous source rocks, the Aalborg Formation showed an increase in maturity over the whole area during the Upper Cretaceous.

The history of transformation ratio shows that in the wells where the source rock is overmature, great deal of the organic matter has been transformed. In the rest of the wells, the source rock is still able to generate hydrocarbon as around 50% of the transformable organic matter has been transformed into hydrocarbon (Figure 63).

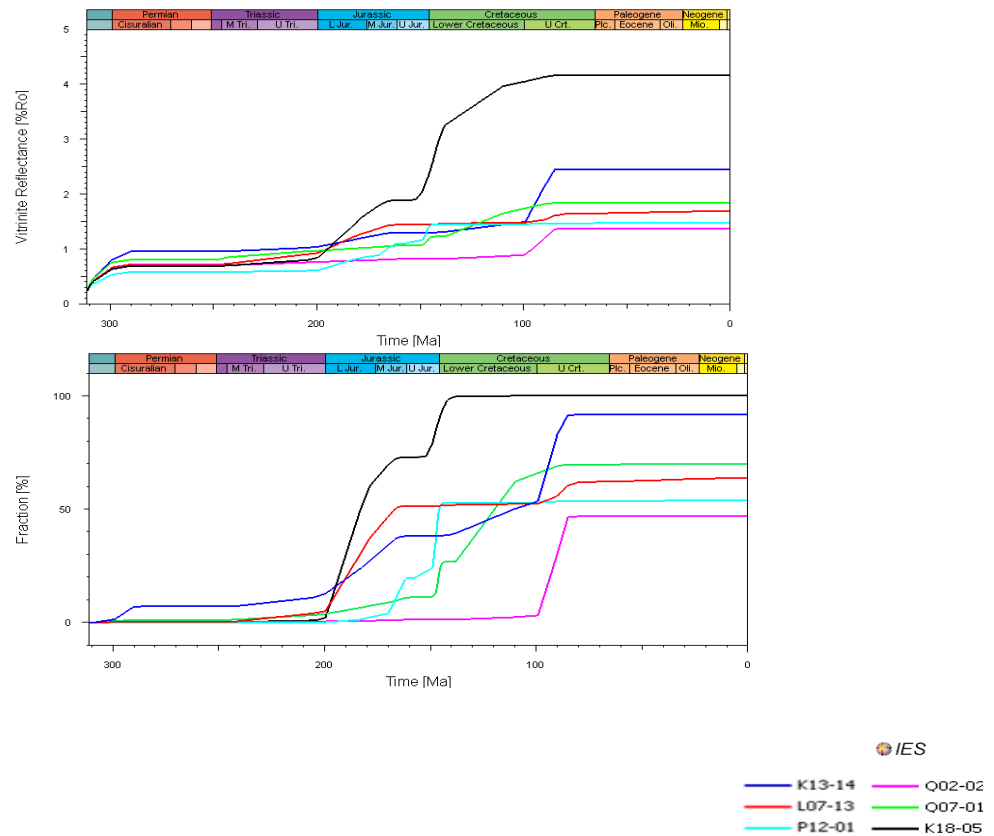


Figure 59: History of maturity (top) and transformation ratio (bottom) of the Ruurlo Formation in 6 well extractions. Location of the well extractions are shown in Figure 58.

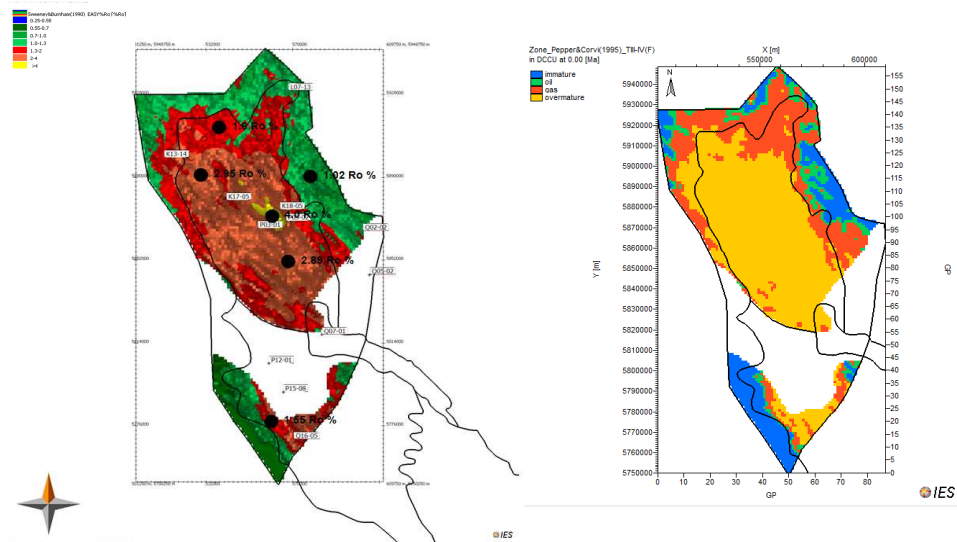


Figure 60: Left: present-day maturity map of the Maurits Formation in the study area. The locations of the well extractions are also indicated on the map. Right: hydrocarbon generation zones of the Maurits formation.

The Posidonia Formation

Our model shows that the Jurassic Posidonia Formation is predominantly in the oil window. The maturity generally ranges between V_r 0.55 -1.3 %Ro (Figure 64). Only in small patches in the BFB the Posidonia has entered the gas window.

The history of source rock maturity at the location of 3 well extractions show that, as in the Aalborg Formation, the maturity started already in the Upper Jurassic. The maximum maturity was reached in the Upper Cretaceous (Figure 65). Only in the area where the source rock is overmature, the transformation ratio is almost 90 %. In the rest of the area, the source rock is still able to generate hydrocarbons. Most of the transformation and therefore hydrocarbon generation took place during the Cretaceous.

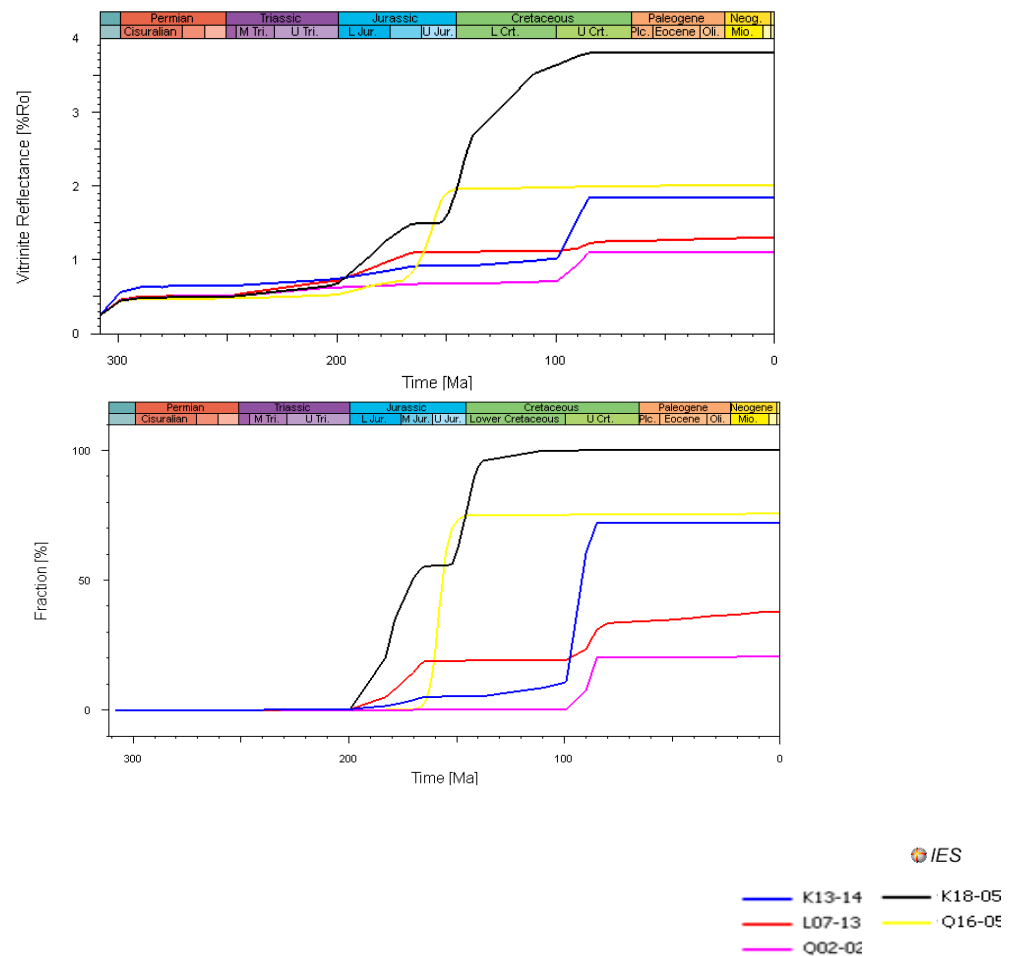


Figure 61: History of maturity (top) and transformation ratio (bottom) of the Maurits Formation in 5 well extractions. Location of the well extractions are shown in Figure 60.

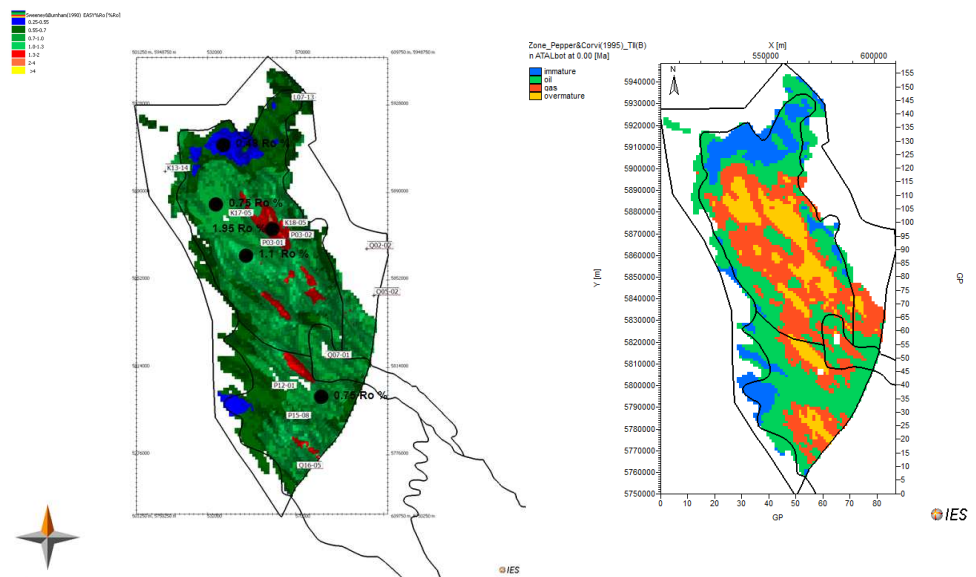


Figure 62: Left: present-day maturity map of the Aalburg Formation in the study area. The locations of the well extractions are also indicated on the map. Right: hydrocarbon generation zones of the Aalburg formation.

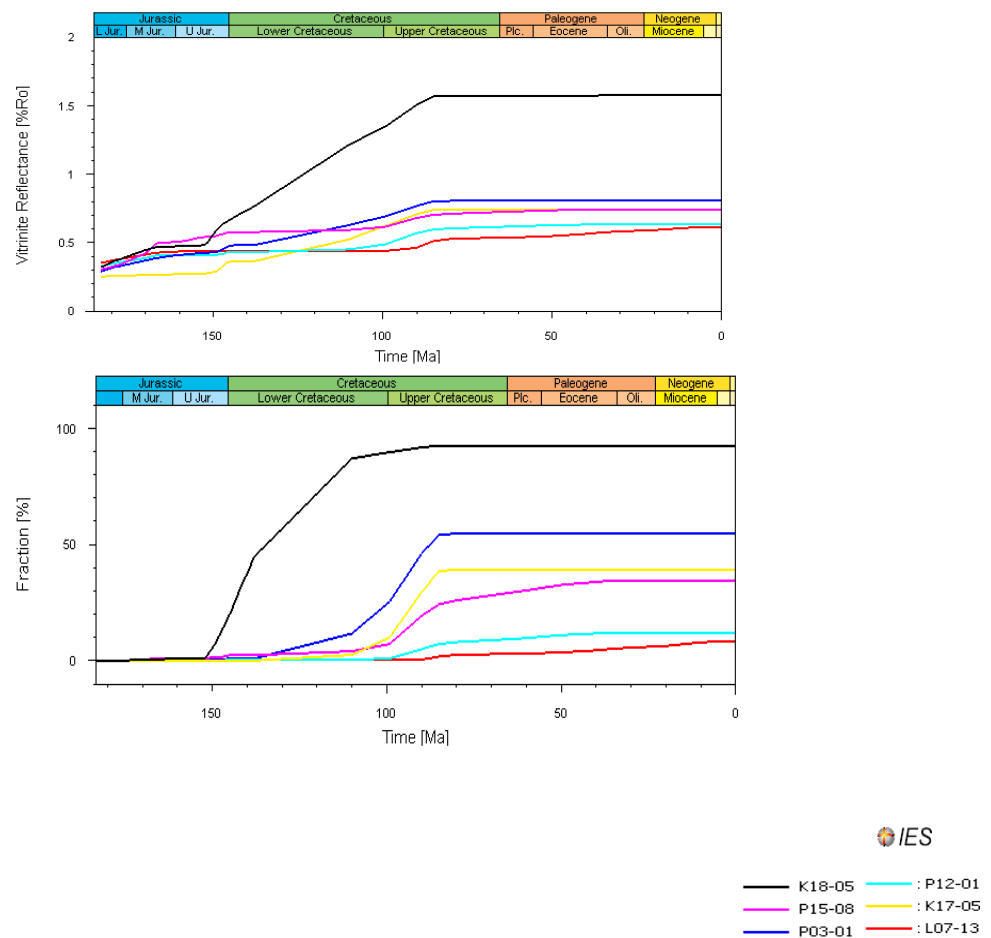


Figure 63: History of maturity (top) and transformation ratio (bottom) of the Aalburg Formation in 5 well extractions. Location of the well extractions are shown in Figure 62.

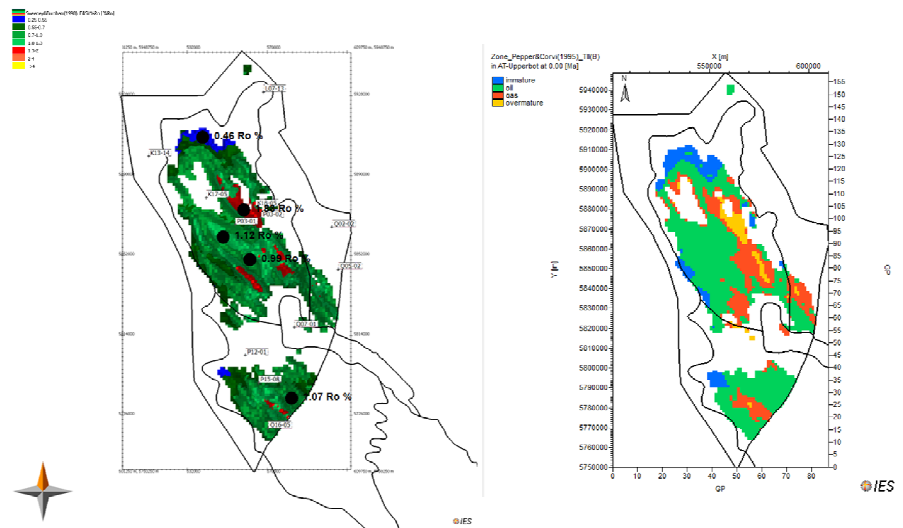


Figure 64: Left: present-day maturity map of the Posidonia Formation in the study area. The Locations of the well extractions are also indicated on the map. Right: hydrocarbon generation zones of the Posidonia formation.

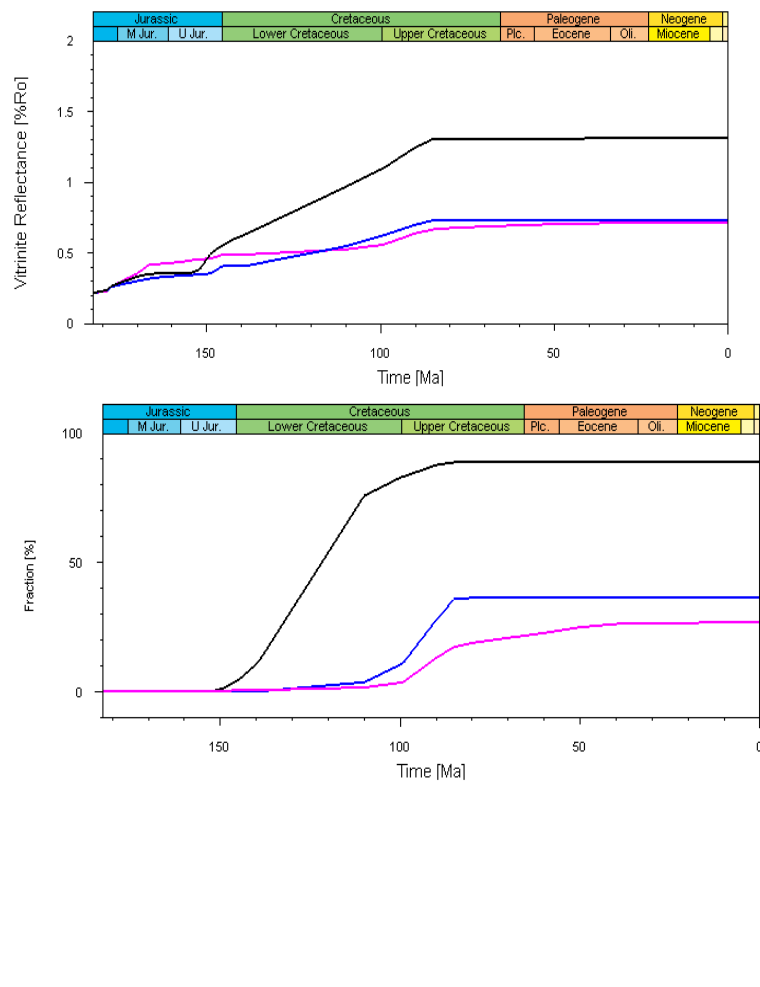


Figure 65: History of maturity (top) and transformation ratio (bottom) of the Posidonia Formation in 3 well extractions. Location of the well extractions are shown in Figure 64.

5 Discussion

5.1 Temperature, burial history and maturity

The maturity history of the source rocks is related to the evolution of the thermal regime in the basin. The relationship between burial history, temperature and maturity is demonstrated in two well extractions from the BFB (well P03-01) and the WNB (well P09-02). Two source rocks are discussed, the Ruurlo Formation from the Westphalian and the Posidonia Formation from the Jurassic. Figure 66 shows maturity and temperature evolution of two source rocks at the location of well P03-01 in the BFB.

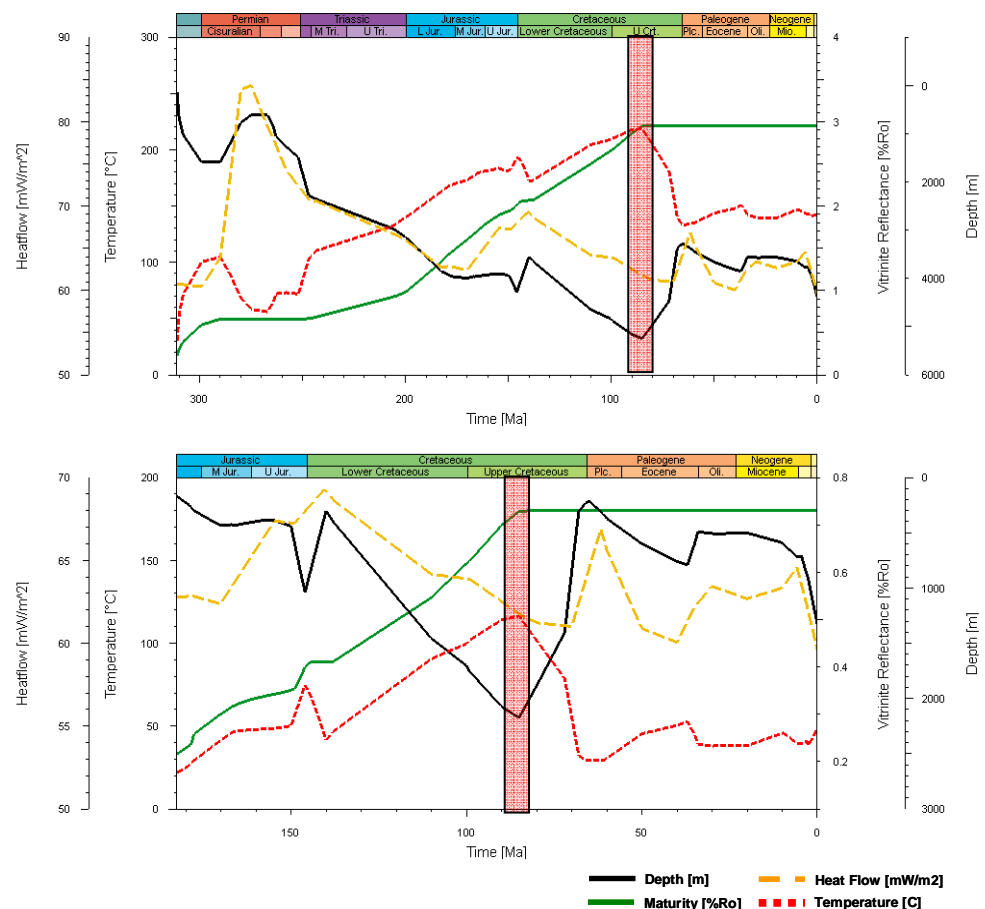


Figure 66: Maturity, temperature, burial and heat flow evolution at the location of well P03-01 (Broad Fourteen Basin) for the Ruurlo Formation (top) and the Posidonia Formation (bottom).

The figure shows that the maximum maturity, reached in the Upper Cretaceous, is associated with a peak in temperature. The maximum temperature in the Upper Cretaceous is related to the burial of the formation which is at its maximum value in the Upper Cretaceous (Figure 66). No heat flow peaks are observed in the Late Cretaceous. Some increase in heat flow is noticed during the Palaeocene. The maximum burial and thus maturity of both source rocks takes place during the subsidence of the basin and prior to the Later Cretaceous inversion event (Laramide – Subhercynian: 85 – 61 Ma) (Figure 66).

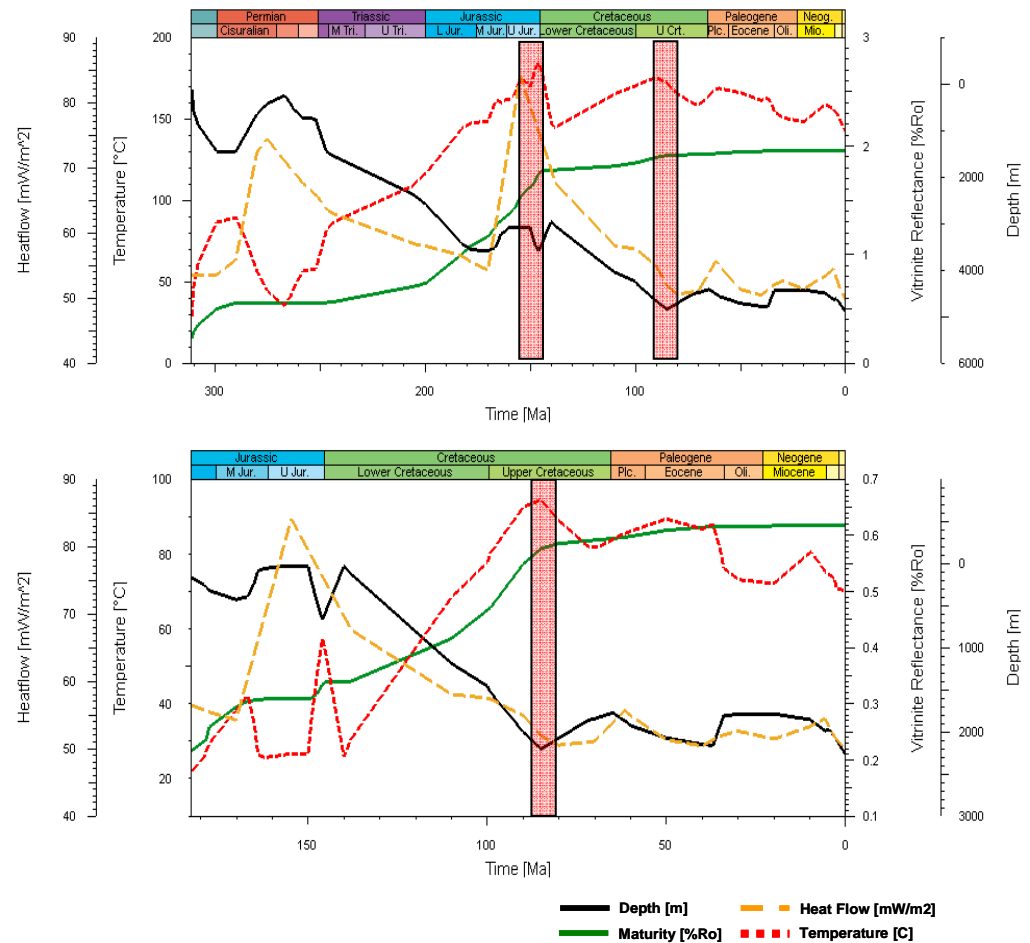


Figure 67: Maturity, temperature, burial and heat flow evolution at the location of well P09-02 (West Netherlands Basin) for the Ruurlo Formation (top) and the Posidonia Formation (bottom).

The temperature evolution of the Ruurlo Formation in well P09-02 (in the WNB) shows that the temperature peak (and the associated maturity peak) is reached in the Upper Jurassic and Lower Cretaceous (Figure 67). The temperature peak is caused mainly by the heat flow peak rather than the deep burial of the layer. The heat flow peak is related to the Late Kimmerian doming and uplift event that was associated with magmatic and underplating activities. The Posidonia Formation reached a temperature peak in Upper Cretaceous which caused an increase in maturity. The temperature peak is related to the deep burial of the formation during the Upper Cretaceous rather than any heat flow peaks (Figure 68).

5.2 Heat flow calibration

The applied heat flow values are based on the calibrated data (maps) that are originally interpolated between a number of 1D heat flow models. Relatively high heat flow values are observed in the calibrated models during certain geological ages. This was especially the case in the WNB and the Zandvoort Ridge, where high heat flow values are modelled during major heat flow peaks (Late Permian and Upper Jurassic). The calibrated heat flow values were resulted from fitting the models with measured temperatures in the wells. High

temperatures and vitrinite reflectance values were measured in many wells in the area which requires high heat flow value to achieve a good fit. The quality of the calibration data (temperature and vitrinite reflectance) is a major source of uncertainty that could lead to unrealistic calibration. The quality of the data was assessed before the selection of calibration data. Some criteria were considered in the selection, such as the type of temperature measurement (corrected bore hole BHT and DST temperatures) and the source of vitrinite reflectance data. Nevertheless, there is still a possibility that some unrealistic measurements are present and used in the calibration process. This is especially valid for the vitrinite data where chance of contamination is present even when the measurement itself is reliable.

The observed high temperature and vitrinite data can be caused by processes within the basin that are not taken into account in our model. This includes for example, heat transfer by convection and magmatic activities. Anomalous temperatures can be caused by circulating fluids in the basin which might transfer heat from deeper levels to shallower strata. This is quite likely in areas with faults and displacements that act as corridors for heat through strata. The West Netherlands Basin is known for deep and intersecting faults that are related to various tectonic activities and ages. The observed high temperatures can therefore be related to these deep faults and the related thermal activities. Since the convection heat circulation is not included in our model, neither are any hydrodynamic aspects, their possible influence on the temperature is neglected in our model.

The other factor that might have caused anomalously high temperatures and vitrinite reflectance is magmatic activities during various geological ages. There have been many indications to magmatic activities (intrusion as well as extrusions) in the region (see for example: van Bergen and Sissingh, 2007). Magmatic processes are taken into account in our model as major tectonic activities that caused, for example, underplating and volcanism. Their influence on the heat flow model was included during heat flow modelling (see above). However, the local impact of such activities (intrusions or volcanism) on maturity is not included. Wells that are located in the vicinity of a magmatic intrusion such as sill, a pluton or a dike, are likely to show high maturity, especially in the formations adjacent to the intrusion. Consequently, the observed vitrinite reflectance in such a well will not be reproducible by simple tectonic heat flow and maturity models. In our study area, igneous rocks have been documented in many wells, especially in the Zandvoort Ridge (Van Bergen and Sissingh, 2007).

The effect of the intrusions on the maturity is not taken into account in our model. Nonetheless, anomalous vitrinite reflectance, which might have been caused by local intrusions, are sometimes used to calibrate the heat flow if quality of the data is reliable. Consequently, fitting such measurements has sometimes resulted in higher heat flow models which can not be explained by our tectonic models.

5.3 Source rock maturity

The modelled maturity of the Limburg Group as well as the Namurian shales appear to have reached its maximum values prior to the Subhercynian inversion event. This is where the formation reached their deepest burial and therefore the highest temperatures.

The formations underwent an increase in maturity during the main syn-rift phases in the Jurassic. The model shows that Carboniferous formations in general are

overmature with the most inverted parts of the Broad Fourteen Basin showing the highest maturities. The formations are still in the gas window in some places, especially in the surrounding platforms. Westphalian source rocks in the BFB entered the gas window in the Jurassic and reached their present-day maturity in the late Cretaceous. Verweij et al. (2003) has shown that the Limburg Group source rocks generally entered the gas window during the rift phase and prior to the Late Cretaceous inversion. Some variations in the degree of maturity and the age of maturity has also been observed in the BFB by Verweij et al. (2003).

Van Balen et al. (2000) modeled hydrocarbon generation in the onshore part of the WNB. The results can be compared with the maturity models in the onshore WNB in this study. Van Balen et al. (2000) showed that the timing of generation from Westphalian source rocks in the WNB is 240 Ma and the at 160 Ma. In some areas the generation continued until now. Some variations in the maturity were observed in the offshore parts of the WNB. The variations were attributed to differences in burial depths in different location (Van Balen et al., 2000). Although these studies are limited to 2D sections and do not cover the whole study area, they do agree with the results of our models.

Jurassic source rocks (Aalburg and Posidonia formations) seem to have been affected by the Upper Cretaceous post-rift maturity pulse. Over the whole basin area, both formations appear to be in the oil generating window, except for small patches that seem to be in the gas window. Variations in original thicknesses and burial histories are the main cause for maturity variations in area. the models shows that Jurassic source rocks started to generate hydrocarbons already during the Kimmerian syn-rift phase. The maturity increased with the rifting and thus the burial and level out during the inversion phase. In the southern part of the BFB and in the WNB, maturity reached the present-day values after the Upper Cretaceous inversion and during the Later Paleogene and the Neogene.

The maturity pattern of the Jurassic formations in this model is generally consistent with that modelled in previous studies (Verweij, 2003; van Balen et al., 2000). Maturity modelling by Verwije et al (2003) of the Posidonia Shale and the Aalburg Formation along across section in the BFB revealed similar results. Their modelling revealed that there was major generation of oil from Jurassic source rocks during post-rift times prior to the inversion. In some places, oil generation continued until the Palaeogene. Most of the oil generation took place in the central part of the BFB prior to the inversion (Verweij et al., 2003). Van Balen et al (2000) demonstrate that the generation of hydrocarbons from Jurassic source rocks in the onshore part of the WNB started in Later Jurassic-Early Cretaceous. This is in agreement with the modelling results from the offshore part of the WNB.

5.4 Migration and trapping

Although the purpose of this study is not to assess the migration and trapping, the timing of maturity can provide insights into the trapping possibilities and possible accumulations. For all major source rocks, the most important maturity phase is prior to the inversion. During the Subhercynian inversion it is likely that many faults came to existence and/or were re-activated. Trapping structures have also been formed during this event. Although these tectonic activities might have helped in trapping the generated hydrocarbons, the faults might have contributed to escaping the generated hydrocarbons. However, the model shows that parts of the source

rocks have not reached an overmature status yet and maturity continued after the inversion. It also shows that since the Cretaceous, there have been enough organic matter in the source rock to generate hydrocarbons. This can clearly be seen in the transformation ratio of the source rocks in different locations (Figures 55,57,59,61,63). It is therefore likely that some of the traps, which were created during the Subhercynian inversion, were charged by hydrocarbons that are generated in the Tertiary later during the Tertiary.

The Namurian, however, seems to have consumed more than 85% of its organic content already in the Permian. In the Jurassic, most of the organic matter in the Namurian was consumed. The Namurian was therefore overmature and no substantial amount of hydrocarbons were generated ever since the Jurassic. Hydrocarbons that were generated during that phase might have escaped in later geological events. During the Upper Cretaceous, the remaining of the organic matter in the Namurian were finally transformed to hydrocarbons. This might have contributed to the charging of the traps in later phase. However, the amount of generated hydrocarbons in the Cretaceous must have been limited and it was probably not sufficient to charge all the reservoirs.

Commercial oil accumulations are found in the Vlieland Sandstone Formation (Rijnland Group) and the Delfland Subgroup (Schieland Group) in mainly faulted anticlines that formed during the Late Cretaceous inversion. Main oil fields in the area are located within the basins (BFB and WNB) where the oil prone Jurassic source rocks are present. The source rock of the oil accumulations is the Posidonia and the Aalborg Shale Formation (Altena Group).

The generation of oil was accelerated during the pre-inversion phase. According to Verweij et al. (2003) the expulsion of oil from the deepest parts of the Posidonia started in the early Cretaceous. The post-rift phase in the late Cretaceous, is the main period of oil expulsion in the central part of the basin. In the southern parts of the basin, expulsion started after the inversion and in the Palaeogene. Charging of present-day accumulations in the Vlieland Sandstone Formation and the Delfland Subgroup took place after the Subhercynian inversion. While some of the charging is related to direct migration from the source rocks, other accumulations were charged by remigration of oil from pre-inversion accumulations (Verweij et al., 2003). Van Balen et al. (2000) indicate that oil filling of anticlinal structures in lower Cretaceous sandstones in the WNB started after the Subhercynian inversion phase.

Major gas accumulations are present in the Slochteren Formation (Upper Rotliegend Group), the Main Buntsandstein Subgroup (Lower Germanic Trias Group) and in the Zechstein Carbonate Member.

The main phase of gas generation from the Limburg Group is during the early Cretaceous pre-rift phase. Peak expulsion of gas in the BFB occurred in the Cretaceous pre-inversion times (Verweij et al., 2003). Gas accumulations in the Slochteren Formation and the Main Buntsandstein Subgroup were charged during the pre-inversion phase (Verweij et al., 2003). The inversion probably caused re-migration of gas in the reservoir. Modelling results from onshore West Netherlands Basin showed that the filling of gas reservoir from Limburg Group started in the Lower Cretaceous and during the pre-rift phase (Van Balen et al., 2000). The filling was completed prior to the inversion phase. Judging from the generation models, it is likely that the filling of gas reservoirs in the offshore WNB happened at similar times as in the onshore.

Most of the gas discoveries are located along the margins of the major tectonic elements and in the platforms (Figure 3). This might be attributed to the maturity status of the source rocks in the platforms especially for the gas prone Carboniferous formations. The effect of the faults in the area on the hydrocarbon accumulations is not covered in this study and faults were not included in the model.. A more detailed study that includes the faults and their properties as well as a complete migration simulation is required for that.

6 Conclusions

A 4D basin modelling study was conducted on the NCP-2F area. This is part of the large-scale mapping project of the Dutch offshore. The study aimed at evaluating the maturity history of the major source rocks in area. It also aimed at developing and evaluating new erosion scenarios for the major erosion intervals.

The NCP-2F area is a complex area with different tectonic elements and structures including basins, platforms and highs. In addition to that, the area has gone through several tectonic events including uplift, extension, inversion, magmatism as well as salt tectonic.

Our model consisted of 24 layers including the basement. Some sub-layers were created in order to include different facies within some layers. The thicknesses of the layers were generally based on seismic and well interpretations. Carboniferous formations were derived from a subcrop map that was based on well data.

Six source rock formations were defined in the model. In addition to the oil prone Namurian Unit, three more gas prone source rocks were defined in the Carboniferous (Baarlo, Ruurlo and Maurits). Two formations were defined as oil prone source rock in the Jurassic; the Aalburg and the Posidonia formations.

- *Heat flow maps*

A number of heat flow maps were modelled and used for maturity analysis in this study. The heat flow maps, 18 maps in total, represent the evolution of heat flow through geologic times from 326 Ma to present day. The maps were initially interpolated between 6 1D heat flow models at the location of 6 wells (Annex V). The 1D heat flow models were calculated based on tectonic models. The interpolated heat flow maps were later calibrated with measured temperatures and vitrinite reflectance in a number of wells over the whole area. The new generated heat flow maps were used for the following analysis.

- *Erosion scenarios*

Several erosion scenarios were discussed and evaluated. New erosion maps were generated and used for basin analysis and maturity modelling.

The initial erosion thicknesses were assumed based on stratigraphic data and paleogeographic concepts from the area. The maturity models, based on the introduced erosion thicknesses, were compared to measured maturity data (vitrinite reflectance) for calibration purposes. Through various scenarios the initial erosional thicknesses were refined for different layers so that a better fit could be achieved. In addition to erosion thicknesses, the erosional and geological model that outlines the erosional phases were also modified and discussed in various scenarios.

The initial geological model comprised four erosional phases, the Saalian, the Late Kimmerian, the Subhercynian-Laramide and the Pyrenean. During the Late Kimmerian erosion, the Jurassic as well as the Upper Triassic Group were eroded. In the Subhercynian-Laramide, the Chalk and the Rijnland Groups were eroded. The Pyrenean erosion phase eroded parts of the Lower North Sea Group. The calibration process with selected vitrinite reflectance measurements form a

selection of wells resulted in refined thickness of the erosional thicknesses of the Chalk Group.

Based on a subcrop map of the Cretaceous and Jurassic formations, a new scenario was developed where the Schieland Formation is entirely eroded during the Subhercynian inversion phase. It was proposed that the inversion event in Later Cretaceous in the central part of the BFB cut deep in the sediments to reach the Upper Trias. Jurassic formations therefore were eroded in two phases, the Late Kimmerian and the Subhercynian-Laramide phases. In a different scenario, the upper part of the Schieland Group (together with great parts of the Altena Group) was eroded during the Late Kimmerian event. The lower part of the Schieland Group in the centre of BFB (with the underlying Altena Group at that location) were eroded during the Subhercynian inversion phase. New erosion maps of the main intervals were generated through calibration with measured maturity data in a selection of wells.

Based on new stratigraphic data and a more refined formation ages, a new erosion scenario was introduced. This scenario, aimed at modifying the burial depth of the formations so that the maturity model is adjusted. It also considered the stratigraphic and paleo geographic concepts from the area which affected the depositional thicknesses of the formations. In this scenario, five erosion phases were introduced. The Kimmerian erosion phase was divided into two phases, the Late Kimmerian I and the Late Kimmerian II. In the Late Kimmerian I, parts of the Altena Group was eroded, especially at the platforms and in the basins. During the Late Kimmerian II, the Schieland Group was eroded in almost the whole area. In the central part of the BFB, the Schieland was preserved together with the underlying Altena formations. During the Subhercynian inversion the Cretaceous formations were eroded as well as the remaining patches of Schieland and Altena Groups in the central part of the BFB.

The calculated temperature and maturity based on this scenario showed acceptable fit with measured data at a number of wells. Besides, the latest erosion scenario was more consistent with the new stratigraphic interpretations. Therefore, this scenario was implemented for maturity and hydrocarbon generation modelling and evaluation of the major source rocks in the NCP-2F area.

- Erosion maps

As a result of the erosion scenarios, a number of erosion maps were generated and used for later basin and maturity modelling in the area.

Four erosion maps of the Carboniferous Formations were generated. These maps included, the erosion maps of the Baarlo Formation, the Ruurlo Formation, the Maurits Formation and the Hunze Subgroup (Annex VII). The erosion thicknesses of the Carboniferous formation were derived from the subcrop map and the initial depositional thicknesses of the formations. The original thickness were based on the analysis of well data as well as paleo geographic models from the area. The erosion thicknesses of the Carboniferous layers were not changed in the subsequent erosion scenarios.

An erosion map of the Lower North Sea Group was generated. This map was not modified during the various erosion scenarios (Annex VII).

The various erosion scenarios has resulted in a set of refined erosion maps for the Cretaceous and the Jurassic formations. Cretaceous erosion maps included an erosion maps of the Chalk Group and the Rijnland Group. Both layers were eroded during the Subhercynian erosion phase. The Schieland was eroded in two phases, the Late Kimmerian II and the Subhercynian phase. Therefore two erosion maps were generated for the Schieland Group.

A total number of eight erosion maps were generated for the Altena Group. According to the adopted erosion scenario, the various formations of the Altena Group were eroded in three phases; the Late Kimmerian I, the Late Kimmerian II and the Subhercynian erosion phase (Annex VII). One erosion map was generated froth Upper Germanic Trias Group which was eroded in the Late Kimmerian I phase.

- Burial History

The burial history in 1D extractions from the study area reflect the main deposition and erosion phases. Variations in the amount of uplift and erosion can be seen over the whole study area.

The Saalian phase in the early Permian affected the whole study area. Some variations is in the amount of uplift and erosion is however noticed over the area.

While the Late Kimmerian I erosion phase is less present in the BFB, it appears to be more pronounced to the south and in the WNB. The Late Kimmerian I erosion has affected the surrounding platforms and the Zandvoort Ridge. The Late Kimmerian II phase is clearly seen in the basin areas (BFB and WNB). The burial histories show that the Subhercynian-Laramide phase mostly affected the BFB and some parts of the platform area. The impact of this phase in the WNB is less prominent.

In the BFB the deepest burial was reached in the late Cretaceous and prior to the inversion. To the south of the basin and in the WNB, the burial during the Cretaceous becomes comparable to present-day burial.

Similar to the Saalian erosion, the Pyrenean uplift is reflected over the whole area. Some versions in the amount of uplift and erosion in the Tertiary can be seen in the area.

Simulation results revealed that burial history has a deciding role on temperature and maturity evolution of the area. Maturity peaks are generally noticed during deep burial phases.

- Source rock maturity

The model indicates that hydrocarbon generation in the Namurian Unit started in the Permian and increased during the Jurassic rifting phases to reach the present-day status in the Upper Cretaceous. Most of its organic matter content was consumed during the Permian through hydrocarbon generation. During the Late Cretaceous, the remaining organic matter was transformed and might have contributed to gas accumulations.

For the Westphalian formations, the Jurassic and Cretaceous mark an important phase of hydrocarbon generation in the whole area. Maturity of these formations started in the Early Jurassic and experienced a jump in Late Cretaceous. While the Baarlo Formation is inertly overmature at present-day in the whole area, the Ruurlo and the Maurits formations are overmature in the basins only.. At the platforms,

both formations appear to be in the gas generating phase. The Westphalian formations in some places are still capable of hydrocarbon generation as shown by the transformation ratio of the model.

Jurassic source rocks (Aalburg and Altena formations) are predominantly in the oil window. Some small patches in the basins area are in the gas window and overmature. Jurassic source rocks appear to be immature in the northern part of the BFB. The maturity started in Late Jurassic and increased during the Cretaceous to reach a peak at Lower Cretaceous. Some increase in maturity is also observed during the Tertiary, especially in the WNB.

The maturity and the timing of hydrocarbon generation can be related to the major tectonic events and the associated structures to understand the distribution of oil and gas fields. The Kimmerian rifting and the Late Cretaceous inversion have caused faulting and folding that might have created conditions for hydrocarbon migration and trapping. Later generation phases, during the Tertiary, might have played an additional role in charging the traps in the area from various source rock units. A more detailed migration study is required for understanding the trapping and distribution of the current fields.

7 References

- Abdul Fattah, R. (trainee, 2007-2008), Van Wees, J-D, Verweij, J.M., Bonte, D., 2008. Tectonic heat flow modelling for the NCP2a area of the Dutch offshore. TNO report 2008-U-R-558/A.
- Bouw, L. & Oude Essink, G.H.P., 2003. Fluid flow in the northern Broad Fourteens Basin during Late Cretaceous inversion. *Geologie en Mijnbouw / Netherlands Journal of Geosciences*, vol. 82, no. 1, p. 55-69.
- Burnham, A.K., 1989. A simple kinetic model of petroleum formation and cracking. Lawrence Livermore National Laboratory Report UCID 21665, 11 p.
- De Jager, J., 2007. Geological Development. In: Wong, Th.E., Batjes, D.A.J. & De Jager, J. (eds): *Geology of the Netherlands*. Royal Netherlands Academy of Arts and Sciences (Amsterdam): p. 5 -26.
- De Jager, J., & Geluk, M.C., 2007. Petroleum Geology. In: Wong, Th.E., Batjes, D.A.J. & De Jager, J. (eds): *Geology of the Netherlands*. Royal Dutch Academy of Arts and Sciences (Amsterdam): p. 241 -264.
- Dirkzwager, J.B., 2002. Tectonic modelling of vertical motion and its near surface expression in the Netherlands, PhD thesis, VU-Amsterdam: 156 pp.
- Dronkert, H., and Remmelts, G. 1996. Influence of salt structures on reservoir rocks in Block L2, Dutch continental shelf. In: Rondeel, H.E., Batjes, D.A.J. & Nieuwenhuijs, W.H. (eds): *Geology of gas and oil under the Netherlands*. Kluwer (Dordrecht), 179-189.
- Duin E.J.T., Doornenbal J.C., Rijkers R.H.B., Verbeek J.W. & Wong Th.E., 2006. Subsurface structure of the Netherlands - results of recent onshore and offshore mapping, *Netherlands Journal of Geosciences - Geologie en Mijnbouw*, 85-4, pp. 245 -276.
- Geluk, M.C., Paar, W.A. & Fokker, P.A., 2007 . Salt. In: Wong, Th.E., Batjes, D.A.J. & De Jager, J. (eds): *Geology of the Netherlands*. Royal Dutch Academy of Arts and Science (Amsterdam): p. 283 – 294.
- Gradstein, F.M., Ogg, J.G. & Smith, A.G. (eds), 2004. *A geologic time scale*. Cambridge University Press: 589 pp.
- Hantschel, T., and Kauerauf, A.I. 2009. *Fundamentals of Basin and Petroleum Systems Modelling*, Springer, Verlag Berlin Heidelberg: 476 pp.
- Hooper, R.J., Goh, L.S. & Dewey, F.J., 1995. The inversion history of the northeastern margin of the Broad Fourteens Basin. In: Buchanan, J.G. & Buchanan, P.G. (eds.). *Basin Inversion*, The Geological Society of London, Special Publication, no. 88, p. 307-317.

- Huyghe, P., Mugnier, J.L., 1994. Basin inversions as a source of information for paleostress determination in the peri-Tethyan domain : an example from the Southern North Sea. In : Peri-Tethyan Platform, Roure F. (ed) Technip, 211-226.
- International Stratigraphic Chart.. 2009. International Commission on Stratigraphy << [http://www.stratigraphy.org/column.php?id=Chart/Time Scale](http://www.stratigraphy.org/column.php?id=Chart/Time%20Scale)>>
- Kombrink, H., Besly, B.M., Collinson, J.D., Den Hartog Jager, D.G., Drozdowski, G., Dusa, M., Hoth, P., Pagnier, H.J.M., Stemmerik, L., Waksmundzka, M.I. & Wrede, V., 2010. Carboniferous. In: Doornenbal, J.C. and Stevenson, A.G. (editors): Petroleum Geological Atlas of the Southern Permian Basin Area. EAGE Publications b.v. (Houten): 81-99.
- Kozur, H.W. and Bachmann, G.H. 2008. Updated correlation of the Germanic Triassic with the Tethyan scale and assigned numeric ages. *Berichte der Geologischen Bundesanstalt Wien*, 76, 53-58.
- Munsterman, D.K., Verreussel, R.M.C.H., Mijnlief, H.F., Witmans, Kerstholt-Boegehold. N., Abbink, O.A, in press. Revision and update of the Callovian-Ryazanian Stratigraphic Nomenclature in the northern Dutch offshore, i.e. Central Graben Subgroup and Scruff Group. Submitted to *Netherlands Journal of Geosciences*.
- Netherlands Institute of Applied Geoscience TNO – National Geological Survey (2004). Geological Atlas of the Subsurface of the Netherlands – onshore, TNO – NITG, Utrecht: 101 pp.
- Sekiguchi, K., 1984. A method for determining terrestrial heat flow in oil basinal areas. *Tectonophysics* v. 103, 67-79.
- Stegers, D., Mijnlief, H. 2009. Rotliegend: A 3D lithofacies model. Distribution model on the Dutch on- and offshore. TNO report. TNO-034-UT-2009-02450/C.
- Sweeney, J.J. and A.K. Burnham. 1990. Evaluation of a simple model of vitrinite reflectance based on chemical kinetics. *AAPG Bulletin*, v. 74, 1559-1570.
- Van Adrichem Boogaert, H.A. and W.F.P. Kouwe, eds, 1993 - 1997. Stratigraphic nomenclature of the Netherlands, revision and update by RGD and NOGEPA, Mededelingen Rijks Geologische Dienst, v. 50, The Netherlands.
- Van Balen, R.T., Van Bergen, F., De Leeuw, C.S., Pagnier, H.J.M., Simmelink, H.J., Van Wees, J.D.A.M. & Verweij, J.M. (2000) Modelling the hydrocarbon generation and migration in the West Netherlands Basin, the Netherlands. *Geologie en Mijnbouw / Netherlands Journal of Geosciences*, vol. 79, no. 1, p. 29-44.
- Van Balen, R.T., Van Bergen, F., De Leeuw, C.S., Pagnier, H.J.M., Simmelink, H.J., Van Wees, J.D.A.M. & Verweij, J.M. (2000) Modelling the evolution of hydrocarbon systems in the inverted West Netherlands Basin, the Netherlands. *Journal of Geochemical Exploration*, vol. 69-70, p. 685- 688.

- Van Bergen, F., 1998. Basin modelling and hydrocarbon generation in the WNB-an organic petrological and organic geochemical approach. Internal report Netherlands Institute of Applied Geoscience TNO – National Geological Survey (Utrecht) 98-148B: 120 pp.
- Van Bergen and W. Sissingh, 2007. Petroleum Geology. In: Th.E.Wong, D.A.J. Batjes and J. de Jager, eds, Geology of the Netherlands. Royal Dutch Academy of Arts and Sciences (Amsterdam), p. 197-221.
- Van Wees, J.D., F. van Bergen, P. David, M. Nepveu, F. Beekman, S. Cloetingh, D. Bonte. 2009. Probabilistic tectonic heat flow modelling for basin maturation: assessment methods and applications. In: Verweij, H., Kacwicz, M., Wendebourg, J., Yardley, G., Cloetingh, S., Düppenbecker, S. (eds.) 2009. Thematic set on Basin Modelling Perspectives, Marine and Petroleum Geology 26, p. 536-551.
- Van Wijhe, D.H. 1987. Structural evolution of inverted basins in the Dutch offshore. Tectonophysics 137: p. 171-219.
- Verweij, J.M., Souto Carneiro Echternach, M., Witmans, N., Abdul Fattah, R. 2009. Reconstruction of basal heat flow, surface temperature, source rock maturity and hydrocarbon generation in salt-dominated Dutch Basins. AAPG Special Publication on Basin modelling: New horizons in research and applications (accepted).
- Verweij, J.M., Souto Carneiro Echternach, M., Witmans, N. 2009. Central Offshore Platform - Area NCP2E, Burial history, temperature, source rock maturity and hydrocarbon generation. TNO Report, TNO-034-UT-2010-01298 / A.
- Verweij, J.M., Souto Carneiro Echternach, M., Witmans, N. 2010. Terschelling Basin and Southern Dutch Central Graben, Burial history, temperature, source rock maturity and hydrocarbon generation – Area 2A. TNO Report, TNO-034-UT-2009-02065.
- Verweij, J.M., 2003. Fluid flow systems analysis on geological timescales in onshore and offshore Netherlands, with special reference to the Broad Fourteens Basin. Thesis, Vrije Universiteit (Amsterdam): 278 pp.
- Verweij, J.M., Simmelink, H.J., Van Balen, R.T. and David, P., 2003. History of petroleum systems in the Broad Fourteen Basin. Netherlands Journal of Geosciences/Geologie en Mijnbouw. 82-1. Special issue 'on Geofluids in the Netherlands', 71-90.
- Wygrala, B.P., 1989. Integrated study of an oil field in the southern Po Basin, Northern Italy. - Ph.D. thesis, University of Cologne, West Germany.
- Wong, Th.E., Batjes, D.A.J. & De Jager J. (eds), 2007. Geology of the Netherlands, Royal Netherlands Academy of Arts and Sciences (Amsterdam) 354 pp.

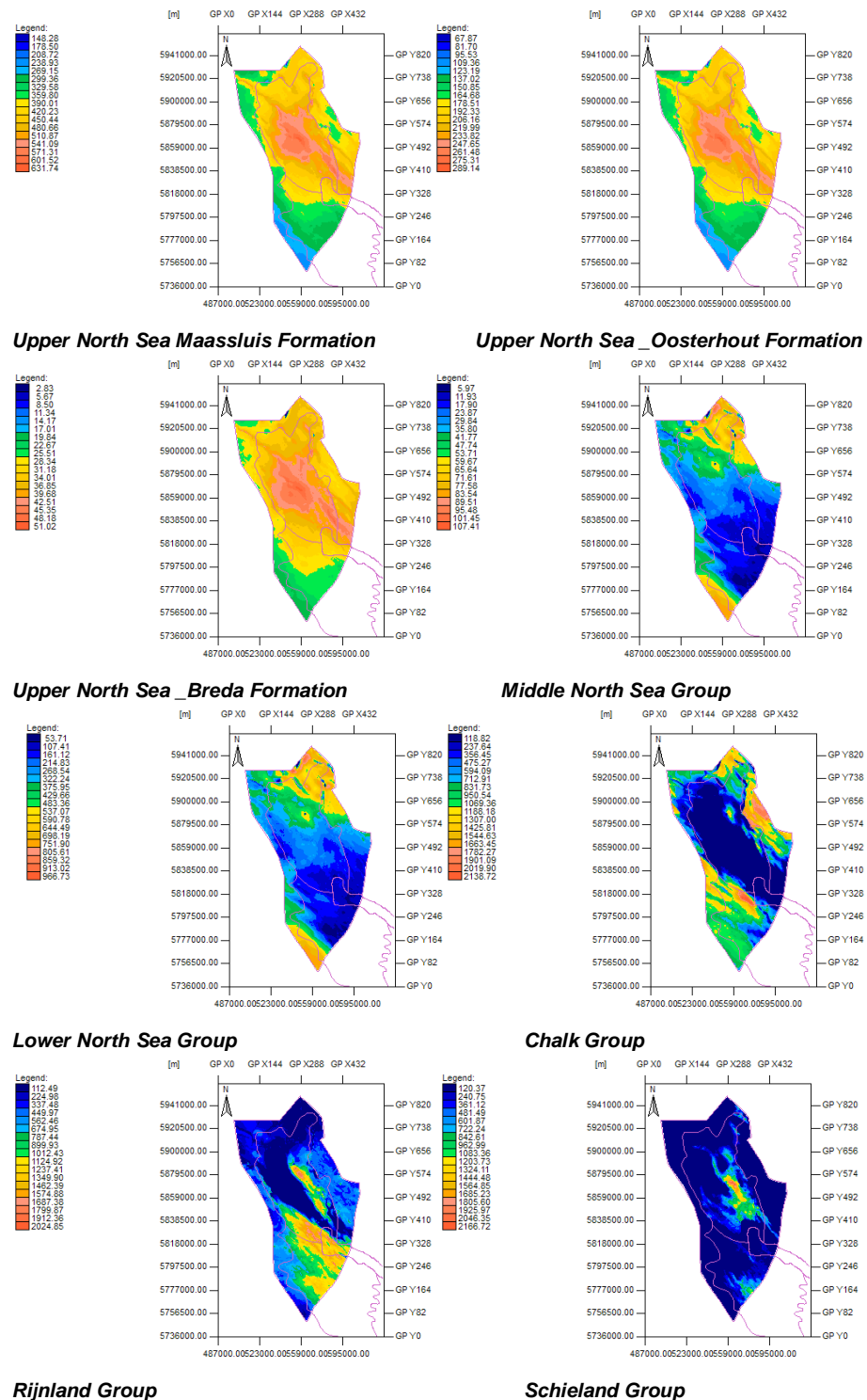
Ziegler, P.A., 1988. Evolution of the Arctic-North Atlantic and the Western Tethys, American Association of Petroleum Geologist Memoir 43: p. 164-196.

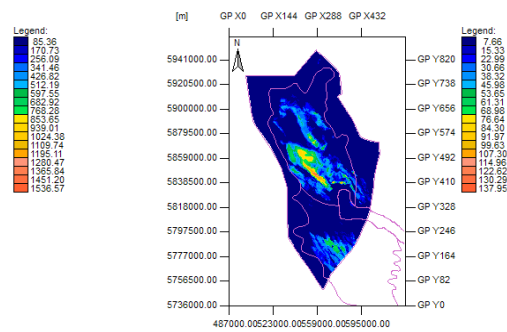
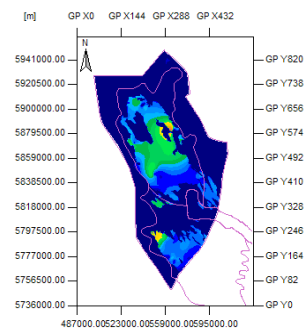
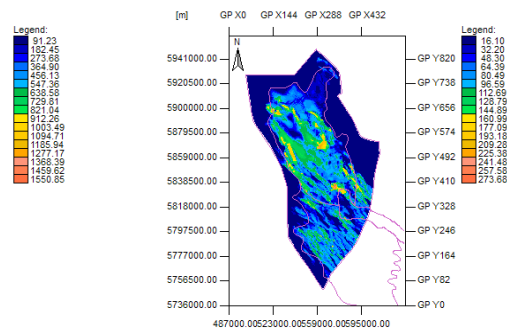
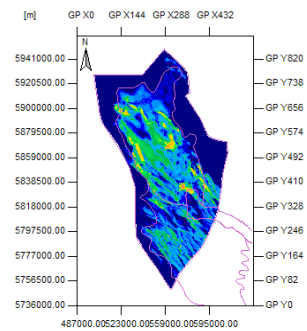
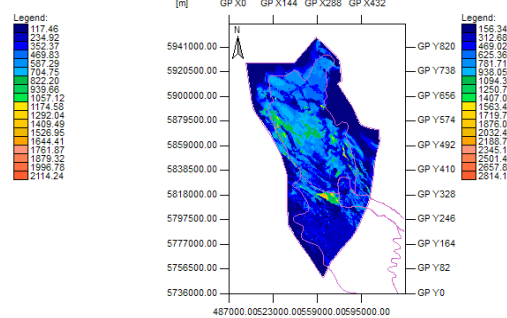
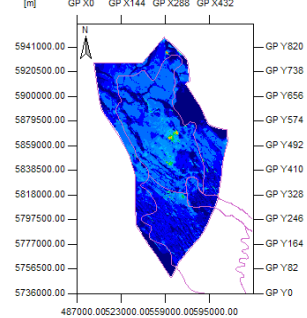
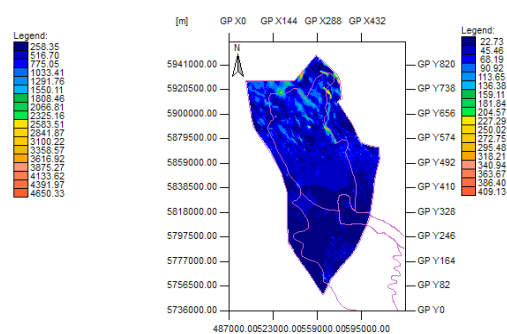
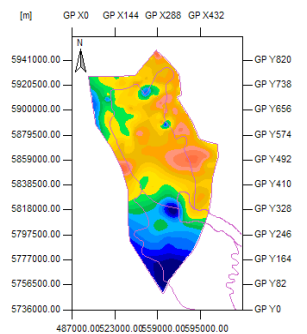
Ziegler, P.A., 1990. Geological Atlas of Western and Central Europe (2nd edition). Shell Internationale Petroleum Maatschappij B.V.; Geological Society Publishing House (Bath): 239 pp.

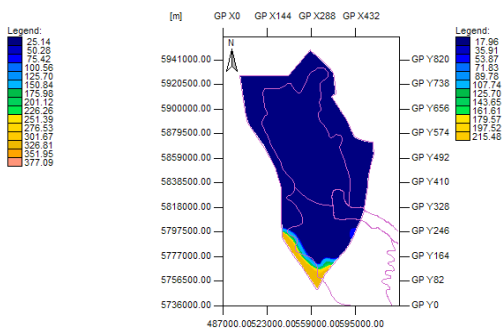
8 Annex

- I. Input thickness maps
- II. Basin modelling parameters, default relations
- III. List of Calibration wells and calibration data
- IV. 1D Heat flow modelling parameters
 - Example of 1D heat flow modelling (Well P06-01)
- V. 3D Heat flow calibration
- VI. Calibration of well data
 - Maturity calibration
 - Temperature calibration
- VII. Erosion maps

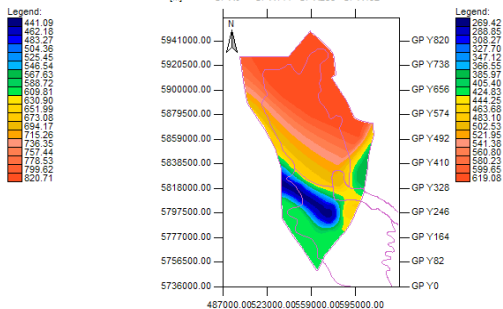
8.1 Annex I : Input thickness maps



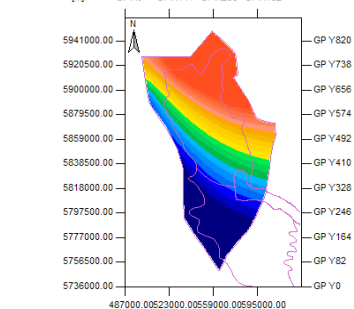
**Altena Group Upper****Altena_Posidonia Formation****Altena_Aalborg Formation****Altena_Sleen Formation****Upper Germanic Trias Group****Lower Germanic Trias Group****Zechstein Group****Rotliegend Group**



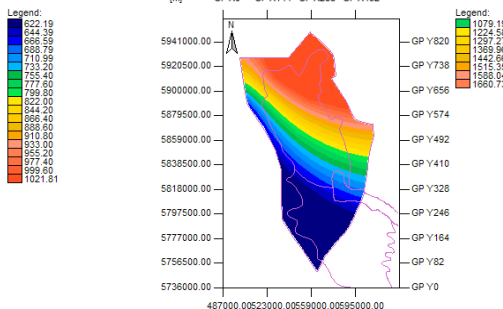
Hunze Sub-Group



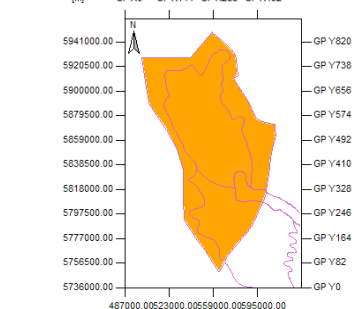
Maurits Formation



Ruurlo Formation



Baarlo Formation



Namurian Unit

Basement

8.2 Annex II: Basin modelling parameters, default relations

Lithology-related properties and relations

Lithology	Model	Matrix thermal conductivity W/m/K	
		at 20oC	at 100oC
Chalk_100	Sekiguchi Model	2.9	2.62
Salt_100	Sekiguchi Model	6.5	5.25
Shale_100	Sekiguchi Model	1.64	1.69
Limestone_100	Sekiguchi Model	3	2.69
Sandstone_100	Sekiguchi Model	3.95	3.38
Sand/Shale_75	Sekiguchi Model	2.66	2.44
Sand/Shale_50	Sekiguchi Model	2.55	2.36
Shale/Sand_90	Sekiguchi Model	1.79	1.8
Sand/Shale_90	Sekiguchi Model	3.62	3.14
Shale/Sand_95	Sekiguchi Model	1.71	1.74
Sand/Shale_80	Sekiguchi Model	3.31	2.92
Shale/Salt_80	Sekiguchi Model	2.16	2.07
Shale/Silt_75	Sekiguchi Model	1.73	1.76
Shale/Sand_60	Sekiguchi Model	2.33	2.2
Shale/Sand_75	Sekiguchi Model	2.04	1.99
Shale/Silt/Sand/Coal _48/25/25/2	Sekiguchi Model	2.09	2.02
Shale/Sand/Coal_80/15/5	Sekiguchi Model	1.72	1.75
Basement	Sekiguchi Model	2.72	2.35

Lithology	Model	Initial porosity	Minimum porosity	Athy's factor km-1
Chalk_100	Athy's Law (Depth)	0.7	0.01	0.9
Salt_100	Athy's Law (Depth)	0.01	0.01	0
Shale_100	Athy's Law (Depth)	0.7	0.01	0.83
Limestone_100	Athy's Law (Depth)	0.35	0.01	0.01
Sandstone_100	Athy's Law (Depth)	0.41	0.01	0.31
Sand/Shale_75	Athy's Law (Depth)	0.49	0.04	0.43
Sand/Shale_50	Athy's Law (Depth)	0.55	0.01	0.57
Shale/Sand_90	Athy's Law (Depth)	0.67	0.01	0.78
Sand/Shale_90	Athy's Law (Depth)	0.44	0.01	0.36
Shale/Sand_95	Athy's Law (Depth)	0.69	0.01	0.8
Sand/Shale_80	Athy's Law (Depth)	0.47	0.01	0.41
Shale/Salt_80	Athy's Law (Depth)	0.56	0.01	0.0769
Shale/Silt_75	Athy's Law (Depth)	0.66	0.01	0.75
Shale/Sand_60	Athy's Law (Depth)	0.58	0.01	0.62
Shale/Sand_75	Athy's Law (Depth)	0.63	0.01	0.7
Shale/Silt/Sand /Coal_48/25/25/2	Athy's Law (Depth)	0.59	0.01	0.61
Shale/Sand/Coal _80/15/5	Athy's Law (Depth)	0.66	0.01	0.73
Basement	Athy's Law (Depth)	0.05	0.05	0

Lithology	Model	Heat Capacity Kcal/kg/K	
		at 20oC	at 100oC
Chalk_100	Waples Model for Rock	0.203	0.23
Salt_100	Waples Model for Rock	0.206	0.24
Shale_100	Waples Model for Rock	0.206	0.24
Limestone_100	Waples Model for Rock	0.2	0.23
Sandstone_100	Waples Model for Rock	0.204	0.24
Sand/Shale_75	Waples Model for Rock	0.185	0.21
Sand/Shale_50	Waples Model for Rock	0.205	0.24
Shale/Sand_90	Waples Model for Rock	0.206	0.24
Sand/Shale_90	Waples Model for Rock	0.204	0.24
Shale/Sand_95	Waples Model for Rock	0.206	0.24
Sand/Shale_80	Waples Model for Rock	0.204	0.24
Shale/Salt_80	Waples Model for Rock	0.206	0.24
Shale/Silt_75	Waples Model for Rock	0.209	0.24
Shale/Sand_60	Waples Model for Rock	0.205	0.24
Shale/Sand_75	Waples Model for Rock	0.205	0.24
Shale/Silt/Sand/Coal _48/25/25/2	Waples Model for Rock	0.21	0.24
Shale/Sand/Coal_80/15/5	Waples Model for Rock	0.211	0.24
Basement	Waples Model for Rock	0.188	0.223

Lithology	Model	Uranium ppm	Thorium ppm	Potassium %	Porosity	Radiogenic heat production (microW/m^3)
Chalk_100	Rybach equation	1.9	1.4	0.25	0	0.6
Salt_100	Rybach equation	0.02	0.01	0.1	0	0.02
Shale_100	Rybach equation	3.7	12	2.7	0	2.03
Limestone_100	Rybach equation	1	1	0.2	0	0.35
Sandstone_100	Rybach equation	1.3	3.5	1.3	0	0.7
Sand/Shale_75	Rybach equation	0.93	3	0.68	0	0.5
Sand/Shale_50	Rybach equation	2.5	7.75	2	0	1.37
Shale/Sand_90	Rybach equation	3.46	11.15	2.56	0	1.9
Sand/Shale_90	Rybach equation	1.54	4.35	1.44	0	0.84
Shale/Sand_95	Rybach equation	3.58	11.57	2.63	0	1.97
Sand/Shale_80	Rybach equation	1.78	5.2	1.58	0	0.97
Shale/Salt_80	Rybach equation	2.96	9.6	2.18	0	1.63
Shale/Silt_75	Rybach equation	3.28	10.25	2.28	0	1.77
Shale/Sand_60	Rybach equation	2.74	8.6	2.14	0	1.5
Shale/Sand_75	Rybach equation	3.1	9.88	2.35	0	1.7
Shale/Silt/Sand/Coal _48/25/25/2	Rybach equation	2.63	7.94	1.88	0	1.4
Shale/Sand/Coa l_80/15/5	Rybach equation	3.23	10.28	2.38	0	1.73
Basement	Rybach equation	0	0	0	0	0

Lithology	Model	Permeability (log mD)	
		at 1% porosity	at 25% porosity
Chalk_100	Multi-Point Model	-6.75	-3.1
Salt_100	Multi-Point Model	-16	-16
Shale_100	Multi-Point Model	-8.52	-3
Limestone_100	Multi-Point Model	-2.44	2.8
Sandstone_100	Multi-Point Model	-1.8	3
Sand/Shale_75	Multi-Point Model	-5.05	1.85
Sand/Shale_50	Multi-Point Model	-5.16	0
Shale/Sand_90	Multi-Point Model	-7.85	-2.4
Sand/Shale_90	Multi-Point Model	-2.47	2.4
Shale/Sand_95	Multi-Point Model	-8.18	-2.7
Sand/Shale_80	Multi-Point Model	-3.14	1.8
Shale/Salt_80	Multi-Point Model	-10.2	-5.6
Shale/Silt_75	Multi-Point Model	-7.96	-2.5
Shale/Sand_60	Multi-Point Model	-5.83	-0.62
Shale/Sand_75	Multi-Point Model	-6.84	-1.5
Shale/Silt/Sand/Coal_48/25/25/2	Multi-Point Model	-6.16	-0.96
Shale/Sand/Coal_80/15/5	Multi-Point Model	-7.22	-2.04
Basement	Multi-Point Model	-16	-16

8.3 Annex III: List of calibration wells

In this table, the wells used for calibration the various models are listed together with the availability of the calibration data. Please contact the author(s) for the calibration data itself.

Wells used for model calibration in the NCP-2F area

Well name	Coordinate (X)	Coordinate (Y)	Depth (m)	Temperature data [C]	Vitrinite Reflectance data [%Ro]
K11-04	534746	5912476	3470	0	
K11-13	536562	5917121	4031	0	
K12-05	547077	5914081	3931	0	
K12-10	546955	5913983	3764	0	
K13-01	515033	5896435	2684		0
K13-06	507926	5907973	2591		0
K13-10	517993	5895902	2548		0
K13-12	520776	5892093	2054		0
K13-14	513726	5899285	2712		0
K14-01	541247	5904563	3284	0	0
K14-02	536137	5901085	3216	0	0
K14-03	537524	5892264	2801	0	
K14-05	539925	5905992	3337	0	
K14-06	524415	5902636	3300		0
K14-07	538853	5877399	1648	0	
K14-08	539613	5892966	2751	0	
K14-09	538742	5893855	3015	0	
K14-10	524778	5905712	3483	0	
K14-12	531150	5899520	3145	0	
K15-01	559858	5897745	2782	0	0
K15-03	557595	5904680	4060	0	0
K15-07	562908	5899648	4065	0	
K15-08	563779	5902030	4007	0	
K15-09	566030	5897085	3922	0	
K15-14	553922	5904495	4026	0	
K17-01	541456	5877548	3400	0	0
K17-02	534455	5880970	3101	0	0
K17-03	528032	5882591	2972		0
K17-04	535164	5880063	2975	0	
K17-05	541100	5879643	3149	0	
K17-06	531973	5873947	2815	0	
K18-01	564818	5881299	2621	0	
K18-03	565267	5883784	2130	0	
K18-05	564515	5875410	2950	0	
L07-13	568216	5929866	4124	0	
L10-02	572940	5919625	3825		0
L10-06	576648	5922552	4119	0	0
L13-01	569306	5902055	3716		0
L16-01	579593	5881506	3695		0
L16-03	567930	5879784	4287	0	0

L16-05	570219	5880640	2512	0	
L16-05	570219	5880640	2512	0	
P02-01	541989	5861174	3799	0	0
P02-02	529339	5866115	3529	0	
P02-03	540868	5862162	3657	0	0
P02-05	531701	5871516	3715	0	0
P03-01	554816	5866785	3790		0
P03-02	567113	5870143	2375	0	
P05-03	537039	5849842	1698	0	
P06-01	556451	5842437	5680	0	0
P06-02	565176	5843568	3145		0
P06-05	551124	5845527	3043	0	
P06-06	548209	5850039	3400	0	
P09-02	548850	5823924	2212	0	0
P12-01	559709	5804743	3581	0	0
P12-11	553847	5807927	3575	0	
P15-01	558638	5790450	3258		0
P15-05	548003	5796713	2176	0	0
P15-08	565956	5791658	2125	0	
P15-10	558310	5790857	2918		0
P18-02	565845	5773940	3751	0	0
Q01-03	576918	5858173	3250	0	0
Q01-04	572846	5864261	1901	0	
Q01-05	576536	5859688	1389	0	
Q01-06	568797	5861580	2178	0	
Q01-08	574301	5869964	2364	0	0
Q01-09	577550	5863775	2096	0	0
Q01-12	579109	5863670	2325	0	
Q01-17	577408	5868028	2469	0	
Q01-20	574308	5869951	1856	0	
Q02-02	600752	5865596	3570	0	0
Q04-01	575859	5838210	3138		0
Q04-04	581950	5850686	1239	0	
Q04-06	569217	5838188	3007	0	
Q04-07	583835	5852157	3498	0	
Q05-02	603761	5845364	2775		0
Q07-01	582900	5817985	2600	0	0
Q07-02	574409	5818436	3900		0
Q07-03	571138	5831191	2334	0	
Q07-04	579615	5826992	3030	0	
Q07-05	588124	5829292	2030	0	0
Q08-01	602743	5829606	2550		0
Q08-02	594336	5828277	2565		0
Q10-01	586236	5800991	2350	0	0
Q11-01	593570	5808642	2497		0
Q11-03	595245	5804892	3197	0	
Q13-01	577752	5783619	2387	0	0
Q13-02	577239	5783023	2810		0
Q14-01	591406	5791989	2222	0	

Q16-01	577764	5772286	2631		0
Q16-03	569027	5777713	2660		0
Q16-04	570498	5774656	3836		0
Q16-05	570560	5769982	2979	0	

8.4 Annex IV: 1D Heat flow modelling parameters

Six wells were used for modelling the basal heat flow. The main input parameters for the modelling procedure were generally similar for the six models. These parameters include:

- Compaction curves for the main lithological units.
- Matrix thermal conductivities for the main lithologies.
- The initial lithosphere parameters.
- The Paleo water depth and paleo surface water interface temperatures.

These parameters are shown below.

The main differences in the modelling parameters for the different wells included, in addition to the stratigraphy, the composition of main stratigraphic units. The tectonic model used to calculate the tectonic subsidence, was in broad senses similar in all the wells (see text for more information). However the ages of the main tectonic events were slightly modified according to different wells. The description of the main erosion and uplift phases as well as subsidence and rifting was specifically tailored for each well.

Common modelling parameters:

LITHOLOGY(1-8)	PHI0	PHI SD	SCALE	SCALE SD	ZDEPTHCHANGE	SCALE2
SANDSTONE	41	0	2600	667	240	3300
SHALE	70	0	1280	16	750	1200
SILT	55	0	1800	621	350	2000
LIMESTONE	51	0	1900	377	1300	1900
SALT	6	0	7000	377	20000	5000
COAL	76	0	2000	377	400	1650
ANHYDRITE	6	0	7000	377	20000	5000
CARBONATE	80	0	1550	377	400	1650

Decompaction Curve Settings used in PetroProb for heat flow analysis

LITHOLOGY	CONDUCTIVITY MEAN	CONDUCTIVITY SD	COND. DISTRIBUTION	HEAT PRODUCTION MEAN	HEAT PRODUCTION SD	HEAT PROD. DISTRIBUTION
sandstone	4.1	0	Triangular	4.03E-07	0	Uniform
shale	2.1	0	Triangular	1.20E-06	0	Uniform
siltstone	2.2	0	Triangular	3.00E-07	0	Uniform
limestone	3.1	0	Triangular	2.50E-07	0	Uniform
salt	6.6	0	Triangular	1.50E-08	0	Uniform
coal	1	0	Triangular	0	0	Uniform
anhydrite	6.6	0	Triangular	0	0	Uniform
dolomite	4.4	0	Triangular	5.00E-07	0	Uniform
water	0.6	0	Uniform	0	0	Uniform
HC	0.5	0	Uniform	0	0	Uniform

Sediment thermal Parameters used in PetroProb for heat flow analysis

PARAMETER NAME	UNITS	VALUE mean	VALUE sd	DISTRIBUTION
lithosphere_thickness	[m]	1.3000E+05	5.0E+04	Uniform
crust_thickness	[m]	3.00E+04	5.0E+03	Uniform
rho0_crust	[kg/m3]	2800	0	Constant
rho0_mantle	[kg/m3]	3400	0	Constant
conductivity_crust	[-]	2.6	0	Constant
conductivity_mantle	[-]	3.4	0	Constant
heat_production_upper_crust_0means40%	[microW/m3]	0	0	Constant
heat_production_lower_crust	[microW/m3]	0.5	0	Constant
lithosphere_thermal_expansion	[-]	3.20E-05	0	Constant
base_temperature	[C]	1330	0	Constant
rho_underplate	[kg/m3]	3000	0	Constant

Lithosphere Parameters used in PetroProb for heat flow analysis (Lithosphere and crustal thickness might slightly be different in different wells)

Tectonic models used for heat flow modelling:

- Well K14-01

BASE FORMATION START	BASE FORMATION END	lithosphere process	iterationmode	start beta	start delta
313.6	DC	bdstretch	bdcoup	1	1
DC	DC-Erosion	bdstretch	bdcoup	1	1
DC-Erosion	RO	bdstretch	bfree	1	1
RO	267.5	bdstretch	bdcoup	1	1
251.6	246.2	bdstretch	bdcoup	1	1
203.6	ATPO	bdstretch	bdcoup	1	1
FAULT	SL-Erosion	bdstretch	bdcoup	1	1
SL-Erosion	140.2	bdstretch	dfree	2	1
CK-Erosion	65	bdstretch	bdcoup	1	1
65	42.1	bdstretch	bdcoup	1	1
42.1	NU-Erosion	bdstretch	bdcoup	1	1
NU-Erosion	19.9	bdstretch	bdcoup	1	1
19.9	11.7	bdstretch	bdcoup	1	1
11.7	5.8	bdstretch	bdcoup	1	1
5.8	PD	bdstretch	bdcoup	1	1

- Saalian erosion phase (DC-Erosion) is introduced as an underplating event (bfree).
- Late Kimmerian erosion event (SL-erosion) is defined as thinning of the crust (rifting) (dfree) associated with magmatism (b=2).

- Well P06-01 (See below for a detailed overview of modelling the heat flow in this well)

BASE FORMATION START	BASE FORMATION END	lithosphere process	iterationmode	start beta	start delta
313.6	312.3	bdstretch	bdcoup	1	1
312.3	DC	bdstretch	bdcoup	1	1
DC	RV-erosion	bdstretch	bdcoup	1	1
RV-erosion	RO	bdstretch	bfree	1	1
RO	264	bdstretch	bdcoup	1	1
264	251	bdstretch	bdcoup	1	1
251	238.9	bdstretch	bdcoup	1	1
238.9	199.6	bdstretch	bdcoup	1	1
199.6	AT-erosion	bdstretch	bdcoup	1	1
AT-erosion	156.4	bdstretch	bdfree	1	1
156.4	131.1	bdstretch	bdcoup	1	1
131.1	124.5	bdstretch	bdcoup	1	1
CK	CK-erosion	bdstretch	bdcoup	1	1
CK-erosion	61.7	bdstretch	bdcoup	1	1
53	NM-erosion	bdstretch	bdcoup	1	1
NM-erosion	33.1	bdstretch	bdcoup	1	1
20.1	5.8	bdstretch	bdcoup	1	1
5.8	PD	bdstretch	bdcoup	1	1

- Saalian erosion phase (RV-erosion) is introduced as an underplating event (bfree).
- A coupled model is used to describe the Late Kimmerian erosion event (AT-erosion) (bdfree) where the model is allowed to vary the b and d stretching factors freely.

- Well P18-02

BASE FORMATION START	BASE FORMATION END	lithosphere process	iterationmode	start beta	start delta
326.27	DCH	bdstretch	bdcoup	1	1
DCH	DC-Er	bdstretch	bdcoup	1	1
DC-Er	L-RO	bdstretch	bfree	1	1
251.6	244	bdstretch	bdcoup	1	1
238.9	203.6	bdstretch	bdcoup	1	1
203.6	183	bdstretch	bdcoup	1	1
ST-Er	156.4	bdstretch	dfree	1.5	1
131.1	113.5	bdstretch	bdcoup	1	1
92.9	CK-Er	bdstretch	bdcoup	1	1
CK-Er	61.7	bdstretch	bdcoup	1	1
61.7	35.4	bdstretch	bdcoup	1	1
35.4	16	bdstretch	bdcoup	1	1
16	5.8	bdstretch	bdcoup	1	1
5.8	PD	bdstretch	bdcoup	1	1

- Saalian erosion phase (DC-Er) is introduced as an underplating event (bfree).
- Late Kimmerian erosion event (ST-Er) is defined as thinning of the crust (rifting) (dfree) where the magnitude for the stretching is derived from the subsidence curve. This is associated with magmatism and underplating where the subcrustal lithosphere is stretched by a magnitude of (b=1.5).

- *Well Q07-01*

BASE FORMATION START	BASE FORMATION END	lithosphere process	iterationmode	start beta	start delta
326.27	DCH	bdstretch	bdcoup	1	1
DCH	DC-Er	bdstretch	bdcoup	1	1
DC-Er	L-RO	bdstretch	bfree	1	1
264	245	bdstretch	bdcoup	1	1
AT-Er	137	bdstretch	dfree	2	1
131	112	bdstretch	bdcoup	1	1
104	CK-Er	bdstretch	bdcoup	1	1
CK-Er	61	bdstretch	bdcoup	1	1
35	NM-Er	bdstretch	bdcoup	1	1
NM-Er	16	bdstretch	bdcoup	1	1
5.8	PD	bdstretch	bdcoup	1	1

- Saalian erosion phase (DC-Er) is introduced as an underplating event (bfree).
- Late Kimmerian erosion event (AT-erosion) is defined as thinning of the crust (rifting) (dfree) associated with magmatism (b=2).

- *Well L10-01*

BASE FORMATION START	BASE FORMATION END	lithosphere process	iterationmode	start beta	start delta
326.27	DCH	bdstretch	bdcoup	1	1
DCH	DC-Er	bdstretch	bdcoup	1	1
DC-Er	L-RO	bdstretch	bfree	1	1
251	245.6	bdstretch	bdcoup	1	1
244	AT	bdstretch	bdcoup	1	1
AT	AT-Er	bdstretch	bdcoup	1	1
AT-Er	140.2	bdstretch	dfree	2	1
92.9	CK	bdstretch	bdcoup	1	1
CK-Er	61.7	bdstretch	bdcoup	1	1
55.4	50.2	bdstretch	bdcoup	1	1
42	NM	bdstretch	bdcoup	1	1
NM-Er	20.1	bdstretch	bdcoup	1	1
5.8	PD	bdstretch	bdcoup	1	1

- Saalian erosion phase (DC-Er) is introduced as an underplating event (bfree).
- Late Kimmerian erosion event (AT-erosion) is defined as thinning of the crust (rifting) (dfree) associated with magmatism (b=2).

8.5 Example of basal heat-flow modelling : Well P06-1 (Broad Fourteens Basin)

The Broad Fourteens Basin (BFB) is a structurally complex element in the Dutch offshore. It has experienced several phases of extension and subsidence as well as inversion, uplift and erosion. The structure is intersected by several fault swarms mainly oriented SE-NW and S-N. There have been several studies aiming at modelling petroleum systems in the basin.

The geological evolution of the basin can be summarized as following:

- Late Carboniferous - Permian: thermal upwelling associated with erosion followed by thermal subsidence.
- Late Triassic: some extension and subsidence.
- Lower Jurassic: gradual and quite subsidence.
- Middle Jurassic to upper Jurassic: uplift and erosion caused by a thermal uplift event associated with volcanism. This is followed by a rifting phase in the later Jurassic (Later Kimmerian rifting).
- Late Cretaceous: inversion of the basin and uplift led to erosion (Alpine orogeny).
- Early Palaeogene: strong inversion that led to significant erosion in some places.

Input well

In order to accurately model the basal heat-flow, the well must meet a number of requirements. First of all, the well should not be located close to a salt diapir. Secondly, there should be a good description of the stratigraphy and the lithology of the well. For calibration purposes, sufficient data (measurements) for temperature and vitrinite reflectance should be available. In addition to that, the penetration depth of the well needs to be sufficient, i.e., ideally the well should include Carboniferous formations.

Considering all these factors, we selected well P06-01 as being representative for tectonic heat-flow modelling in the BFB. The present-day stratigraphy of the well is shown in Table 1.

The litho-stratigraphy of the well was extended by adding available information of the subdivision of the North Sea Super Group from wells surrounding P06-01. In addition, stratigraphic information of the Carboniferous and upper Permian from surrounding wells was added to the well. Erosion values of various geological phases are taken from published data and previous studies.

The well is intersected by a normal-component fault around 2333 m depth which explains the absence of part of the stratigraphy in the well. This stratigraphic information needs to be re-included before conducting the modelling.

Table 1: Stratigraphy in well P06-01

Name	Top	Base	Thickness	Dep From	Dep To	Lithology
N	0	915.5	915.5	60.5	0	50_Sand_50_Shale
KNGL	915.5	1145	229.5	124.5	97	50_Shale_25_Marl_25_Sand
KNNC	1145	1823	678	140.7	122	100_Shale
KNNSI	1823	1887	64	133.5	131.8	100_Sandstone
SLDN	1887	2333.5	446.5	145	134	48_Shale_25_Sand_25_Silt_2_Coal
FAULT	2333.5	2333.5	0			0
RNKPL	2333.5	2375	41.5	237	227.5	80_Shale_10_Anhy_10_Lime
RNMUU	2375	2408	33	240	238	50_Marl_50_Lime
RNMUA	2408	2432	24	240	238	100_Marl
RNMUE	2432	2450	18	240	238	75_Salt_25_Anhy
RNMUL	2450	2530	80	240	238	50_Marl_50_Lime
RNROC	2530	2608	78	241	240	50_Shale_50_Silt
RNRO1	2608	2631	23	241	240	90_Salt_10_Anhy
RNSO	2631	2658	27	243	241	50_Sand_50_Shale
RBMH	2658	2684	26	245	241	75_Sand_25_Shale
RBMDL	2684	2705	21	245	241	100_Shale
RBMDL	2705	2723	18	245	241	75_Sand_25_Shale
RBMVC	2723	2806	83	245	241	34_Shale_33_Sand_33_Silt
RBMVL	2806	2883	77	245	241	100_Sandstone
RBSHR	2883	3031	148	247.5	243.4	50_Shale_25_Lime_25_Silt
RBSHM	3031	3173	142	247.5	243.4	75_Shale_25_Silt
ZEUC	3173	3190	17	252	251	100_Shale
ZEZ4A	3190	3191	1	256.1	245	100_Anhydrite
ZEZ4R	3191	3204	13	256.1	245	75_Shale_25_Anhy
ZEZ3C	3204	3240	36	256.1	245	100_Dolomite
ZEZ3G	3240	3252	12	256.1	245	100_Shale
ZEZ2T	3252	3257	5	256.1	245	100_Anhydrite
ZEZ2M	3257	3295	38	256.1	245	80_Shale_20_Dolo
ZEZ1M	3295	3340	45	256.1	245	75_Shale_25_Silt
ZEZ1F	3340	3378	38	256.1	245	50_Lime_50_Dolo
ZEZ1G	3378	3452	74	256.1	245	50_Shale_50_Marl
ZEZ1K	3452	3455	3	256.1	245	100_Shale
ROSL	3455	3680	225	268.8	256.1	100_Sandstone

When restoring the missing stratigraphy it should be kept in mind that the Late Kimmerian erosion phase accounts for ~564 m of erosion of the upper part of the Altona group. The absence of the Lower Altona group and the Upper Germanic Trias Group in the well is explained by the fault offset and needed to be restored. The thicknesses of these layers are extracted from literature and other wells in the area where the layers are preserved and not affected by faulting. The surrounding wells used to reconstruct the modelling well are: P06-02, P06-A-06, P06-C-01, P06-C-02, P09-07.

The Carboniferous stratigraphy is based completely on literature, whereas the Saalian erosion phase is assumed to have resulted in removal of ~800 m of early Permian rocks.

The final set-up of the well, as it was incorporated in the model, is shown in Table 2.

Table 2: The final set-up of well P06-01 as it was introduced to the model.

	Formation	Depth (from)	Depth (to)	Thickness (m)	Erosion (m)	Age (from)	Age (to)	Lithology
UNG	NUMS	0	532.5	532.5		3.10	0	75_Sand_25_Shale
	NUOT	532.5	622.5	90		5.80	3.10	75_Sand_25_Shale
	NUBA	622.5	648.5	26		20.10	9.60	75_Sand_25_Shale
MNG	NMRF	648.5	661.5	13	15	33.10	28.60	75_Shale_25_Sand
NL					450	37.90	33.10	
	NLFF	661.5	774.5	113		50.20	37.90	50_Sand_50_Shale
	NLFFY	774.5	867.5	93		53.00	50.20	100_Shale
	NLFFT	867.5	879.5	12		55.10	53.00	50_Sand_50_Shale
	NLFFD	879.5	887.5	8		55.40	55.10	50_Shale_50_Tuff
	NLLFC	887.5	915.5	28		61.7	55.4	100_Shale
CK					2000	99.1	61.7	
KN	KNGL	915.5	1145	229.5		124.5	99.1	50_Shale_25_Marl_25_Sand
	KNNC	1145	1823	678		131.1	124.5	100_Shale
	KNNSI	1823	1887	64		137.4	131.1	100_Sandstone
SL	SLDN	1887	2333.5	446.5		156.4	137.4	48_Shale_25_Sand_25_Silt_2_Coal
AT	ATBR				564	168.2	156.4	
	ATWD					177.6	168.2	
	ATPO					183	177.6	
AT	ATAL	2333.5	2634	300.5		199.6	183	75_Shale_25_Silt
	ATRT	2634	2650.5	16.5		203.6	199.6	100_Shale
RN	RNKPU	2650.5	2654.5	4		207.2	203.6	75_Shale_25_Marl
	RNKPD	2654.5	2676.5	22		211.4	207.2	75_Shale_25_Dolo
	RNKPR	2676.5	2679.5	3		213.6	211.4	50_Shale_50_Marl
	RNKPE	2679.5	2681.5	2		220.1	213.6	40_Anhy_40_Shale_20_Silt
	RNKPM	2681.5	2690.5	9		221.5	220.1	100_Shale
	RNKPS	2690.5	2708.5	18		225.6	221.5	90_Salt_10_Anhy
	RNKPL	2708.5	2750	41.5		233.5	225.6	80_Shale_10_Anhy_10_Lime
	RNMUU	2750	2783	33		237.0	233.5	50_Marl_50_Lime
RB	RNMUA	2783	2807	24		238.9	237.0	100_Marl
	RNMUE	2807	2825	18		240.7	238.9	75_Salt_25_Anhy
	RNMUL	2825	2905	80		244.0	240.7	50_Marl_50_Lime
	RNROC	2905	2983	78		245.3	244.0	50_Shale_50_Silt
	RNRO1	2983	3006	23		245.6	245.3	90_Salt_10_Anhy
	RNSO	3006	3033	27		246.2	245.6	50_Sand_50_Shale
	RBMH	3033	3059	26		247.2	246.2	75_Sand_25_Shale
	RBMD	3059	3080	21		247.6	247.2	100_Shale
	RBMDL	3080	3098	18		247.8	247.6	75_Sand_25_Shale
	RBMVC	3098	3181	83		248.7	247.8	34_Shale_33_Sand_33_Silt
	RBMVL	3181	3258	77		249.0	248.6	100_Sandstone
	RBSHR	3258	3406	148		250.0	249.0	50_Shale_25_Lime_25_Silt
	RBSHM	3406	3548	142		251.0	250.0	75_Shale_25_Silt
	ZEUC	3548	3565	17		251.6	251.0	100_Shale
	ZEZ4A	3565	3566	1		252.6	252.4	100_Anhydrite
	ZEZ4R	3566	3579	13		252.8	252.6	75_Shale_25_Anhy
ZE	ZEZ3C	3579	3615	36		254.3	253.8	100_Dolomite
	ZEZ3G	3615	3627	12		254.6	254.3	100_Shale
	ZEZ2T	3627	3632	5		255.0	254.6	100_Anhydrite

	ZEZ2M	3632	3670	38		256.0	255.3	80_Shale_20_Dolo
	ZEZ1M	3670	3715	45		257.4	256.4	75_Shale_25_Silt
	ZEZ1F	3715	3753	38		257.6	257.4	50_Lime_50_Dolo
	ZEZ1G	3753	3827	74		257.8	257.6	50_Shale_50_Marl
	ZEZ1K	3827	3830	3		258.0	257.8	100_Shale
RO	ROSL	3830	4055	225		264.0	258.0	100_Sandstone
DC					800	290.0	280.0	
	DCD/DCH	4055	4655	600		311.0	308.7	75_Shale_25_Sand
	DCCU	4655	4855	200		312.3	311.0	80_Shale_15_Sand_5_Coal
	DCCR	4855	5455	600		313.1	312.3	78_Shale_20_Sand_2_Coal
	DCCB	5455	6055	600		313.6	313.1	48_Shale_25_Sand_25_Silt_2_Coal

In well P06-01, the North Sea Super Group is divided into three groups, the Upper North Sea Group (NU), the Middle North Sea Group (NM) and the Lower North Sea Group (NL). An erosion phase is introduced during the Pyrenean uplift which accounts for around 450 m of erosion of the upper part of the Lower North Sea group. The Subhercynian and Laramide uplift phases are combined in a single phase that accounts for approximately 2000 m of erosion of the upper Chalk group. This estimated amount of erosion needs to be constrained by the heat-flow modelling and adjusted accordingly.

The calibration data available for this well include good quality temperature data as well as some vitrinite measurements that are conducted by external parties (Figure 8.4). The latter are regarded less reliable. The vitrinite data points shown in Figure 8.4 show the average of several measurements within a specific depth range.

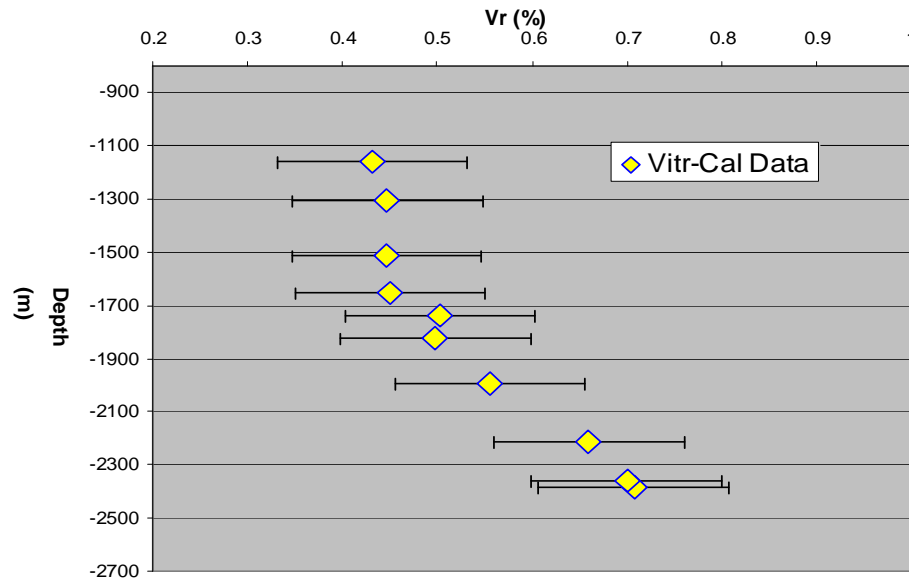


Figure 8.5: calibration data used in the modelling. Temperature data are good quality. Vitrinite reflectance (Vr) data shown here represent the average value over a specific depth range.

Modelling parameters

Model definition

The stratigraphic units and their ages are introduced to the model together with amounts and ages of erosion phases. The effect of the fault is defined as an erosion phase that removed all the layers that are displaced by the fault (Figure 8.6).

FORMATION	EROSIVE	ISO mean	ISO sd	ISO dist	ERODED mean	ERODED sd	ERODED dist	AGE mean	AGE sd	AGE dist	OUTPUT
313.6	<input type="checkbox"/>	600	0	Constant	0	0	Constant	313.6	0	Constant	<input checked="" type="checkbox"/>
313.1	<input type="checkbox"/>	600	0	Constant	0	0	Constant	313.1	0	Constant	<input checked="" type="checkbox"/>
312.3	<input type="checkbox"/>	200	0	Constant	0	0	Constant	312.3	0	Constant	<input checked="" type="checkbox"/>
311	<input type="checkbox"/>	600	0	Constant	0	0	Constant	311	0	Constant	<input checked="" type="checkbox"/>
DC	<input type="checkbox"/>	0	0	Constant	800	0	Constant	308.7	0	Constant	<input checked="" type="checkbox"/>
RV-erosion	<input checked="" type="checkbox"/>	0	0	Constant	2	0	Constant	290	0	Constant	<input checked="" type="checkbox"/>
RO	<input type="checkbox"/>	0	0	Constant	0	0	Constant	280	0	Constant	<input checked="" type="checkbox"/>
264	<input type="checkbox"/>	225	0	Constant	0	0	Constant	264	0	Constant	<input checked="" type="checkbox"/>
258	<input type="checkbox"/>	3	0	Constant	0	0	Constant	258	0	Constant	<input checked="" type="checkbox"/>
257.8	<input type="checkbox"/>	74	0	Constant	0	0	Constant	257.8	0	Constant	<input checked="" type="checkbox"/>
257.6	<input type="checkbox"/>	38	0	Constant	0	0	Constant	257.6	0	Constant	<input checked="" type="checkbox"/>
257.4	<input type="checkbox"/>	45	0	Constant	0	0	Constant	257.4	0	Constant	<input checked="" type="checkbox"/>
256	<input type="checkbox"/>	38	0	Constant	0	0	Constant	256	0	Constant	<input checked="" type="checkbox"/>
255	<input type="checkbox"/>	5	0	Constant	0	0	Constant	255	0	Constant	<input checked="" type="checkbox"/>
254.6	<input type="checkbox"/>	12	0	Constant	0	0	Constant	254.6	0	Constant	<input checked="" type="checkbox"/>
254.3	<input type="checkbox"/>	36	0	Constant	0	0	Constant	254.3	0	Constant	<input checked="" type="checkbox"/>
252.8	<input type="checkbox"/>	13	0	Constant	0	0	Constant	252.8	0	Constant	<input checked="" type="checkbox"/>
252.6	<input type="checkbox"/>	1	0	Constant	0	0	Constant	252.6	0	Constant	<input checked="" type="checkbox"/>
251.6	<input type="checkbox"/>	17	0	Constant	0	0	Constant	251.6	0	Constant	<input checked="" type="checkbox"/>
251	<input type="checkbox"/>	142	0	Constant	0	0	Constant	251	0	Constant	<input checked="" type="checkbox"/>
250	<input type="checkbox"/>	148	0	Constant	0	0	Constant	250	0	Constant	<input checked="" type="checkbox"/>
249	<input type="checkbox"/>	77	0	Constant	0	0	Constant	249	0	Constant	<input checked="" type="checkbox"/>
248.7	<input type="checkbox"/>	83	0	Constant	0	0	Constant	248.7	0	Constant	<input checked="" type="checkbox"/>
247.8	<input type="checkbox"/>	18	0	Constant	0	0	Constant	247.8	0	Constant	<input checked="" type="checkbox"/>
247.6	<input type="checkbox"/>	21	0	Constant	0	0	Constant	247.6	0	Constant	<input checked="" type="checkbox"/>
247.2	<input type="checkbox"/>	26	0	Constant	0	0	Constant	247.2	0	Constant	<input checked="" type="checkbox"/>
246.2	<input type="checkbox"/>	27	0	Constant	0	0	Constant	246.2	0	Constant	<input checked="" type="checkbox"/>
245.6	<input type="checkbox"/>	23	0	Constant	0	0	Constant	245.6	0	Constant	<input checked="" type="checkbox"/>
245.3	<input type="checkbox"/>	78	0	Constant	0	0	Constant	245.3	0	Constant	<input checked="" type="checkbox"/>
244	<input type="checkbox"/>	80	0	Constant	0	0	Constant	244	0	Constant	<input checked="" type="checkbox"/>
240.7	<input type="checkbox"/>	18	0	Constant	0	0	Constant	240.7	0	Constant	<input checked="" type="checkbox"/>
238.9	<input type="checkbox"/>	24	0	Constant	0	0	Constant	238.9	0	Constant	<input checked="" type="checkbox"/>
237	<input type="checkbox"/>	33	0	Constant	0	0	Constant	237	0	Constant	<input checked="" type="checkbox"/>
233.5	<input type="checkbox"/>	42	0	Constant	0	0	Constant	233.5	0	Constant	<input checked="" type="checkbox"/>
225.6	<input type="checkbox"/>	0	0	Constant	18	0	Constant	225.6	0	Constant	<input checked="" type="checkbox"/>
221.5	<input type="checkbox"/>	0	0	Constant	9	0	Constant	221.5	0	Constant	<input checked="" type="checkbox"/>
220.1	<input type="checkbox"/>	0	0	Constant	2	0	Constant	220.1	0	Constant	<input checked="" type="checkbox"/>
213.6	<input type="checkbox"/>	0	0	Constant	3	0	Constant	213.6	0	Constant	<input checked="" type="checkbox"/>
211.4	<input type="checkbox"/>	0	0	Constant	22	0	Constant	211.4	0	Constant	<input checked="" type="checkbox"/>
207.2	<input type="checkbox"/>	0	0	Constant	4	0	Constant	207.2	0	Constant	<input checked="" type="checkbox"/>
203.6	<input type="checkbox"/>	0	0	Constant	16	0	Constant	203.6	0	Constant	<input checked="" type="checkbox"/>
199.6	<input type="checkbox"/>	0	0	Constant	300.5	0	Constant	199.6	0	Constant	<input checked="" type="checkbox"/>
AT	<input type="checkbox"/>	0	0	Constant	564	0	Constant	183	0	Constant	<input checked="" type="checkbox"/>
AT-erosion	<input checked="" type="checkbox"/>	0	0	Constant	2	0	Constant	165	0	Constant	<input checked="" type="checkbox"/>
156.4	<input type="checkbox"/>	446	0	Constant	0	0	Constant	156.4	0	Constant	<input checked="" type="checkbox"/>
137.4	<input type="checkbox"/>	64	0	Constant	0	0	Constant	137.4	0	Constant	<input checked="" type="checkbox"/>
131.1	<input type="checkbox"/>	678	0	Constant	0	0	Constant	131.1	0	Constant	<input checked="" type="checkbox"/>
124.5	<input type="checkbox"/>	230	0	Constant	0	0	Constant	124.5	0	Constant	<input checked="" type="checkbox"/>
CK	<input type="checkbox"/>	0	0	Constant	1000	0	Constant	99	0	Constant	<input checked="" type="checkbox"/>
CK-erosion	<input checked="" type="checkbox"/>	0	0	Constant	2	0	Constant	71	0	Constant	<input checked="" type="checkbox"/>
61.7	<input type="checkbox"/>	28	0	Constant	0	0	Constant	61.7	0	Constant	<input checked="" type="checkbox"/>
55.4	<input type="checkbox"/>	8	0	Constant	0	0	Constant	55.4	0	Constant	<input checked="" type="checkbox"/>
55.1	<input type="checkbox"/>	12	0	Constant	0	0	Constant	55.1	0	Constant	<input checked="" type="checkbox"/>
53	<input type="checkbox"/>	93	0	Constant	0	0	Constant	53	0	Constant	<input checked="" type="checkbox"/>
50.2	<input type="checkbox"/>	113	0	Constant	435	0	Constant	50.2	0	Constant	<input checked="" type="checkbox"/>
NM-erosion	<input checked="" type="checkbox"/>	0	0	Constant	2	0	Constant	37.9	0	Constant	<input checked="" type="checkbox"/>
33.1	<input type="checkbox"/>	13	0	Constant	0	0	Constant	33.1	0	Constant	<input checked="" type="checkbox"/>
20.1	<input type="checkbox"/>	26	0	Constant	0	0	Constant	20.1	0	Constant	<input checked="" type="checkbox"/>
5.8	<input type="checkbox"/>	90	0	Constant	0	0	Constant	5.8	0	Constant	<input checked="" type="checkbox"/>
3.1	<input type="checkbox"/>	532	0	Constant	0	0	Constant	3.1	0	Constant	<input checked="" type="checkbox"/>

Figure 8.6: Model definition of well P06-01 as introduced to PetroProb.

The paleo water-depth (PWD) values are based on the new values published by the Geo-biology department and specifically focus on refinement of the Tertiary water depths. The surface water interface temperatures (SWIT) are also taken from data provided by the Geo-biology department (Figure 8.7, 8.8).

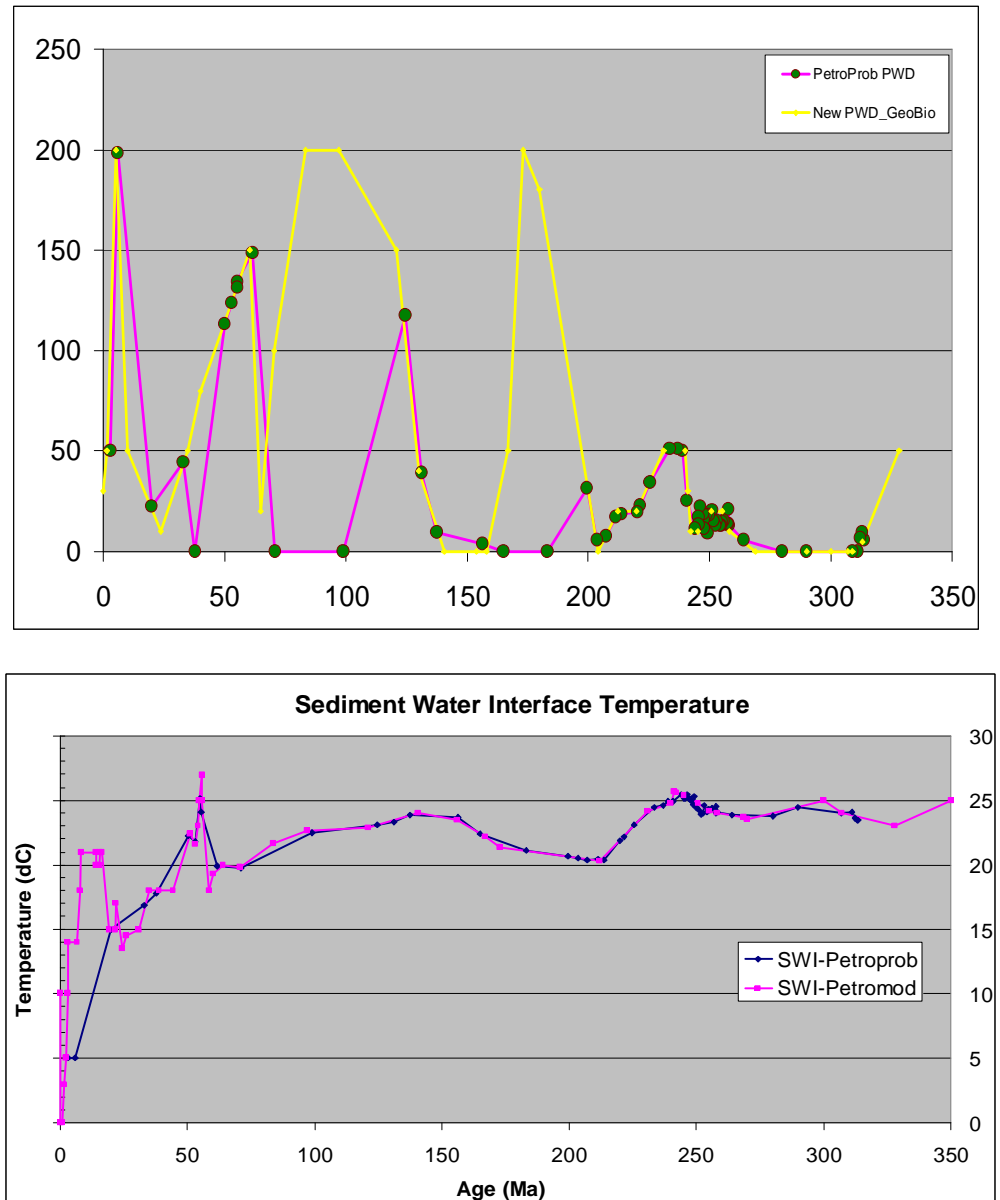


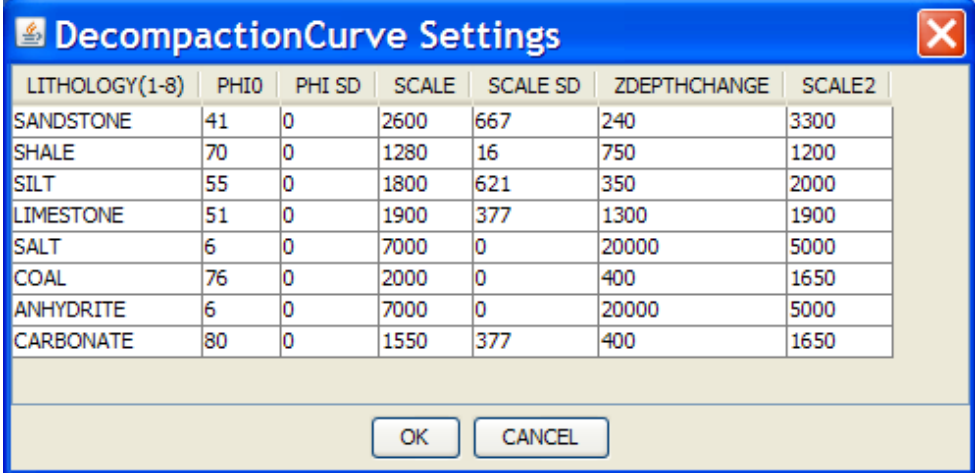
Figure 8.7: Paleo Water Depth (PWD) and Sediment Water Interface Temperature (SWIT) used in PetroProb calibrated with data produced by the GeoBiology department.

Paleo waterdepths			
FORMATION	PAL WD mean	PAL WD sd	PAL WD dist
313.6	9.4	0	Constant
313.1	6.5	0	Constant
312.3	20	0	Constant
311	20	0	Constant
DC	20	0	Constant
RV-erosion	0	0	Constant
RO	5.9	0	Constant
264	13.1	0	Constant
258	13.8	0	Constant
257.8	21.1	0	Constant
257.6	13.8	0	Constant
257.4	15.3	0	Constant
256	14.6	0	Constant
255	13.1	0	Constant
254.6	13.1	0	Constant
254.3	15.3	0	Constant
252.8	13.1	0	Constant
252.6	15.3	0	Constant
251.6	20.4	0	Constant
251	18.2	0	Constant
250	9	0	Constant
249	18.2	0	Constant
248.7	15.8	0	Constant
247.8	11.7	0	Constant
247.6	18.8	0	Constant
247.2	22.3	0	Constant
246.2	17	0	Constant
245.6	13.5	0	Constant
245.3	11.7	0	Constant
244	25.2	0	Constant
240.7	50	0	Constant
238.9	51.1	0	Constant
237	51.1	0	Constant
233.5	34.6	0	Constant
225.6	22.9	0	Constant
221.5	19.4	0	Constant
220.1	18.8	0	Constant
213.6	17	0	Constant
211.4	7.6	0	Constant
207.2	5.9	0	Constant
203.6	31.7	0	Constant
199.6	0	0	Constant
AT	0	0	Constant
AT-erosion	4	0	Constant
156.4	9.4	0	Constant
137.4	39.3	0	Constant
131.1	117.4	0	Constant
124.5	0	0	Constant
CK	0	0	Constant
CK-erosion	148.5	0	Constant
61.7	134.4	0	Constant
55.4	131.5	0	Constant
55.1	123.8	0	Constant
53	113.3	0	Constant
50.2	0	0	Constant
NM-erosion	44.6	0	Constant
33.1	22.3	0	Constant
20.1	198.4	0	Constant
5.8	70	0	Constant
3.1	30	0	Constant
OK CANCEL			

T surface Dialog			
FORMATION	DISTRIBUTION	TSURFACE mean	TSURFACE SD
313.6	Constant	23.5	0
313.1	Constant	23.5	0
312.3	Constant	23.6	0
311	Constant	24.07	0
DC	Constant	24	0
RV-erosion	Constant	24.45	0
RO	Constant	23.8	0
264	Constant	23.83	0
258	Constant	24.1	0
257.8	Constant	24	0
257.6	Constant	24.5	0
257.4	Constant	24.3	0
256	Constant	24.4	0
255	Constant	24.3	0
254.6	Constant	24.3	0
254.3	Constant	24.1	0
252.8	Constant	24.6	0
252.6	Constant	24	0
251.6	Constant	23.9	0
251	Constant	24.25	0
250	Constant	24.44	0
249	Constant	25.3	0
248.7	Constant	24.69	0
247.8	Constant	24.98	0
247.6	Constant	25.07	0
247.2	Constant	25.12	0
246.2	Constant	25.45	0
245.6	Constant	25.17	0
245.3	Constant	25.17	0
244	Constant	25.41	0
240.7	Constant	24.88	0
238.9	Constant	24.88	0
237	Constant	24.59	0
233.5	Constant	24.45	0
225.6	Constant	23.11	0
221.5	Constant	22.15	0
220.1	Constant	21.87	0
213.6	Constant	20.33	0
211.4	Constant	20.43	0
207.2	Constant	20.33	0
203.6	Constant	20.48	0
199.6	Constant	20.67	0
AT	Constant	21.15	0
AT-erosion	Constant	22.39	0
156.4	Constant	23.73	0
137.4	Constant	23.88	0
131.1	Constant	23.35	0
124.5	Constant	23.11	0
CK	Constant	22.49	0
CK-erosion	Constant	19.76	0
61.7	Constant	19.9	0
55.4	Constant	24.11	0
55.1	Constant	25.17	0
53	Constant	21.77	0
50.2	Constant	22.25	0
NM-erosion	Constant	17.8	0
33.1	Constant	16.84	0
20.1	Constant	14.98	0
5.8	Constant	5	0
3.1	Constant	5	0
PD	Constant	10	0
OK CANCEL			

Figure 8.8: Paleo Water Depth (PWD) and Sediment Water Interface Temperature (SWIT) input parameters used in PetroProb.

The compaction parameters of the main lithologies are calculated through calibration with the compaction curves in Petro-Mod. The parameters are shown in the Figure 8.9.



LITHOLOGY(1-8)	PHI0	PHI SD	SCALE	SCALE SD	ZDEPTHCHANGE	SCALE2
SANDSTONE	41	0	2600	667	240	3300
SHALE	70	0	1280	16	750	1200
SILT	55	0	1800	621	350	2000
LIMESTONE	51	0	1900	377	1300	1900
SALT	6	0	7000	0	20000	5000
COAL	76	0	2000	0	400	1650
ANHYDRITE	6	0	7000	0	20000	5000
CARBONATE	80	0	1550	377	400	1650

Figure 8.9: Screen shot of the compaction parameters of the main lithologies as introduced in PetroProb..

The thermal conductivity values of the main lithologies were calculated through comparison with the standard conductivity curves from PetroMod. The values were then modified through comparing maturity and temperature models from simple layer-cake models of the main lithologies in both PetroProb and PetroMod (Table 3).

Table 3: Thermal conductivity values based on calibration data.

Lithology	Conductivity Mean	Conductivity SD	Cond. Distribution	Heat Production	Heat Production SD	Heat Production Distribution
Sandstone	4	0	Triangular	4.03E-07	0	Uniform
Shale	1.9	0	Triangular	1.20E-06	0	Uniform
Siltstone	2.1	0	Triangular	3.00E-07	0	Uniform
Limestone	3.1	0	Triangular	2.50E-07	0	Uniform
Salt	6.7	0	Triangular	1.50E-08	0	Uniform
Coal	1	0	Triangular	0	0	Uniform
Anhydrite	6.7	0	Triangular	0	0	Uniform
Dolomite	4.4	0	Triangular	5.00E-07	0	Uniform
Water	0.6	0	Uniform	0	0	Uniform
HC	0.5	0	Uniform	0	0	Uniform

Figure 8.10 shows a comparison between the modelled and modified temperature and maturation using the standard matrix thermal conductivity of shale.

Due to the effect of over-pressuring, which is caused by the evaporites and shale layers, the comparisons of modelled maturation and temperature between PP and PM using the latest value of thermal conductivities does not provide a good fit. This can be explained by the fact that in PM pressure variations and their impact on porosity and therefore thermal conductivity are considered, while in PP, this factor is not taken into account. One way to compensate for that is to reduce the values of the thermal conductivities which simulates the effect of higher porosity due to over-pressuring.

For our modelling procedures we used decreased values of thermal conductivities after having done some modelling a maturity calibration with the actual litho-stratigraphy of the well. The applied values are shown in Figure 8.11.

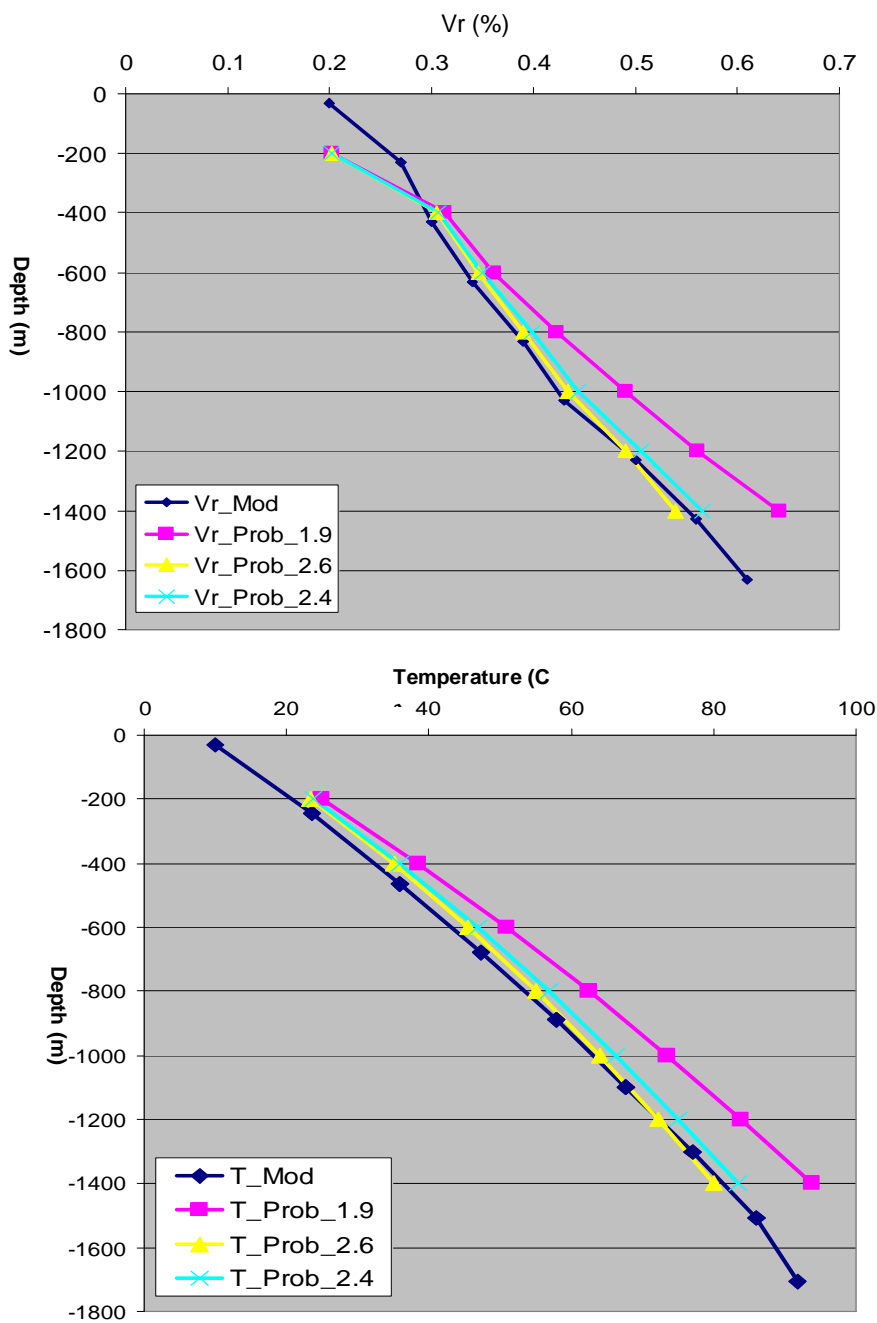


Figure 8.10: Maturation (vitrinite reflectance V_r) and temperature (T) calculated in PetroMod and PetroProb for various conductivity values for shale.

LITHOLOGY	CONDUCTIVITY MEAN	CONDUCTIVITY SD	COND. DISTRIBUTION	HEAT PRODUCTION MEAN	HEAT PRODUCTION SD	HEAT PROD. DISTRIBUTION
sandstone	4.2	0.0	Triangular	4.03e-07	0	Uniform
shale	2.1	0.0	Triangular	1.203e-06	0	Uniform
siltstone	2.2	0.0	Triangular	3.00e-07	0	Uniform
limestone	3.1	0.0	Triangular	2.50e-07	0	Uniform
salt	7	0.0	Triangular	1.50e-08	0	Uniform
coal	1	0.0	Triangular	0	0	Uniform
anhydrite	6.75	0.0	Triangular	0	0	Uniform
dolomite	4.4	0.0	Triangular	5.00e-07	0	Uniform
water	0.6	0.0	Uniform	0	0	Uniform
HC	0.5	0.0	Uniform	0	0	Uniform

Figure 8.11: Screenshot of the modified thermal conductivity values used in PetroProb. The values are obtained through calibration of maturation and temperature values from layer-cake models.

The initial lithosphere parameters used in the modelling are presented in Figure 8.12. The thickness of the lithosphere and the crust are derived from previous studies in the Dutch offshore.

PARAMETER NAME	UNITS	VALUE mean	VALUE sd	DISTRIBUTION
lithosphere_thickness	[m]	1.1500E+05	2.0E+04	Uniform
crust_thickness	[m]	3.50E+04	5.0E+03	Uniform
rho0_crust	[kg/m3]	2800	0	Constant
rho0_mantle	[kg/m3]	3400	0	Constant
conductivity_crust	[-]	2.6	0	Constant
conductivity_mantle	[-]	3.4	0	Constant
heat_production_upper_crust_0means40%	[microW/m3]	0	0	Constant
heat_production_lower_crust	[microW/m3]	0.5	0	Constant
lithosphere_thermal_expansion	[-]	3.20E-05	0	Constant
base_temperature	[C]	1330	0	Constant
rho_underplate	[kg/m3]	3000	0	Constant

Figure 8.12: Screenshot of the lithosphere properties and parameters used in modelling well P06-01.

The burial history of well P06-01 is presented in Figure 8.12. The major uplift and erosion phases are clearly seen in the burial history.

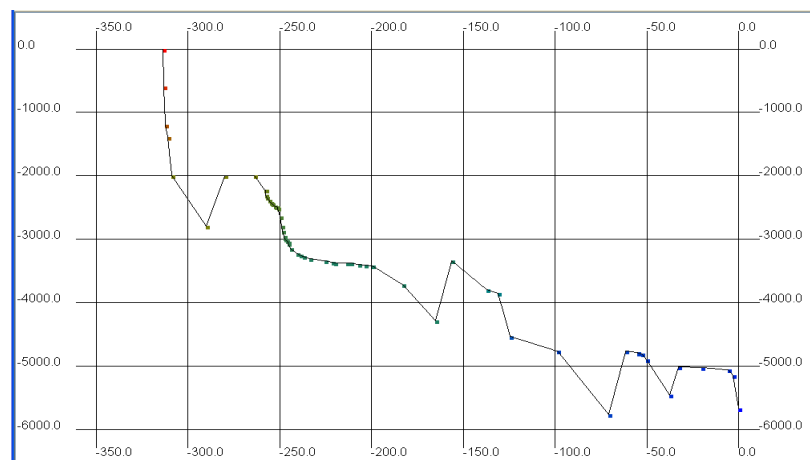
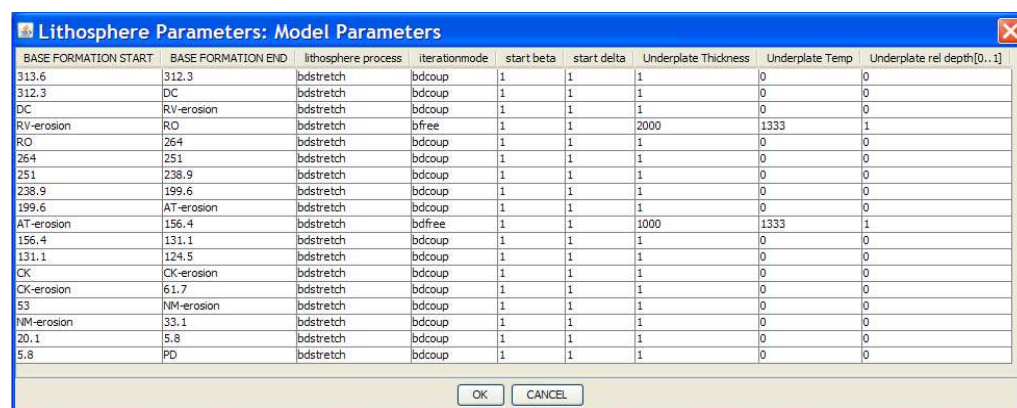


Figure 8.13: Burial curve of well P06-01.

Tectonic model and the calibration of data

The tectonic model used for the inversion of the subsidence curve of the well included the major uplift and erosion phases. The Saalian erosion phase is defined as caused by a thermal uplift phase in the early Permian. In this phase we assume a subcrustal extension ($b = \text{free}$) which is accompanied by no crustal extension ($a = \text{constant}$). We enter a 2000 m thick underplated layer below the crust with a temperature of ~ 1333 C. In the Late Kimmerian I erosion phase there was an uplift and erosion associated with volcanism, but there was also extension which means that the subcrustal lithosphere as well as the crust underwent extension. For this reason we start with a scenario where both factors (a , b) can vary freely and independently. We also introduce an underplating of 1000 m at the base of the crust. This scenario can be changed and tested to see the impact on the model.

The Subhercynian-Laramide uplift and erosion event is introduced as an inversion phase. Uplift due to inversion is defined in PetroProb as a coupled model (e.i. $a=b$), where both factors are left to be determined by the subsidence curves. The lithospheric compression during the inversion is reflected in the extension factors ($a = b < 1$) which indicates shortening of the lithosphere. This is also applied for the later Cenozoic uplift phases (Figure 8.14).



BASE FORMATION START	BASE FORMATION END	lithosphere process	iterationmode	start beta	start delta	Underplate Thickness	Underplate Temp	Underplate rel depth[0..1]
313.6	312.3	bdstretch	bdcoup	1	1	1	0	0
312.3	DC	bdstretch	bdcoup	1	1	1	0	0
DC	RV-erosion	bdstretch	bdcoup	1	1	1	0	0
RV-erosion	RO	bdstretch	bfree	1	1	2000	1333	1
RO	264	bdstretch	bdcoup	1	1	1	0	0
264	251	bdstretch	bdcoup	1	1	1	0	0
251	238.9	bdstretch	bdcoup	1	1	1	0	0
238.9	199.6	bdstretch	bdcoup	1	1	1	0	0
199.6	AT-erosion	bdstretch	bdcoup	1	1	1	0	0
AT-erosion	156.4	bdstretch	bdfree	1	1	1000	1333	1
156.4	131.1	bdstretch	bdcoup	1	1	1	0	0
131.1	124.5	bdstretch	bdcoup	1	1	1	0	0
CK	CK-erosion	bdstretch	bdcoup	1	1	1	0	0
CK-erosion	61.7	bdstretch	bdcoup	1	1	1	0	0
53	NM-erosion	bdstretch	bdcoup	1	1	1	0	0
NM-erosion	33.1	bdstretch	bdcoup	1	1	1	0	0
20.1	5.8	bdstretch	bdcoup	1	1	1	0	0
5.8	PD	bdstretch	bdcoup	1	1	1	0	0

Figure 8.14: Screenshot of the tectonic steps used in the modelling. Some changes in the model will be made and new scenarios will be discussed later.

The temperature and vitrinite data used for calibrating the model are shown in Figures 8.4. Multiple modelling and calibration runs showed that the amount of erosion during the late Cretaceous and early Palaeocene are an important source of uncertainty. Various scenarios for erosion were tested starting with an erosion amount of 2000 m for the Chalk and ~ 450 m of erosion for the Lower North Sea group (Based on regional thickness distribution outside inverted areas). The erosion estimates were based on stratigraphic correlation and comparison with wells in the area. In order to get a good fit with the temperature and vitrinite data the erosion of the Chalk group was reduced from 2000 m to 800 m. The effect of the erosion of the Lower North Sea Group on the calibration was also tested. The erosion value of the Lower North Sea group seemed to have less effect on the calibration and implementing less amount of erosion (~ 250 m) did not improve the fit between the model and the measured data. Both assumed amounts of erosion for the Lower North Sea Group (~ 450 m and ~ 250 m) resulted in a similar fit (Figure 8.15).

The resulting heat-flow and tectonic models are based on the best-fit between temperature and vitrinite values and are shown in Figure 8.16. The associated

initial lithosphere thickness is around 128.310 m and the crust thickness is 34.643 m.

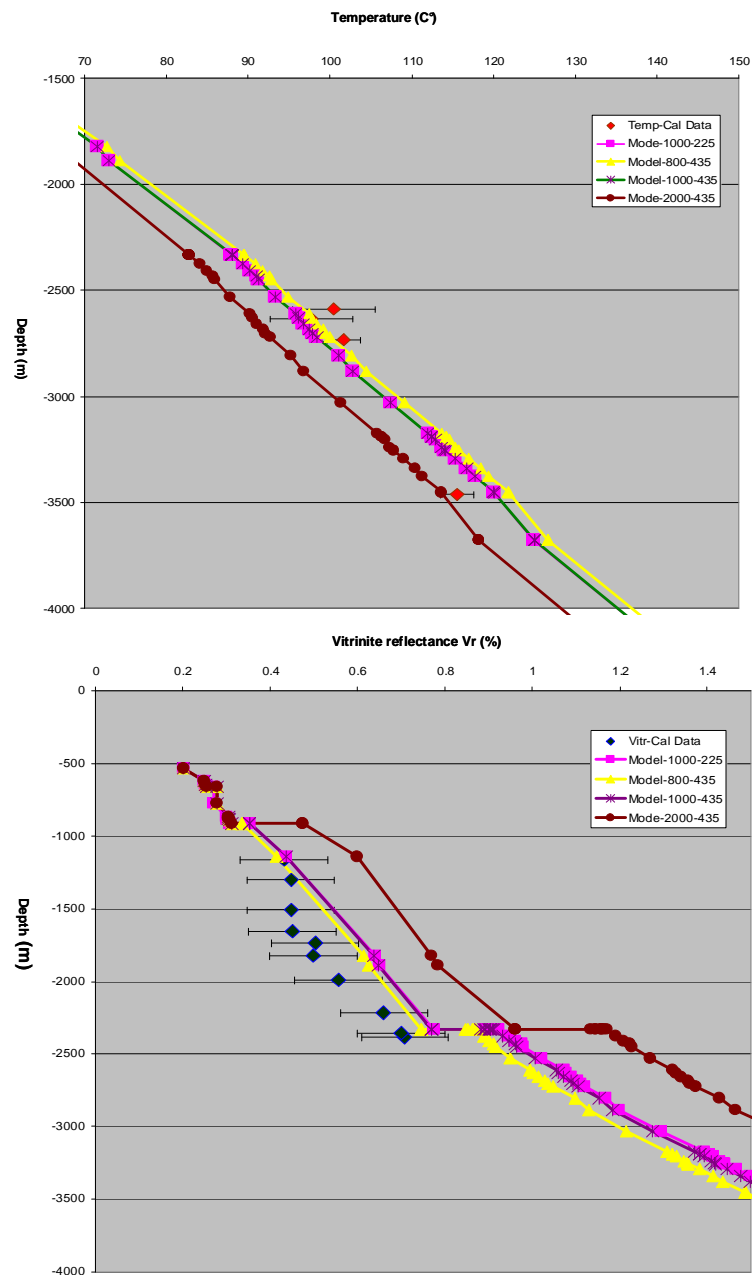


Figure 8.15: Calibration results and the effect of reducing the amount of erosion load during the Late Cretaceous and Late Palaeogene.

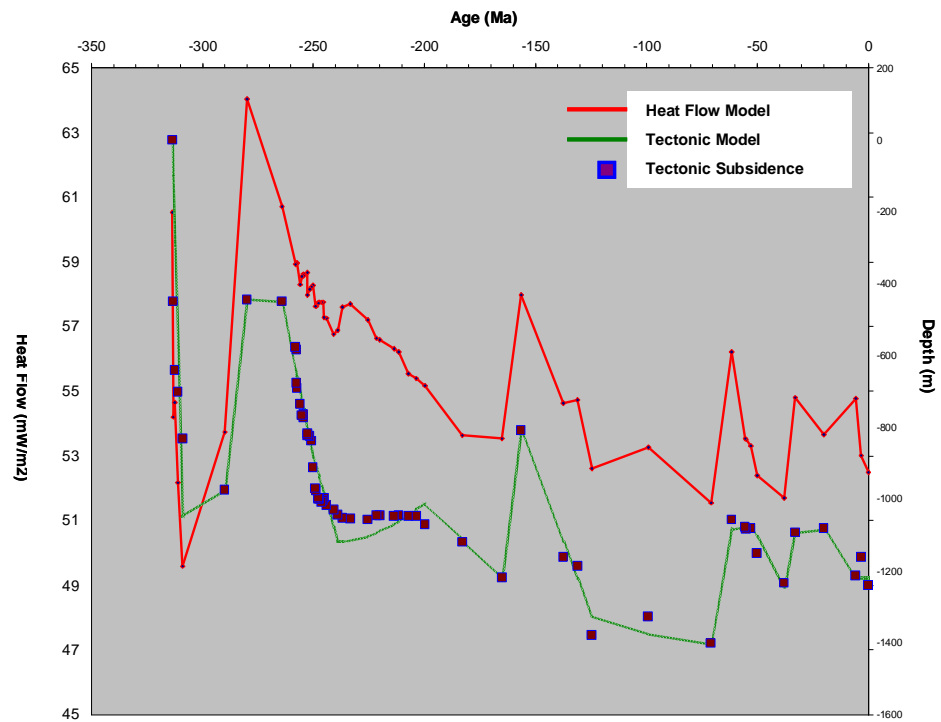


Figure 8.16: Modelled basal heat-flow, tectonic model and observed tectonic subsidence. Good fit is obtained between modelled and observed tectonic subsidence. The modelled heat-flow is used to achieve good fit between observed and measured calibration data (T_r and V_r)

Alternative tectonic models

In the Late Kimmerian I erosion phase the uplift and erosion was associated with volcanism as well as extension. The starting model included a scenario where both extension factors (a , b) could change freely and independently, i.e. $a, b = \text{free}$. To what extent this model is representative is not well known and therefore other models were introduced to describe this phase and the results were compared to the initial model.

Two more scenarios were tested concerning the Later Kimmerian erosion phase. The first was defined as b : free and a fixed to 1. An underplating of around 1000 m was introduced and it was given a temperature of 1333 C. According to this scenario, the same lithospheric settings are applied as those for the Saalian. In the second scenario the subcrustal extension factor b was set to 1.5 and the crustal extension factor was set to free. This means that there was a mantle thinning, which resulted in volcanism and crustal thinning. For both scenarios, the results indicate that the calibration is mainly determined by the erosion of the Upper Chalk. The alternative tectonic model does not result in significant differences in the modelled tectonic subsidence (Figure 8.17). There is however some changes in the modelled basal heat flow especially during the Late Jurassic and Early Cretaceous Late Kimmerian phases (Figure 8.18). However, the impact the modelled heat-flow difference is not observed in the modelled maturity as it can be seen in the calibration with measured data (Figure 8.19). This is because the heat-flow model in the new tectonic scenario is higher during the Late Kimmerian phase and as such

influences the maturation as the deepest burial is achieved around Later Cretaceous (Figure 8.17, 8.18, 8.19).

From this we conclude that the resulted heat-flow from the first scenario can be used for further analyses and can be considered representative for the well P06-01.

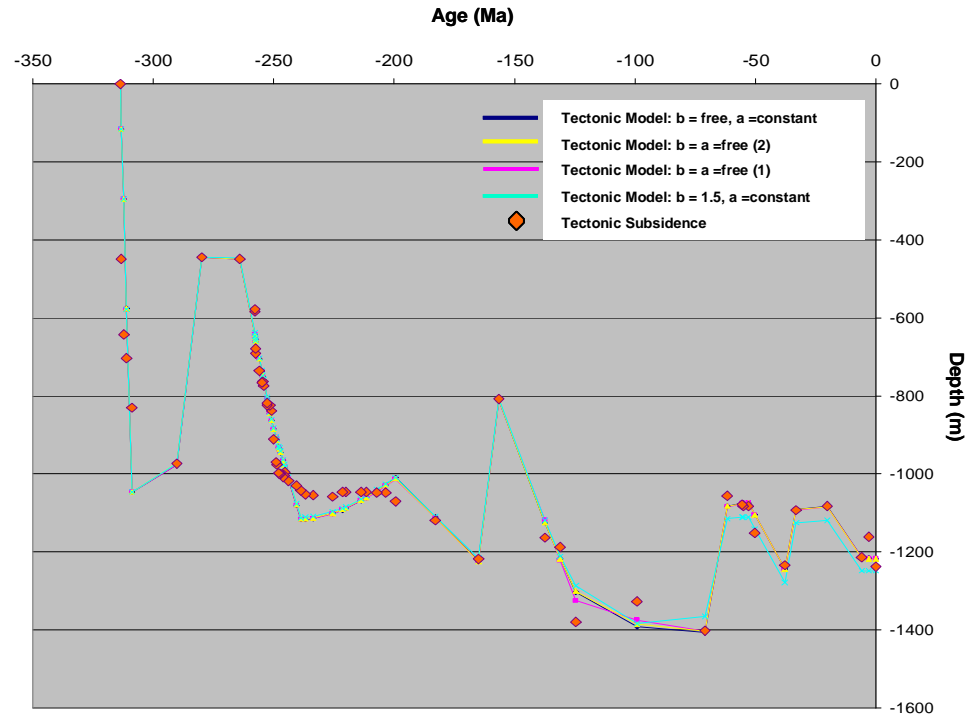


Figure 8.17: Tectonic models for various scenarios for the Late Kimmerian phase. Different scenarios do not seem to have big impact.

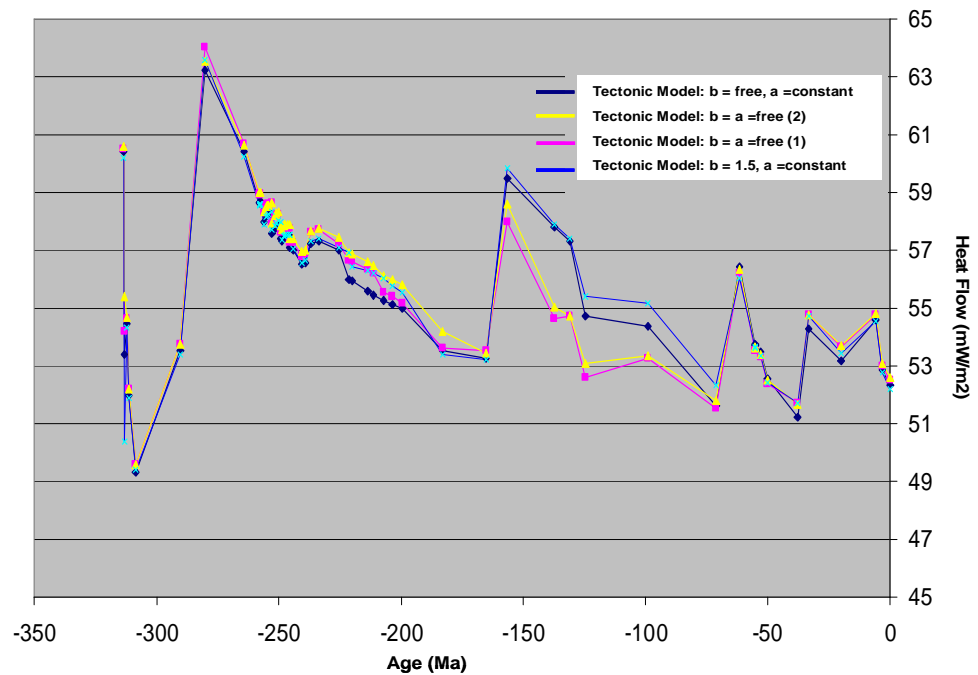


Figure 8.18: Modelled heat-flows for various scenarios for the Late Kimmerian phase.

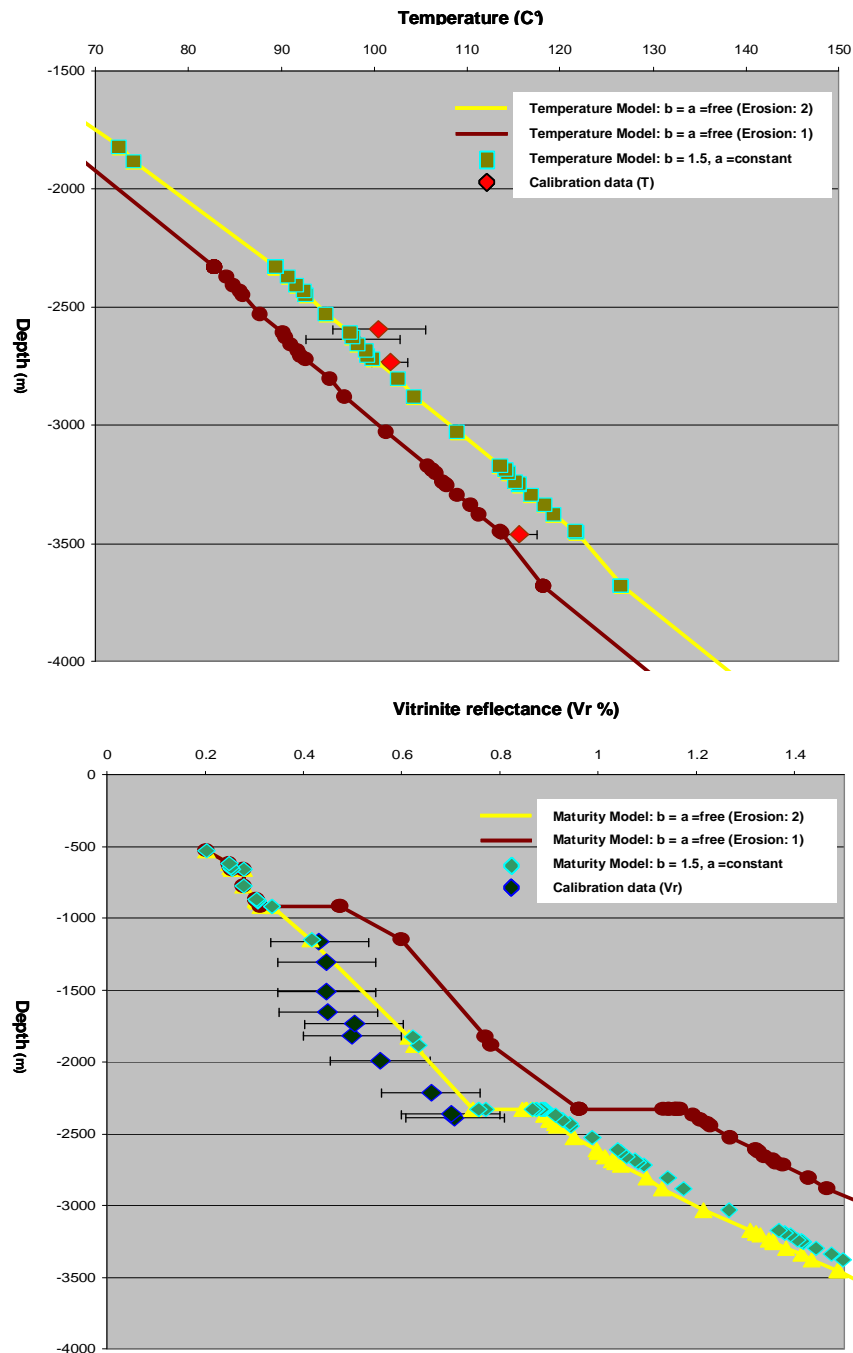


Figure 8.19: Calibration results showing the impact of using a different tectonic scenario for the Late Kimmerian event (Temperature (above), Maturity (below)). The effect of the erosion (Chalk erosion) is also shown. Erosion 1: $er-CK = 800$ m. Erosion 2: $er-CK = 2000$ m.

For both scenarios, the modelled heat-flow at well P06-01 shows two major heat-flow peaks that are produced during thermal uplift phases and associated with major erosion. This implies that the heat peaks observed are not only related to the amount of erosion, but also to the depth of the magmatic event, the thickness of the under plating as well as its temperature. In this well, the present-day heat-flow is about 53 mW/m², while the highest peak is reached during the Saalian phase when the heat-flow reached a value of around 65 mW/m².

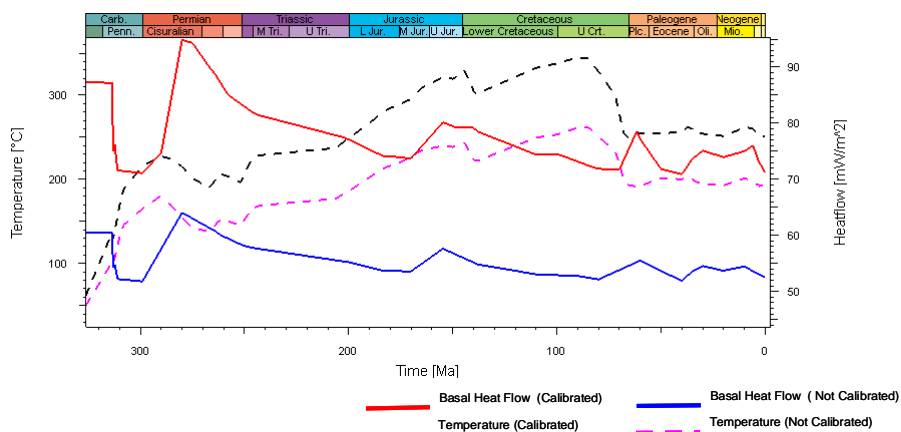
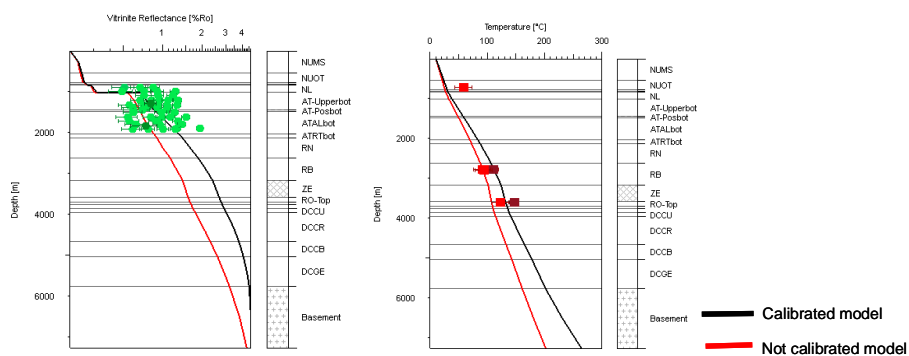
8.6 Annex V: 3D Heat flow calibration

Initial basal heat flow maps were interpolated between six 1D heat flow models. The maps were calibrated to measured data (temperature, vitrinite reflectance) at the location of the six 1D models (wells). However the maps were not calibrated to data from other wells in the study area. The 3D heat flow calibration tool allows us to calibrate the input initial maps to those data. When the data are introduced and the quality of the data are defined, the model runs the simulation where heat flow values are modified in an area surrounding the calibration wells until a good fit is achieved. The new heat flow values at the location of the wells are stored and new maps are created. The maps are then smoothed over the area and between the calibrated wells. The new maps are then exported and reused for the simulation and the maturity calculation.

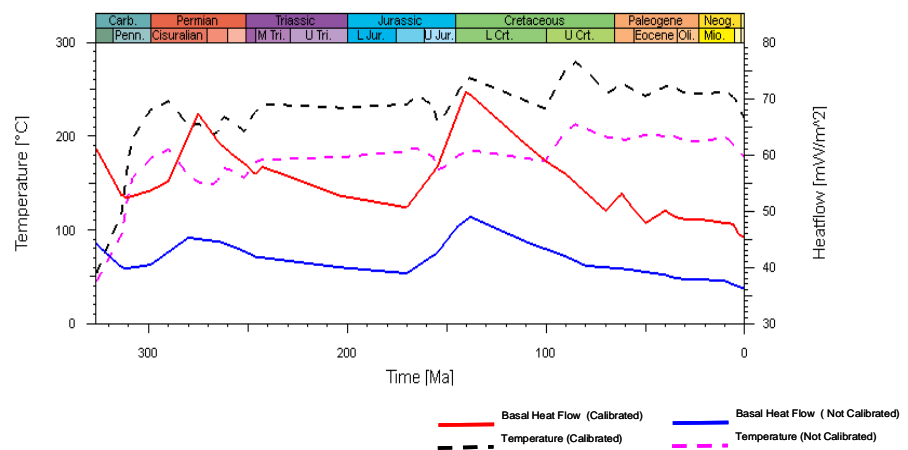
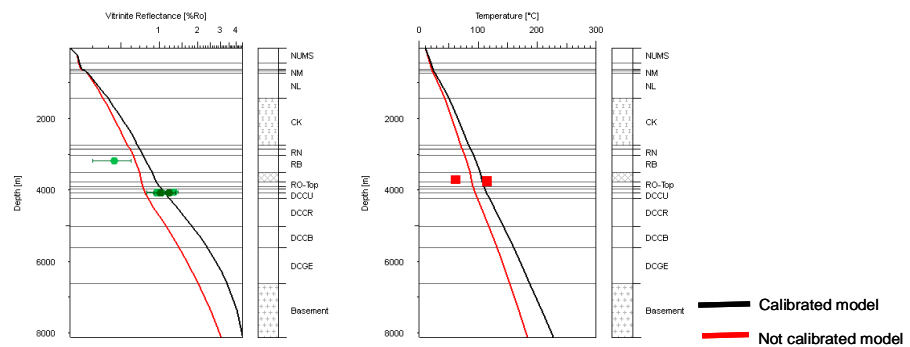
In our study, 36 wells were used to calibrate the heat flow maps. Some examples of the calibration results are preselected below.

8.6.1 Examples of heat flow calibration in few wells

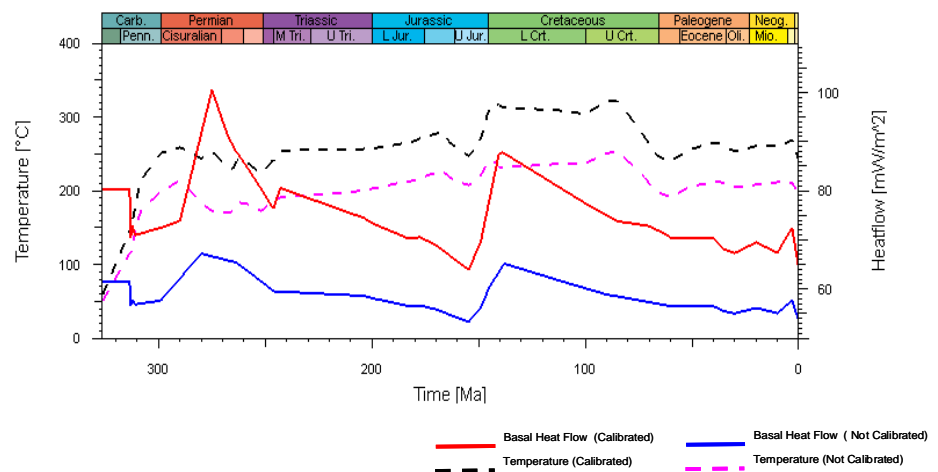
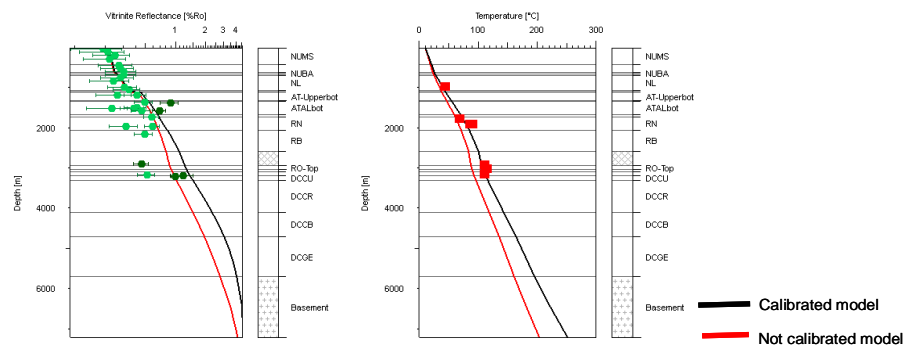
Well P02-03



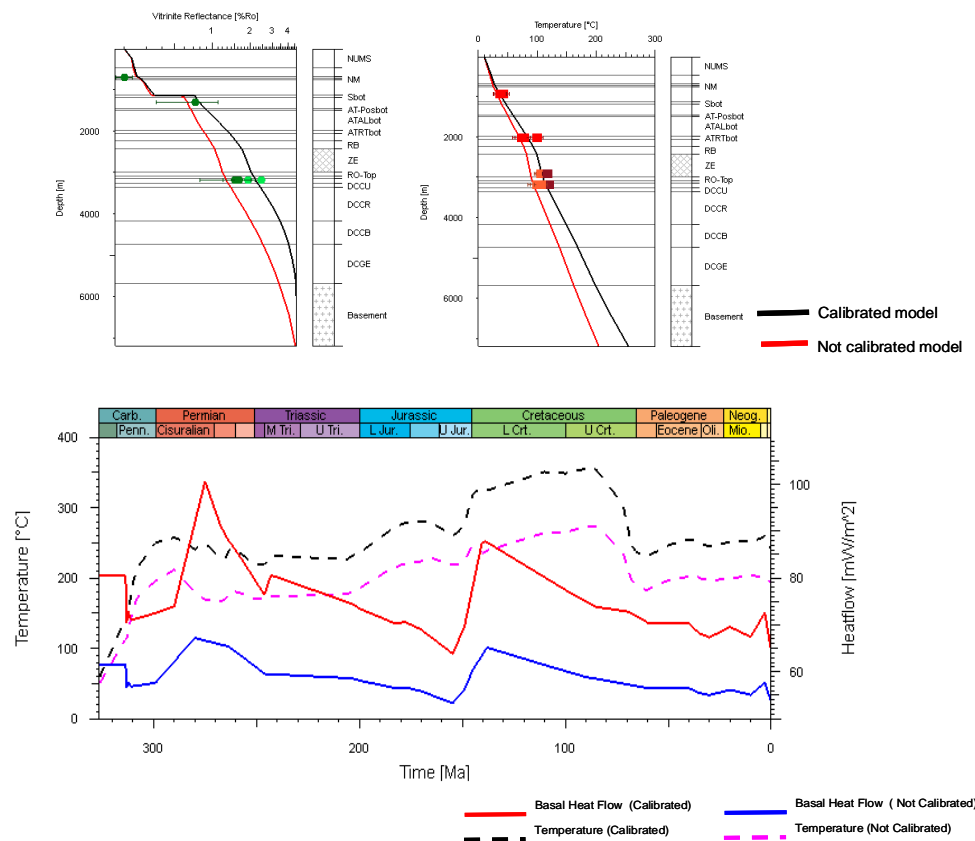
Well L10-06



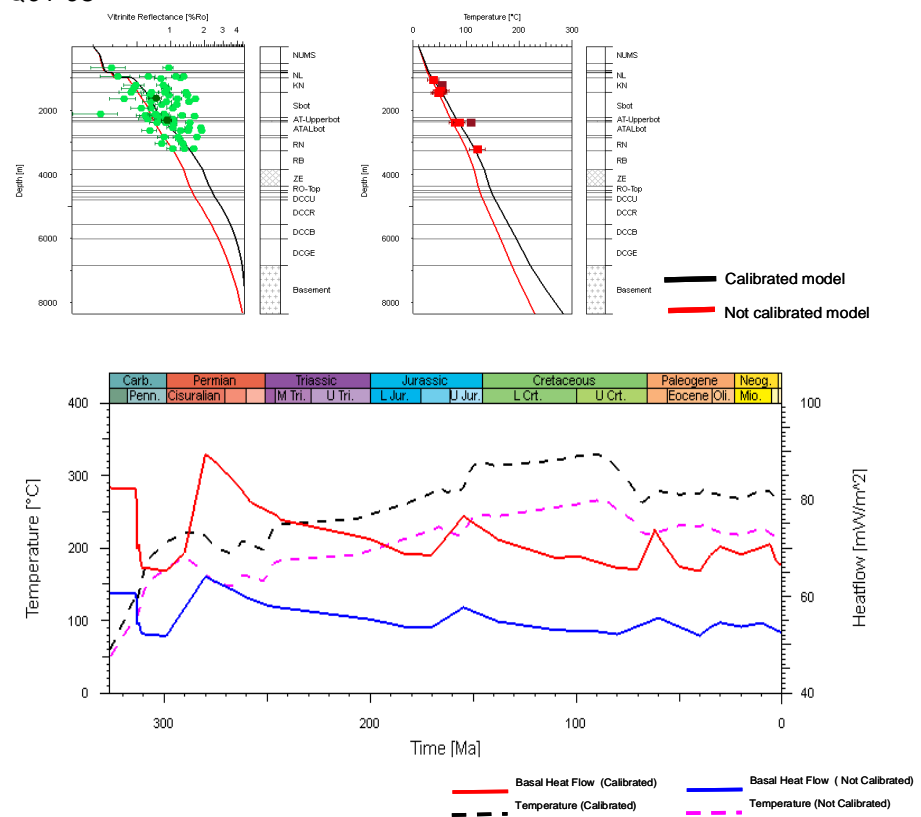
Well K14-01



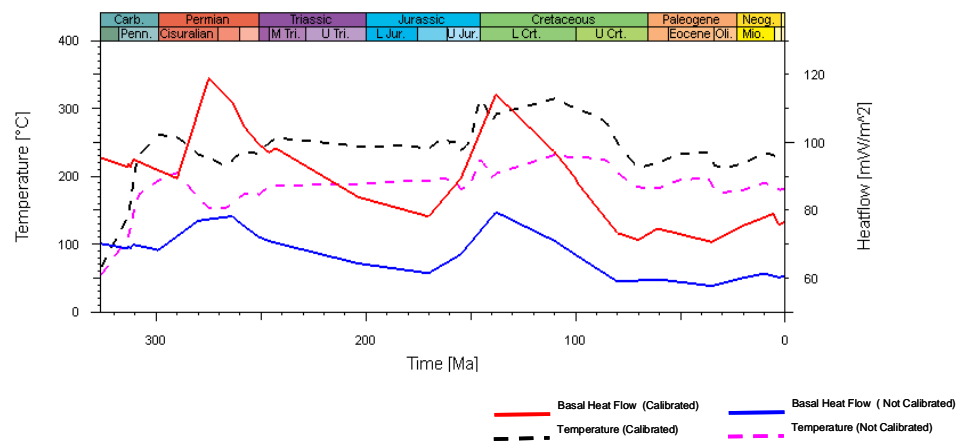
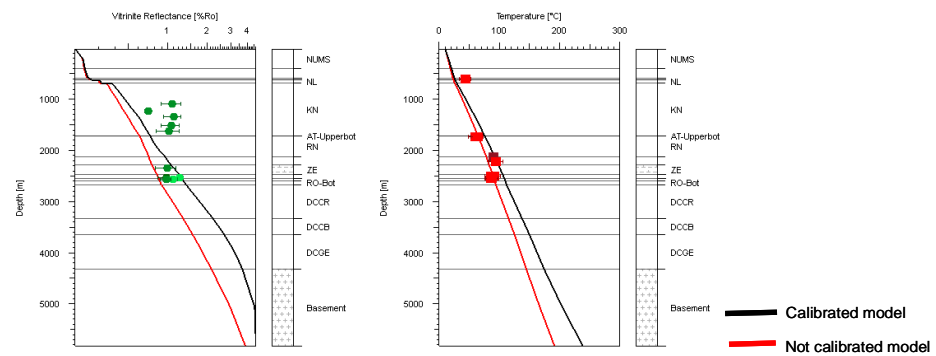
Well K14-02



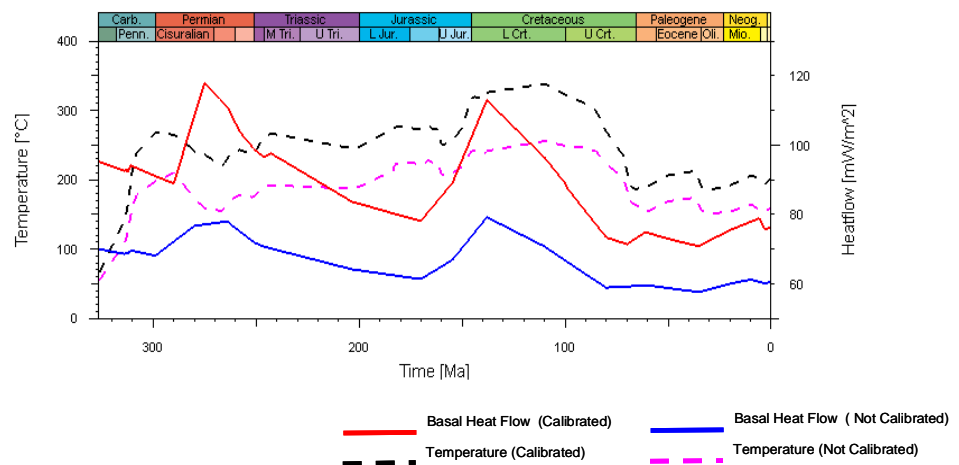
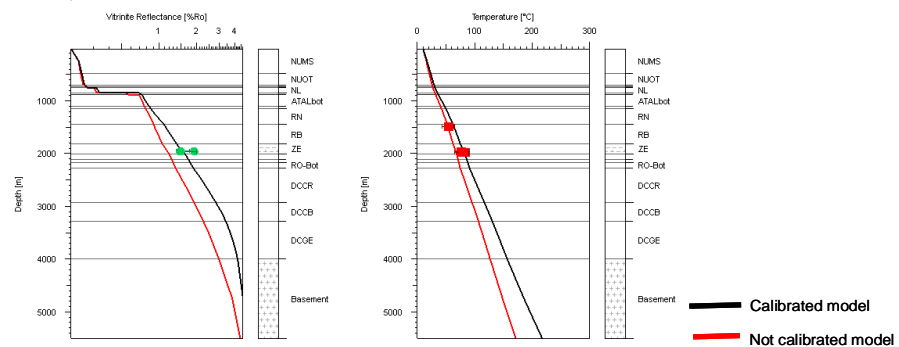
Well Q01-03



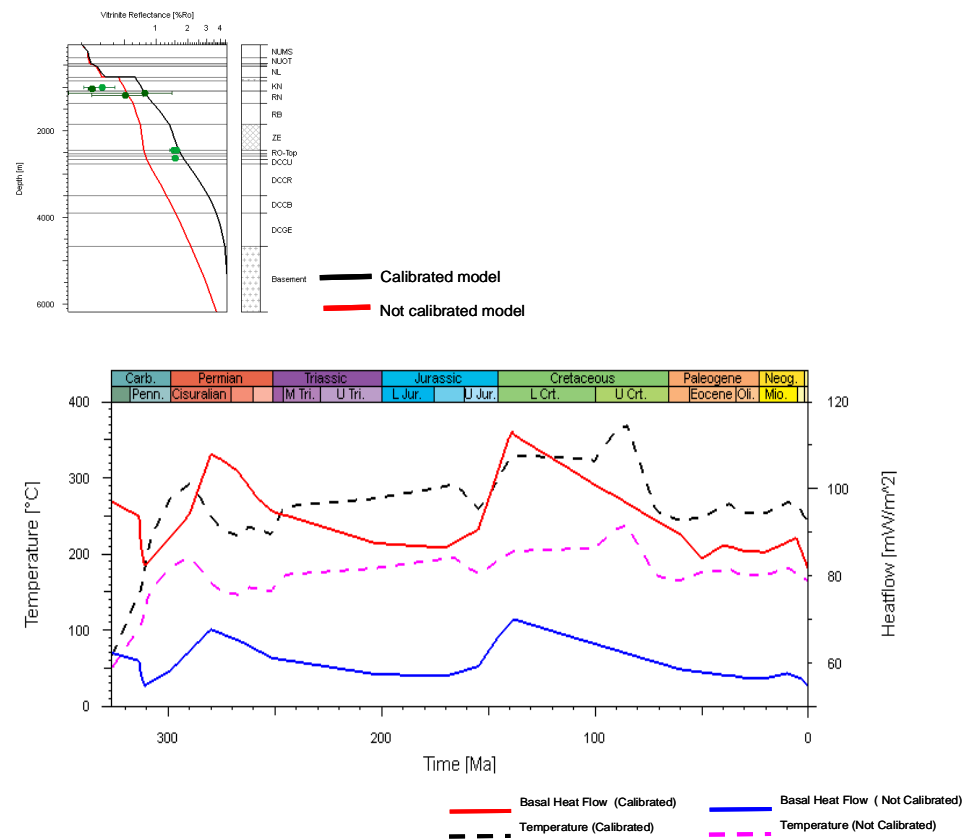
Well Q07-01



Well Q07-05

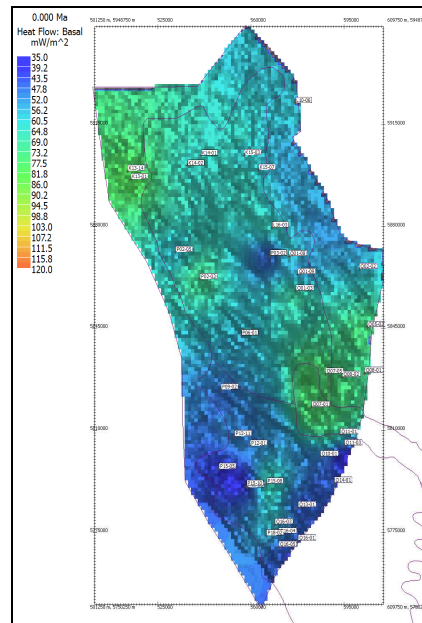
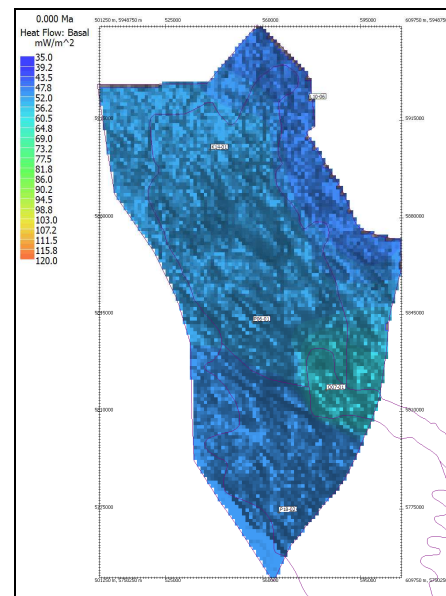
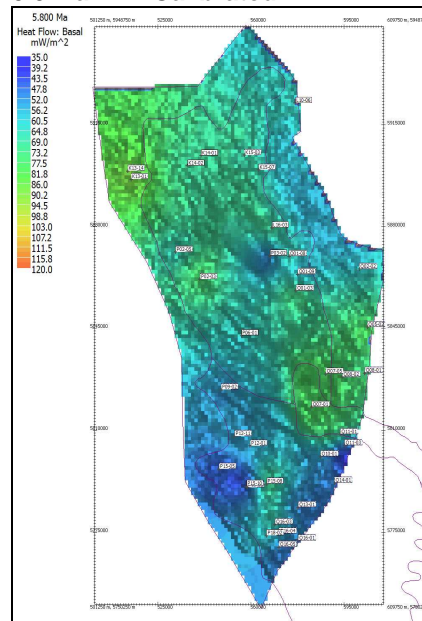
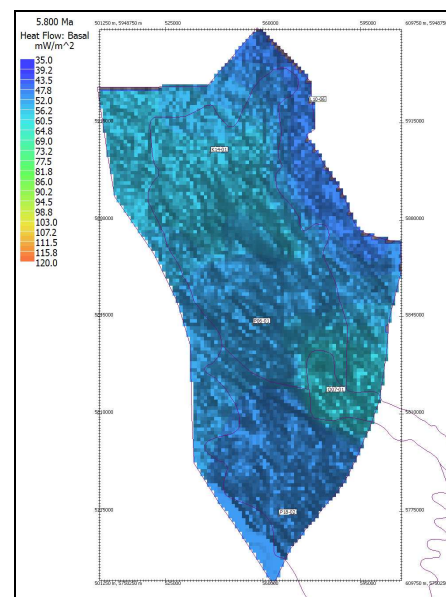


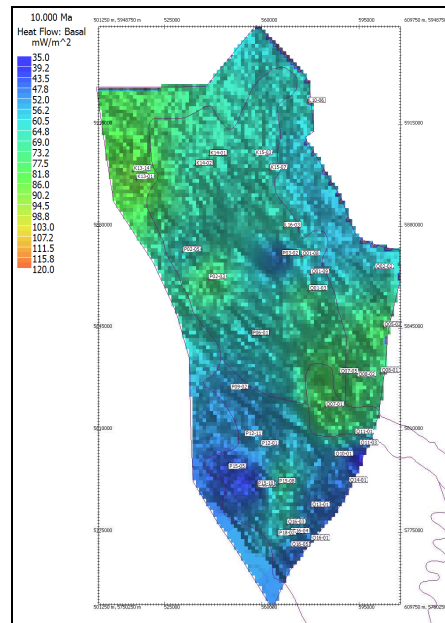
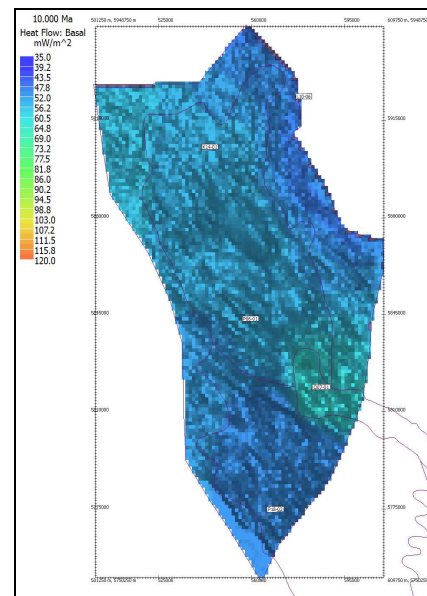
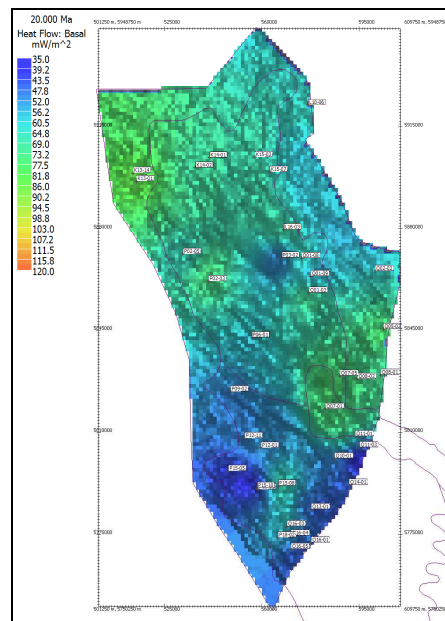
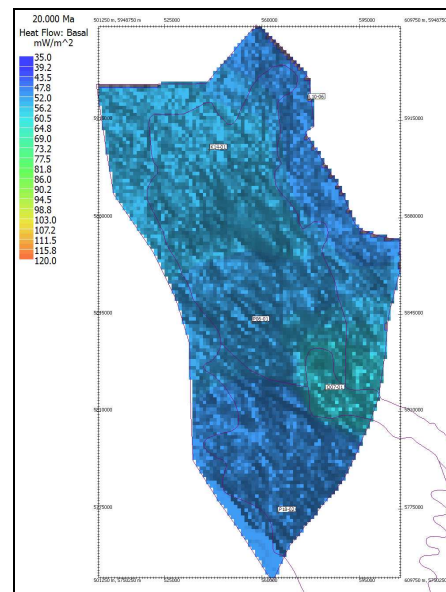
Well K13-01

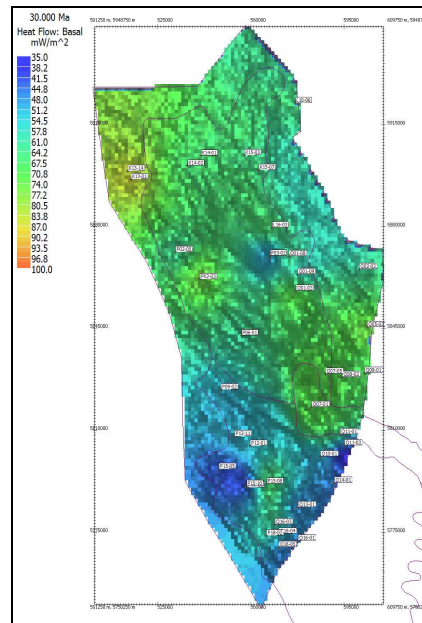
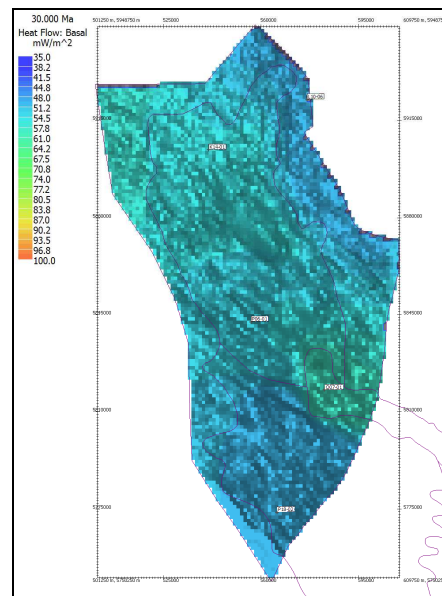
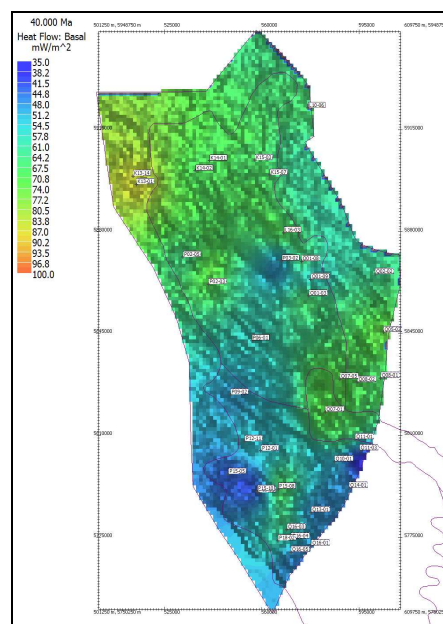
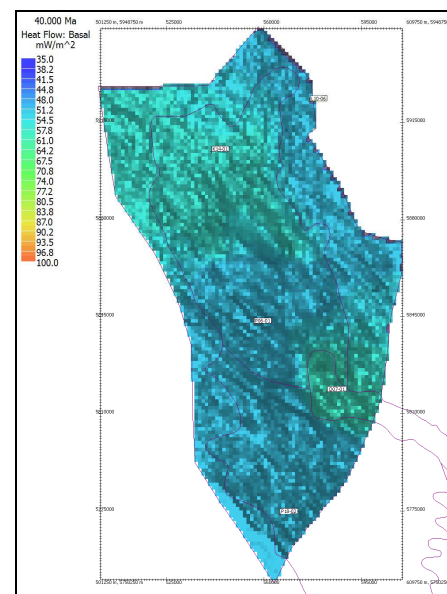


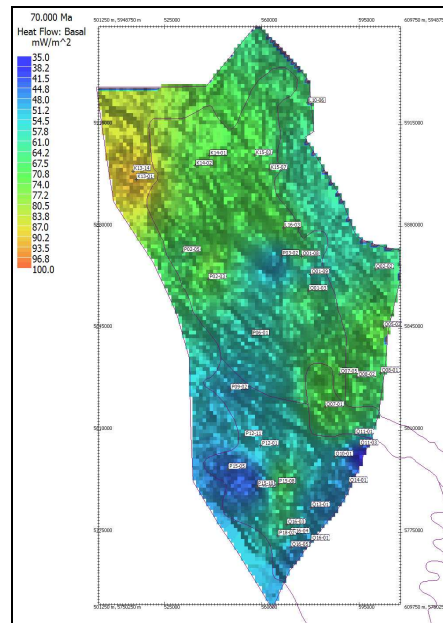
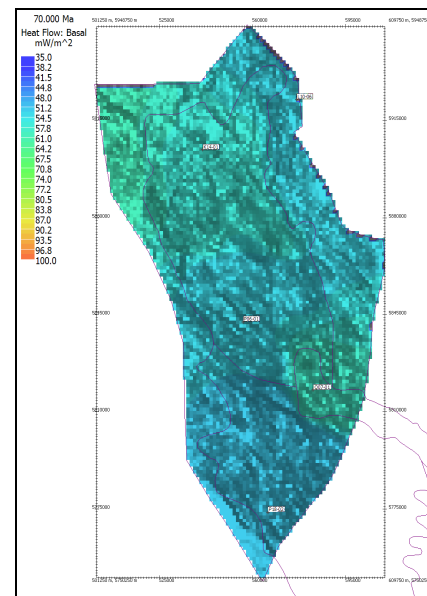
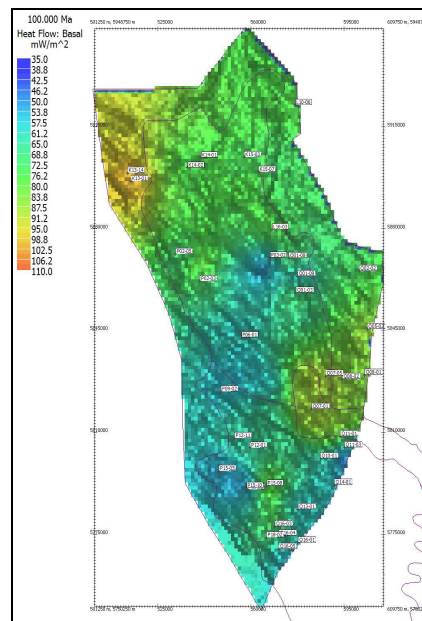
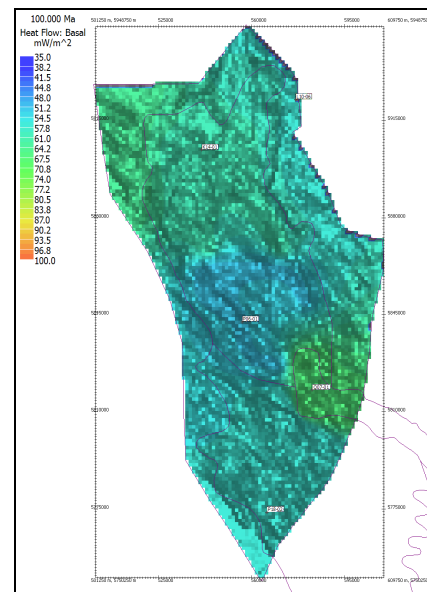
8.6.2 Basal heat flow maps before and after calibration:

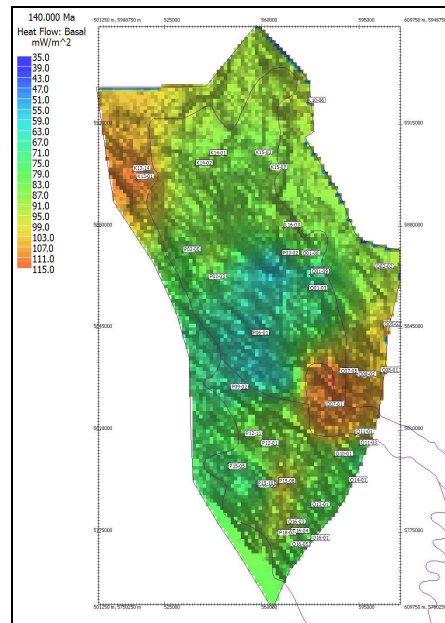
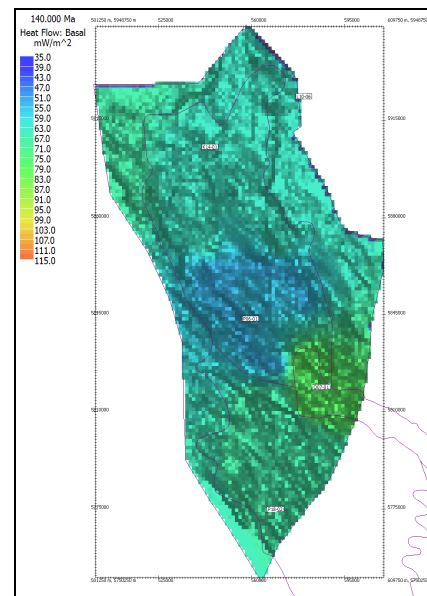
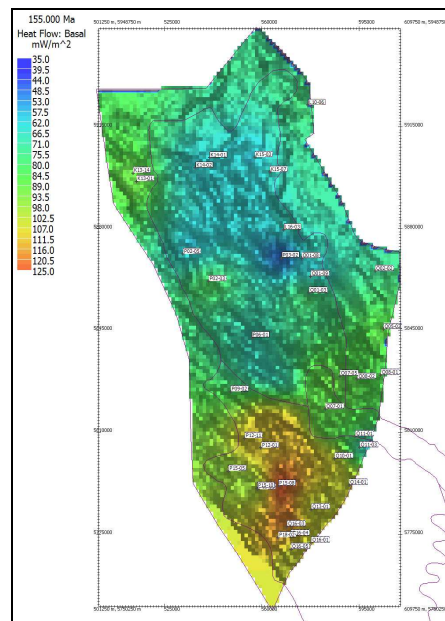
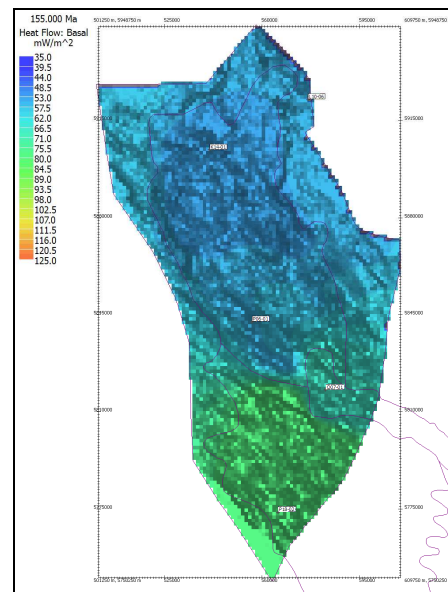
Several basal heat flow maps used in the simulation are presented below. Both calibrated and un-calibrated (initial) heat flow maps are shown for comparison purposes. Wells used for the calibration are overprinted on the calibrated heat flow maps (left). Wells used 1D heat flow modelling and used for generating initial heat flow maps through interpolations are also shown (right). Six wells were used in total for 1D heat flow calibration. Five of these wells are located within the NCP-2F area and one well is located in the NCP-2D area (not shown here).

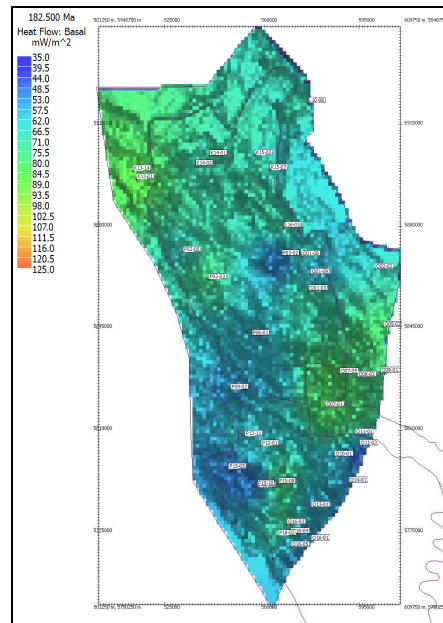
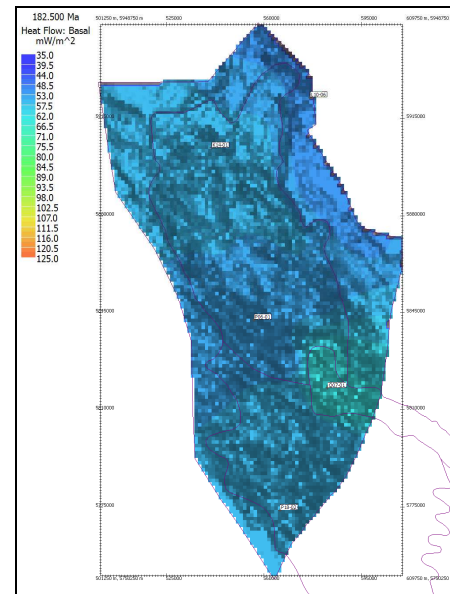
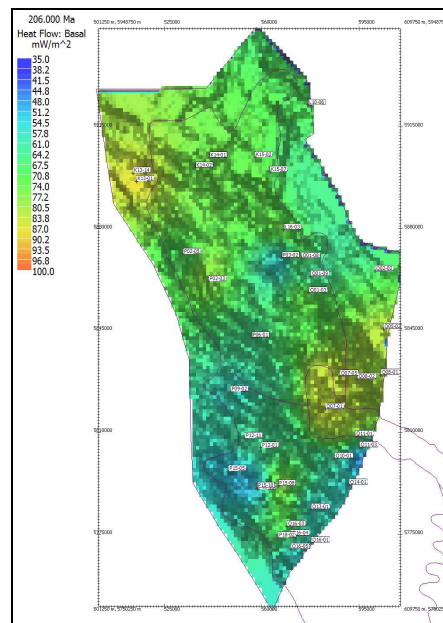
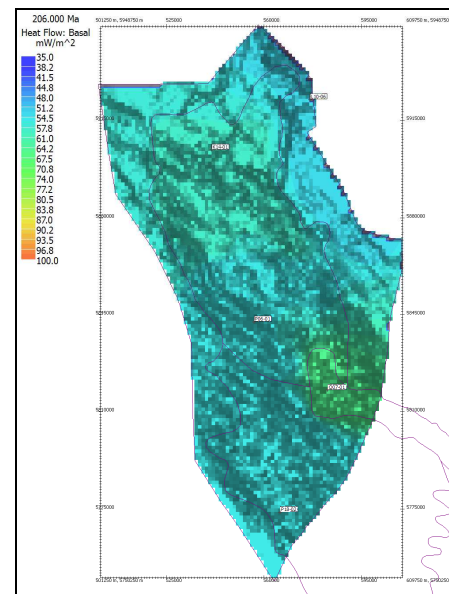
**0.0 Ma Calibrated****Un-calibrated****5.8 Ma Calibrated****Un-calibrated**

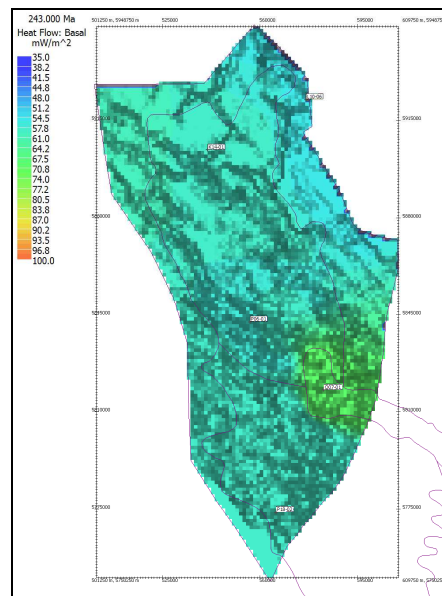
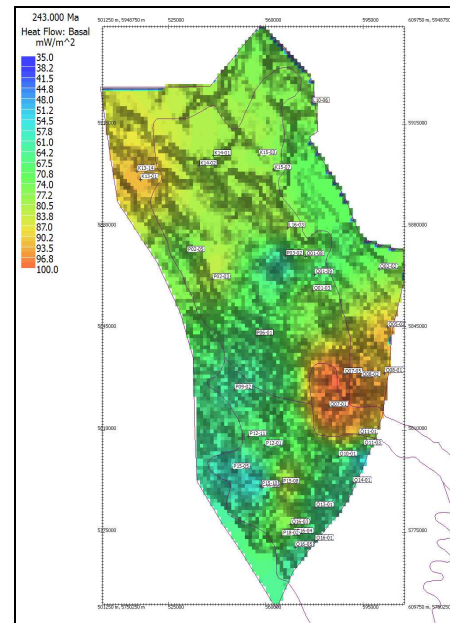
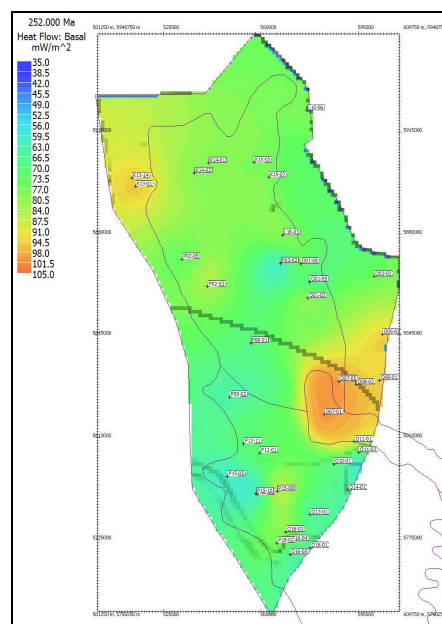
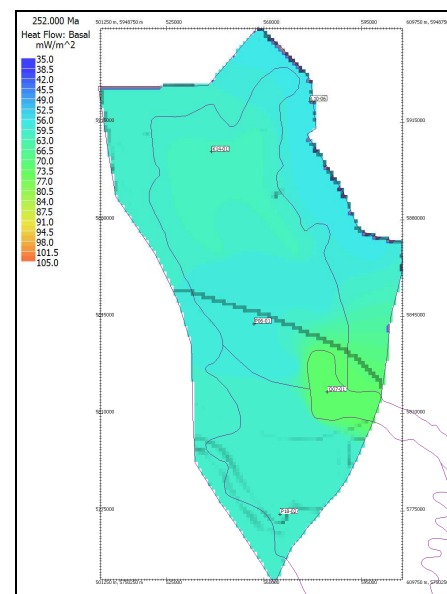
**10.0 Ma Calibrated****Un-calibrated****20.0 Ma Calibrated****Un-calibrated**

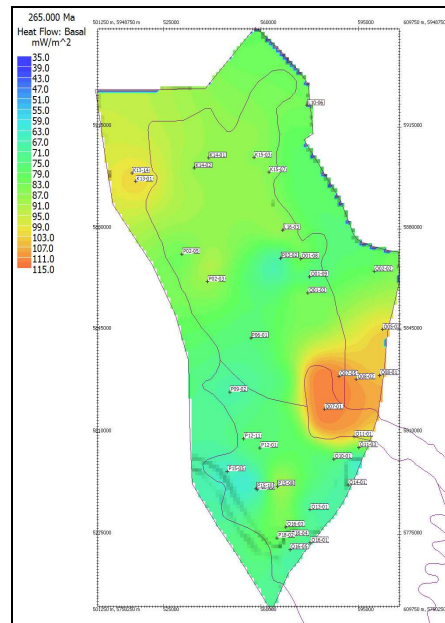
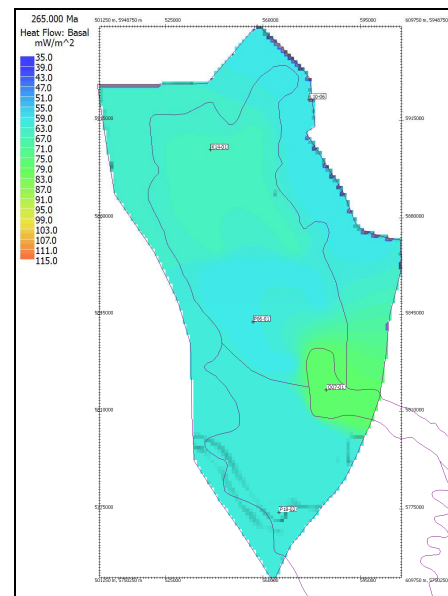
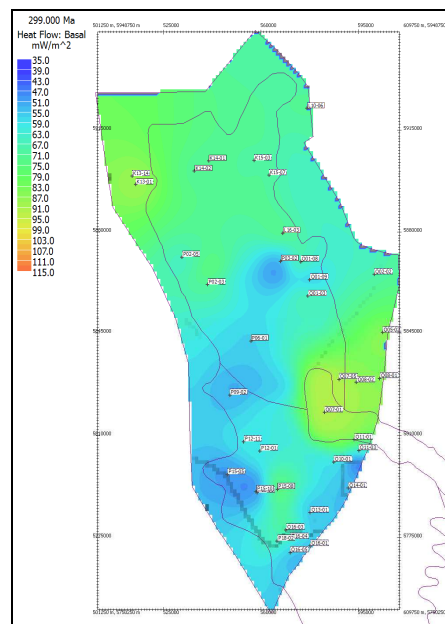
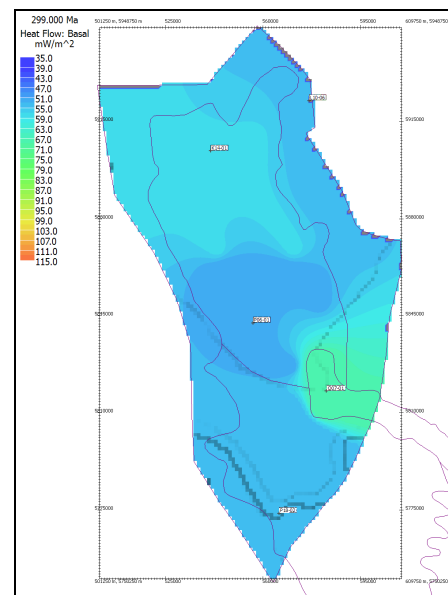
**30.0 Ma Calibrated****Un-calibrated****40.0 Ma Calibrated****Un-calibrated**

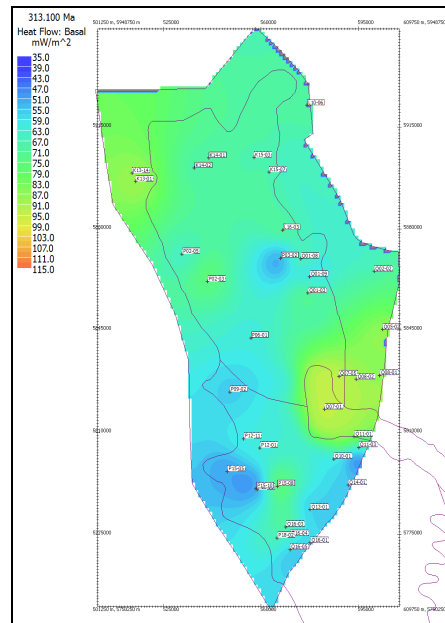
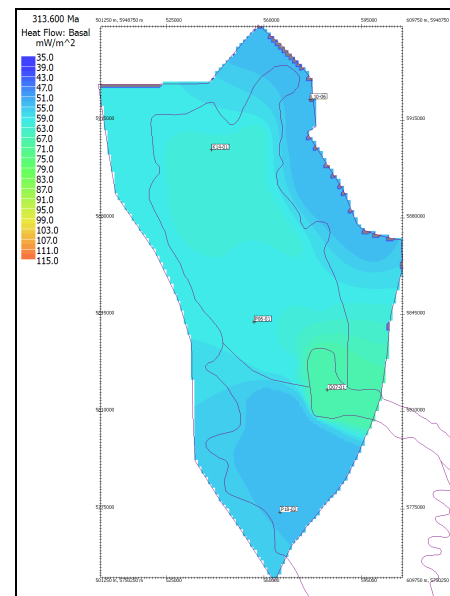
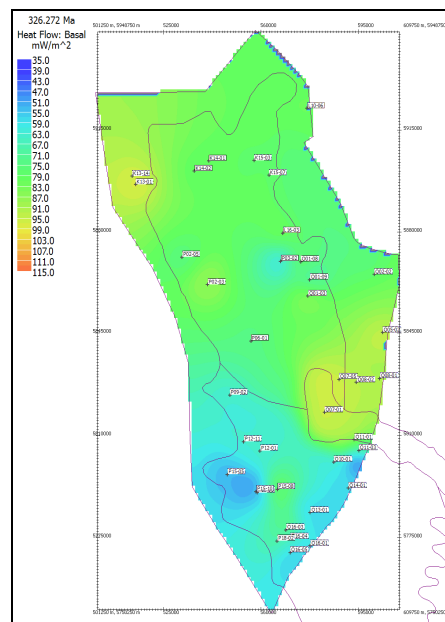
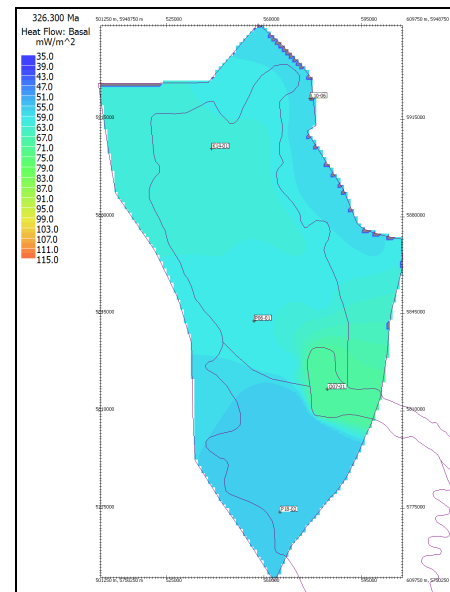
**70.0 Ma Calibrated****Un-calibrated****100.0 Ma Calibrated****Un-calibrated**

**140.0 Ma Calibrated****Un-calibrated****155.0 Ma Calibrated****Un-calibrated**

**182.5 Ma Calibrated****Un-calibrated****206.0 Ma Calibrated****Un-calibrated**

**243.0 Ma Calibrated****Un-calibrated****252.0 Ma Calibrated****Un-calibrated**

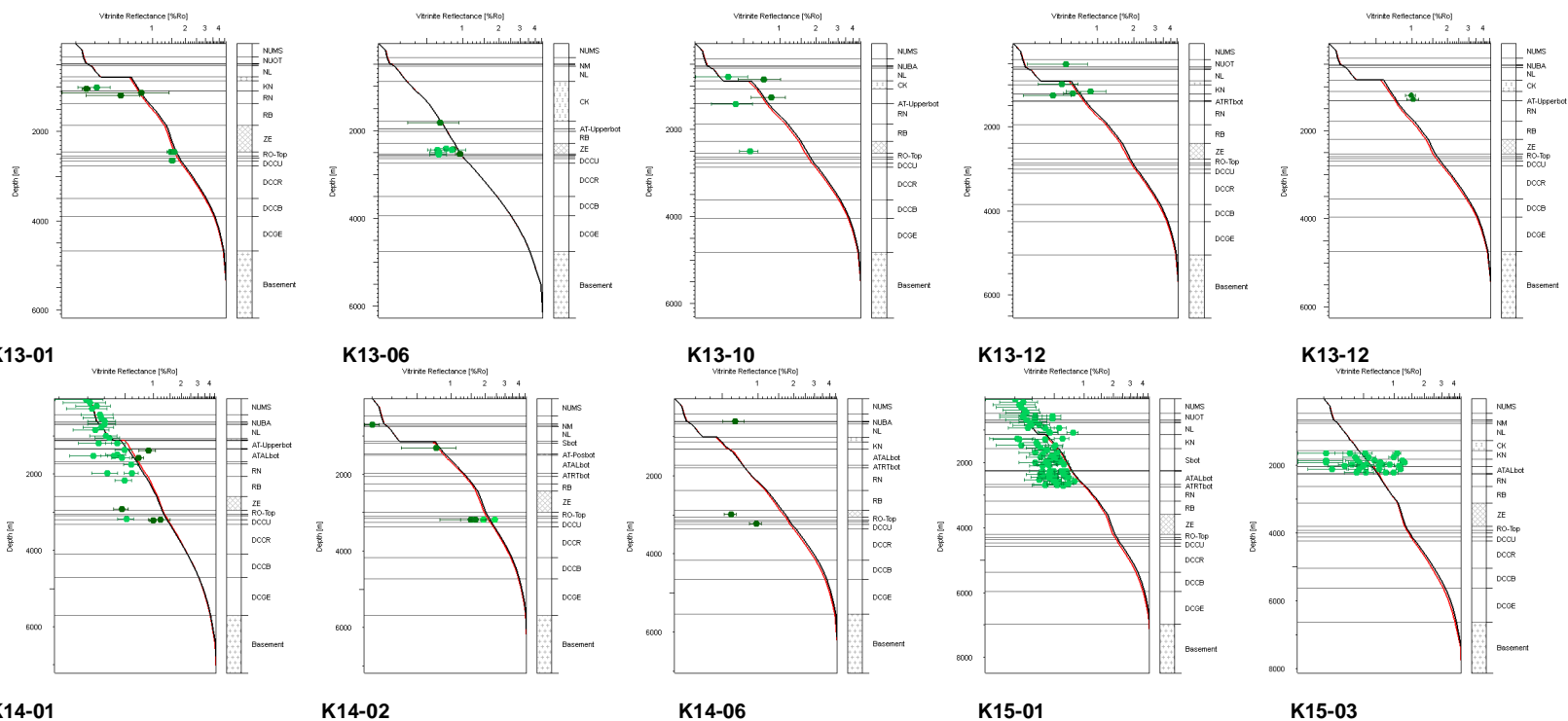
**265.0 Ma Calibrated****Un-calibrated****299.0 Ma Calibrated****Un-calibrated**

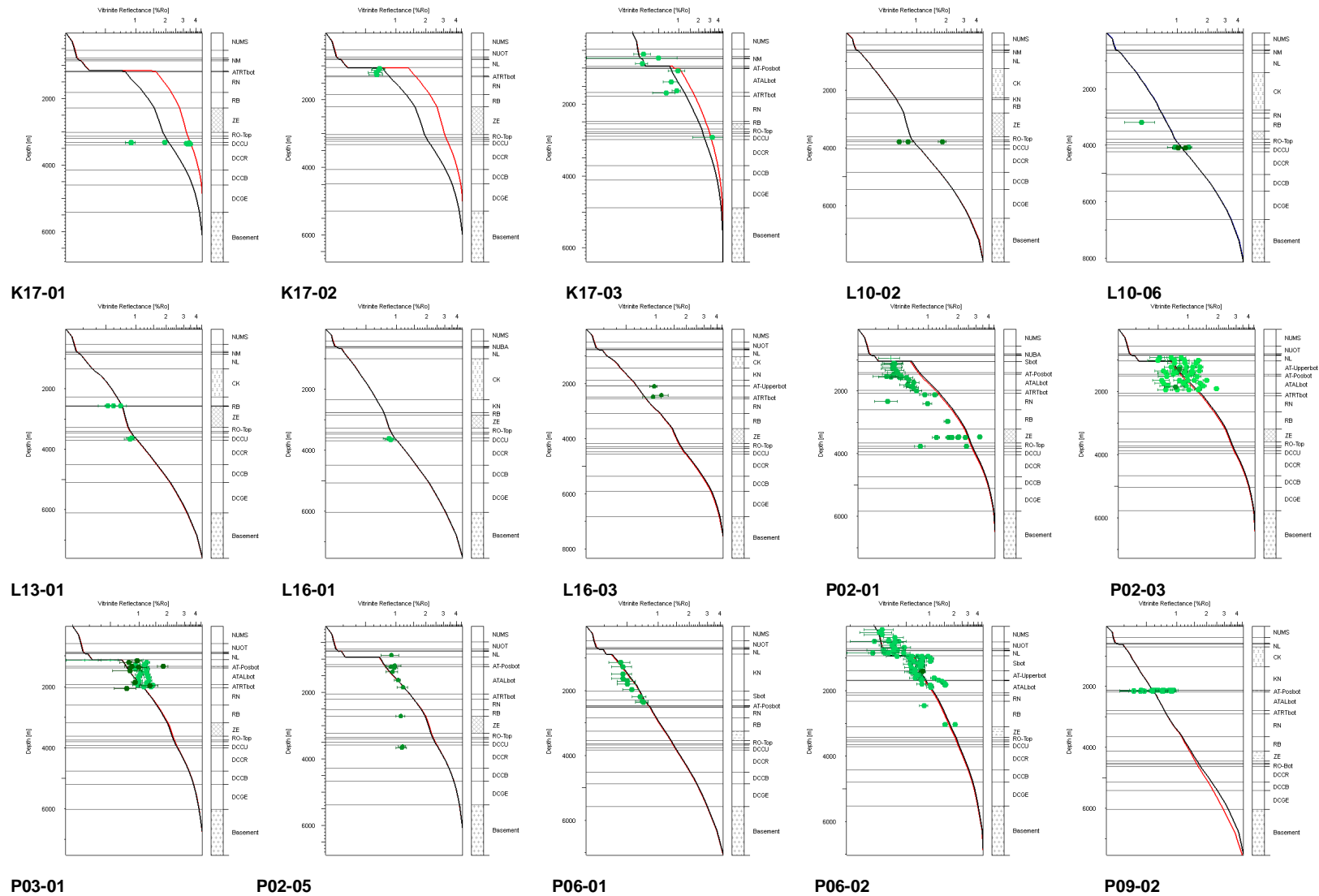
**313.1 Ma Calibrated****Un-calibrated****326.2 Ma Calibrated****Un-calibrated**

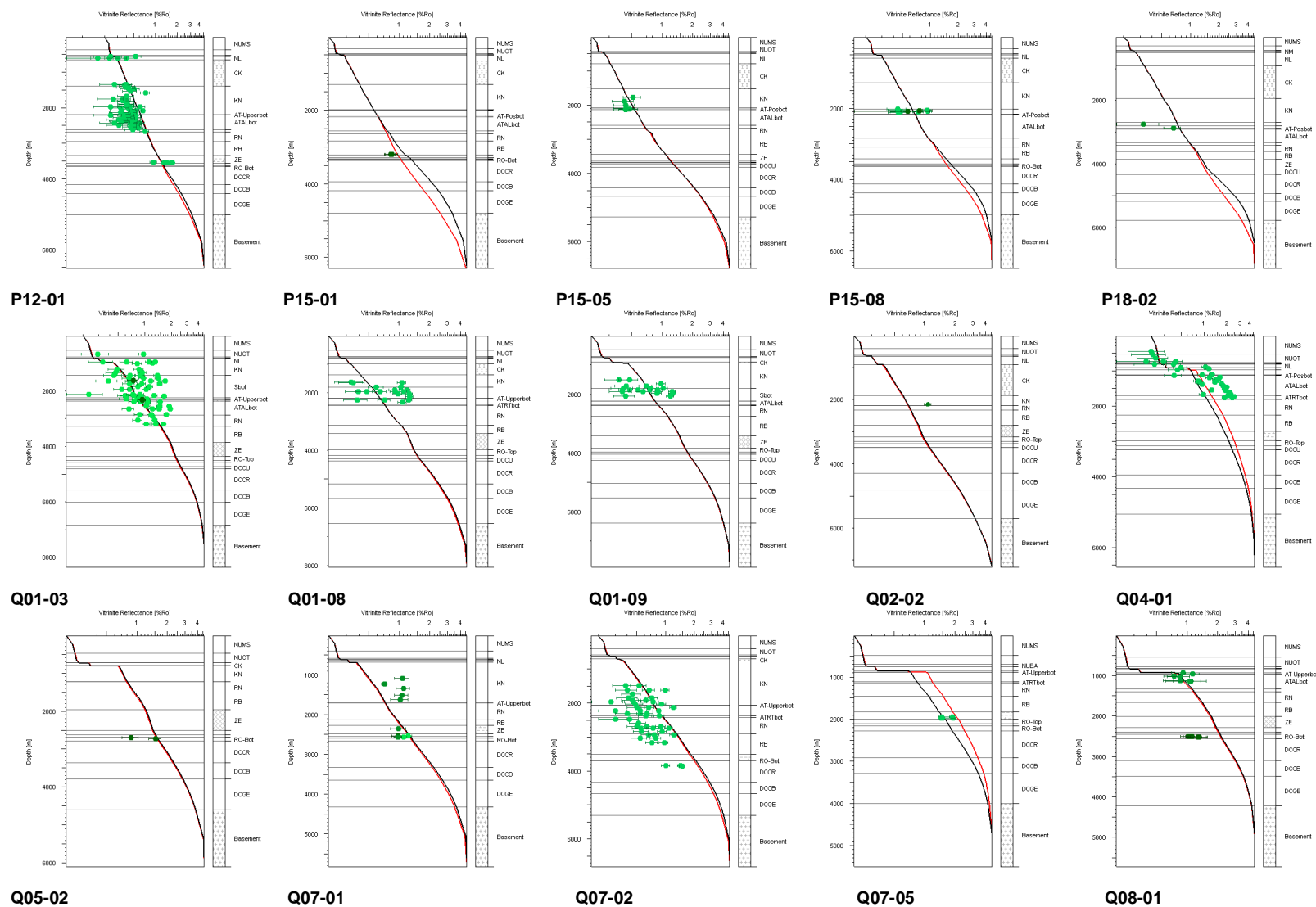
8.7 Annex VI: Calibration of well data

8.7.1 Maturity (Vitrinite reflectance)

— Scenario V
— Scenario IV

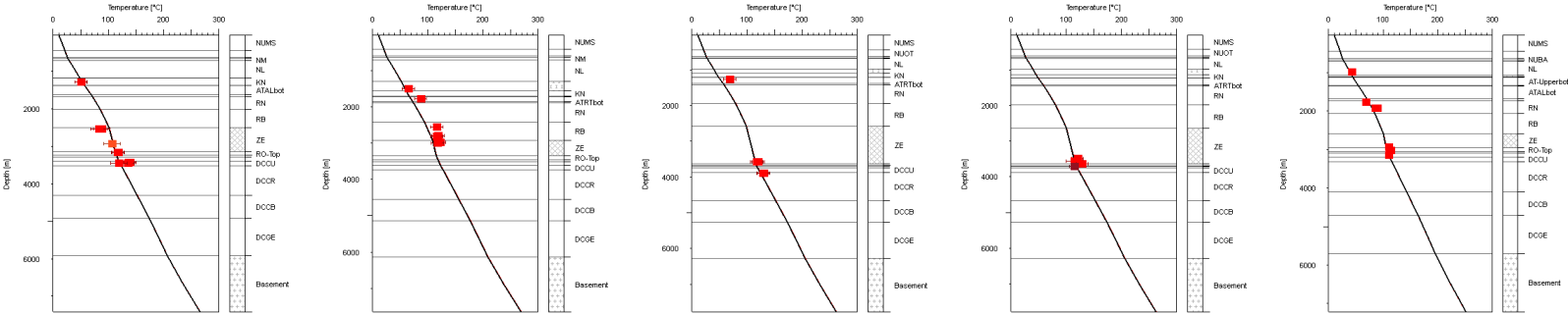






8.7.2 Temperature

— Scenario V
— Scenario IV



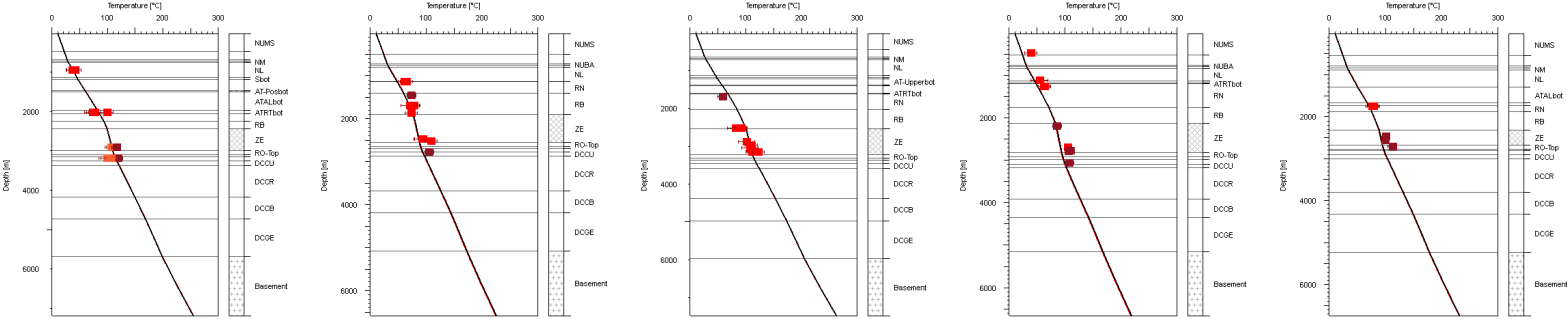
K11-04

K11-03

K12-05

K12-10

K14-01



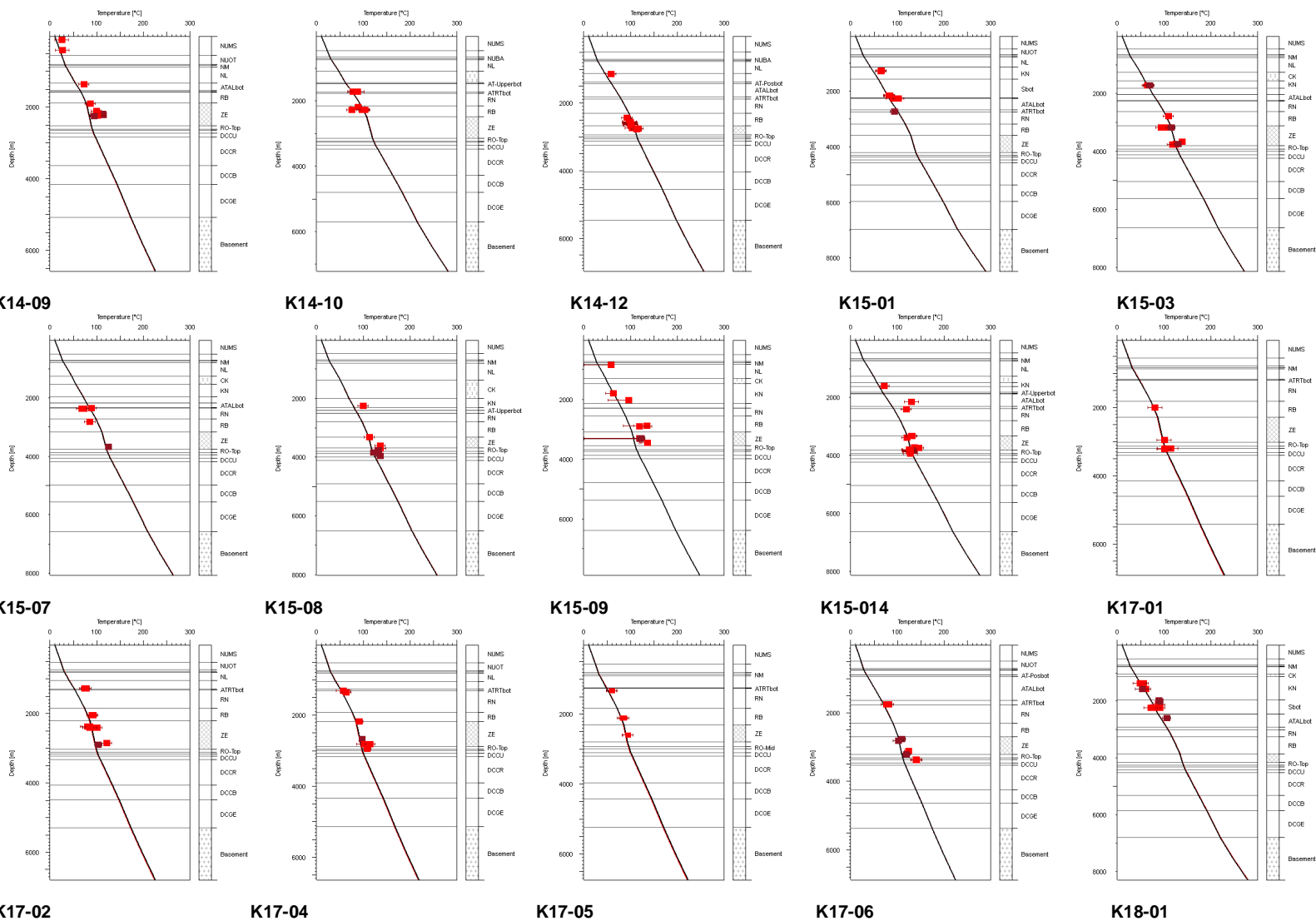
K14-02

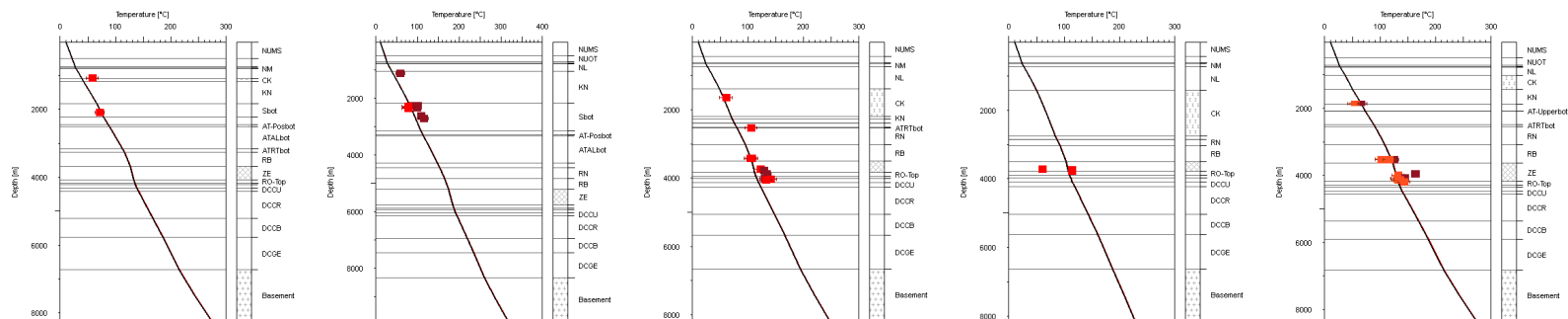
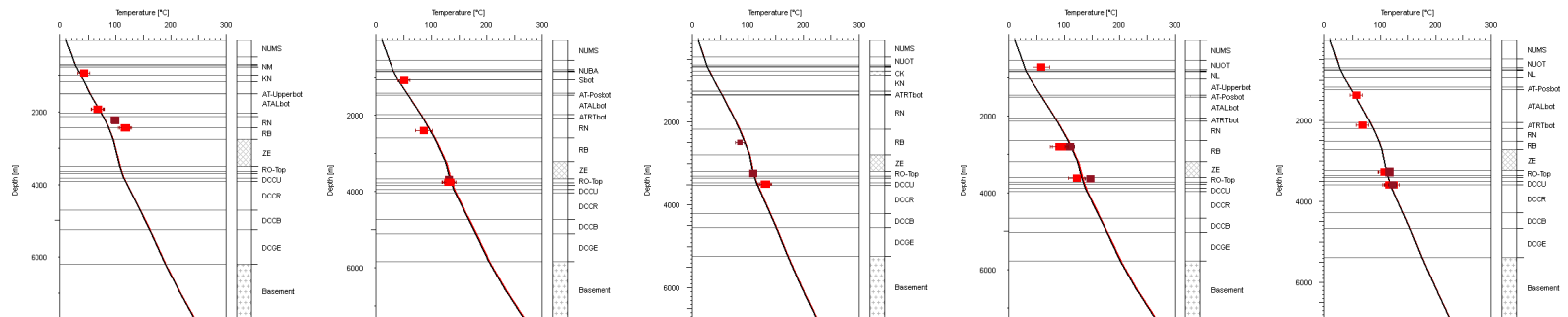
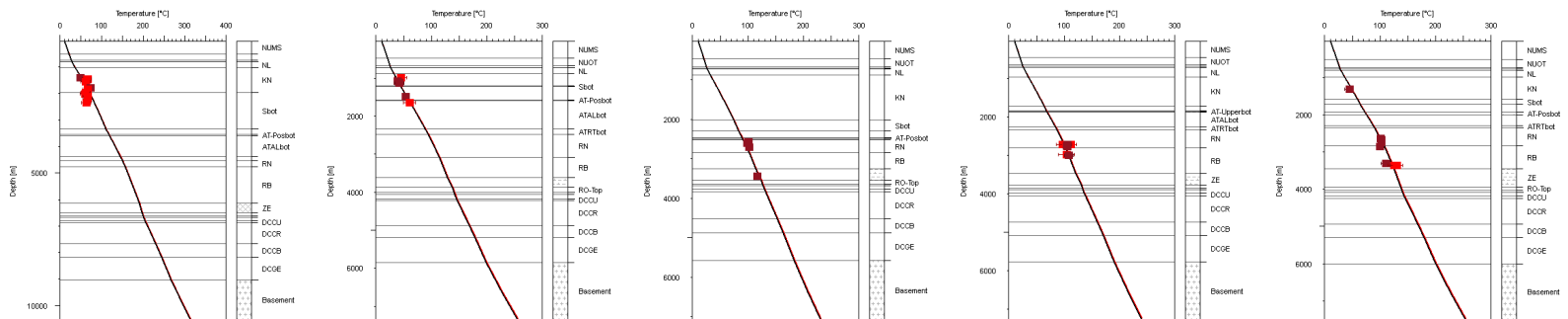
K14-03

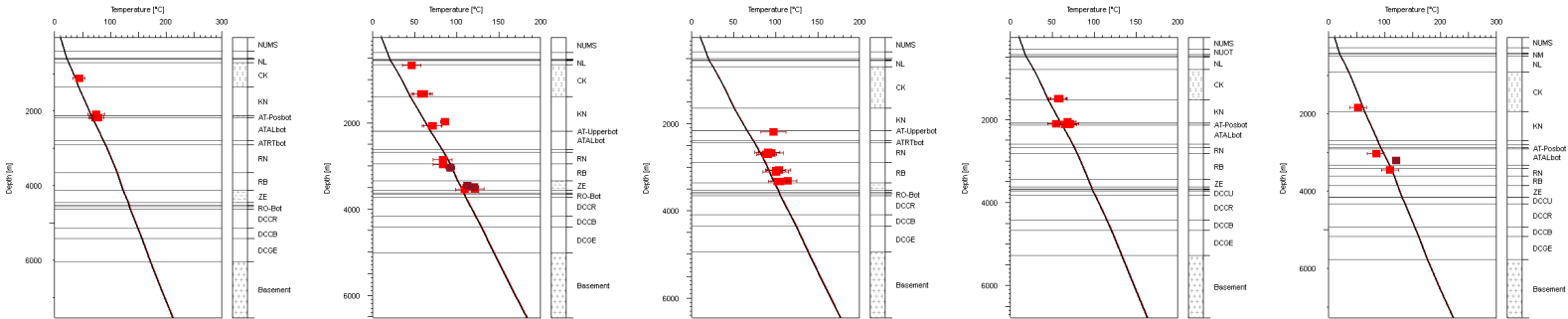
K14-05

K14-07

K14-08



**K18-04****K18-05****L17-03****L10-06****L16-03****L16-05****P02-01****P02-02****P02-03****P02-05****P03-02****P05-03****P06-01****P06-05****P06-06**



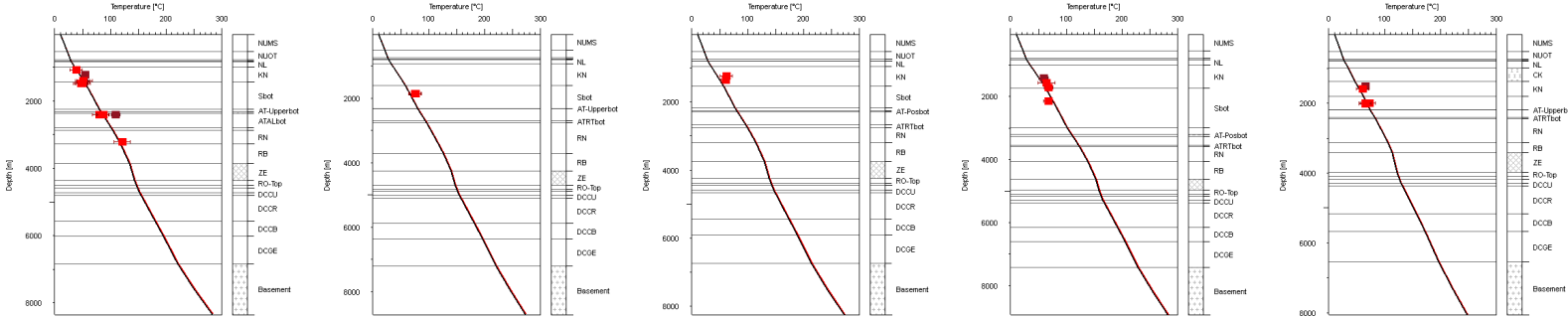
P09-02

P12-01

P12-11

P15-05

P18-02



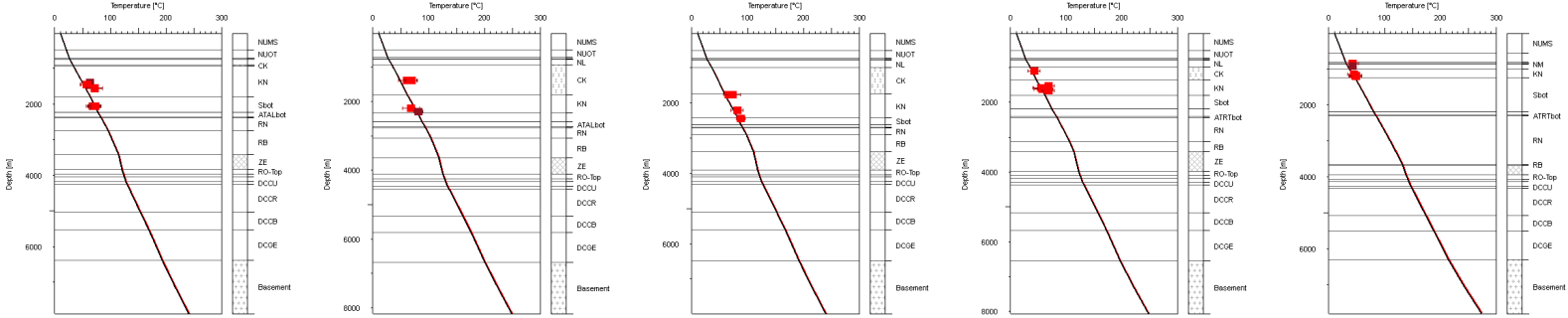
Q01-03

Q01-04

Q01-05

Q01-06

Q01-08



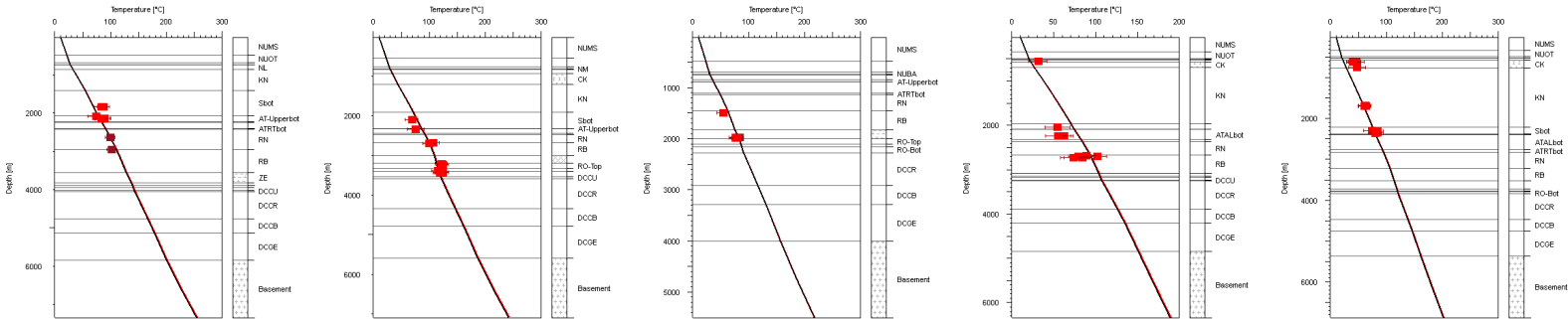
Q01-09

Q01-12

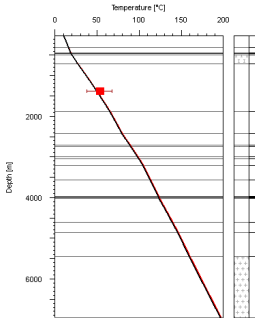
Q01-17

Q01-20

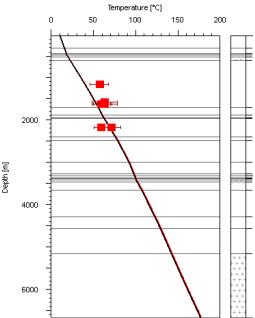
Q04-04



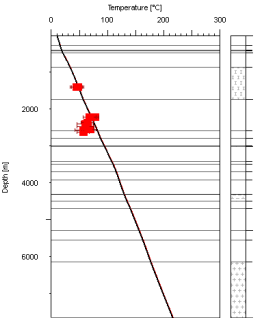
Q04-06



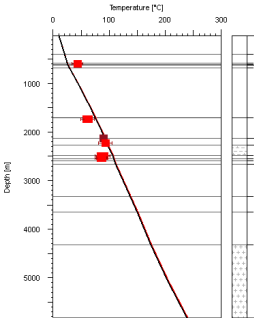
Q04-07



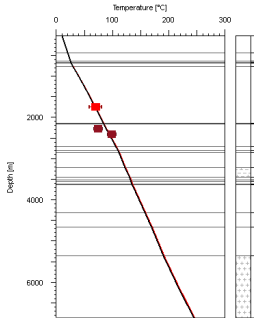
Q07-05



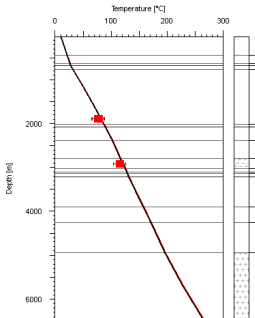
Q11-03



Q10-01



Q13-01



Q14-01



Q16-05



Q07-01



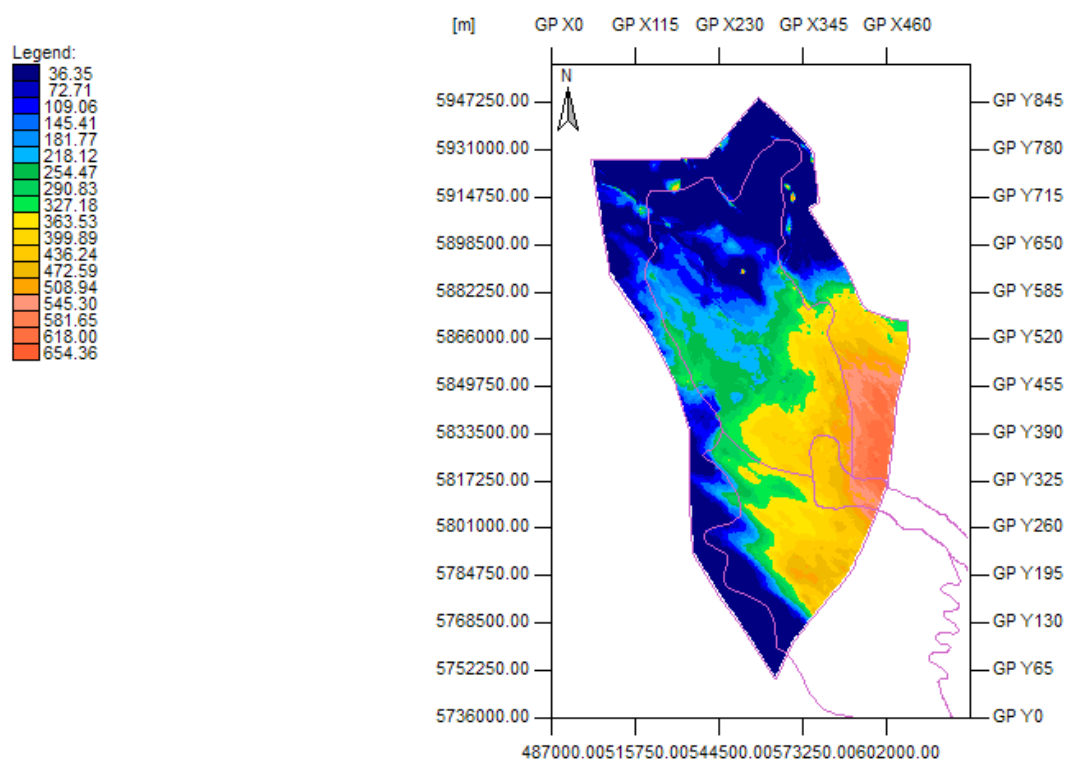
Q07-03



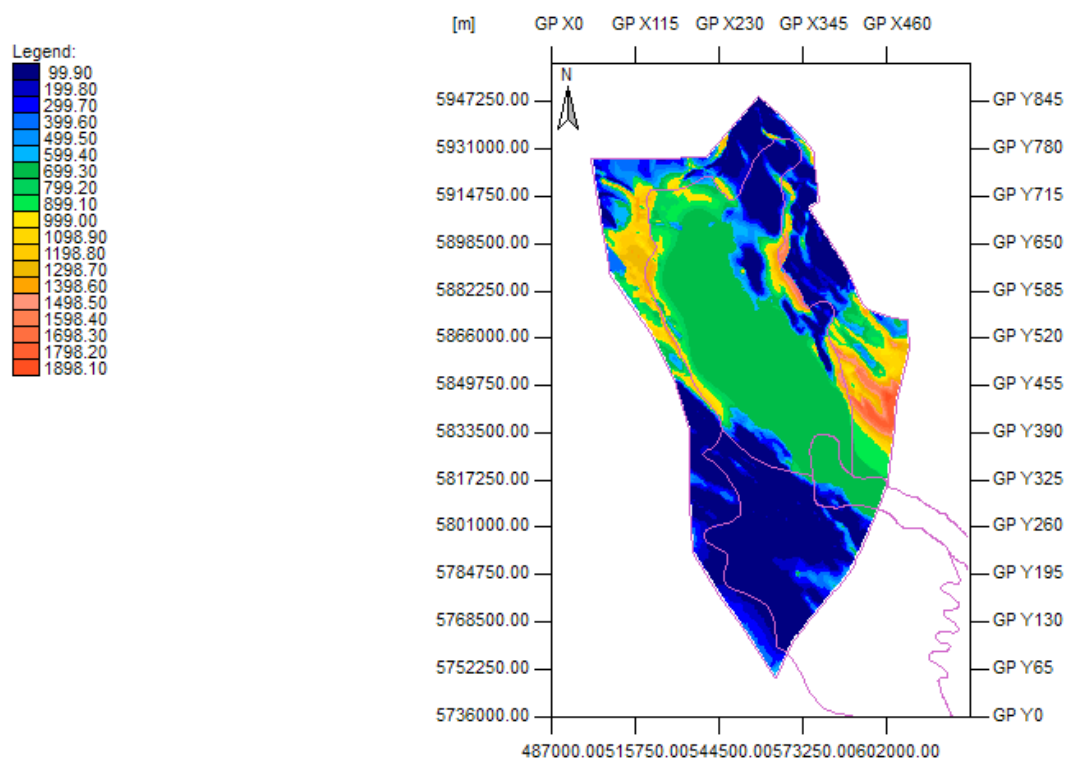
Q07-04



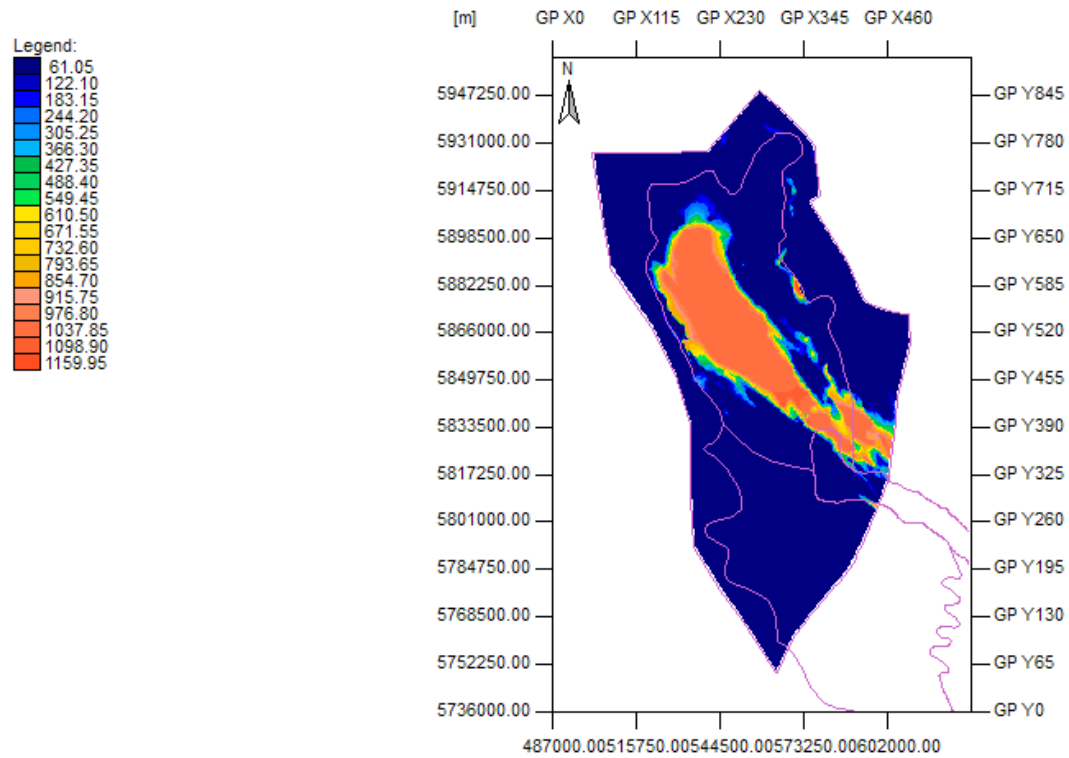
8.8 Annex VII: Erosion maps (Maturity scenario)



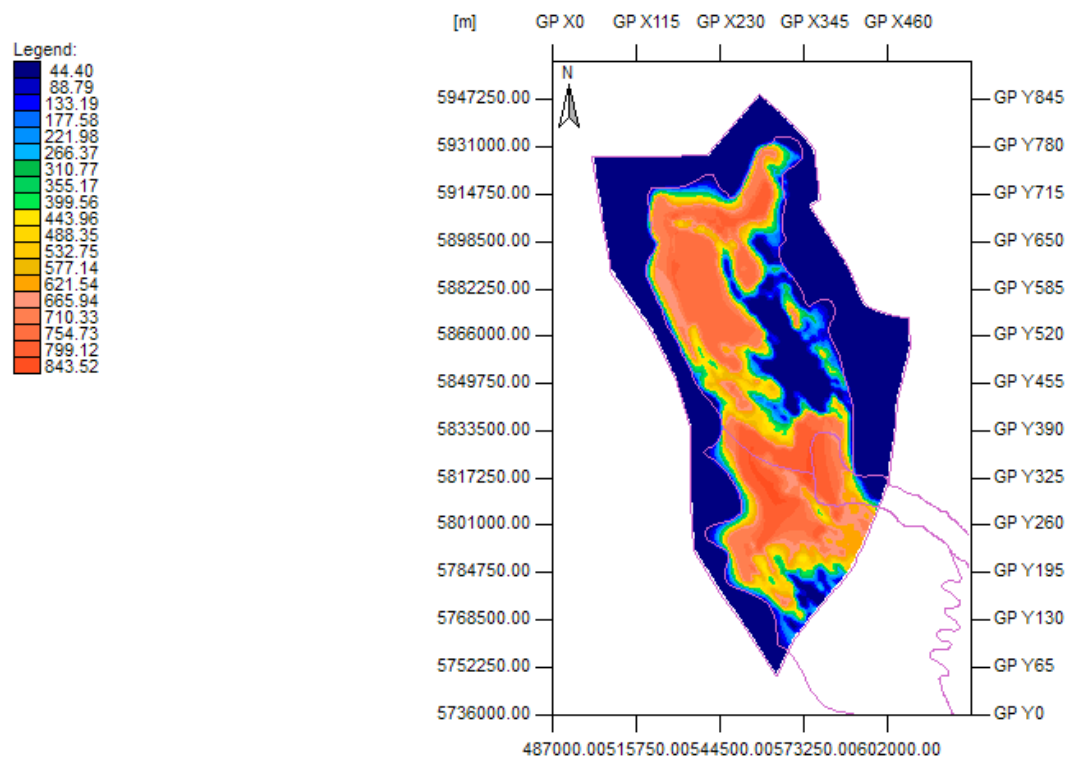
Lower North Sea Group



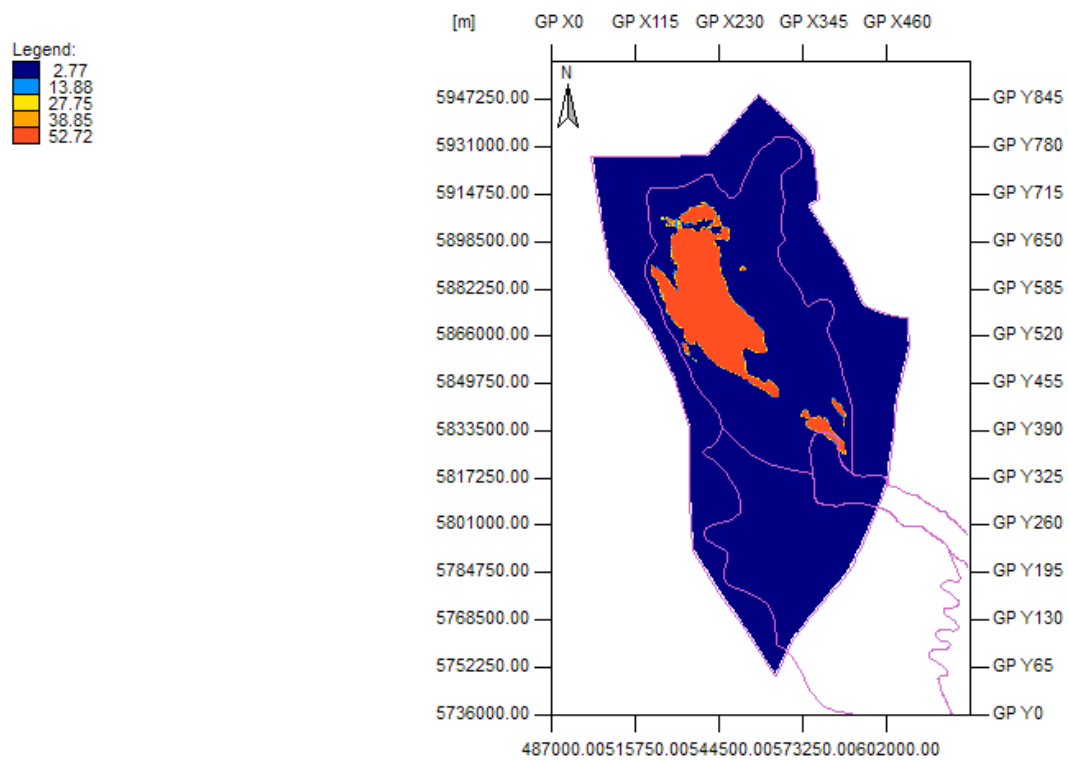
Chalk Group (Subhercynian Erosion)



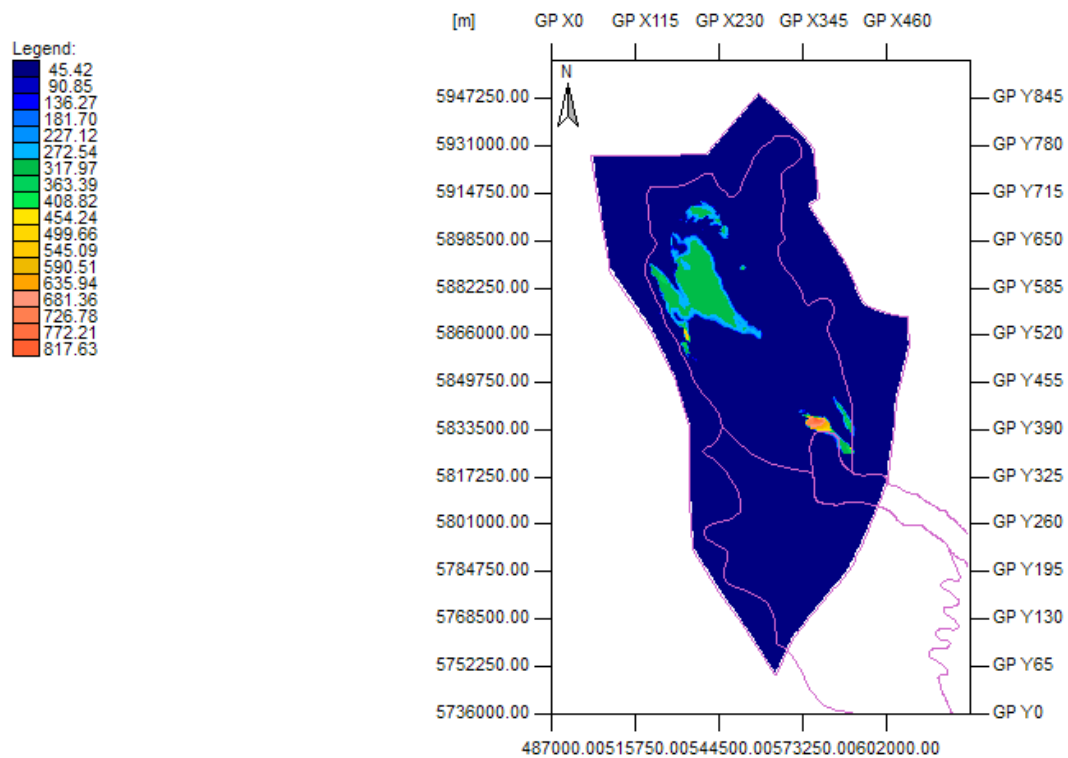
Rijnland (Subhercynian Erosion)



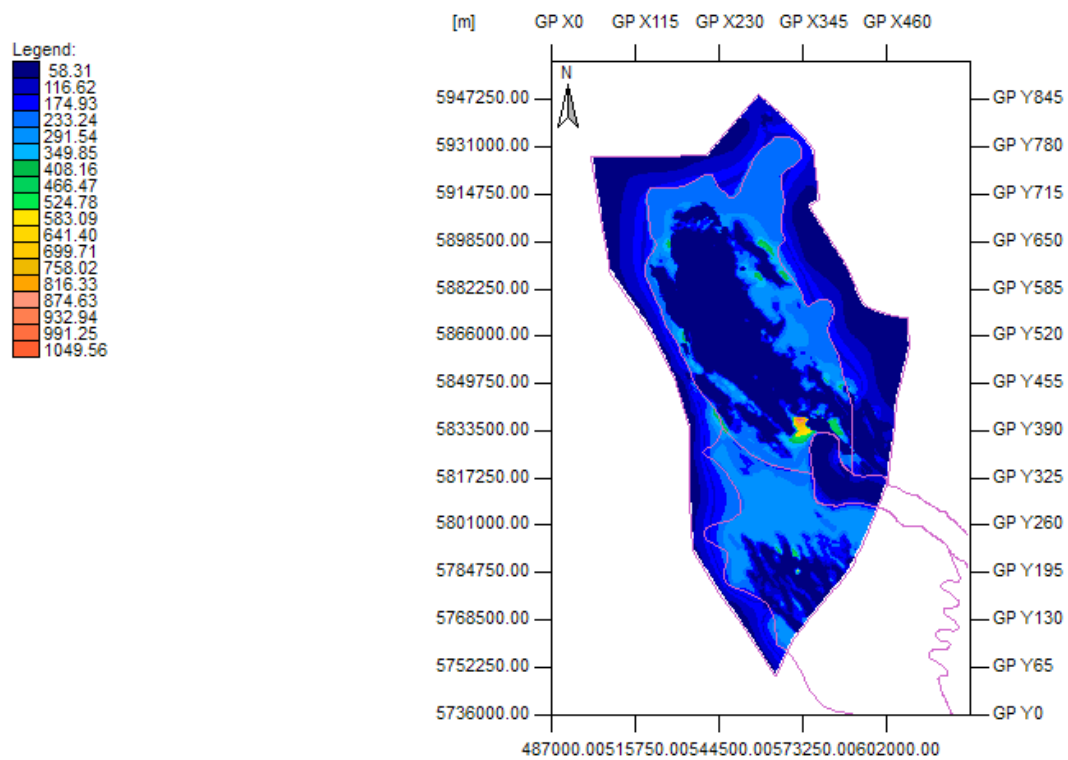
Schieland Group (Late Kimmerian II Erosion)



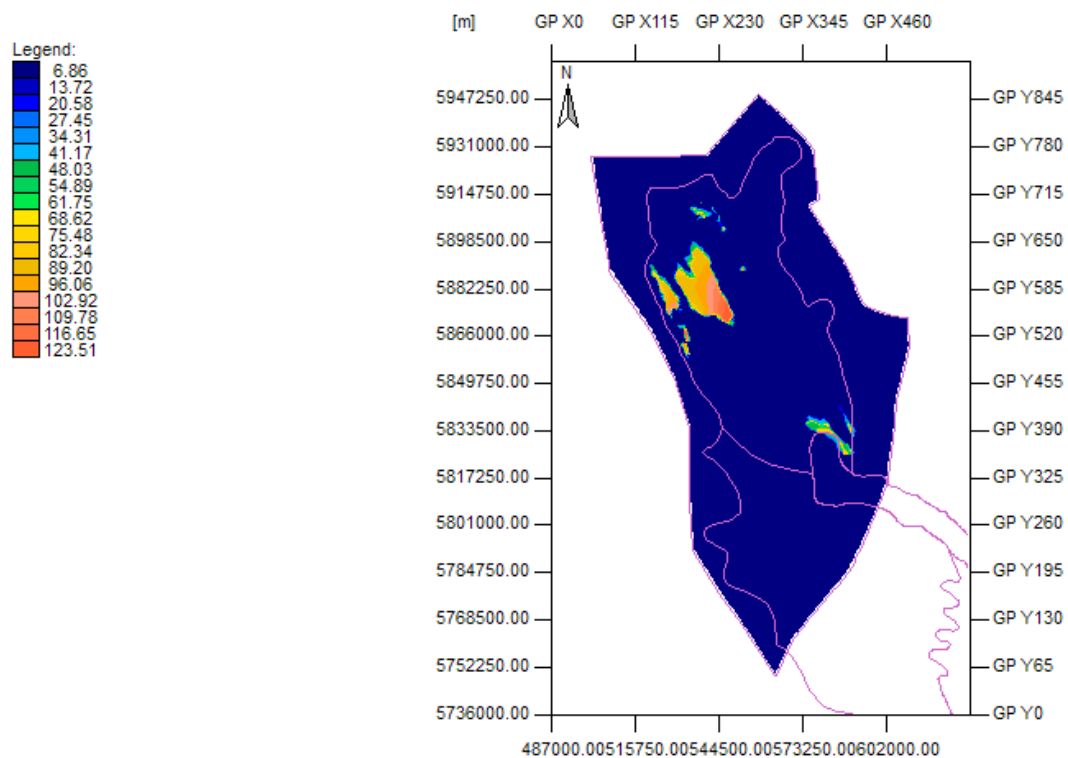
Schieland Group (Subhercynian Erosion)



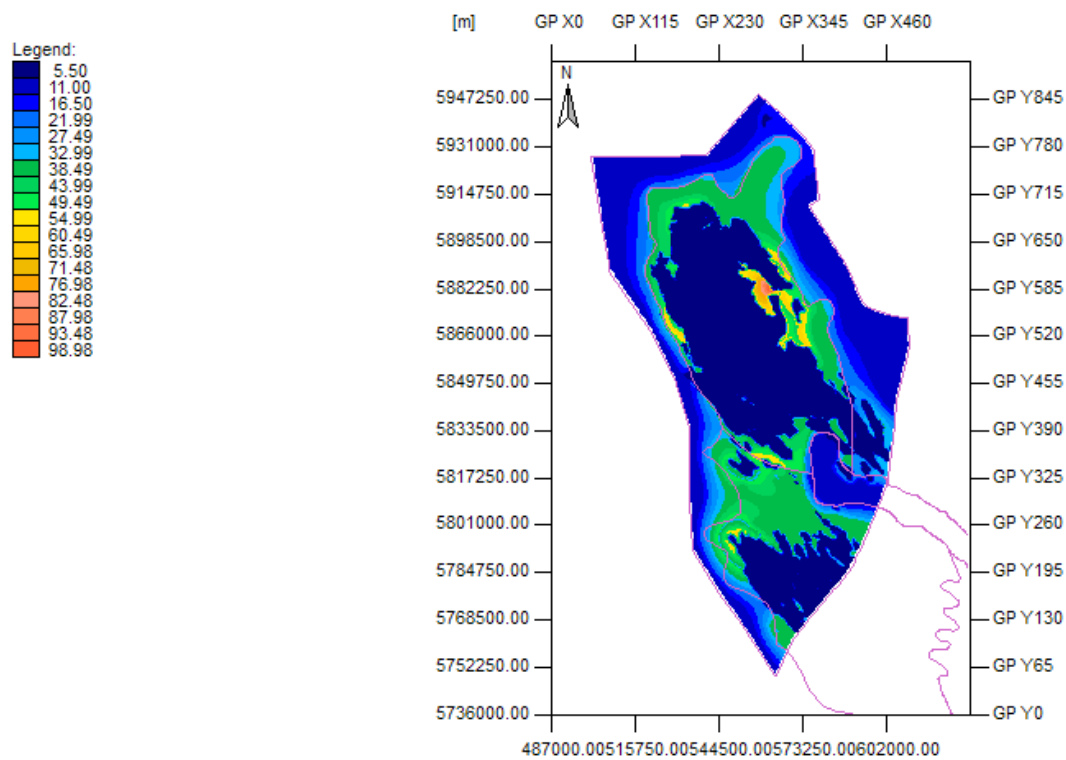
Altena Group Upper (Subhercynian Erosion)



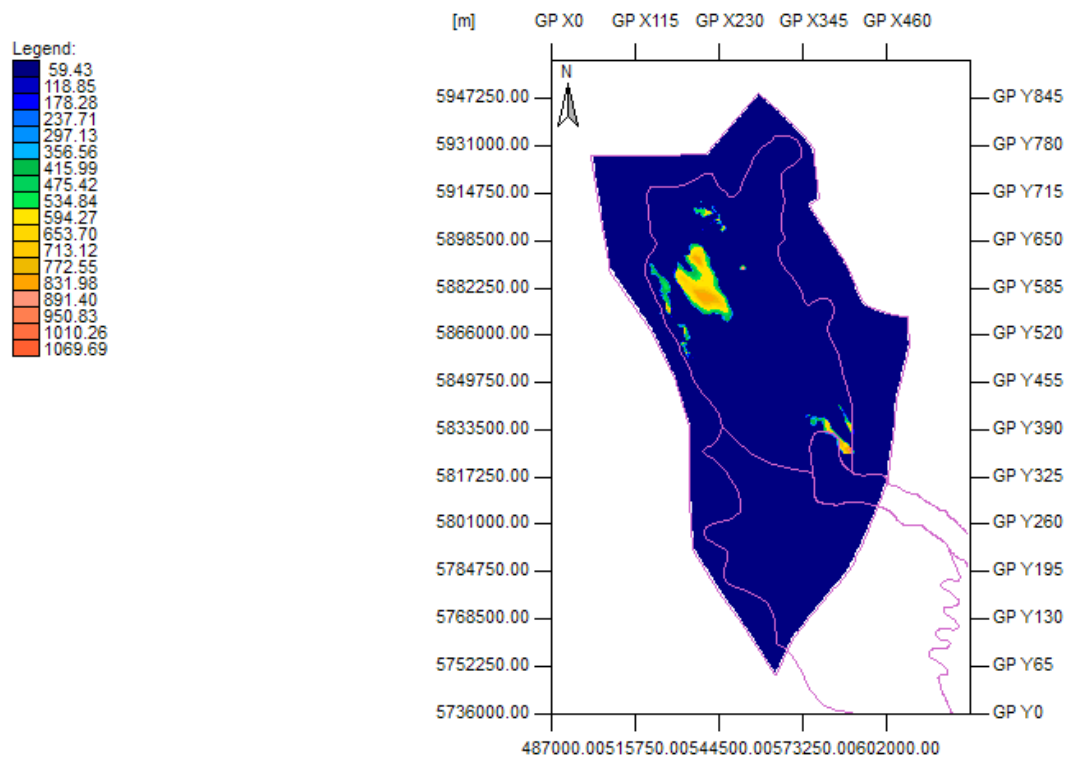
Altena Group Upper (Mid- Late Kimmerian I Erosion)



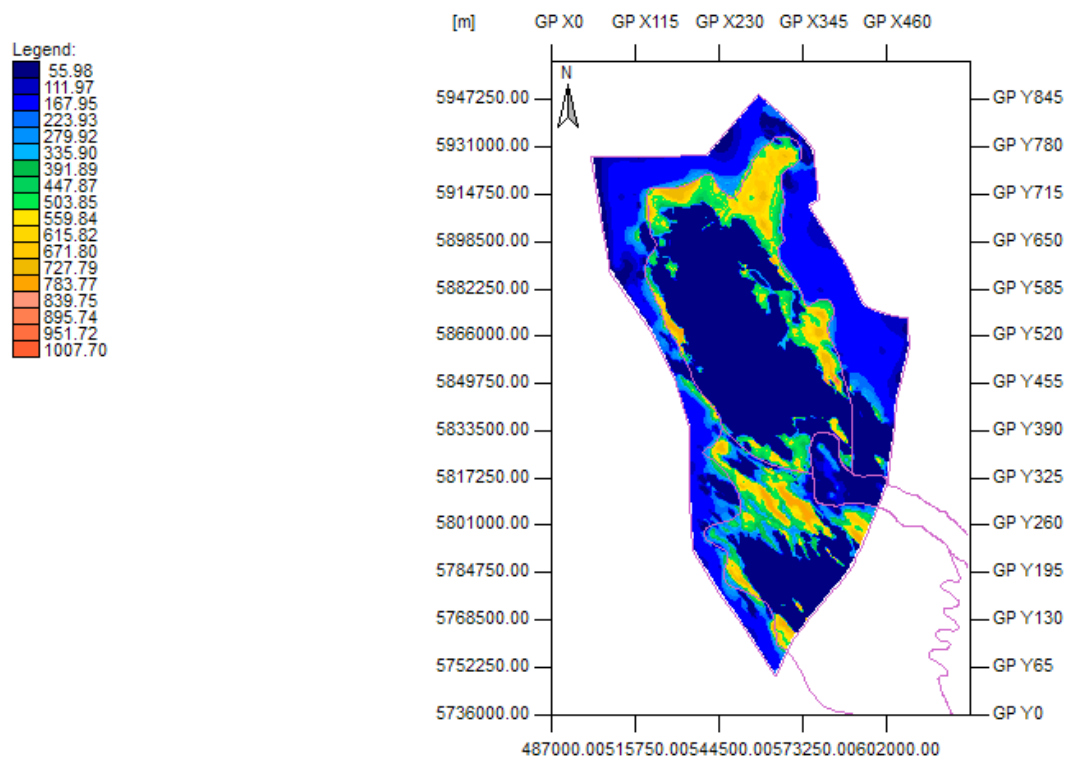
Altena_Posidonia Formation (Subhercynian Erosion)



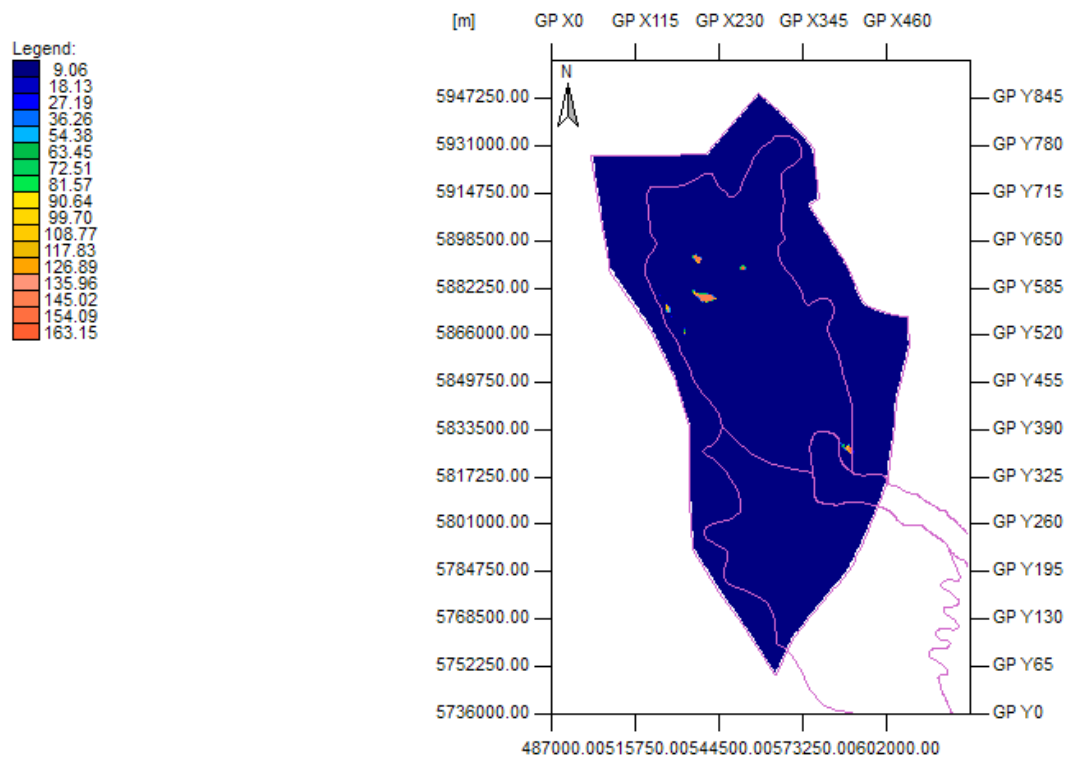
Altena_Posidonia Formation (Mid- Late Kimmerian I Erosion)



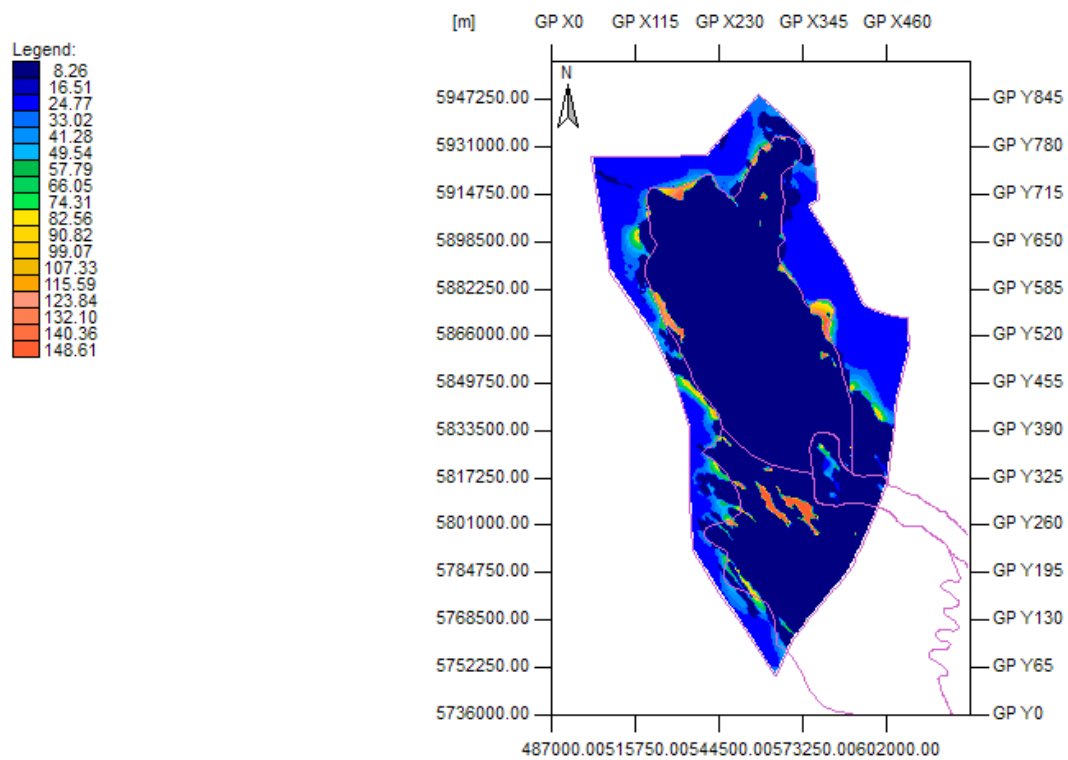
Altena_Aalburg Formation (Subhercynian Erosion)



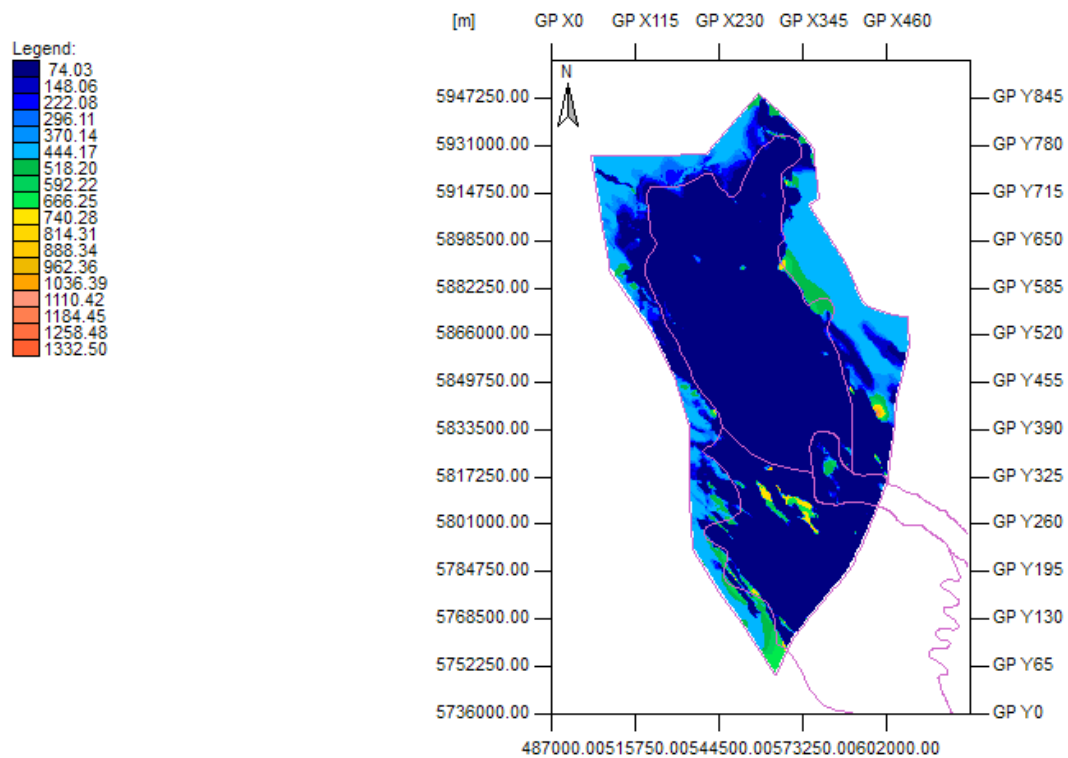
Altena_Aalborg Formation (Mid-Late Kimmerian I Erosion)



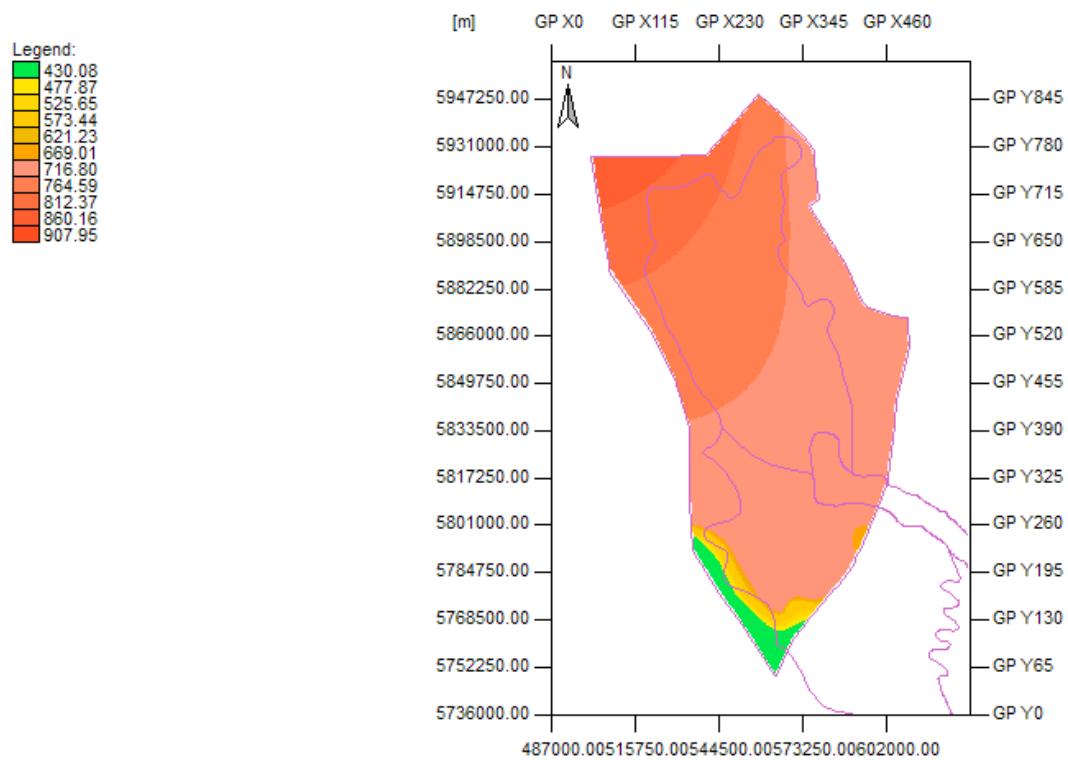
Altena_Sleen Formation (Subhercynian Erosion)



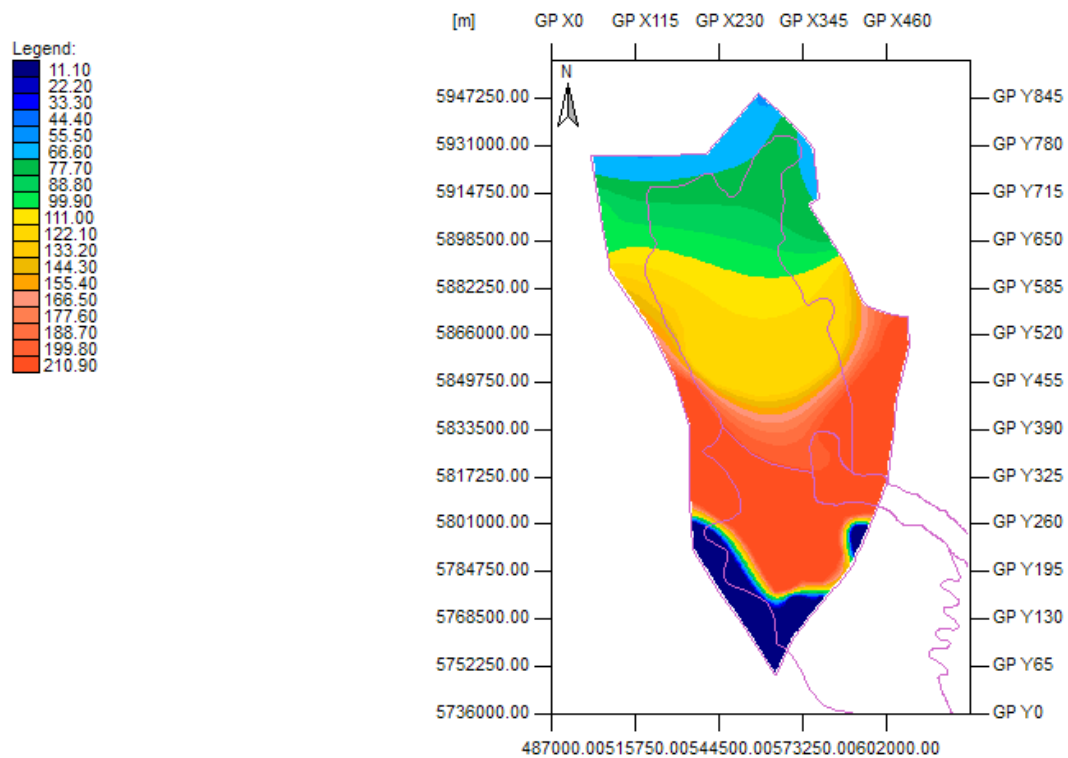
Altena_Sleen Formation (Mid-Late Kimmerian I Erosion)



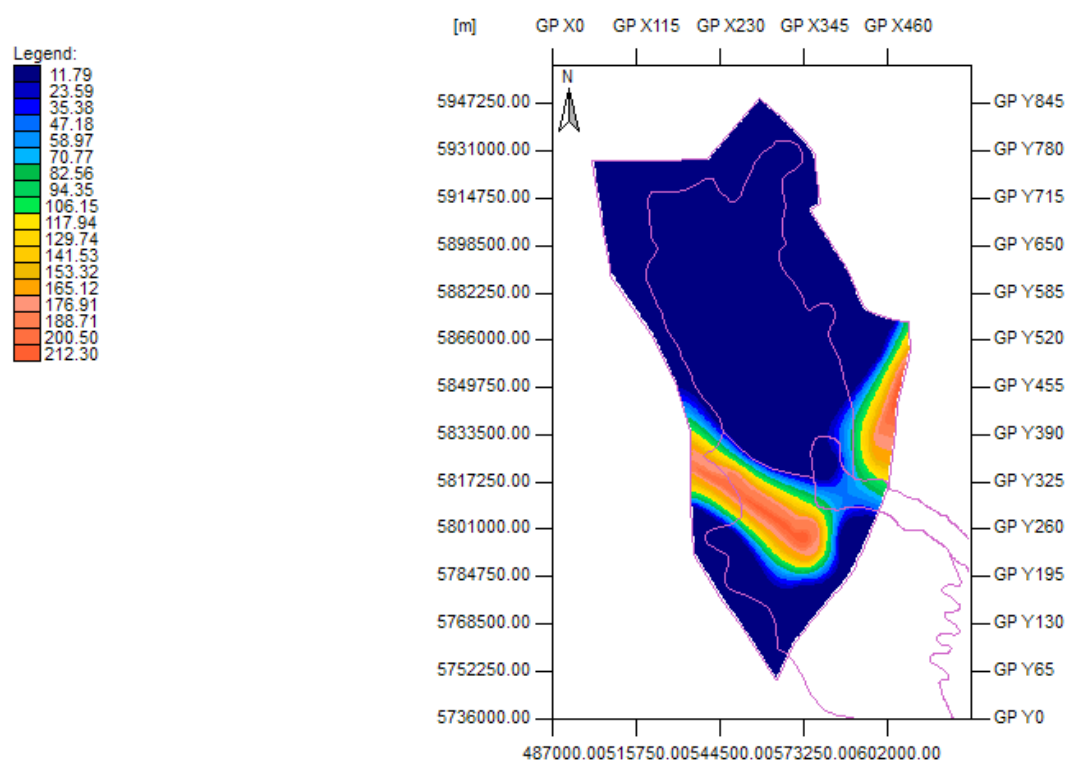
Upper Germanic Trias Group



Hunze Sub-Group



Maurits Formation



Ruurlo Formation

9 Signature

Utrecht, <datum>

Placeholder

<naam afdelingshoofd>

J.M. Verweij

N. Witmans

J.T.Veen

Head of department

R. Abdul Fattah

Author